2012

Study of coal sorption characteristics and gas drainage in hard-to-drain seams

Lei Zhang
University of Wollongong

STUDY OF COAL SORPTION CHARACTERISTICS AND GAS DRAINAGE IN HARD-TO-DRAIN SEAMS

A thesis submitted in fulfilment of the requirements for the award of the degree

DOCTOR OF PHILOSOPHY

from

UNIVERSITY OF WOLLONGONG

by

Lei Zhang

B.Sc. Mining Engineering (Hons)

School of Civil, Mining and Environmental Engineering

2012

AFFIRMATION

I, Lei Zhang, declare that this thesis, submitted in fulfilment of the requirements for the award of Doctor of Philosophy, in the school of Civil, Mining and Environmental Engineering, University of Wollongong, is wholly my own work unless otherwise referenced or acknowledged. The thesis was completed under the supervision of Dr Ting X Ren and Professor Naj Aziz and has not been submitted for qualifications at any other academic institution.

Lei Zhang

The following publications are the result of this thesis:

Zhang, L., Aziz, N., Ren, T., Wang, Z., 2011. Influence of temperature on the gas content of coal and sorption modelling. In *Proceedings of the 11th Underground Coal Operators' Conference (Coal 2011)*, University of Wollongong, Wollongong, Australia, pp 269-276. http://ro.uow.edu.au/cgi/viewcontent.cgi?article=2028&context=coal

Zhang, L., Ren, T., Aziz, N., Wang, Z., 2011. Influence of temperature and moisture on the gas content of coal. In *Proceedings of the 3rd ASIA Pacific Coalbed Methane Symposium*, Brisbane, Queensland, Australia, Paper No. 11.

Zhang, L., Aziz, N., Ren, T., Wang, Z., 2011. Influence of temperature on coal sorption characteristics and the theory of coal surface free energy. In *Proceedings of the 1st International Symposium on Mine Safety Science and Engineering*, Beijing, China, pp 1207-1216. *(This conference paper was indexed by ELSEVIER and published in Journal of Procedia Engineering)*

Zhang, L., Aziz, N., Ren, T., Wang, Z., 2012. Permeability testing of coal under different triaxial conditions. In *Proceedings of the 12th Underground Coal Operators' Conference (Coal 2012)*, University of Wollongong, Wollongong, Australia, pp 278-286. http://ro.uow.edu.au/cgi/viewcontent.cgi?article=2077&context=coal

Zhang, L., Ren, T., Aziz, N., Nemcik J., Wang, Z., 2012. Investigation into variations in the drainability of coal in different sections of the Bulli Seam, NSW, Australia, in *Proceedings of the 18th Coal Congress of Turkey*, Chamber of Mining Engineers of Turkey, Zonguldak, Turkey, pp 173-184.

Zhang, L., Aziz, N., Ren, T., Nemcik J., Wang, Z., 2012. Permeability testing of Bulli Seam coal under triaxial condition, in *Proceedings of the 18th Coal Congress of Turkey*, Chamber of Mining Engineers of Turkey, Zonguldak, Turkey, pp 71-83. (*These two papers won the Acknowledgement and Contribution Award of the 18th Coal Congress of Turkey*)

Zhang, L., Ren, T., Aziz, N., Wang, Z., 2012. A study of laboratory testing and calculation methods for coal sorption isotherms, *Journal of China Coal Society*. (Accepted and in press)

Zhang, L., Ren, T., Aziz, N., Nemcik J., Hyslop A., 2013. A critical analysis of gas data in relation to gas drainability in Bulli seam. In *Proceedings of the 13th Underground Coal Operators' Conference (Coal 2013)*, University of Wollongong, Wollongong, Australia, pp 300-306.

ACKNOWLEDGEMENTS

I would like to express my sincere acknowledgement to my supervisors Dr Ting X Ren and Professor Naj Aziz, School of Civil, Mining and Environmental Engineering (CME), University of Wollongong for their generous love, supervision, support, guidance and patience throughout the PhD studying period, not only in the aspect of study but also life, they treat me as their student in my research and also as their son in my everyday life in Australia.

This thesis has been reviewed by Bob Kininmonth, whose invaluable help and comments in improving the thesis are gratefully acknowledged.

Thanks also extend to the following staff and organisations:

- Andrew Hyslop, Wayne Mulholland and other technical staff from Metropolitan Colliery for supporting the gas drainage investigation research project.
- Shane Domaschen, Matt Hill and Chris Davey and other staff from GeoGas for supporting my industry laboratory study programme.
- Murry Bull, Salvador Castelo and other staff from BHP Gas Lab for providing the coal seam gas measurement study programme.
- Darren Brady, Sean Muller and other staff from Simtars for providing the GC training and assisting my study visit.
- Metropolitan Colliery, West Cliff Colliery and Mandalong Colliery for providing coal samples, field data and field work discussion and underground visits.

Sincere appreciation extends to the financial support of the Scholarship from University of Wollongong and China Scholarship Council (CSC).

I would also like to thank the technical staff in the School of CME, especially Col Devenish and Alan Grant for their laboratory assistances and also Rick McLean, Ian Laird and other technical staff; thanks are due to Rodger Paton, Ben Brien, Peter Turner and staff from the ITS for their assistance, Eren Mehmet, Zhongwei Wang and Dalin Cai, for their support and friendship, and all my fellow friends, who have ever helped me, thank you all.

Most importantly, I would also like to express my deepest gratitude to my father Lide Zhang, my mother Jianping Liu and my elder sister Yao Zhang for their enduring love and support in everyday during the past 25 years. This study would not have been finished without their care, love and encouragements.

ABSTRACT

The subject of coal sorption characteristics and investigations into the reasons for coal seam gas drainability of the Bulli seam in Sydney Basin were undertaken by focusing on Metropolitan Colliery, where certain parts of the seam have been found to be especially hard-to-drain. Specifically, one part of this study was to examine gas generation and flow mechanism in coal, to understand coal isotherm testing and calculation methods and the environmental influences on the coal sorption characteristics such as temperature and moisture content and coal particle size variations. Another part of this study was to investigate the possible reasons resulting in hard-to-drain coal at Metropolitan Colliery, including coal cleat system variation, sorption capacity, coal microstructure, coal permeability, gas content and composition. Laboratory tests were conducted to investigate the impact of nitrogen injection to promote gas desorption from hard-to-drain coals.

Worldwide, different types of apparatus and methods are used to generate coal sorption isotherms, but in general, there are of two types; volumetric and gravimetric methods. In this study, both methods were introduced in detail and comparatively examined. The unique gravimetric apparatus in the University of Wollongong, called the indirect gravimetric method apparatus, including its setup, operation procedure, calculation theory, and calculation methods were comprehensively modified and introduced.

Different factors influence coal sorption characteristics. Concluded from both dry and moist coals' test results, the adsorbed volume of CO_2 and CH_4 is decreased with increasing temperature. The adsorption capacity of coal (Langmuir volume) also decreases with coal moisture. Ash content of coal samples and the density of coal determined by helium were found to increase with increasing coal particle size. The experiments of CO_2 and CH_4 adsorption of different particle size coal sample were conducted. The tested coal isotherms were compared and Langmuir volumes were examined and concluded. Coal sorbed volume decreased with the increasing coal particle size, both on a dry basis and dry ash free basis. Coal surface free energy theory was found to fit the experimental test result, and it could be used to explain theoretically the sorption behaviour of coal at higher temperature and moist conditions.

In the investigation of the main reasons resulting in hard-to-drain coal at Metropolitan Colliery, coal cleat systems were identified both in the lab and field. Geological background

was examined and geological variations could be the explanations of coal permeability change and CO_2 concentration variation, hence inducing gas drainage problem. Scanning Electron Microscopy (SEM) was used to analyse the coal microstructures. It was observed that the microstructures of the hard-to-drain coal samples appeared to be tighter and less porous when compared with the easy-to-drain samples.

Two different types of the permeability tests were conducted and showed that the Metropolitan coal permeability decreased with the increasing gas pressure and stress. The permeability converges to a steady level below 1 mD under high triaxial stress conditions. Such a relative low permeability could be another one of the possible factors causing the problem of hard-to-drain in the Bulli seam.

As the hard-to-drain area is typically CO_2 rich, the CO_2 isotherm should affect the gas drainage more than the CH_4 isotherm. Evidently, the experiment results shows coal adsorption capacity for CO_2 is much higher than CH_4, indicating that coal seams with higher CO_2 concentration and high gas adsorption capacity (7% ash content) can result in low gas saturation, contributing to poor gas drainage problems as these in the Bulli Seam.

A critical examination of the whole gas database (519 samples) and typical hard-to-drain database (97 samples) at Metropolitan were conducted. The relationships of Q_1, Q_2 and Q_3 gas content and their ratio in response to total gas content Q_T were statistically analysed. Comparative analysis of gas content and composition between the whole gas database and the hard-to-drain area was also carried out. Apparently, a direct warning index for the hard-to-drain area in the field can include relatively lower gas content (6-10 m^3/t), high gas composition of CO_2 (CO_2>80 %, CH_4<20 % or $CH_4/(CH_4+CO_2)$<0.2) and geological variations.

Laboratory tests were conducted to systemically analysis the N_2 injection enhancement process. It was observed that the coal seam gas (CO_2 and CH_4) can be flushed out by N_2 injection. The experiments results in terms of gas concentration, gas volume and gas content were examined in different stages. Furthermore results also show both N_2 gas flushing and gas desorption processes have influences on the coal swelling and shrinkage behaviour. Results from these tests provide invaluable knowledge for field trials of this innovative technology that could potentially lead to enhanced gas recovery from hard-to-drain or low permeability seams.

TABLE OF CONTENTS

AFFIRMATION ..... **i**

ACKNOWLEDGEMENTS ..... **iii**

ABSTRACT ..... **iv**

TABLE OF CONTENTS ..... **vi**

LIST OF FIGURES ..... **xii**

LIST OF TABLES ..... **xvii**

LIST OF SYMBOLS AND ABBREVIATIONS ..... **xviii**

CHAPTER ONE – GENERAL INTRODUCTION **1**

1.1 INTRODUCTION 1

1.2 COAL SORPTION CHARACTERISTICS 3

1.3 GAS DRAINAGE IN HARD-TO-DRAIN SEAMS 4

1.4 STATEMENT OF THE PROBLEM 5

1.5 OBJECTIVES OF RESEARCH 6

1.6 RESEARCH PROGRAMME 7

1.7 THESIS OUTLINE 8

CHAPTER TWO – GAS GENERATION, STORAGE AND FLOW MECHANISM IN COAL IN RELATION TO GAS DRAINAGE **10**

2.1 INTRODUCTION 10

2.2 GAS GENERATION AND STORAGE 10

2.2.1 Coalification process 10

2.2.2 Generation of coal seam gas 12

2.2.3 Storage of coal seam gas 14

2.3 PHYSICAL STRUCTURE OF COAL 16

2.4 GAS TRANSPORT IN COAL 17

2.4.1 Gas adsorption and desorption from coal surface 18

2.4.2 Gas diffusion in coal matrix 19

2.4.3 Factors impacting on gas diffusion in coal 20

2.4.3.1 Effect of coal moisture 20

2.4.3.2 Effect of temperature 20

2.4.3.3 Effect of gas type 21

2.4.3.4 Effect of coal particle size 21

2.4.3.5 Effect of confining stress 22

2.4.4 Gas flow through the cleats 22

2.4.5 Factors impacting on gas flow in coal cleat 23

2.4.5.1 Effect of water 23
2.4.5.2 Effect of temperature 24
2.4.5.3 Effect of gas type, pressure and saturation 25
2.4.5.4 Effect of geological variation 26
2.4.5.5 Effect of effective and confining stress 27
2.4.6 Coal behaviour with different gases 28
2.4.6.1 Gas adsorption and desorption 28
2.4.6.2 CO_2 gas injection 30
2.4.6.3 N_2 gas injection 31
2.5 GAS DRAINAGE FROM COAL 31
2.5.1 Surface gas drainage 32
2.5.2 Enhanced surface gas drainage 32
2.5.2.1 Technologies to increase borehole surface area for gas drainage 32
2.5.2.2 Secondary lateral drilling technology 34
2.5.2.3 Surface drainage with stress relief 35
2.5.3 Underground gas drainage 38
2.5.4 Enhanced underground gas drainage 39
2.5.4.1 Technologies to increase borehole surface area 39
2.5.4.2 In-seam directional drilling technology 44
2.5.4.3 Underground ventilation and gas drainage strategy 46
2.6 SUMMARY 50
CHAPTER THREE – GAS SORPTION ISOTHERM TEST OF COAL 52
3.1 INTRODUCTION 52
3.2 ISOTHERM TESTING APPARATUS AND CALCULATION METHOD 53
3.2.1 Volumetric method 53
3.2.1.1 Sample cell (equilibrium cell) and injection pumps 53
3.2.1.2 Both sample cell and reference cell (or reference volume) 55
3.2.2 Gravimetric method 57
3.2.2.1 Sample cell and suspension magnetic balance 57
3.2.2.2 Both sample cell and reference cell (or reference volume) 59
3.2.3 OTHER METHODS 60
3.2.3.1 Under-confining stress 60
3.2.3.2 Direct determining method 61
3.3 UNCERTAINTIES IN RECORDING SORPTION ISOTHERM 62

3.3.1 Helium as a reference gas 62
3.3.2 Temperature 62
3.3.3 Equations of state (EOS) 63
3.3.4 Volume calculation 63
3.3.5 Impurity in the measurement gas 64
3.3.6 Gas dissolution in water and gas sorption on mineral matter 64
3.3.7 Other sources of errors 64
3.4 COMPARISON OF DIFFERENT METHODS 65
3.5 COMPARISON BETWEEN DIFFERENT LABORATORIES 67
3.6 COAL SORPTION ISOTHERM TESTING IN UNIVERSITY OF WOLLONGONG 69
3.6.1 Apparatus 69
3.6.2 Experimental procedure 70
3.6.3 Calculation method 71
3.6.3.1 SRK equation calculation 71
3.6.3.2 Calibration curve calculation 72
3.6.3.3 Gibbs adsorbed volume and absolute adsorbed volume 73
3.6.3.4 Discussion regarding the two calculation methods 74
3.7 SUMMARY 75
CHAPTER FOUR – FACTORS INFLUENCING SORPTION CHARACTERISTICS AND SURFACE FREE ENERGY OF COAL 77
4.1 INTRODUCTION 77
4.2 EXPERIMENTAL SET UP AND SAMPLE PREPARATION 77
4.2.1 Coal sorption apparatus and coal samples 77
4.2.2 Coal sample retrieval and preparation for testing 78
4.2.3 Ash content test 82
4.3 INFLUENCE OF TEMPERATURE ON COAL ADSORPTION ISOTHERMS 83
4.3.1 Coal adsorption isotherm 84
4.3.2 Coal adsorption capacity 85
4.4 INFLUENCE OF MOISTURE ON COAL ADSORPTION ISOTHERMS 87
4.4.1 Coal adsorption isotherm 87
4.4.2 Coal adsorption capacity 89
4.5 INFLUENCES OF COAL PARTICLE SIZE ON COAL ADSORPTION AND DESORPTION ISOTHERMS 92
4.5.1 Coal ash content and helium density 92
4.5.2 Coal adsorption isotherms 95

4.5.3 Coal adsorption capacity 96
4.5.4 Coal desorption isotherms 97
4.5.5 Coal desorption capacity 99
4.6 COAL SURFACE FREE ENERGY THEORY 99
4.6.1 Calculation 100
4.6.2 Result analysis 101
4.6.2.1 Dry coal sample test analysis 101
4.6.2.2 Moist coal sample test analysis 104
4. 7 SUMMARY 106
CHAPTER FIVE – STUDY OF GEOLOGICAL VARIATION AND COAL MICROSTRUCTURE 108
5.1 INTRODUCTION 108
5.2 GEOLOGICAL VARIATION 110
5.2.1 Geological background 110
5.2.2 Mineralisation 112
5.2.3 Coal cleat system 113
5.2.4 Geological variation induced permeability change 115
5.2.5 Geological variations inducing high CO_2 concentration 116
5.3 COAL MICROSTRUCTURE STUDY 119
5.3.1 Scanning Electron Microscopy (SEM) test 119
5.3.2 SEM analysis of coal samples from hard-to-drain area 123
5.3.3 SEM analysis of coal samples from easy-to-drain area 126
5.3.4 Identification of coal porous structure 129
5.4 SUMMARY 130
CHAPTER SIX – DRAINABLITY ASSESSMENT OF THE BULLI SEAM AT METROPOLITAN COLLIERY 132
6.1 INTRODUCTION 132
6.2 COAL PERMEABILITY 133
6.2.1 Multi Function Outburst Research Rig test 134
6.2.1.1 Multi Function Outburst Research Rig 134
6.2.1.2 Coal sample preparation 135
6.2.1.3 Testing procedure 136
6.2.1.4 Results and analysis 136
6.2.2 Triaxial Compression Apparatus test 138
6.2.2.1 Triaxial Compression Apparatus 138
6.2.2.2 Coal sample preparation 139

6.2.2.3 Testing procedure 140
6.2.1.4 Results and analysis 140
6.2.3 Comparative analysis of MFORR and Triaxial Compression Apparatus test results 142
6.2.4 Permeability classification of coalbeds 143
6.3 COAL SORPTION CAPACITY 145
6.3.1 Ash content test 145
6.3.2 Adsorption isotherm test 146
6.4 STUDY OF GAS CONTENT AND GAS COMPOSITION 151
6.4.1 Measurement of coal seam gas content and gas composition 151
6.4.1.1 Lost gas component 152
6.4.1.2 Desorbed gas component 152
6.4.1.3 Residual gas component 153
6.4.1.4 Measured total gas Content 153
6.4.2 Analysis of whole gas database 153
6.4.2.1 Bulli Seam outburst threshold limits (TLV) 153
6.4.2.2 Q_1 gas content component 154
6.4.2.3 Q_2 gas content component 156
6.4.2.4 Q_3 gas content component 157
6.4.2.5 Gas content component summary 159
6.4.3 Analysis of the hard-to-drain area 160
6.4.3.1 Bulli Seam outburst threshold limits (TLV) 160
6.4.3.2 Q_1 gas content component 161
6.4.3.3 Q_2 gas content component 162
6.4.3.4 Q_3 gas content component 163
6.4.3.5 Gas content component summary 164
6.4.4 Comparative analysis of gas content and composition between the whole gas database and the hard-to-drain area 165
6.5 SUMMARY 169
CHAPTER SEVEN – GAS INJECTION TO FLUSH COAL SEAM GAS 172
7.1 INTRODUCTION 172
7.2 HARD-TO-DRAIN SEAMS 173
7.3 STUDY OF GAS INJECTION TO FLUSH COAL SEAM GAS 175
7.4 LABORATORY TEST OF INJECTION WITH MULTI FUNCTION OUTBURST RESEARCH RIG 177
7.4.1 Multi Function Outburst Research Rig (MFORR) and Gas Chromatograph 177

7.4.2 Coal sample preparation 178
7.5 INJECTION OF N_2 TO FLUSH CO_2 179
7.5.1 Stage 1 - Coal sorption process 179
7.5.2 Stage 2 - N_2 injection to flush CO_2 process 180
7.5.3 Stage 3 - Desorption test after N_2 injection 182
7.6 INJECTION OF N_2 TO FLUSH CH_4 185
7.6.1 Stage 1 - Coal sorption process 185
7.6.2 Stage 2 - N_2 injection to flush CH_4 process 185
7.6.3 Stage 3 - Desorption test after N_2 injection 188
7.7 COMPARISON OF N_2 TO FLUSH CO_2 AND CH_4 190
7.7.1 Stage 1 - Coal sorption comparison 191
7.7.2 Stage 2 - N_2 injection process comparison 192
7.7.3 Stage 3 - Desorption process comparison 194
7.8 SUMMARY 196
CHAPTER EIGHT – CONCLUSIONS AND RECOMMENDATIONS 199
8.1 CONCLUSIONS 199
8.2 RECOMMENDATIONS 204
REFERENCES 205
APPENDICES 223
APPENDIX A: LANGMUIR EQUATION 223
APPENDIX B: SOAVE-REDLICH-KWONG EQUATION OF STATE 224
APPENDIX C: COAL SOPRTION ISOTHERM CALCULATION WITH SRK EQUATION METHOD 225
APPENDIX D: COAL SOPRTION ISOTHERM CALCULATION WITH CALIBRATION CUREVE METHOD 227
APPENDIX E: COAL PERMEABILITY TEST RESULT WITH MFORR 228
APPENDIX F: COAL PERMEABILITY TEST RESULT WITH TRIAXIAL COMPRESSION APPARATUS 229
APPENDIX G: COMPARISON OF ADSORPTION ISOTHERMS (HARD-TO-DRAIN AND EASY-TO-DRAIN AREAS) 231
APPENDIX H: SUMMARY OF GAS CONTENT AND GAS COMPOSITION DATA (WHOLE DATABASE-PASS SAMPLES) 232
APPENDIX I: SUMMARY OF GAS CONTENT AND GAS COMPOSITION DATA (WHOLE DATABASE-FAIL SAMPLES) 235
APPENDIX J: SUMMARY OF GAS CONTENT AND GAS COMPOSITION DATA (HARD-TO-DRAIN DATABASE) 237

LIST OF FIGURES

Figure 1.1: Location of Australian black coal resources....1
Figure 1.2: Main structure of the thesis....8
Figure 2.1: Details of the processes, stages and products of coalification (after UWYO, 2002)....11
Figure 2.2: Location of the Southern and Hunter Coalfields, Sydney Basin, New South Wales, Australia (after Faiz *et al.*, 2007)....12
Figure 2.3: Schematic of bidisperse coal pore structure showing macro- and micropores containing gas in free, adsorbed and dissolved states (after Yi *et al.*, 2009)....15
Figure 2.4: Schematic illustration of coal cleat geometries. (a) Cleat-trace patterns in plan view. (b). Cleat hierarchies in cross-section view. (after Laubach *et al.*, 1998)....16
Figure 2.5: Transport of coal seam gas in coal. (after Harpalani and Schraufnagel, 1990)....18
Figure 2.6: Gas drainage enhancement methods ranked according to cost and application relative to coal seam permeability (after Loftin, 2009 and Johnson, 2010)....33
Figure 2.7: Pinnate pattern of multi-lateral wells (after Spafford, 2007)....35
Figure 2.8: Perm-based completion tree for CBM: vertical wells (after Palmer, 2010).....35
Figure 2.9: The schematic diagram of the vertical distribution of mining fractures in overlying strata (after Sang *et al.*, 2010)....36
Figure 2.10: Underground stope stress zoning. I - normal stress zone; II - stress concentration zone; III - stress relief zone; IV - stress resume zone. 1 - initial surface; 2 - surface subsidence curve; 3 - strata subsidence curve. (after Sang *et al.*, 2010)....37
Figure 2.11: Pressure relief gas migration and surface vertical wells drainage (after Sang *et al.*, 2010)....38
Figure 2.12: Gas sources in a coal mine (after SAWS, 2006)....39
Figure 2.13: Directional drilling system schematic layout (after Hungerford *et al.*, 2012b)....44
Figure 2.14: Inseam drilling patterns available for CSG drainage (after Thomson, 1998)....46
Figure 2.15: Gas control methods developed in Chinese coal mines for multi-seam mining with cross measure drilling (after Wang *et al.*, 2011)....47
Figure 2.16: 'U+L' ventilation scheme combined with cross measure boreholes (after You *et al.*, 2008a)....47
Figure 2.17: 'U+I' ventilation scheme based gas control technique (after You, 2008)....48
Figure 2.18: 'Y' ventilation scheme based gas control technique (after Yuan, 2008)....50
Figure 3.1: Schematic layout of volumetric method of gas sorption apparatus with injection pump (after Mohammad *et al.*, 2008)....54
Figure 3.2: Schematic diagram of the experimental set-up for gas adsorption using; (a) stainless steel sample cell containing coal and a pressure transducer, and (b) sample cell volume and reference volume (after Krooss *et al.*, 2002)....56
Figure 3.3: Schematic diagram of gravimetric method with sample cell and suspension magnetic balance (after Charriere *et al.*, 2010)....58
Figure 3.4: Schematic diagram of gravimetric method with both sample cell and reference cell (after Saghafi *et al.*, 2007)....59
Figure 3.5: Schematic diagram of under-confining stress method (after Pone *et al.*, 2009)....61
Figure 3.6: Schematic diagram of sorption direct determining method (after Hol *et al.*, 2011)....62
Figure 3.7: Schematic diagram of the modified gravimetric method with sample cells....70

Figure 4.1: Schematic diagram of the gas sorption apparatus (a) sorption apparatus including bombs, water bath and charging board, (b) sorption bomb, (c) pressure calibration apparatus for pressure transducer 78
Figure 4.2: Mine plan showing the location of longwall panel 520, Area 5, West Cliff Colliery (blue lines represent the underground gas drainage boreholes) (after Black, 2012) 79
Figure 4.3: Coal sample preparation (a) temperature controlled oven, (b) coal sample with water-sorbing silicon, (c) coal sample with saturated solution of potassium sulphate 80
Figure 4.4: Moisture content equilibrium in coal samples at different particle size 81
Figure 4.5: Ash content test (a) furnace, (b) coal sample before incineration, (c) coal sample after incineration 82
Figure 4.6: CO_2 and CH_4 adsorption isotherms at different temperature (Dry samples) 84
Figure 4.7: CO_2 and CH_4 adsorption isotherms at different temperature (Moist samples) 85
Figure 4.8: CO_2 and CH_4 adsorption capacity of dry and moist at different temperature 86
Figure 4.9: CO_2/CH_4 sorption ratio for different moist and dry coal samples at various temperatures as a function of coal rank. Values were picked between 1 and 5 MPa. Data fit for moist samples only (after Busch and Gensterblum, 2011) 87
Figure 4.10: Dry and moist adsorption isotherms in terms of different temperature: (a), (b) and (c) is CO_2 at 35 ℃, 45 ℃ and 55 ℃ respectively; (d), (e) and (f) is CH_4 at 35 ℃, 45 ℃ and 55 ℃ respectively 88
Figure 4.11: CO_2 and CH_4 adsorption capacity of dry and moist coal at different temperature 89
Figure 4.12: Sorption sites of each gas at one given fixed surface coverage (fixed P,T) and the intersection for multi-component sorption isotherms (after Busch and Gensterblum, 2011) 91
Figure 4.13: (a) Schematic diagram of sorption capacity of coals at different moisture contents and as a function of temperature; (b) schematic plot of the sorption capacity in the dry and moisturized state as a function of temperature (after Busch and Gensterblum, 2011) 92
Figure 4.14: Relationship of different analytical bases to various coal components (after Busch and Gensterblum, 2011) 93
Figure 4.15: Coal samples before the ash content test (a) 16 mm, (b) 8mm, (c) 2.4mm, (d) 150 µm .. 93
Figure 4.16: Coal samples after the ash content test (a) 16 mm, (b) 8mm, (c) 2.4mm, (d) 150 µm 94
Figure 4.17: Coal helium density and ash content test results 95
Figure 4.18: Coal adsorption isotherm results with CO_2 95
Figure 4.19: Coal adsorption isotherm results with CH_4 96
Figure 4.20: Langmuir volume of adsorption isotherm with CO_2 and CH_4 97
Figure 4.21: Coal desorption isotherm results with CO_2 and CH_4 98
Figure 4.22: Langmuir volume of desorption isotherm with CO_2 and CH_4 99
Figure 4.23: CO_2 adsorption isotherm and surface free energy calculation at different temperature (Dry sample) 102
Figure 4.24: CO_2 isotherm and surface free energy calculation in terms of adsorption and desorption (Dry sample) 103
Figure 4.25: Adsorption isotherm and surface free energy calculation in terms of CO_2, CH_4 and N_2 (Dry sample) 103
Figure 4.26: CO_2 adsorption isotherm and surface free energy calculation at different temperature (moist sample) 104
Figure 4.27: CO_2 isotherm and surface free energy calculation in terms of adsorption and desorption (moist sample) 105

Figure 4.28: CO_2 adsorption isotherm and surface free energy calculation in terms of dry and moist samples 105
Figure 5.1: Metropolitan mine plan showing the hard-to-drain and easy-to-drain areas 109
Figure 5.2: Generalised Permian stratigraphy for the southern Sydney Basin (after Faiz *et al.*, 2007) 110
Figure 5.3: Map showing major geological structures and regions of igneous intrusions in the Illawarra Coal Measures (after Faiz *et al.*, 2007) 111
Figure 5.4: Typical hard-to-drain area with fault structure and mylonite presence 112
Figure 5.5: Picture of the lump coal sample showing the cleat systems relative to the coal bedding direction 114
Figure 5.6: Picture of the lump coal sample showing the face cleat and butt cleat from roof side of the lump coal sample 114
Figure 5.7: Mine plan picture of typical hard-to-drain area showing the drainage borehole layout 115
Figure 5.8: Field observation of gas drainage borehole location 116
Figure 5.9: Carbon dioxide concentrations and δ13C CO_2 (VPDB) values for coal seam gases from the southern Sydney Basin (after Faiz *et al.*, 2007) 117
Figure 5.10: Burial and thermal history reconstruction for the southern Sydney Basin based on data from Bootleg-8 well ('iso-VR' signifies lines of equal vitrinite reflectance) (ater Faiz *et al.*, 2007) 117
Figure 5.11: Bulli Seam outburst threshold limits (Typical hard-to-drain area) 118
Figure 5.12: Illustration showing coal matrix blocks and cleat system of a coal (after Black, 2012) 119
Figure 5.13: The diagram of SEM equipment 121
Figure 5.14: Pictures of sample piece in SEM test, (a) 11-12 c/t, MG 22 (perpendicular to bedding), (b) 11-12 c/t, MG 22 (parallel to bedding), (c) 9-10 c/t, MG 22 (perpendicular to bedding), (d) 9-10 c/t, MG 22 (parallel to bedding), (e) GME 2193 (perpendicular to bedding), (f) GME 2193 (parallel to bedding), (g) GME 2237 (perpendicular to bedding), (h) GME 2237 (parallel to bedding) 122
Figure 5.15: SEM image showing the coal face and butt cleat system (from 11-12 c/t, MG 22, perpendicular to bedding) 123
Figure 5.16: SEM images showing the coal face cleat, (a) open face cleat, (b) close face cleat (from 11-12 c/t, MG 22, perpendicular to bedding) 123
Figure 5.17:SEM images showing the coal solid surface(from 11-12 c/t, MG 22, perpendicular to bedding) 124
Figure 5.18: SEM images showing the coal solid surface (from 11-12 c/t, MG 22, parallel to bedding) 124
Figure 5.19: SEM images showing the solid surface (from 9-10 c/t, MG 22, parallel to bedding) 124
Figure 5.20: SEM images showing the coal porous structure (from 11-12 c/t, MG 22, parallel to bedding) 125
Figure 5.21: SEM images showing the intrusion filling the coal cleat (11-12 c/t, MG 22, parallel to bedding) 126
Figure 5.22: SEM images showing porous structure (from GME2193, perpendicular to bedding) 126
Figure 5.23: SEM images showing porous structure (from GME2193, parallel to bedding) 127
Figure 5.24: SEM images showing porous structure (from GME2237, perpendicular to bedding) 128
Figure 5.25: SEM images showing solid surface (from GME2237, parallel to bedding) 128
Figure 5.26: SEM images showing coal fracture, (a) from GME2193, parallel to bedding, (b) from GME2193, perpendicular to bedding 128

Figure 5.27: SEM images showing coal porous structure, (a) with SE mode, (b) with BSE mode (from GME 2193, parallel to bedding) 129
Figure 5.28: Element mapping images, (a) element C mapping, (b) element O mapping, (c) element Al mapping, (d) element Si mapping 130
Figure 6.1: Multi Function Outburst Research Rig (MFORR) 135
Figure 6.2: Coal samples for permeability test with MFORR 136
Figure 6.3: Coal permeability test result with MFORR 137
Figure 6.4: Coal strain behaviour in the permeability test with MFORR (ppm refers to part per million, dimensionless unit) 138
Figure 6.5: Triaxial Compression Apparatus 139
Figure 6.6: Coal samples for triaxial permeability test with Triaxial Compression Apparatus 140
Figure 6.7: Coal triaxial permeability test with a certain vertical stress 141
Figure 6.8: Coal triaxial permeability test with a certain horizontal stress 142
Figure 6.9: MFORR permeability and triaxial permeability test results comparison 143
Figure 6.10: Classification of coal-beds based on their permeability (after Santillan, 2004 and Sereshki, 2005) 144
Figure 6.11: Permeability bands for CBM well completions (after Palmer, 2010) 144
Figure 6.12: Permeability and gas content relationship with depth (after Thomson and MacDonald, 2003) 145
Figure 6.13: Relationship between Langmuir Volume representing coal sorption capacity and ash content (after Laxminarayana and Crosdale, 1999) 146
Figure 6.14: Coal adsorption isotherms at 25 °C (pictures a, b, c are from typical hard-to-drain area) 147
Figure 6.15: Coal adsorption isotherms at 25 °C (pictures a, b and c are from easy-to-drain area A, pictures d, e, f, g and h are from easy-to-drain area B) 148
Figure 6.16: Coal adsorption isotherm comparisons at 25 °C (picture a is for CO_2 adsorption isotherm, picture b is for CH_4 adsorption isotherm) 149
Figure 6.17: Critical desorption point of a typical CO_2 and CH_4 rich Bulli seam coal sample. (after Black and Aziz, 2010) 149
Figure 6.18: Desorbed gas volume measurement apparatus (after AS3980:1999) 153
Figure 6.19: Bulli Seam outburst threshold limits (whole data base) 154
Figure 6.20: Distribution of Q_1 gas content and Q_1:Q_M ratio relative to Q_M (whole data base) 155
Figure 6.21: Distribution of Q_1 gas content and Q_1:Q_M ratio relative to gas composition (whole data base) 156
Figure 6.22: Distribution of Q_2 gas content and Q_2:Q_M ratio relative to Q_M (whole data base) 156
Figure 6.23: Distribution of Q_2 gas content and Q_2:Q_M ratio relative to gas composition (whole data base) 157
Figure 6.24: Distribution of Q_3 gas content and Q_3:Q_M ratio relative to Q_M (whole data base) 158
Figure 6.25: Distribution of Q_3 gas content and Q_3:Q_M ratio relative to gas composition (whole data base) 158
Figure 6.26: Gas content component relative to Q_M (whole data base, linear relationship) 159
Figure 6.27: Gas content component relative to Q_M (whole data base, power relationship) 160
Figure 6.28: Bulli Seam outburst threshold limits (Typical hard-to-drain area) 161
Figure 6.29: Distribution of Q_1 gas content and Q_1:Q_M ratio relative to Q_M (Typical hard-to-drain area) 161

Figure 6.30: Distribution of Q_1 gas content and Q_1:Q_M ratio relative to gas composition (Typical hard-to-drain area) 162
Figure 6.31: Distribution of Q_2 gas content and Q_2:Q_M ratio relative to Q_M (Typical hard-to-drain area) 162
Figure 6.32: Distribution of Q_2 gas content and Q_2:Q_M ratio relative to gas composition (Typical hard-to-drain area) 163
Figure 6.33: Distribution of Q_3 gas content and Q_3:Q_M ratio relative to Q_M (Typical hard-to-drain area) 163
Figure 6.34: Distribution of Q_3 gas content and Q_3:Q_M ratio relative to gas composition (Typical hard-to-drain area) 164
Figure 6.35: Gas content component relative to Q_M (typical hard-to-drain area, linear relationship) 164
Figure 6.36: Gas content component relative to Q_M (typical hard-to-drain area, power relationship) 165
Figure 6.37: Comparative analysis of gas content component Q_1 and Q_1:Q_M ratio 167
Figure 6.38: Comparative analysis of gas content component Q_2 and Q_2:Q_M ratio 167
Figure 6.39: Comparative analysis of gas content component Q_3 and Q_3:Q_M ratio 168
Figure 6.40: Comparative analysis of gas content component Q_M 169
Figure 7.1: Summary of investigation of hard-to-drain 175
Figure 7.2: A combination set up of MFORR and GC 177
Figure 7.3: A combination set up of MFORR and GC (modified after Florentin *et al.*, 2010) 178
Figure 7.4: Coal samples for N_2 flushing test 178
Figure 7.5: Coal strain gauges behaviour during coal sorption 179
Figure 7.6: Gas composition during N_2 injection 181
Figure 7.7: Gas volume during N_2 injection 181
Figure 7.8: Coal strain gauges behaviour during N_2 injection 182
Figure 7.9: Gas pressure drop during desorption 183
Figure 7.10: Gas composition during desorption 183
Figure 7.11: Gas volume during coal desorption 184
Figure 7.12: Coal strain gauges behaviour during desorption 184
Figure 7.13: Coal strain gauges behaviour during coal sorption 185
Figure 7.14: Gas composition during N_2 injection 186
Figure 7.15: Gas volume during N_2 injection 187
Figure 7.16: Coal strain gauges behaviour during N_2 injection 187
Figure 7.17: Gas pressure drop during desorption 188
Figure 7.18: Gas composition during desorption 189
Figure 7.19: Gas volume during coal desorption 189
Figure 7.20: Coal strain gauges behaviour during desorption 190
Figure 7.21: Comparison of strain change in Stage 1 191
Figure 7.22: Comparison of strain change in Stage 2 192
Figure 7.23: Comparison of collected gas volume in Stage 2 193
Figure 7.24: Comparison of gas content in coal in Stage 2 194
Figure 7.25: Comparison of strain change in Stage 3 195
Figure 7.26: Comparison of collected gas volume in Stage 3 195
Figure 7.27: Comparison of gas content in coal in Stage 3 196

LIST OF TABLES

Table 1.1: Research activities and timetable 7
Table 4.1: Coal density and proximate analysis (after Saghafi and Roberts, 2008) 79
Table 4.2: Coal Petrography (after Saghafi and Roberts, 2008) 79
Table 4.3: Moisture content of coal samples at different particle size 81
Table 4.4: Sorption experiments performed by various authors (h.v.b, m.v.b. and l.v.b are high, medium and low volatile bituminous coals.) (after Busch and Gensterblum, 2011) 83
Table 5.1: JSM-6490 LV Key Product Features (after JEOL, 2012) 121
Table 5.2: Top 4 elements percentage in the mapping area 130
Table 6.1: Langmuir parameters for the tested samples in terms of CO_2 and CH_4 (hard-to-drain area) 150
Table 6.2: Langmuir parameters for the tested samples in terms of CO_2 and CH_4 (easy-to-drain area) 150
Table 6.3: Average gas analysis data summary 166
Table 7.1: The comparative result between hard-to-drain and easy-to-drain area 174
Table 7.2: The important stages of flushing CO_2 test 190
Table 7.3: The important stages of flushing CH_4 test 191

LIST OF SYMBOLS AND ABBREVIATIONS

A	cross section area
Å	Angstrom (1 x 10^{-10} metres)
AS	Australia Standard
BSE	back-scattered electron
Bt	billion tonne
c	gas composition
CBM	coalbed methane
cc/g	cubic centimetres per gram
c_f	free gas content
CSG	coal seam gas
c/t	cut through
cm	centimetre (1x10^{-2} metres)
d	density
daf	dry ash free
DDM	directional drill monitor
D_e	the effective diffusion coefficient
DGS	drill guidance system
ECBM	enhanced coalbed methane
EOS	equation of state
g	gram
GC	gas chromatograph
GHG	greenhouse gas
g/cm^3	gram per cubic centimetre
h	height of the sample
H	hour
Hz	hertz
J/m^2	joule per square metre
K	permeability of coal
kg	kilogram
kN	kilonewton
kPa	kilopascal
kV	kilovolts
L	litre
LV	low vacuum
L/min	litres per minute
MECCA	modular electrically-connected cable assembly
MG	main gate
m	metre
M	mass
mD	milli darcy
MFORR	multi function outburst research rig

min	minute
mm	millimetre ($1x10^{-3}$ metres)
MPa	megapascal
Mt	million tonne
m^2/g	square metres per gram
m^3/min	cubic metre per minute
m^3/t	cubic metre per tonne
n	amount of substance
n_a	adsorbed gas content
nm	nanometre ($1x10^{-9}$ metres)
NTP	normal temperature and pressure (20 ℃ and 101.325 kPa)
N_2-ECBM	N_2 injection to coalbed methane
P	absolute gas pressure
Pa	pascal
P_{atm}	atmospheric pressure (101.325 kPa)
P_c	critical temperature
P_L	Langmuir pressure
ppm	part per million
Q	flow rate of gas
Q_M	total measured gas content; sum of Q_1, Q_2 and Q_3 (m^3/t)
Q_1	gas lost during coal core sample recovery (m^3/t)
Q_2	gas released from coal core sample during desorption testing (m^3/t)
Q_3	gas released from coal sample after crushing (m^3/t)
r	radius
R	the universal constant
S	specific surface area
SCA	soundless cracking agent
SE	secondary electron
SEM	scanning electron microscopy
SRK	Soave-Redlich-Kwong equation
T	temperature
TLV	threshold limit value
μ	viscosity of gas
μg	microgram ($1x10^{-6}$ gram)
μm	micrometre, or micron ($1x10^{-6}$ metres)
v	gas volume
V	cell or bomb volume
v_f	flow velocity
V_L	Langmuir volume
VR	vitrinite reflectance
VPDB	IAEA international standard defining Vienna Peedee Belemnite
V_0	molar volume of gas
x	space dimension

Z	compressibility factor
Ɛ	porosity
λ	gas permeability coefficient
$\boldsymbol{\gamma}$	surface tension
Γ	surface excess
ψ_d	gas diffusive flux
$\delta^{13}C$	isotope carbon-13
℃	degree centigrade
%	one in a hundred
‰	one in a thousand

CHAPTER ONE – GENERAL INTRODUCTION

1.1 INTRODUCTION

Australia has the fourth largest reserves of coal in the world with 76.4 Billion Tonnes (Bt) proved coal resources, including 37.1 Bt anthracite and bituminous coals and 39.3 Bt sub-bituminous and lignite coals (SRWE, 2012). The total coal production in Australia is 415.5 Million Tonnes (Mt) in 2011, making Australia the fourth largest coal producing country behind China, the United States of America and India with Australia remaining the world's largest coal exporter (SRWE, 2012). Australia has significant black coal resources (anthracite, bituminous and sub-bituminous coals) and about 325 Mt of saleable black coal produced each year, some 80 Mt is consumed locally and the rest is exported. Most of the domestic coal utilisation is for electricity production, whereby black coal accounts for more than 55% of the total power generation (Saghafi, 2010).

The majority of Australia's economic black coal resources exist in Queensland and New South Wales, which jointly produced 98 % of Australian black coal. The majority of Australia's metallurgical (coking) coal is produced in Queensland, while New South Wales produces predominantly thermal (steaming) coal. In addition, brown coal is mined in Victoria and South Australia, where it is used for domestic electricity generation (Black, 2012). Figure 1.1 shows the location of Australian black coal resources and two major coal basins in Australia; Bowen Basin in Queensland and Sydney Basin in New South Wales.

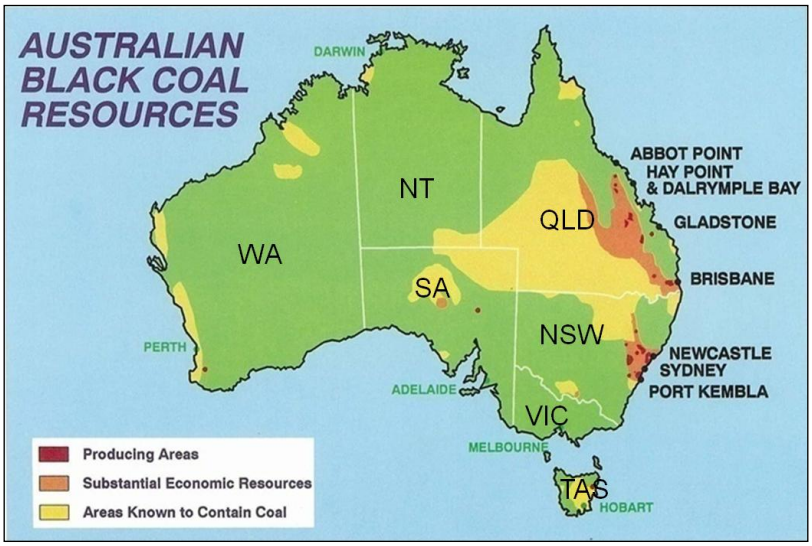

Figure 1.1: Location of Australian black coal resources

In addition to coal, Coalbed Methane (CBM) has also become a resource of global significance. Beside USA, countries such as Canada, Australia, China and India have active CBM activities (Faiz *et al.*, 2007; Kinnon *et al.*, 2010; Sang *et al.*, 2010; Liu *et al.*, 2011). CBM is a rapidly growing industry in Australia and becoming an important energy source along the eastern seaboard both in Queensland (Kinnon *et al.*, 2010) and NSW (Faiz *et al.*, 2007). Faiz *et al.* (2007) stated that bituminous coals of the Sydney Basin contain a large resource of methane, which is located in proximity to the largest gas market in Australia. The economic production of CH_4 from Sydney Basin coals is a challenge because of low permeability, high stress and variable gas saturation levels. Therefore, a thorough understanding of the factors that affect variations in these properties is critical for efficient commercial methane production.

Reliance on fossil fuel has put Australia amongst the world's top greenhouse gas (GHG) emitters and in recent years Australia has become one of the world's largest commercial producers of Coal Seam Gas (CSG) and the production is predicted to increase in the coming years (Saghafi, 2010). Consequently, the industry is seeking reliable short to medium term options to reduce CO_2 emissions. One such option is the capture of CO_2 and its geo-sequestration in coal seams (Liu *et al.*, 2010; Massarotto *et al.*, 2010; Pone *et al.*, 2010; Saghafi, 2010; Wong *et al.*, 2010). CO_2 is mostly stored in coal seams as sorbed gas attached to the coal surface with only a small amount as free gas within pore spaces or dissolved in pore space liquids (Liu *et al.*, 2010). Sorption induces the density of CO_2 increasing in the sorbed phase and hence, provides high CO_2 storage capacity even at quite low-pressure. As the sorbed gas is bound to the coal, the potential risk of gas leakage is reduced. A recent CO_2 natural analogue study of the Sydney Basin sheds light on some of the specifics of the coalfields in this basin with respect to the CO_2 storage (Faiz *et al.*, 2007 and Saghafi, 2010).

With the growing interest in enhanced CBM recovery (ECBM), the utilisation of CO_2 and N_2 injection has been found to help CBM recovery (Reeves *et al.*, 2002; Reeves and Oudinot, 2005; Massarotto *et al.*, 2010; Kiyama *et al.*, 2011). Specifically, the use of N_2 injection has been found to help incremental methane recovery of approximately 10-20 % of the original gas in place, and the future use of N_2 injection has been predicted to add an additional 25-40 % to the total gas recovery (Reeves and Oudinot, 2005). Also, Reeves and Oudinot (2005) stated that future N_2 injection at Tiffany is forecasted to be economic. In concept, the process of coal seam gas enhancing is simple, during which N_2 is injected into a coal reservoir, it

displaces the gaseous CBM from the cleat system, decreasing the CBM partial pressure and creating a compositional disequilibrium between the gaseous and adsorbed phases. These combined influences cause the CO_2 or CH_4 to desorb and diffuse into the cleat system. The CBM then migrates to and is produced from production wells (Reeves and Oudinot, 2004).

Coal swells with gas adsorption, and shrinks with gas desorption and as coal permeability is highly sensitive to stress (Pan *et al.*, 2010). Kiyama *et al.* (2011) and Florentin *et al.* (2010) found that the coal permeability decreases after CO_2 injection and subsequent N_2 flooding tests following CO_2 injection showed slow strain recovery. For a successful sequestration of carbon dioxide in coal seams and subsequent ECBM, knowledge of coal seam gas flow mechanism, coal sorption characteristics, structural properties and their variation under replicated *in situ* stress conditions is required (Holloway, 1997; White *et al.*, 2005; Wang *et al.*, 2007; Pone *et al.*, 2010).

1.2 COAL SORPTION CHARACTERISTICS

Mining experience in Australia shows that CO_2 content can vary significantly within short distances in the same seam and within the same coal mine (Lama and Saghafi, 2002). Differences in the behaviour of CH_4 and CO_2 have been noted for more than a century from coal mining operations worldwide.

Gas outbursts can occur at lower gas contents for CO_2 than for CH_4, and the presence of high CO_2 content in coal seams has been the cause of numerous gas outbursts during underground coal mining (Saghafi *et al.*, 2007). During the last 50 years, many outbursts occurred in Australian mines. In some instances where the dominant gas is CO_2, outbursts happened more frequently. For instance, at Tahmoor, Metropolitan and West Cliff collieries in the Illawarra Coalfield in the southern part of the Sydney Basin, gas outbursts were caused mainly by CO_2. Due to the common occurrence of CO_2 in Australian coal seams and its implications for coal mining, the mechanism of CO_2 storage and flow in coal has been investigated during the last two decades (Lama and Bodziony, 1996).

Measurement of the amount of gas adsorbed per unit mass of coal with increasing pressure at a certain temperature produces an isotherm that describes the coal's gas storage capacity. Accurately tested and well interpreted coal sorption isotherms play an important role, not only in coal mine safety, but also in enhanced gas drainage for gas recovery applications, and it is commonly used in the areas of CBM reservoir resource assessment as well as the CO_2

sequestration in coal seams which has also been identified as an attractive option that may aid in mitigating emissions for greenhouse gas (GHG). The undersaturation of the coal seams seems to be a common aspect. As the adsorption data show higher storage capacity for CO_2 than for CH_4, therefore, the phenomenon of undersaturation is more pronounced in CO_2 rich coal seams than CH_4 rich coal seams, particularly for the Bulli seam of Sydney Basin, Australia.

1.3 GAS DRAINAGE IN HARD-TO-DRAIN SEAMS

Coal seams in Australia often contain large volumes of gas and in many cases mixed gas conditions prevail where CSG consists of a mixture of CO_2 and CH_4. The productivity of underground mines, regardless of the mining method, is significantly impacted by the prevailing geological conditions, such as faults and dykes, the presence of coal seam gas, and the relative ease with which these gases can be drained. It is estimated that 40 % of Australian longwall mines require regular gas drainage to manage coal seam gas emissions (Black, 2012).

While in most coalfields of the world CH_4 is the dominant gas, in Australian coalfields either of the two gases can be the dominant gas (Saghafi, 2010). Actually in the Bulli seam of the Sydney Basin the main seam gas is CO_2 rather than CH_4 in some parts of the longwall blocks. A mixture of CH_4 and CO_2 gas with a high concentration of CO_2 has been found in a number of locations in Tahmoor, Metropolitan, Appin and West Cliff mines. In Metropolitan Colliery, in some areas, the mine site has experienced difficulty in reducing gas content within the available drainage lead time, as the coal seam would not drain even with additional drainage boreholes. These areas are identified as hard-to-drain areas.

In this study, both laboratory tests and field study were conducted to understand coal sorption and transport characteristics and the hard-to-drain problem in Bulli seam, particularly focusing on Metropolitan Colliery. The aim of these studies was to add new knowledge to the CO_2 geo-sequestration and CBM industries, to improve the understanding of gas drainability and help drain gas efficiently and reduce the risk of outburst and gas explosion, and generally improve gas exploration and hence ensure coal mine safety.

1.4 STATEMENT OF THE PROBLEM

For a long time, because of inadequate knowledge about sorption characteristics of coal in different gases under varying conditions, engineers were unable to accurately determine the gas content of coal and avoid gas related accidents in coal mines. Especially with the continued increase of coal production, mine operators need to face the reality of underground mining in various conditions with high risk of gas explosion and outbursts. Thus a better understanding of the coal-gas interaction mechanism, accurately identifying the sorption characteristics of coal in a changing geological condition becomes crucially important.

Many Australian underground coal mines are mining in areas that require the use of gas drainage to reduce coal seam gas content to below a prescribed Threshold Limit Value (TLV). In a number of cases, these mines encounter areas where the gas is hard to drain from the coal, ahead of mining. Factors contributing to poor drainage may include high coal rank and *in situ* conditions resulting in high sorption capacity, low gas content, high CO_2 gas composition and high *in situ* gas pressure causing low coal saturation as well as coal microstructure and permeability affecting gas transport. In various parts of the Bulli seam of the Sydney Basin, the main seam gas is CO_2 rather than CH_4, thus high CO_2 and mixed gas CH_4 and CO_2 have been found in a number of locations in Tahmoor, Metropolitan, Appin and West Cliff mines, where operators have to deal with the increasing problems of gas drainage. In particular the difficult-to-drain longwall panels of area 5 at West Cliff has been well documented (Black, 2012).

In the case of Metropolitan Colliery, the mine site has experienced difficulty in reducing gas content in the Bulli seam within the available drainage lead time, particularly in an area of MG 22, as the coal seam would not drain even with additional drainage boreholes. Research was therefore conducted to:

- Identify the main reasons contributing to “difficult-to-drain” areas between 8-11 c/t of MG 22;
- Establish the fingerprints of coals that are able to give early warning signs for future drainage process; and
- Develop a new method based on nitrogen flushing to help the drainage of coal in these areas.

1.5 OBJECTIVES OF RESEARCH

The objectives of this thesis are:

1. To review the gas storage and flow mechanism in coal, gas drainage and different coal isotherm testing approaches and provide the general principle of accurate testing methods as well as introduce a unique isotherm testing apparatus;
2. To investigate the influences of various factors such as temperature, moisture and coal particle size on the coal sorption characteristics of coal samples from hard-to-drain seams;
3. To identify coal microstructures, pore system and cleat systems of the hard-to-drain seams using SEM technology and element mapping method;
4. To conduct laboratory tests to determine the permeability of coal samples under triaxial stress conditions portraying the *in-situ* conditions at Metropolitan;
5. To identify and conclude the differences of gas content and gas composition between the whole gas database and typical hard-to-drain areas, as well as those differences between "Pass" and "Fail" drainage samples, by analysing the results tested from fast desorption methods for determining gas content.
6. To identify and summarise the main reasons for poor coal seam gas production in the typical hard-to-drain areas, such as geological variation, coal sorption capacity, coal microstructure, coal permeability and gas content and composition; and
7. To provide new knowledge for the development of an innovative technology based on nitrogen flushing to enhance coal seam gas recovery from hard-to-drain or tight seams hence help improve gas drainage in underground coal mines.

1.6 RESEARCH PROGRAMME

The research programme was conducted at different stages. Table 1.1 provides the research schedule and the main research activities at each stage.

Table 1.1: Research activities and timetable

TASK	2010		2011		2012	
	S_1	S_2	S_1	S_2	S_1	S_2
Literature review of coal seam gas generation and coal sorption characteristics.						
A survey of various gas sorption isotherm testing methods and calculations; and modification of existing equipment and calculation.						
Research into influence of temperature, moisture and coal particle size on coal sorption characteristics.						
Literature review study of gas drainage and of experimental tests of ash content, sorption capacity and permeability.						
Study of coal microstructures using SEM technology and analysis of gas content and composition of gas database.						
Laboratory testing of nitrogen gas injection to flush coal seam gas.						
Thesis preparation and submission of final thesis.						

S_1= 1st Academic Session, S_2= 2nd Academic Session

1.7 THESIS OUTLINE

This thesis is presented in eight chapters. A flowchart showing the chapters of the thesis is given in Figure 1.2.

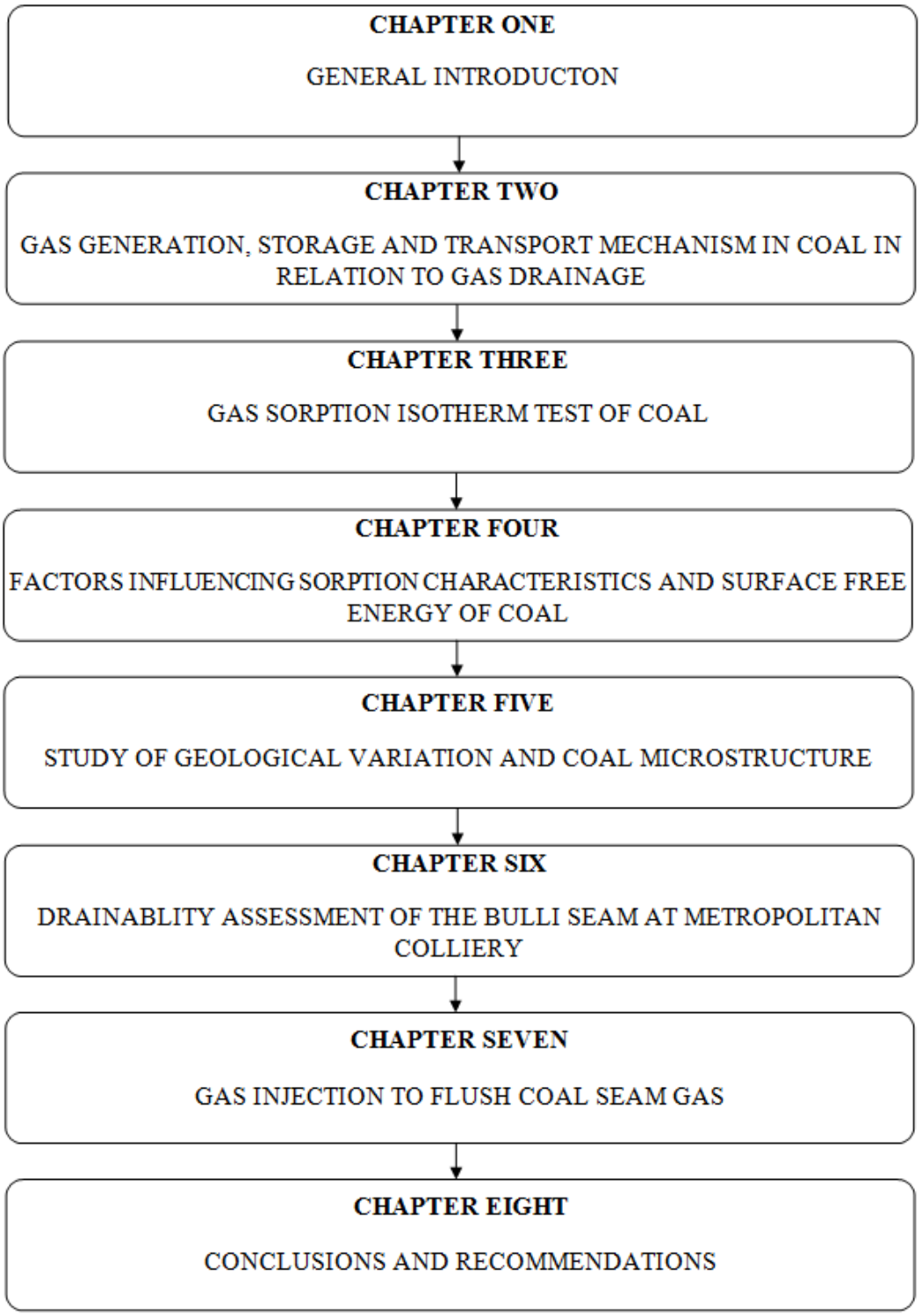

Figure 1.2: Main structure of the thesis

- Chapter 1 presents a general introduction of the research and objectives of the thesis work.
- Chapter 2 describes the mechanisms of the coal seam gas generation, gas storage and transport in coal and coal seam gas drainage and its enhancement technologies.
- Chapter 3 describes the gas sorption isotherm testing of coal, including factors impacting on gas sorption testing, isotherm testing apparatus and calculation methods worldwide and introduction of isotherm testing method in the University of Wollongong.
- Chapter 4 analyses the influences of temperature, moisture and coal particle size on coal sorption characteristics and introduces theory of coal surface free energy and explains this theory in terms of gas type, temperature and moisture influence.
- Chapter 5 presents the study of the hard-to-drain problem in Bulli seam at Metropolitan Colliery, including a study of geological variation investigation and coal microstructure SEM analysis of coal samples from both hard-to-drain and easy-to-drain areas.
- Chapter 6 presents the drainability assessment at Metropolitan Colliery, including the investigation of coal permeability of hard-to-drain areas and coal sorption capacity, gas content and composition of the coal seam. Coal permeability tests are conducted using the MFORR and the Triaxial Compression Apparatus. Gas content and gas composition investigation is carried out within the whole gas database (519 samples) and typical hard-to-drain areas (94 samples).
- Chapter 7 presents a summary of the investigation of hard-to-drain seam, and laboratory tests of N_2 injection to flush coal seam gas. The procedure and result of injection of N_2 to flush CO_2 and CH_4 are discussed and compared.
- Chapter 8 summarises the results and principal conclusions of the research work presented in the thesis and recommendations for future research.

CHAPTER TWO – GAS GENERATION, STORAGE AND FLOW MECHANISM IN COAL IN RELATION TO GAS DRAINAGE

2.1 INTRODUCTION

Both coal and CSG are important resources for the coal mining and CBM industries. Once the pressure on the coal reservoir decreases, the gas molecules start detaching themselves from the surface of the pores and microfractures and the process of desorption is initiated, making more gas available for flow towards the gas drainage well. Three distinct processes are involved in the transport of CSG; namely, desorption from the internal coal surfaces, then diffusion through the coal matrix and micropores towards the cleats/fractures, finally the Darcy flow in the natural fracture network.

In order to understand the coal and gas behaviour, this chapter reviews the coalification process, generation and the storage of CSG. The three processes of gas transport in a coal seam are introduced and the environmental factors impacting on gas diffusion and gas flow in cleats, such as coal moisture, temperature, gas type, coal particle size and confining stress are presented. Gas drainage technology is also reviewed in two sections in this chapter in terms of surface and underground gas drainage. Different technologies are introduced worldwide to enhance gas drainage from coal, generally including increasing the surface area, advanced drilling technology, stress relief gas drainage as well as drainage arrangement strategy according to different *in situ* conditions.

2.2 GAS GENERATION AND STORAGE

2.2.1 Coalification process

Coalification is the process of coal formation through the physical and chemical transformation of peat material. During coalification the peat material undergoes several changes resulting from bacterial decay and the effects of compaction, heat and time. With increasing pressure, heat and time the complex hydrocarbon compounds in peat material break down and change in a variety of ways. There are two main processes involved in coalification, diagenesis and metamorphism (UWYO, 2002). Figure 2.1 shows the processes and stages involved in the coalification process along with the products throughout

coalification. As the depth of burial of the peat material increases by basin subsidence, the peat enters the geochemical stage of coalification, known as metamorphism, where the material is subjected to rising temperature and pressure (UWYO, 2002). Many physical and chemical changes, governed by biological and geological factors, occur during these processes. Whereas darkening in colour and increase in hardness and compactness are the main physical changes, loss of moisture and volatile contents, and increase in carbon content are the main chemical changes (Singh and Singh, 1999).

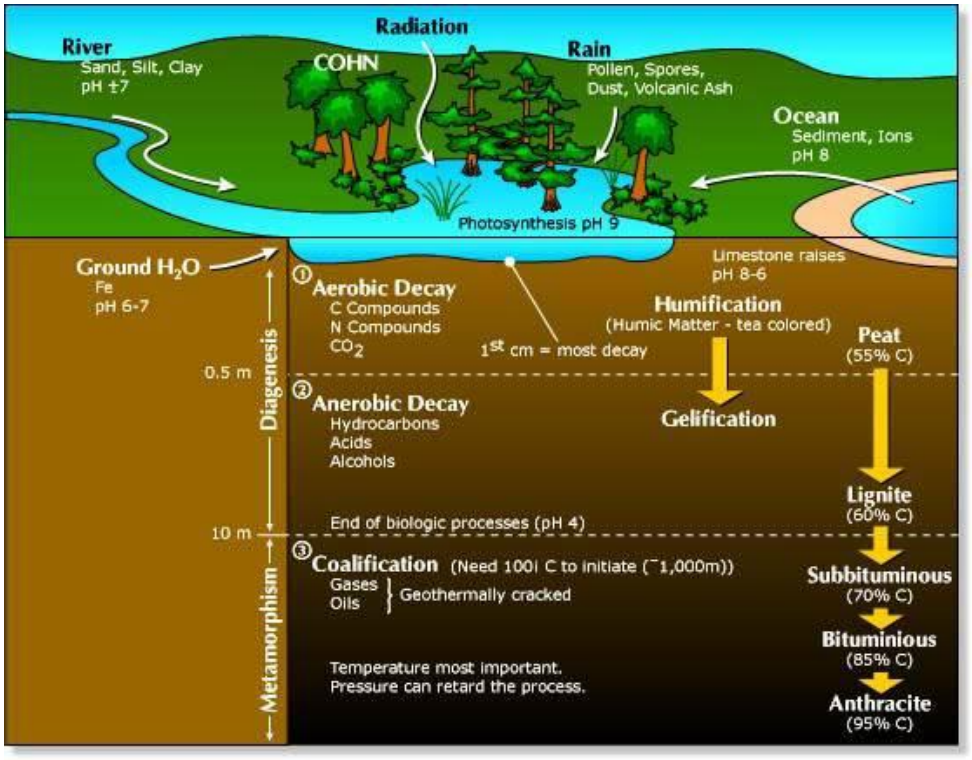

Figure 2.1: Details of the processes, stages and products of coalification (after UWYO, 2002)

The Sydney Basin, which is located in New South Wales (NSW) shown in Figure 2.2, contains four major coalfields: Hunter, Newcastle, Western and Southern Coalfields. Sydney Basin coals range in rank from high volatile bituminous to low volatile bituminous with mean maximum vitrinite reflectance values ranging from about 0.7 % to 1.9 % (Faiz *et al.*, 2007). All coals are Permian and their rank is generally medium to high volatile bituminous, except for the Southern Coalfield coals which are generally low to high volatile bituminous. Coal in the Southern Coalfields of Sydney Basin is >300 m deep and is mined underground whereas most coals in northern coalfields are extracted from open-cut operations. Open-cut mining produces half of the total coal production of NSW (Saghafi *et al.*, 2007).

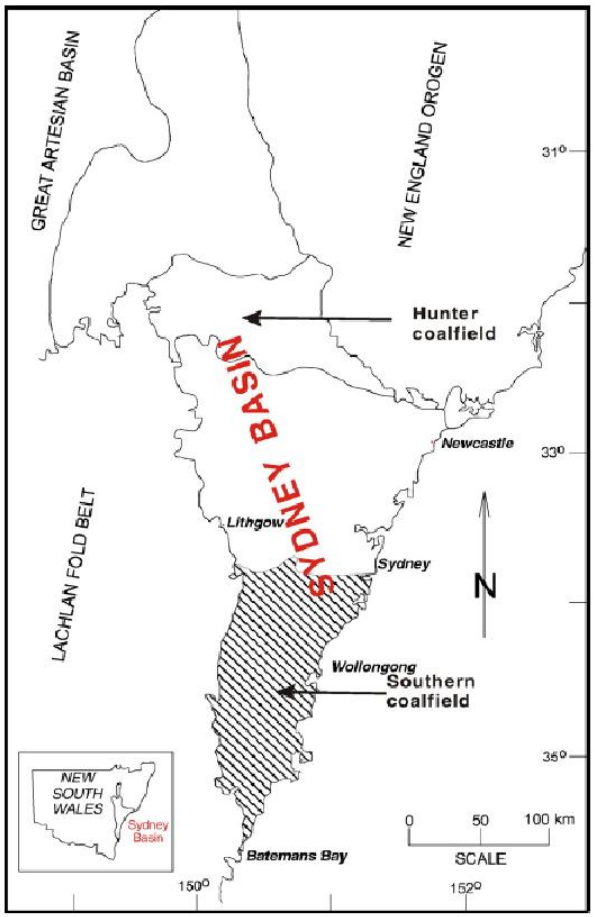

Figure 2.2: Location of the Southern and Hunter Coalfields, Sydney Basin, New South Wales, Australia (after Faiz *et al.*, 2007)

The Sydney Basin is a retro-arc, foreland basin with the sedimentary sequence deposited during the Late Carboniferous to Early Triassic on Devonian and Ordovician basement rocks. The majority of the coals targeted for CBM production were deposited in the Late Permian, primarily in fluvio-deltaic environments. The Sydney Basin sequence also contains numerous Permian to Tertiary igneous intrusions (Faiz *et al.*, 2007). Radiometric dating and other stratigraphic studies indicate that igneous activity occurred throughout the geological history of the basin, with peak activity at about 250, 180 and 50 million years ago (Facer and Carr, 1979 and Embleton *et al.*, 1985).

2.2.2 Generation of coal seam gas

CSG generation has been studied and discussed by different researchers (Faiz and Hutton, 1995; Clayton, 1998; Singh and Singh, 1999; Faiz *et al.*, 2007). It is generally believed that CSG generated at shallow depths (<10 m) and lower-rank stage (sub-bituminous) by the first process (active up to 50-80 ℃) is termed biogenic or diagenetic methane. Methane generated

during this process is about 10 % of the total methane generation of coalification (Singh and Singh, 1999). Though most of the gas generated during early stages of coalification generally escapes into the atmosphere, some can accumulate under certain specific geologic conditions like rapid subsidence, and thus may get trapped in shallow reservoirs. Gas produced at greater depths and higher rank stages of the second process, the thermogenic methane, constitutes the large proportion of the coalbed methane. The gas generation in this process, begins with peak rank near the boundary between the medium-volatile and low-volatile bituminous coal stages, temperature 100-150 ℃, and declines further with the rise in temperature and reflectance values. It could reasonably be presumed that the generation of CSG is more in the regions of high palaeogeothermal gradient as well as in the vicinity of intrusion bodies (Singh and Singh, 1999).

Thus, the generation of CSG during coalification occurs in two ways (Singh and Singh, 1999):

- Metabolic activity of biological agencies (biological process), and
- Thermal cracking of hydrogen-rich substances (thermogenic process).

In comparison, gas in Sydney Basin coals has been derived from multiple sources, including (Faiz *et al.*, 2007):

- Thermogenic CH_4 and higher hydrocarbons formed during deep burial during the Jurassic and Early Cretaceous,
- Secondary biogenic CH_4 formed since Late Cretaceous uplift, and
- CO_2 derived mostly from intermittent igneous activity between the Permian and Tertiary.

CSG generally comprises CH_4 with subordinate amounts of CO_2, C_2H_6, higher hydrocarbons (C_{2+}) and N_2. However, in some parts of the Sydney Basin, the coals contain over 90% CO_2 and up to 12% C_2H_6 (Faiz *et al.*, 2007).

Clayton (1998) reviewed the geochemistry of seam gas and listed four sources for CO_2 gas in coal seams: a) decarboxylation reactions of kerogen and soluble organic matter during burial heating of the coal, b) mineral reactions such as thermal decomposition or dissolution of carbonates or other metamorphic reactions, c) bacterial oxidation of organic matter and d) magmatic intrusion.

Faiz and Hutton (1995) reported variable amounts of CO_2 and CH_4 occur within the Illawarra Coal Measures. It is believed that the CH_4 and other hydrocarbons present within the Southern Coalfield were formed as a by-product of coalification and most of the CO_2 was introduced during periodic igneous activity. The variations of CO_2 and CH_4 are mainly related to the geological structure and depth. The variations in gas composition have no clear relationship with coal composition or rank but show well-defined relationships with stratigraphy and geological structure. High proportions of CH_4 occur in synclinal structures whereas the CO_2 content increases towards structural highs. Extensive areas of pure CO_2 gas occur on anticlines and domes. In structural lows, local pockets of high CO_2 concentrations are found near some dykes and related faults. Increasing concentrations of CO_2 also occur in the stratigraphically higher levels. Migration of gases mainly occurred upwards in aqueous solution, down the pressure gradient. During the upward migration of gas-saturated solutions, gas was continually released from the solution due to decreasing pressure. Due to the lower solubility of CH_4 relative to CO_2, CH_4 was desorbed within the deeper strata whereas increasing amounts of CO_2 were desorbed within the shallower strata. Therefore, in most parts of the Southern Coalfield, increasing amounts of CO_2 gas occur at shallower depths.

2.2.3 Storage of coal seam gas

Although coal is a reservoir rock for gas, it differs markedly from conventional petroleum reservoirs in that the volume of gas, which it can store, exceeds its open pore volume by an order of magnitude. The volume of pores in coal is small and the majority of gas in coal consists of adsorbed gas which covers the surfaces of micropores (Saghafi *et al.*, 2007). Murry (1991) demonstrated that gases could be retained in a coalbed in four different ways: (a) adsorbed molecules within micropores (<2 nm in diameter); (b) trapped gas within matrix porosity; (c) free gas and (d) as dissolved gas in ground water within a coal fracture.

In the study of Yi *et al.* (2009), a bidisperse coal structure viewed as a microporous matrix, which contains pores on the order of a few molecular diameters, penetrated throughout by interconnected macropores was used to describe the gas storage situation with coal (Figure 2.3). It was conceptualized that the microporous matrix retains the bulk of the gas, while the macropores have relatively negligible gas sorption capacity compared to micropores. In addition, since the matrix exhibits a large internal surface area for gas sorption and a relatively strong affinity for gas, it is expected that an additional diffusive mass transport in the adsorbed phase develops in the direction of free gas mass fluxes. Thus, it is assumed that

gas sorption rates and flow in and out of coal are controlled by combined pore and surface diffusive mass fluxes.

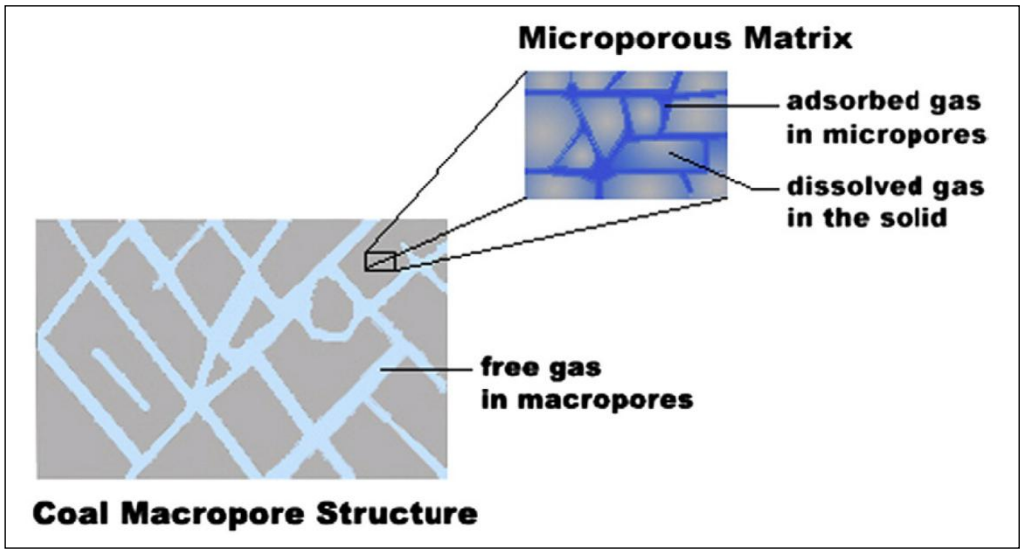

Figure 2.3: Schematic of bidisperse coal pore structure showing macro- and micropores containing gas in free, adsorbed and dissolved states (after Yi *et al.*, 2009)

Coal micropore surface area can reach several hundreds of square metres per gram, making large areas available for gas adsorption. For instance, Griffith and Hirst (1944) measured pore surface area using the heat of wetting of coal in methanol, showing that the surface area of coal is in the order of 20 to 200 m^2/g. As mentioned above, the surface areas of pore systems in coal greatly exceed the pore volume; therefore, most gas is stored in an adsorbed phase.

In situ coal contains gas both on micropore surfaces, in an adsorbed phase, and as a free phase compressed within macropores. Adsorbed gas content of coal can be directly measured from drill cores using standard techniques (AS3980:1999). As shown by Saghafi *et al.* (2007), free gas content can be expressed as:

$$c_f = \frac{\varepsilon P}{d P_{atm}} \qquad (2\text{-}1)$$

Where c_f is the free gas content of coal expressed in terms of volume of gas per unit mass of coal; P, ε and d are gas pressure, porosity and density of the coal, respectively and P_{atm} is atmosphere pressure.

The relationship between free gas and adsorbed gas is a dynamic system, in which gas content is not fixed but changes when equilibrium conditions within the reservoir are

disrupted and is strongly dependent upon multiple hydrogeologic factors and reservoir conditions (Scott, 2002). In the case of Sydney Basin coals, although a large amount of methane and other hydrocarbon gases would have been generated at maximum burial during the Early Cretaceous, a large proportion of the gas might not have been sorbed within the coal due to limited gas sorption capacities and enhanced diffusivity at high temperatures. Upon uplift, gas that migrated from deeper in the sequence or from shallower biological activity may have been sorbed into the coals (Faiz *et al.*, 2007).

2.3 PHYSICAL STRUCTURE OF COAL

Fractures occur in nearly all coalbeds, and exert fundamental control on coal stability, minability, and fluid flow. It is therefore not surprising that coal fractures have been investigated since the early days of coal mining, and that published descriptions and speculation on fracture origins date from early in the nineteenth century, cited by Kendall and Briggs (1933).

Coal seams are characterised by a natural fracture network commonly referred to as cleat. Cleats are fractures that usually occur in two sets, which are, in most instances, mutually perpendicular to each other and to the bedding, as shown in Figure 2.4. Through-going cleats formed first and are referred to as face cleats; cleats that end at intersections with through-going cleats formed later are called butt cleats (Laubach *et al.*, 1998; Solano-Acosta *et al.*, 2007).

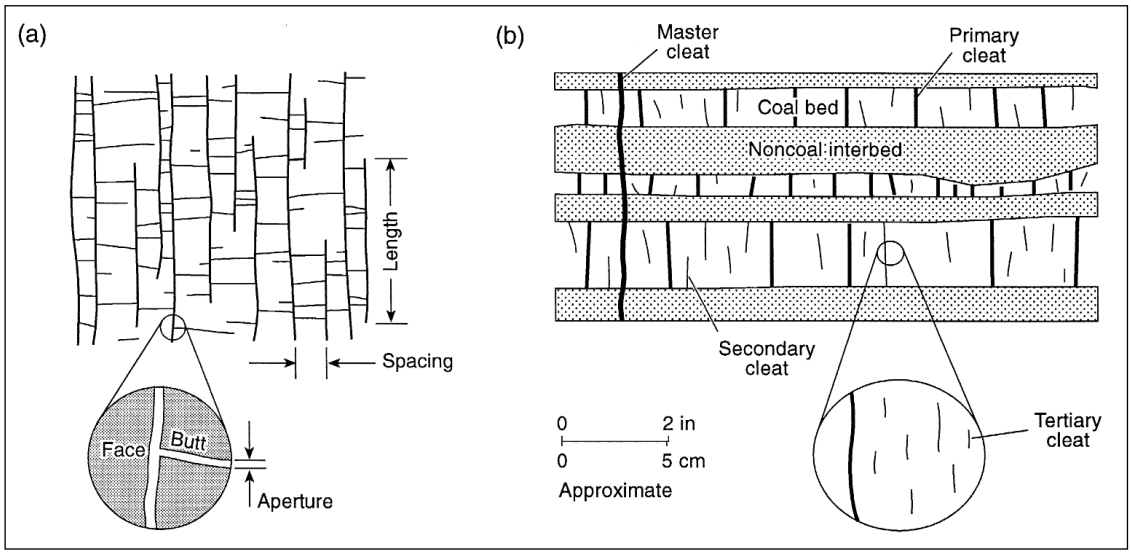

Figure 2.4: Schematic illustration of coal cleat geometries. (a) Cleat-trace patterns in plan view. (b). Cleat hierarchies in cross-section view. (after Laubach *et al.*, 1998)

Cleat space accounts for less than 2 % of the seam bulk volume (Gregory *et al.*, 1986) and the porosity of the micropores accounts for as much as 85 % of coal's total effective porosity. The pore diameter of micropores is typically less than 10 Angstrom (Å), which makes the coal matrix have a large internal surface area.

Except fractures and cleats, coal is a porous material, which is classified on the basis of pore width. Van Krevelen (1993) defines the matrix pore system as follows:

- Macropores: The pore size is larger than the mean free path of the molecules.
- Mesopores: The pore size is smaller than the mean free path of the molecules.
- Micropores (<2 nm): Activated diffusion.

As noted by Busch and Gensterblum (2011), the mean free path length depends on temperature and pressure, so this classification cannot be applied to specific pore radius. This classification is further specified and classified by the International Union of Pure and Applied Chemistry (IUPAC, 2001):

- Macropores: pores with widths exceeding about 0.05 μm (50 nm)
- Micropores: pores with widths not exceeding about 2.0 nm (20 Å)
- Mesopores: pores of intermediate size (2.0 nm<width<50 nm)

2.4 GAS TRANSPORT IN COAL

As pointed out by other researchers (Harpalani and Schraufnagel, 1990; Gamson and Beamish, 1992; Sereshki, 2005), once the pressure in the coalbed is reduced, coal becomes less capable of retaining coal seam gas molecules in adsorbed form. The gas molecules start detaching themselves from the surface of the pores and microfractures and the process of desorption initiated, making more gas available for flow towards the gas drainage well. The rate of flow is primarily dependent on the diffusion characteristics and the permeability of coal. Figure 2.5 shows the three distinct processes involved in the transport of CSG, starting with desorption from the internal coal surfaces, then diffusion through the matrix and

micropores towards the cleats/fractures, finally the Darcy flow of gas in the natural fracture network.

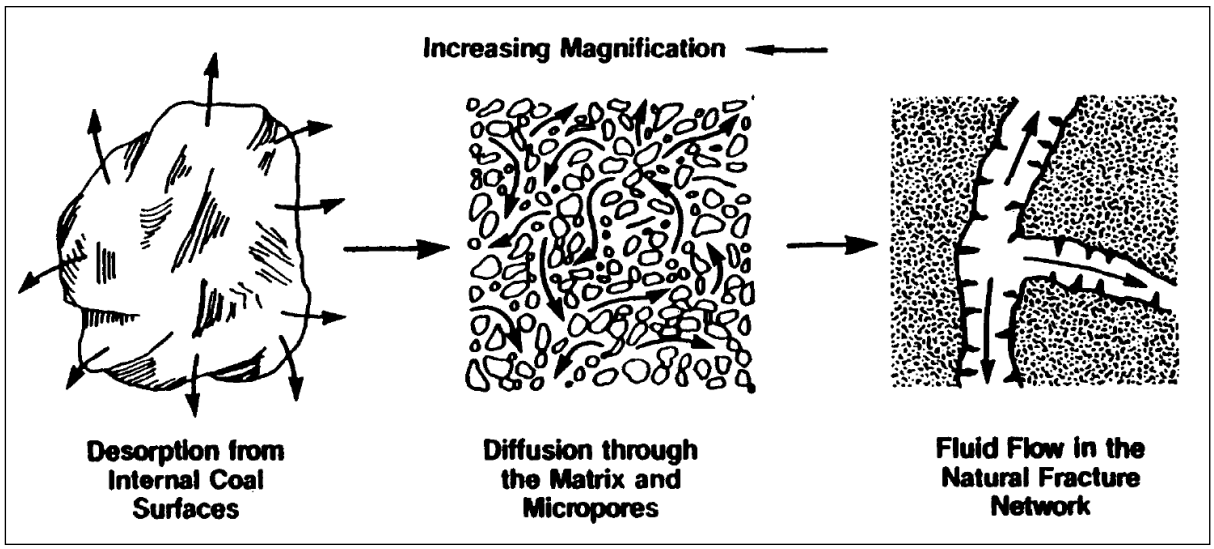

Figure 2.5: Transport of coal seam gas in coal. (after Harpalani and Schraufnagel, 1990)

2.4.1 Gas adsorption and desorption from coal surface

Desorption is the process by which methane molecules detach from the micropore surfaces of the coal matrix and enter the cleat system where they exist as free gas. The desorption isotherm defines the relationship between the adsorbed gas concentration in the coal matrix and the free gas pressure in the cleat system.

Crosdale *et al.* (1998) stated, since methane is physically adsorbed on coal, the time required for desorption is negligible compared to the diffusion step. According to the study of Gamson *et al.* (1993), gas migration is governed by two main factors. First, the diffusion distance depends upon the fracture spacing, which delineates the matrix block size of the coal. Second, gas flow volume through the fractures depends on fracture width, length, continuity and permeability. This model of gas transport through coal may best apply to predominantly vitrinite-rich coals in which fracture systems are open and unmineralised. However, complexities may arise due to secondary mineralisation inhibiting gas flow and the presence of other macropore systems, especially phyteral porosity predominant in some inertinites, enhancing gas flow.

The desorption isotherm is the link between the flow in the matrix system, where flow is controlled by concentration gradients, and flow in the cleat system, where flow is controlled

by pressure gradients. The relationship between gas concentration and pressure is a non-linear function that is generally defined by Langmuir's equation (Appendix A).

$$n_a = \frac{V_L P}{P + P_L} \tag{2-2}$$

Where n_a is adsorbed gas content (gas volume per unit mass of coal), P is gas pressure, and V_L and P_L are experimental coefficients. The coefficient V_L represents the maximum gas storage capacity of the coal and is termed the 'Langmuir volume'. The coefficient P_L is the 'Langmuir pressure' and represents the gas pressure at which coal adsorbs a volume of gas equal to half of its maximum capacity. Saghafi *et al.* (2007) pointed out that at low pressures the Langmuir equation reduces to a linear equation of pressure (Henry's Law) with a linearity coefficient of V_L/P_L. As the Langmuir equation is based on a mono-layer adsorption mechanism, it is applicable for low pressures (<6 MPa for CO_2) and for gases where the molecule sizes and coal pore diameter are of the same order of magnitude. Currently in Australia, the Langmuir equation is the most commonly employed mathematical expression used in industry to describe adsorption of gas onto coal (Crosdale *et al.*, 2005).

2.4.2 Gas diffusion in coal matrix

Diffusion is a process where flow occurs as a result of random molecular motion from an area of high concentration to an area of lower concentration (Crank, 1975 and Kolesar, 1986). Diffusive flow can be a combination of various flow mechanisms depending on coal pore structure and gas type; molecular, Knudsen and surface diffusion mechanisms may all contribute depending on the pore structure of coal and the type of gas (Saghafi *et al.*, 2007).

Saghafi *et al.* (2007) pointed out that gas diffusivity of coal indicates the ease with which gas migrates from micropores into macropores and fractures. Diffusive flux is proportional to the gas concentration gradient, with the coefficient of proportionality termed the diffusivity and, it is a fundamental property of a coal-gas system. In a one dimensional space it is written as Fick's equation:

$$\psi_d = -D_e \frac{\partial c}{\partial x} \tag{2-3}$$

Where D_e is the effective diffusion coefficient combining various diffusive flow mechanisms, c is the gas concentration, x is the space dimension and ψ_d is the gas diffusive flux.

Three different techniques have been applied to determine the gas diffusion parameters of coals (Crosdale *et al.*, 1998): (1) gas passing through a solid coal disc and from the measured pressure drop and flow rate, a diffusion coefficient can be calculated (Thimons and Kissell, 1973), (2) the gas solid chromatography method (Olague and Smith, 1989) and (3) after undergoing a step-change in surface concentration, the rate of sorption from small particles is used to determine a diffusion coefficient (Bielicki *et al.*, 1972).

2.4.3 Factors impacting on gas diffusion in coal

2.4.3.1 Effect of coal moisture

Researchers have confirmed that the gas diffusivity for dry coals was faster than for the corresponding moist coals, indicating that the sorption rate decreased with coal moisture (Clarkson and Bustin, 1999; Busch *et al.*, 2004; Gruszkiewicz *et al.*, 2009). As mentioned above, the rate of sorption of coal can represent the gas diffusivity (Bielicki *et al.*, 1972), thus gas diffusion in coal decreased with coal moisture.

Similarly, decreasing rate of gas sorption with increasing moisture content was reported (Gruszkiewicz *et al.*, 2009), for example, the study by Gruszkiewicz *et al.* (2009) showed that water saturation decreased the rates of CO_2 and CH_4 adsorption on coal surfaces, but it appeared to have minimal effects on the final magnitude of CO_2 or CH_4 adsorption if the coal was not previously exposed to CO_2.

2.4.3.2 Effect of temperature

As the coal sorption and desorption is a thermodynamical process, coal sorption and desorption is influenced by temperature. Increasing temperature generally causes sorption rate increase as reported by various researchers (Marecka and Mianowski, 1998; Busch *et al.*, 2004; Gruszkiewicz *et al.*, 2009; Pan *et al.*, 2010).

For instance, Pan *et al.* (2010) found that the rate of adsorption of CO_2 and CH_4 strongly depends on the temperature: an increase in temperature causes a decrease in equilibrium time. Charrière *et al.* (2010) carried out experiments on CO_2 sorption kinetics, performed for dried coal at the same equilibrium pressure (0.1 MPa) for five different temperatures, between 10 and 60 ℃, showing that the sorption rate increases with increasing temperature.

While some other researchers found that temperature caused slight or negligible influence on coal sorption rate. Marecka and Mianowski (1998) found slightly increasing rates for

increasing temperatures. In another similar study, Li *et al.* (2010) found no distinct differences in rates were observed for the three temperatures chosen (35, 45, 55 ℃).

2.4.3.3 Effect of gas type

Several researchers confirmed that CO_2 had a higher sorption rate than CH_4 (Marecka and Mianowski, 1998; Clarkson and Bustin, 1999; Cui *et al.*, 2004; Charrière *et al.*, 2010). Marecka and Mianowski (1998) observed that higher rates for CO_2 compared to CH_4 (factor around 10–20). In another similar study, Li *et al.* (2010) found three dry Chinese coals, having faster sorption rates for CO_2 than CH_4. The tested coals were ranged in rank from sub-bituminous to anthracite.

For a moisture equilibrated high volatile bituminous coal, Cui *et al.* (2004) found decreasing sorption rates in the order $CO_2 > CH_4 > N_2$ at 30 ℃ while the difference between CH_4 and N_2 is small. Authors related these changes to the differences in kinetic diameter of the gas species ($CO_2 < N_2 \approx CH_4$). Gruszkiewicz *et al.* (2009) confirmed that CO_2 adsorption on both dry and water-saturated coal was much more rapid than CH_4 adsorption and CO_2 was preferentially adsorbed from equimolar CO_2 and CH_4 mixture.

Charrière *et al.* (2010) found that the kinetic rate of CO_2 was generally one or two orders of magnitude larger than that of CH_4 due to its difference in kinetic diameter in interactions with coal. They reported that the higher sorption rate of CO_2 than CH_4 observation under all temperature or pressure conditions and for almost all coal samples was typically attributed to the smaller kinetic diameter of CO_2 compared to CH_4 and the ability of CO_2 to dissolve in the coal polymer structure. The dissolution of CO_2 into coal can play a more important role in the transport of CO_2 than CH_4 which was mainly adsorbed by the coal.

2.4.3.4 Effect of coal particle size

Studies showed that the coal sorption process increases with decreasing coal particle size (Marecka and Mianowski, 1998; Busch *et al.*, 2004; Gruszkiewicz *et al.*, 2009). Marecka and Mianowski (1998) studied CO_2 and CH_4 sorption rates on semi-anthracite coal using different grain size fractions. They found decreasing sorption rates with increasing particle size (i.e. lower specific surface area). Gruszkiewicz *et al.* (2009) found that adsorption in the smallest size fraction (45-150 μm) was much faster than adsorption in the two larger fraction.

Busch *et al.* (2004) performed CO_2 and CH_4 sorption kinetic experiments on high volatile bituminous coal from the Upper Silesian Basin, Poland at 32 ℃ and 45 ℃. They reported decreasing sorption rates with increasing grain size (<0.063 mm to 3 mm), while sorption rates did not change significantly at grain sizes larger than 100 μm. This indicates transport limiting grain sizes at a scale of 100 μm, i.e. above this size small transport pathways in the form of cleats or cracks can trigger fast gas distribution around the matrix blocks.

2.4.3.5 Effect of confining stress

Pone *et al.* (2009) studied the sorption rates of powdered and solid coal under unconfined and confined conditions (confining stresses 6.9 and 13.8 MPa) and found that the overall gas movement, specifically diffusion, was hindered by confining stresses at rates significantly less than unconfined condition. For both gases CO_2 and CH_4, it was found that diffusivities reduced (factor around 1.5) with the increasing sample size in the unconfined experiments and an even higher reduction in diffusivity when applying stress on the sample. The latter reduction was found to be proportional to the applied stress.

Pone *et al.* (2009) also reported that their observations emphasized that it was necessary to use coal samples confined at representative *in situ* confining stress for reliable evaluation of the sorption capacities and sorption rates. Investigation of sorption and diffusion of gases in coal at *in situ* stress conditions were limited and should be investigated further across the rank range and with inclusion of other competing processes. The difference in sorption and flow behaviour observed from the coal samples at different physical state of stress can be best explained in terms of macropore and micropore and matrix components of the coal. These components were affected differently by the confining stress and the subsequent deformation induced by exposure to gas.

2.4.4 Gas flow through the cleats

After gas molecules diffuse through the coal matrix in response to concentration gradients and upon reaching the cleat system, they migrate in response to pressure gradients. The flow of the CSG can be treated as linear percolation, mainly laminar flow. Thus, the flow obeys Darcy's law (Hadden and Sainato, 1969; Meaney *et al.*, 1995; Scott, 2002; Yang *et al.*, 2010):

$$v_f = -\lambda \frac{dp}{dx} \qquad (2\text{-}4)$$

Where v_f is the flow velocity, λ is the gas permeability coefficient, dp is the pressure gap along the distance of dx and dx is the smallest distance along the flow direction.

Gas migration through the cleat system occurs at a much greater rate than diffusion through the coal matrix, indicating that a well-developed cleat system is critical to successful CBM productivity (Scott, 2002).

Gamson and Beamish (1992) showed that from Darcy's law the general behaviour of methane flow through macroscopic structures in coal such as the natural cleat network could be modelled, since the cleats were regarded as having a uniform pore geometry (size, shape and spacing) that was representative of coal as a whole. Moreover, the model assumed the matrix blocks, as defined by the cleats comprised micropores of the same diameter. Gas migration was governed by two main factors. First, the distance methane had to diffuse was dependent upon the face and butt cleat spacing that delineates the size of the matrix blocks in the coal. Second, the amount of gas flowing through the cleat was dependent upon the width, length, continuity and permeability of the cleats.

2.4.5 Factors impacting on gas flow in coal cleat

2.4.5.1 Effect of water

The presence of water in a coal seam has a significant impact on a coal seam's ability to produce gas (Sereshki, 2005 and Black, 2012). In virgin coal seams, water normally fills pore spaces, cleats, and fractures and any gas present is dissolved within the seam water or absorbed on the internal surface of the coal, while the reservoir and its fluid components are in equilibrium (Van der Meer, 2004).

Meszaros *et al.* (2007) pointed out that the coal cleat system which was saturated with water was orthogonal with one direction cross-cutting the other, impacting the deliverability of CSG. Most of the methane in coal was adsorbed inside the micropore spaces in the coal. Water contained within the cleats exerts hydrostatic pressure on the adsorbed methane, keeping it from moving out of these micropores into the cleats in the coal. Whenever reservoir pressure was reduced, the methane desorbed off the coal surfaces, diffused through the matrix material, and then flowed though the cleat system and into the gas well.

The relative permeability of a coal seam increases as the water in the seam decreases, thus making more space available for the gas phase to flow. The rate at which water is produced

steadily decreases during the initial production phase, whereas the gas production rate steadily increases until it reaches a plateau, or peak gas production rate, following which the gas production rate will decline as per a normal gas well (Lamarre, 2007).

Generally, permeability is reduced by an increase in moisture content (Bartosiewicz and Hargraves, 1985). Confirming that, Black (2012) analysed the relationship between inherent moisture and gas production within the West Cliff Colliery mining area in Sydney Basin, Australia. The research results showed that there was some evidence of increased gas production from coal with reduced inherent moisture content, however there was a high degree of scatter and this relationship was rather weak.

2.4.5.2 Effect of temperature

Temperature influence on gas flow in cleat systems in terms of permeability has been studied in recent years (Yang and Zhang, 2008; Li and Xian, 2009; Li *et al.*, 2009; Feng *et al.*, 2010; Xu *et al.*, 2011; Yin *et al.*, 2011). Li *et al.* (2009) studied the relationship between coal permeability and the temperature as well as stress of the sample with CH_4 and He gases. The results showed that the relationship between coal permeability and temperature under different effective stress was not always a monotonically increasing or decreasing function, which was also confirmed by Li and Xian (2009). There was an inflection in permeability when the temperature increased. Under low effective stress, the stress from thermal expansion was larger than the applied effective stress. Then the coal expands externally and the permeability increased with temperature increase in a positive exponential relationship. Under high effective stress, thermal stress was smaller than the effective stress and the coal expanded internally. Then the permeability decreased with temperature increase in a negative exponential relationship.

Feng *et al.* (2010) carried out the research of permeability of coal under *in situ* stress at a depth of 500 m and different temperatures up to 600 ℃. The research results indicated that: (1) A critical temperature was found when the permeability of samples experienced changes with temperature from room temperature to 300 ℃, the permeability decreased from room temperature to the critical temperature; (2) A peak temperature was also found from 300 to 600 ℃, the permeability increased between the critical temperature and the peak temperature; (3) Above the peak temperature, the permeability decreased again with increasing temperature.

Experimental results of Nakajima *et al.* (1995) showed gas permeability of coal decreased irreversibly in response to an increase in applied hydrostatic stress or temperature. In the field trial, the fracturing activity not only caused an increasing gas emission, but also the irreversible closing of the cleats by the effects of stress changes at high temperature. Moreover, this caused irreversible lower gas permeability and increasing gradient of gas pressure. This effect of geological temperature on the permeability of stressed coal explained the reason why coal and gas outbursts frequently occur at the deep level development in a coal field. The result was confirmed by a recent study (Yin *et al.*, 2011), which showed that with the increase of temperature, the compressive strength of coal decreased and the elastic ratio of coal increased, the permeability of coal generally appeared a decreasing trend with increasing stress. Thus the low permeability of coal seam caused negative effect on gas drainage in mining and due to the fast increasing permeability of coal with high temperature in the yield phase, the risk of coal and gas outburst increased.

2.4.5.3 Effect of gas type, pressure and saturation

Permeability of cleated coal varies with different coal seam gases (Somerton *et al.*, 1975; Xue and Thomas, 1995; Sereshki, 2005). Somerton *et al.* (1975) used N_2 and CH_4 to study coal permeability and found that coal permeability with CH_4 was lower than the permeability with N_2. The provided explanation was that the sorption of methane on coal was a possible reason for this phenomenon. Experimental results of Xue and Thomas (1995) showed that coal consistently had a higher permeability with CH_4 than CO_2. The results of the permeability measurements performed with different gases (N_2, CH_4, CO_2, CH_4/CO_2 mixture), also showed the variation of coal permeability of different gases (Sereshki, 2005). The order of coal permeability value from high to low was N_2, CH_4, CH_4/CO_2 mixture and finally CO_2. Xue and Thomas (1995) reported a decreased coal permeability result with the increasing ratio of carbon dioxide in CO_2/CH_4 mixture in their mixture gas permeability study. The flow of the gas through pores and cleats depends on the size of the cleats and pores as well as the range and its distribution. Small pores with diameters of a few Angstrom (Å) can behave as a molecular sieve and permit some molecules to pass. Thus the flow rate of the passing gases will be reduced with bigger gas molecules in the same dimension of pore sizes (Sereshki, 2005).

The gas pressure had an apparent influence on the permeability of all coal samples. Zhang *et al.* (2012) used two different triaxial apparatus with different calculation principles to study

coal permeability and reported that, at each horizontal and vertical stress condition, coal permeability decreased with the increasing gas pressure. With a unique testing apparatus and by setting the gas pressure as the same as the confining pressure, Sereshki (2005) found that with increasing confining gas pressure the permeability decreased. The permeability reduction was greater for methane than carbon dioxide with increasing confining gas pressures (Sereshki, 2005). In addition, when gases such as CO_2 and CH_4 are present in the coal matrix, the coal swells due to gas sorption. This swelling could cause significant cleat closure and reduction in the transmissivity of the cleats with high gas pressure.

Gas saturation is a measure of the actual *in situ* gas content of a coal seam relative to the maximum gas storage capacity of that coal under the same environmental conditions (Black, 2012). Gas saturation is believed to be related to the stages of gas desorption, diffusion and flow through the cleat system. It also affects the gas emission from the coal seam (Cui and Bustin, 2006; Seidle and O'Connor, 2007; Black, 2012). Coal deposits are usually undersaturated to some extent and require pressure reduction to initiate gas release from the matrix into the cleats (Seidle and O'Connor, 2007). Where the cleat and fracture of the undersaturated coal are filled with water, the rate of gas desorption from the coal will be impeded until sufficient water has been pumped out and the pressure reduced to the critical desorption point (Cui and Bustin, 2006; Lamarre, 2007). Slow gas drainage rates and low total gas production with deep undersaturation in the CO_2 rich areas of the Bulli seam was found. Black (2012) compared the gas drainage data from the two areas with similar gas drainage boreholes located in CH_4 rich and CO_2 rich areas of the 518 panel at West Cliff Colliery. The analysis showed that both the gas flow rate and total produced volume from the deeply undersaturated CO_2 rich area was significantly less than the near saturated CH_4 rich area.

2.4.5.4 Effect of geological variation

The permeability of coal seams can be influenced by geological structure variations. Coal seam permeability is sometimes enhanced in the vicinity of a fault, dyke or fold. Generally, favourable areas for CSG drainage are likely to have a relatively simple geological structure ensuring the continuity of reservoirs (Sereshki, 2005). Wallace (1990) reported that gently folded areas in coal seams tended to have higher permeability than steeply folded and faulted areas. Circumstances of low permeability can occur *in situ* as a result of geological anomalies

such as sheared zones and intrusions; it is also reported that gas pressure increased and permeability decreased around the region of intrusions (Sereshki, 2005).

Optimal gas production was generally achieved from coal seams characterised by highly fractured coal and cleat networks with wide cleat apertures, great cleat density and intermediate cleat spacing (Dabbous *et al.* 1974; Lingard *et al.*, 1984; Cui and Bustin, 2006; Solano-Acosta *et al.*, 2007). Coal seams with high cleat permeability and low cleat porosity were expected to achieve peak production and a high production rate in a shorter time.

Bartosiewicz and Hargraves (1984) examined various coal samples from Australian coal basins, and the results demonstrated significant variations in permeability in different directions. Bedding plane permeability was significantly greater than the permeability perpendicular to the bedding. However, Lingard *et al.* (1982) reported no significant permeability difference between coal samples cut parallel and perpendicular to the bedding plane.

Cleat orientation has proved to be an important parameter for the permeability of coal (Wolf *et al.*, 2001), the greatest permeability parallel to the major (face) cleat was observed (Osisanya and Schaffitzel, 1996). Therefore in coal seams with a more developed face cleat, higher gas production can be expected from boreholes oriented perpendicular to the major (face) cleat (Osisanya and Schaffitzel, 1996). Whilst, the study of impact of operational factors on gas drainage (Black, 2012) indicated that in the coal with greater degree of saturation, there was an increased gas production from boreholes oriented between 5 and 60 degrees to the face cleat, suggesting neither face or butt cleat was a more dominant path for gas flow.

In the study of stress relief CBM drainage by surface vertical wells in China, Sang *et al.*, (2010) concluded that with the coal extraction process, secondary cleats and fractures were formed anisotropically in the coal seam. Many additional fractures were also formed along the layers as the protected coal expands in response to stress relief. As the stress relief and fracture generation had a positive effect on the physical characteristic of overlying reservoir (Whittaker *et al.*, 1979), the coal permeability is effectively enhanced.

2.4.5.5 Effect of effective and confining stress

The permeability of coal is significantly dependent on effective stress and confining stress (Xue and Thomas, 1995; Scott, 2002; Sereshki, 2005; Pan *et al.*, 2010; Jasinge *et al.*, 2011).

The permeability of coal is sensitive to the effective stress (Connell *et al.*, 2010; Chen *et al.*, 2011; Jasinge *et al.*, 2011; Kiyama *et al.*, 2011) and it deceases with increasing effective stress. Meanwhile, coal swells with gas adsorption, and shrinks with gas desorption. Under reservoir conditions these strain changes affect the cleat porosity and thus permeability. Cleat compressibility is also changed with gas species and pressure, confirmed by Scott (2002), a significant decrease in permeability with increasing depth indicated that cleat apertures were becoming narrower as effective stress increases.

This phenomenon was explained as being due to the fact that, by applying stress to the coal matrix the fractures and cleats were tightened or closed, the movement of gases was restricted and therefore permeability dropped (Sereshki, 2005). In his study the permeability of Tahmoor coal samples in Australia was shown to decrease by an average factor of 1.5 to 2 when the axial load was increased from 100 to 1000 kg under 0.5 MPa methane gas confining pressure.

Sang *et al.* (2010) summarised the practical utilisation and research related to stress relief CBM drainage using surface wells in China. The high gassy mining areas were often related with low permeability, stress relief CBM surface well drainage had been successfully implemented as a practical CBM exploitation technology. One of the most important reasons was that the stress relief inducing permeability increase in the protected coal seams during mining operations. The research results indicated that the maximum principal stress could drop by 37 % from the original stress in the protected seam located 70 m above the mining coal seam (Liu *et al.*, 2009). The decrease in maximum principal stress continuously recovered the deformation of coal seam as well as surrounding rock strata and hence increased the regional permeability during the continuous coal mining operation process.

2.4.6 Coal behaviour with different gases

2.4.6.1 Gas adsorption and desorption

Coal swells with adsorption and shrinks with desorption of coal seam gases. The experimental studies by various researchers (Sereshki, 2005; Connell *et al.*, 2010; He *et al.*, 2010; Pan *et al.*, 2010; Pone *et al.*, 2010) demonstrated that the influence of gas sorption on coal can cause volume change, coal swelling value change following the gas type order of CO_2, CO_2/CH_4, CH_4 and N_2. The level of coal shrinkage was also affected by the type of gas desorbed and the magnitude of shrinkage was followed with the same gas order (Sereshki,

2005). Among those gases, CO_2 appeared to have the greatest influence on the matrix and nitrogen the least. This was understandable in view of the fact that carbon dioxide had greater affinity to coal than the other gases. Research also found that coal swelled even under confining stress (Pone *et al.*, 2010).

Day *et al.* (2008) used directly observing techniques to study the swelling of coal in CO_2 and other gases. The system was used to measure CO_2-induced swelling in three Australian bituminous coals with pressures up to 15 MPa (Day *et al.*, 2008). All three coals showed similar behaviour, with swelling increasing as a function of pressure up to about 8 to 10 MPa, after which no further increase in swelling was observed. Combined with gas adsorption results, swelling was roughly proportional to the amount of CO_2 adsorbed up to intermediate pressures, but at high pressures, the relationship was no longer linear; adsorption continued to increase but swelling did not. The maximum volumetric swelling was between about 1.7 and 1.9 %, even in liquid CO_2. Significant anisotropy was observed; swelling in the plane perpendicular to the bedding plane was always substantially higher than in the parallel plane. They also found that temperature did not directly affect the maximum amount of swelling, however, the swelling tended to occur at lower pressures with decreasing temperature.

The deformation of coal structure due to CO_2 sorption was irreversible as noted by Briggs and Sinha (1932). This result is confirmed by a recent study (Pone *et al.*, 2010), swelling of the matrix during sorption was not balanced by the shrinkage after desorption. The hysteresis of coal swelling through adsorption, desorption, and readsorption of CO_2 can be observed at subcritical conditions (He *et al.*, 2010). However, according to the study (Day *et al.*, 2008), the swelling in these coals was completely reversible with each sample returning to its original dimensions after the gas was removed, even after multiple exposures.

Connell *et al.* (2010) claimed that gas in coal seams was largely stored by adsorption, which introduced a complication in the understanding of coal permeability behaviour (Chen *et al.*, 2011); as gas desorbed from coal the coal seam matrix shrinks, with gas adsorption the matrix swelled. Thus there are two competing effects on coal seam permeability; lowering the pore pressure acted to increase the effective stress and thus reduced the permeability due to cleat compression. However the drawdown also resulted in desorption of methane leading to matrix shrinkage and increased coal cleat apertures and thus permeability. Conversely, raising the pore pressure and gas content will reverse the processes.

2.4.6.2 CO_2 gas injection

With the developing technology of CO_2 geo-sequestration and CO_2 injection to enhance the coalbed methane recovery (CO_2-ECBM), investigations were undertaken with coal behaviours with CO_2 gas injection (Viete and Ranjith, 2006; Mazumder and Wolf, 2008; Fujioka *et al.*, 2010; Liu *et al.*, 2010; Massarotto *et al.*, 2010; Kiyama *et al.*, 2011). Geo-sequestration of CO_2 is widely seen as a prospective method for greenhouse gas control (Kiyama *et al.*, 2011). Coal seams particularly containing higher contents of CBM are chosen as attractive storage areas.

Alternating positive and negative strain values observed during compression, sorption and desorption, respectively, which emphasized that both compression/compaction and expansion of coal will occur during CO_2 sequestration (Pone *et al.*, 2010). Pore structure changing of coal during the CO_2 geo-sequestration was one of the key issues that significantly affect the sequestration process significantly (Liu *et al.*, 2010).

Liquid CO_2 injection into a water-saturated coal specimen and then heated and injected as supercritical CO_2 was used to simulate the initial stage of CO_2 injection in the field when the coal seam was saturated with water. Study showed a volumetric swelling strain of 0.25 to 0.5 % was observed after injecting liquid CO_2 (Kiyama *et al.*, 2011). The investigations of Massarotto *et al.* (2010) showed that mineral matter in coal, both in the matrix and in the cleats, was dissolved and mobilised during reaction with supercritical CO_2 and de-ionised water in a batch reactor at *in situ* conditions. This occurred for both dull and bright coal samples of Permian age, creating new porosity and additional permeability.

Fujioka *et al.* (2010) showed that the feasibility of extracting gas from a coal seam while storing carbon dioxide underground was evaluated in Japan. In the CO_2-ECBM project in Japan, injection tests suggested that injectivity of CO_2 into the virgin coal seam saturated with water was eventually increased as the water saturation near the injector was decreased by the injected CO_2. It was estimated that low injectivity of CO_2 was caused by the reduction in permeability induced by coal swelling. It was also indicated that the coal matrix swelling might create a high stress zone near to the injection well. Fracture opening pressure of the virgin coal seam surrounding the well has the possibility to significantly increase CO_2 adsorption.

One of the key issues with geological sequestration of carbon dioxide in coal seams was the change of permeability caused by CO_2 injection, and especially the induced reduction in injectivity. Injection caused changes in pressure and effective stress, with further changes caused by coal matrix swelling associated with adsorption of CO_2. The test results clearly depicted an exponential reduction of coal permeability to CO_2 when effective stress increases (Jasinge *et al.*, 2011).

2.4.6.3 N_2 gas injection

With the developing technology of N_2 injection to enhance the coalbed methane recovery (N_2-ECBM) and N_2 flushing to enhance underground CSG drainage, research was carried out to better understand coal behaviour with N_2 gas injection (Fujioka *et al.*, 2010; Yang *et al.*, 2010; Kiyama *et al.*, 2011; Zhang *et al.*, 2012).

Trials had demonstrated that N_2 flooding could be used, not only to recover the reduction of permeability caused by swelling (Shi and Durucan, 2005), but also boost the gas production rate. Fujioka *et al.* (2010) tested N_2 flooding to evaluate the effectiveness of N_2 injection on improving well injectivity. The N_2 flooding test showed that daily CO_2 injection rates were boosted, but only temporarily. Moreover, the permeability did not return to the initial value after CO_2 and N_2 were repeatedly injected.

In the test by Kiyama *et al.* (2011), supercritical CO_2 was injected into a coal specimen saturated with N_2, and then N_2 and CO_2 were repeatedly injected. This test was to simulate the case of N_2 injection and CO_2 re-injection in the field. Tests showed the coal was firstly swelled after injecting supercritical CO_2. Following further injection of N_2, slow strain recovery was observed in the coal, suggesting that N_2 displaced the adsorbed CO_2 in the coal matrix. The permeability of the coal core also recovered to a certain degree after N_2 injection, although it dropped rapidly after CO_2 injection. Further injections of N_2 and supercritical CO_2 caused little subsequent change in permeability. The results indicated that coal swelling was likely to be the main cause for the permeability change in the field tests and coal behaviour can be significantly influence by N_2 injection.

2.5 GAS DRAINAGE FROM COAL

The aim of gas drainage in underground coal mining is to control gas emissions into mine ventilation and to reduce the outburst risk. The aim of the CBM industry is to explore the coalbed methane, treating the CSG as a fuel resource. Based upon gas sources, gas drainage

techniques are divided into working seam drainage, adjacent seam drainage, and goaf drainage. In terms of where gas flows, the techniques are categorised into borehole and tunnel techniques. Gas drainage techniques are also classified as drainage with and without stress relief. Gas drainage can also be divided into surface drainage and underground drainage (Wang and Xue, 2008). In the following, the gas drainage technology is reviewed according to the categories of gas drainage from the surface and underground.

2.5.1 Surface gas drainage

Coal mine gas underground drainage and *in situ* CBM surface well drainage have developed as two different technologies for methane extraction from coal reservoirs. Underground drainage is mature and used mainly for mining safety reasons, while surface well development to recover CBM is encouraged by governments in the world and has consequently been the subject of rapid development. Underground gas drainage shows good outcomes, but the extracted methane concentration often has low purity, the collection, transmission and utilization of the diluted gas are relatively difficult. For CBM drainage using surface vertical wells, the methane concentration can be much higher, and the collection, transmission and utilization are relatively easier (Sang *et al.*, 2010).

2.5.2 Enhanced surface gas drainage

2.5.2.1 Technologies to increase borehole surface area for gas drainage

A variety of methods are available to increase the surface area of well with the natural fracture networks of the coal seam. The main technologies include open hole cavity completion, under-reaming and hydraulic fracturing (Loftin, 2009; Johnson, 2010; Black, 2012). Figure 2.6 shows the various enhancement methods including medium radius borehole technology, ranked according to their cost and applicability to varying coal seam permeability conditions (Loftin, 2009 and Johnson, 2010).

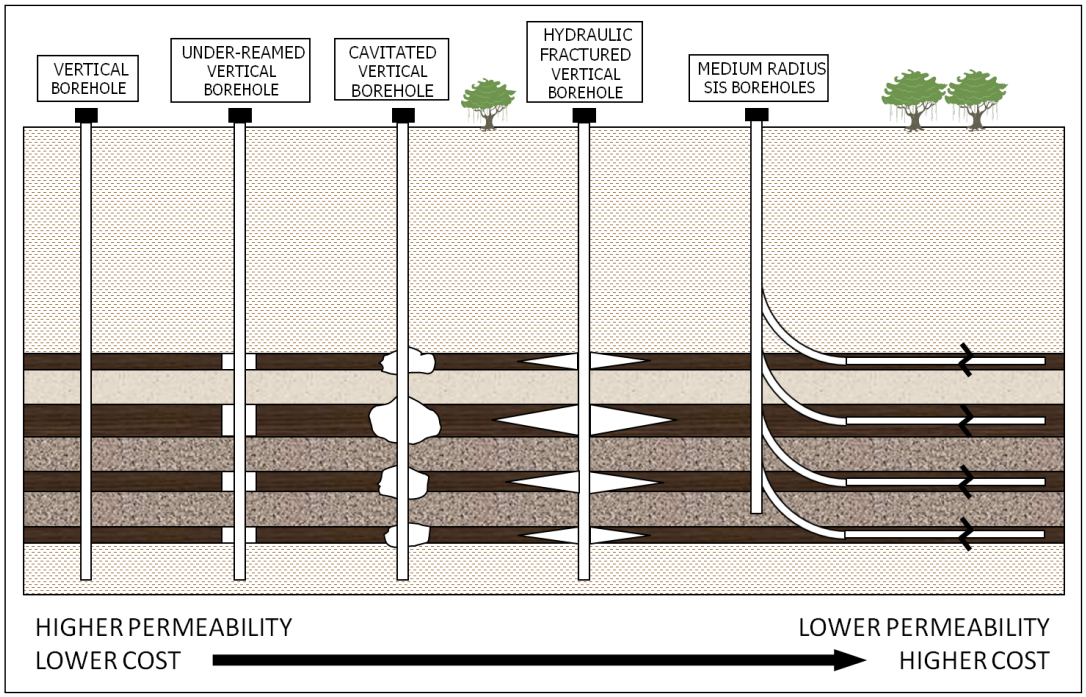

Figure 2.6: Gas drainage enhancement methods ranked according to cost and application relative to coal seam permeability (after Loftin, 2009 and Johnson, 2010)

Open hole cavity completion involves creating a cavity in the coal seam sufficiently large to remove any coal in contact with the borehole that may have been damaged during the drilling process. The cavity completion effectively connects the coal natural fracture system and the well. Mavor *et al.* (1992) suggested open hole cavity completion was the preferred method for enhancing gas production from coal seams with moderate permeability such as the coal seams in the Fruitland formation of the San Juan Basin in United States, as in many cases the cavity completed boreholes often produced gas and water at a significantly greater rate than the hydraulic fractured wells which did not appear to have effective communication with the reservoir.

Under-reaming involves using a reaming tool to increase the diameter of the borehole equivalent to the fully deployed diameter of the cutting arms. After casing is set and cemented to the top of the coal, a special reaming tool with rotating blades, jets or drill cones, is used to ream out a cavity in the coal (USEPA, 2009). Under-reaming is a technique that can be applied to multiple seams. Once the wellbore has been widened at each seam, slotted casing is inserted across the coal interval and, where needed, gravel is packed between the walls of the cavity and the casing to keep the cavity open. Under-reaming is commonly used in CBM projects in the Powder River Basin, United States and in the high permeability coal

seams in the Surat Basin, Australia (USEPA, 2009). After under-reaming, the well is cleaned out with a fresh water flush and a down-hole submersible pump produces water up the tubing while the gas that separates from the water is produced up the annulus (USEPA, 2009).

Hydraulic fracturing involves injecting a proper fluid at a high rate into a coal seam to initiate and propagate a fracture (Kahil and Masszi, 1982 and Stewart and Barro, 1982). Mavor *et al.* (1992) stated that numerous types of hydraulic fracture stimulation treatments had been applied in coal reservoirs and the following injection and proppant carrying fluids have been used: water, hydrochloric acid, hydrofluoric/hydrochloric acid, nitrogen foam, carbon dioxide foam, nitrogen and carbon dioxide foam, linear gelled water and cross-liked gelled water. Hydraulic fracturing in a coal seam attempts to: (a) bypass any formation damage caused during drilling; (b) increase the connection between the borehole and the natural fracture system of the CSG reservoir; and (c) distribute the pressure drawdown over an increased area to reduce fines production (Zahid *et al.*, 2007). In the design and execution of an effective hydraulic fracture stimulation program, Holditch *et al.* (1988) suggested that consideration should be given to the selection of suitable injection fluid and proppant material type, size and loading schedule, adverse impacts of high injection pressures, complex fracture systems, screen-outs and the production of proppant as well as coal fines post-treatment.

2.5.2.2 Secondary lateral drilling technology

Secondary lateral drilling involves drilling multiple branches from the primary lateral of a horizontal inseam directionally drilled borehole. Drilling secondary laterals effectively increases borehole density and contact with the CSG reservoir to increase total gas extraction potential whilst reducing the number of surface installations required (Black, 2012).

The arena for multi-lateral wells can be trilateral, quadrilateral, or pinnate (Palmer, 2010). Study by Palmer (2010) showed that the use of secondary lateral drilling was well suited to gas drainage applications in low permeability, medium thickness coal seams with no geological structures. Figure 2.7 shows a pattern of pinnate wells (Spafford, 2007). The wells are designed for full coverage of the reservoir, to initiate gas flow faster, and to recover gas more quickly. The laterals are unlined, which may cause them to collapse in some situations. Sometimes the downdip quadrant is left undrilled because it is more difficult for gas to lift water in an updip direction.

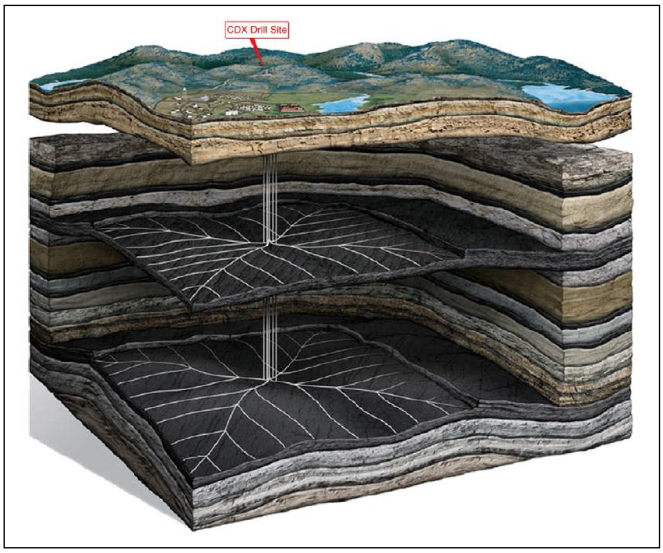

Figure 2.7: Pinnate pattern of multi-lateral wells (after Spafford, 2007)

Figure 2.8 is a summary for vertical wells, while pinpoint (each seam fractured individually) give the most effective stimulation of multiple seams, staged fractures often result in at least one seam with no effective fracture. Limited entry fractures are a special class of staged fractures, but with the same disadvantage. Branch fractures are unproven yet, but hold promise especially for permeability <3 mD where conventional fractures are not effective (Palmer, 2010).

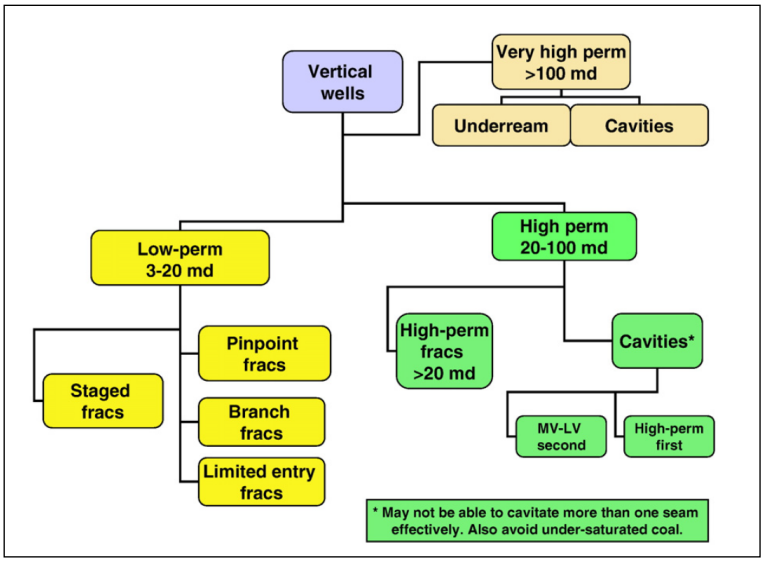

Figure 2.8: Perm-based completion tree for CBM: vertical wells (after Palmer, 2010).

2.5.2.3 Surface drainage with stress relief

Mine gas drainage in China started from 1938, and industrial application started in 1952. Initially, an underground CBM drainage test was operated by Longfeng mine in Liaoning Province (Sang *et al.*, 2010). Being demonstrated with success, the method was gradually

extended over the years, with deformed coal seams, damaged coal seam structures, and low permeability of many Chinese coal measures.

Surface well drainage with stress relief is utilized significantly to enhance the CBM well production rate and methane recovery ratio in low permeability coal seams (Thakur, 1981). Stress relief gas, refers to the gas which is contained in the goafs and coal seams influenced by coal mining operation. According to the seam being mined, the stress relief gas can be divided into the following three categories: gas distributed in the mined coal seam; gas in the adjacent coal seams; and gas in distant overlying coal seams. The following shows the fundamental theories of stress relieved surface gas drainage or post goaf drainage.

The rock strata surrounding the mining area can be divided into different zones, as shown in Figure 2.9 (Cervik, 1979; Singh and Kendorski, 1981; Yu *et al.*, 2004). In the vertical direction above the roof, the rock strata zone can be divided into the caving zone, the fractured zone and the bending zone (Singh and Kendorski, 1981 and Karacan *et al.*, 2007). In the plan view, the whole area can be divided into the compaction area, relief area with fractures and distant coal seam supporting area. The zones and areas move with the advance of working face. Adjacent coal seams and the mining coal seams are stress relieved and gas permeability increased due to stress relief (Esterhuizen and Karacan, 2005 and Whittles *et al.*, 2006).

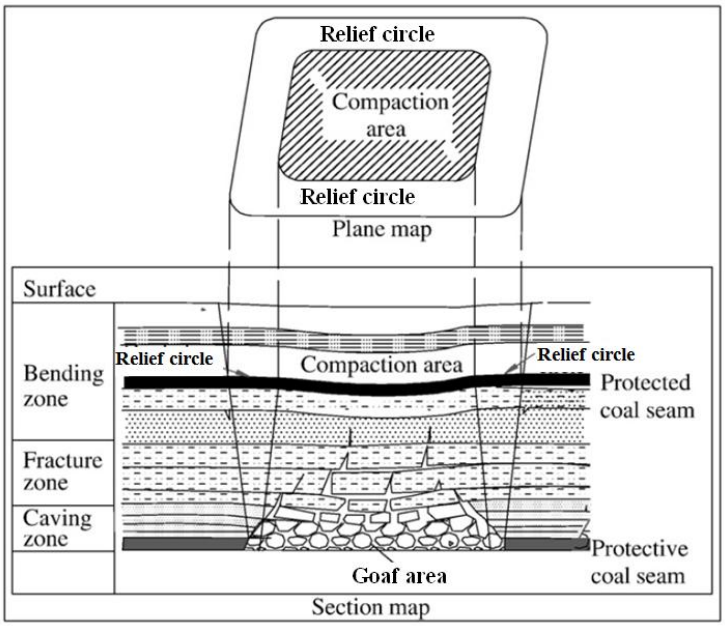

Figure 2.9: The schematic diagram of the vertical distribution of mining fractures in overlying strata (modified after Sang *et al.*, 2010)

The strata ahead of the working face deforms first. The horizontal displacement is relatively larger than the vertical displacement as the strata is still supported by the unmined coal seam. As the goaf grows larger, the strata around the working face moves towards the centre of the goaf, while the rock layers in the centre of the goaf begin to go downwards. The deformation of the strata in different locations varies greatly causing the rock layer to split by tension, forming vertical fractures. The strata overlying the goaf move down at different rate. This difference between the bending of the strata forms the relief layer (Qian and Liu, 1984).

Strata deformation is caused by a variation of the stress during the mining operation, which redistributes forces in the surrounding strata. The weight of overlying strata is supported by the barrier pillar and the stress is decreased to a limited extent above the goaf roof, whereas the stress around the working face is increased greatly. Consequently the strata around the working face are stretched and compressed causing deformation (Sang *et al.*, 2010).

According to the stress situation, the region above the working face can be divided into four zones: normal stress zone, stress concentrated zone, relieved zone and stress resuming zone. These four zones move with the advance of the working face (Yu, 2005), as shown in Figure 2.10.

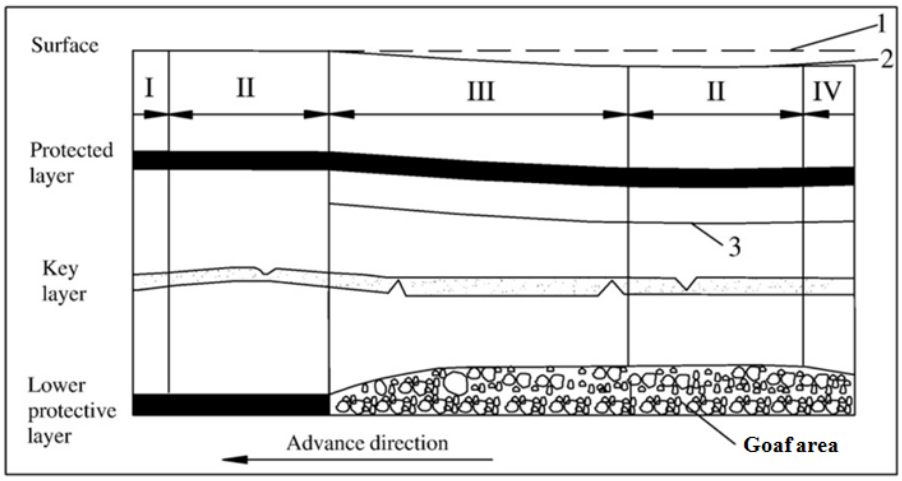

Figure 2.10: Underground stope stress zoning. I - normal stress zone; II - stress concentration zone; III - stress relief zone; IV - stress resume zone. 1 - initial surface; 2 - surface subsidence curve; 3 - strata subsidence curve (after Sang *et al.*, 2010)

The protected coal seam is relieved because of the decreasing stress due to mining. Stress relief leads to expansion of coal which results in fracture generation (Palchik, 2003). The adsorbed methane is released from the stress relief strata, which is also dewatered in these

layers flowing into the goaf through the fractured zone. The gas flows under the pressure gradients from regions of high reservoir pressure to lower reservoir pressure. The gas in the working seam and the adjacent seam will flow into the goaf through the secondary fractured network and accumulate in the fractured zone around the goaf roof. In particular, the layer around the goaf is well developed with a large amount of gas released. Thus, the free gas migration in the goaf and the protected seam along with the fracture development improve the condition for surface gas drainage (Sang *et al.*, 2010), as shown in Figure 2.11.

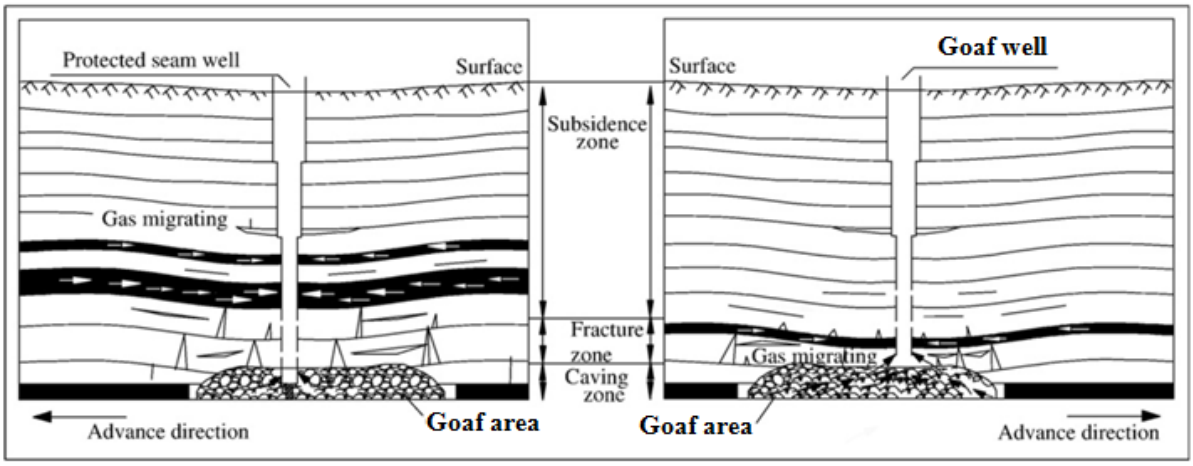

Figure 2.11: Pressure relief gas migration and surface vertical wells drainage (modified after Sang *et al.*, 2010)

2.5.3 Underground gas drainage

Coal mines typically undertake gas drainage to maintain roadway gas concentrations below specified limits to ensure mining safety. A typical category of gas sources in a coal mine is shown in Figure 2.12, from which it can be seen that coal mine gas emission can be categorised into two main sources, active panel gas emission and abandoned panel gas emission (SAWS, 2006).

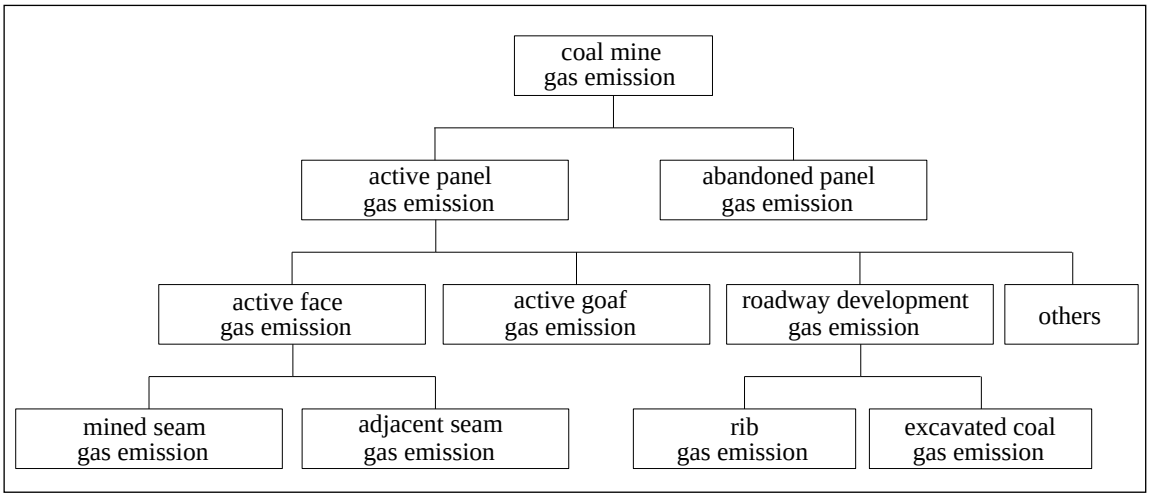

Figure 2.12: Gas sources in a coal mine (after SAWS, 2006)

Ventilation is the most basic and common method for gas control, and for less gassy mines, ventilation is normally sufficient to dilute the gas concentration below the required safety limit. Where the volume of gas liberated into the mine environment exceeds the diluting capacity of the mine ventilation system, three options are available to the mine operator (Black, 2012): (a) remove the excess gas through systematic gas drainage, (b) dilute the excess gas by increasing the ventilation air quantity, or (c) reduce the rate of gas emission by reducing the mining rate. Thus, efficient drainage strategies are necessary for highly gassy coal mines where large quantities of gas may migrate into underground workings from adjacent strata and ventilation dilution capacity is limited. A reasonable combination of a well-designed ventilation system and an efficient gas drainage system is critical to ensure a safe working environment (Wang *et al.*, 2011).

2.5.4 Enhanced underground gas drainage

2.5.4.1 Technologies to increase borehole surface area

A variety of methods are available to increase the surface area of the borehole with the natural fracture networks in underground coal mines. The main technologies include hydraulic fracturing (normal fracturing as well as high pressure pulsating hydraulic fracturing), hydraulic water-jet cutting (normal hydraulic water-jet cutting as well as high pressure pulsating hydraulic water-jet cutting), hydraulic flushing, controlled blasting (normal controlled blasting, static blasting and cumulative blasting). Results of hydraulic coal cracking and controlled blasting in long boreholes at some sites indicated that: (a) seam permeability was increased 2-5 times by controlled blasting in long boreholes, and the

amount of gas drained after blasting was increased by 50-90 %; (b) seam permeability was increased 10-100 times by hydraulic coal cracking, and amount of gas drained after cracking was increased by 100-200 % (Wang and Xue, 2008).

Normal hydraulic fracturing

Many researchers (Sun *et al.*, 2010; Guo *et al.*, 2011; Huang *et al.*, 2011) studied normal hydraulic fracturing to improve coal permeability in underground mine gas drainage. Hydraulic fracturing of coal can be used to control hard roof, to transfer the stress directionally, to release the local concentrated stress, to weaken the coal strength, to increase the permeability and hence to prevent coal seam from outbursting. Huang *et al.* (2011) analysed the structure and physico-mechanical properties of coal and the hydraulic crack propagation and physical chemistry effect of hydraulic fracturing. The field studies showed that with normal hydraulic fracturing in underground mining, the seam permeability was improved by 800 times, the gas production of a single drainage borehole by 120 times. After normal hydraulic fracturing, the coal and gas outburst indexes were dramatically reduced. The borehole gas natural flow was also improved by 127. 6 times and the influence radius of the borehole along the seam strike direction could exceed 50 m (Sun *et al.*, 2010).

High pressure pulsating hydraulic fracturing

High pressure pulsating hydraulic fracturing can make some physical quantities of coal change repeatedly from compression to expansion, which can generate fatigue failure, dredge the pores and enhance the permeability (Lin *et al.*, 2011; Zhai *et al.*, 2011). This technology can effectively enlarge the influencing range of a single borehole and increase the drainage efficiency (Lin *et al.*, 2011). The effect of pressure relief was best with the pulsating pressure of 24 MPa and the frequency of 20 Hz, the extraction concentration and the gas flow increased by twice after fracturing, resulting in the values of outburst risk indexes being reduced (Lin *et al.*, 2011). Zhai *et al.* (2011) concluded that compared with general methods of hydraulic fracturing, the results of field trial showed that pulsating hydraulic fracturing had a better effect on pressure relief and permeability improvement, meanwhile, the concentration and drainage gas flow were remarkably enhanced.

Normal hydraulic water-jet cutting

Normal hydraulic water-jet cutting was treated as a new drilling method for the accurate and efficient installation of long in-seam boreholes tested in Australia (Lunarzewski, 2001). This involved the integration of pure water-jet drilling technology with the conventional directional drilling technique. Actually, the system was similar to the conventional directional drilling method, but instead of relying on a down-hole motor rotating a mechanical drill bit for cutting, a high pressure water-jet cutting technique was used (Lunarzewski, 2001). Compared with general methods of coal seam drilling, industrial experiments indicated that the high pressure hydraulic-cutting across strata layers could have a better effect on pressure relief and permeability improvement, while the drainage gas flow and influencing range increased substantially, which resolved the problem of gas and coal outburst in the drilling process of low permeability coal seams with high gas concentration (Shen *et al.*, 2011; Song *et al.*, 2011; Zhang *et al.*, 2012). Field test results (Shen ,*et al.*, 2011) showed that after hydraulic water-jet cutting application, coal seam permeability increased up to 113 times of the original value with the effective gas drainage influence radius almost doubled.

High pressure pulsating hydraulic water-jet cutting

High pressure pulsating hydraulic water-jet cutting technology was also used in recent years (Li *et al.*, 2008; Liu *et al.*, 2010; Lu *et al.*, 2011). The results of Li *et al.* (2008) showed that the impacting effect, denudation effect and vibration effect caused by high pressure pulsating hydraulic water-jet cutting were effective in coal crack generation and permeability improvement. Lu *et al.* (2011) concluded that High pressure pulsating hydraulic water-jet cutting could also promote coal matrix shrinkage according to their theoretical analysis of coal matrix stress. The gas flow rate of each borehole after high pressure pulsating hydraulic water-jet achieved 0.19-0.26 m^3/min with 4.2 times enhancement (Liu *et al.*, 2010).

Hydraulic flushing

Hydraulic flushing is another gas drainage enhancement technology used in underground coal mines (Liu *et al.*, 2009; Liu *et al.*, 2010; Fan and Wang, 2012; Wang *et al.*, 2012). The distribution of stress and permeability of the coal around flushing holes, is in a dynamic status. Four regions are formed after flushing, from hole to coal seam direction; they are full gas emission region, gas emission region, gas pressure transition region and natural gas

region (Wang *et al.*, 2012). Liu *et al.*, (2010) stated that the optimised hydraulic coal flushing pressure was determined at 12−20 times as high as the Protodyakonov coefficient. The research results showed that after hydraulic flushing application to the high outburst risk seams, the elasticity potential of coal was released, the gas pressure gradient was reduced, the permeability of the seam was improved and the stress to cause outbursts could be effectively eliminated. The results of Liu *et al.* (2009) showed the average value of gas drainage volume fraction increased from 718 % to 5619 % after flushing. The average value of initial gas emission dropped from 2412 L/min to 2128 L/min after flushing. Similarly, the results of Fan and Wang (2012) showed that after hydraulic flushing, the initial gas emission increased by 6 times; the borehole gas emission attenuation coefficient reduced by 85 %; the coal seam permeability coefficient increased by 53 times; the influence radius of boreholes extended 2-3 times.

Controlled hydraulic blasting

Controlled blasting technology is used to generate fractures and enhance the coal seam permeability (Cai *et al.*, 2007; Yu *et al.*, 2007; Guo *et al.*, 2008; Sun *et al.*, 2010; Li *et al.*, 2011). Controlled blasting includes different types, such as normal controlled blasting, static blasting method and cumulative blasting. Yu *et al.* (2007) reported a gas flow increase of more than 1.9 times from the field trail tests of controlled blasting. Research results showed that this technique was feasible to improve gas drainage under suction in hard and low permeability coal seams. The technology of controlled hydraulic blasting of deep crossing-hole which could take the advantage of explosion and water power, was developed and applied in head development (Sun *et al.*, 2010). The results showed that the technology can promote the connections of the fractures around the borehole and help gas drainage, thus it can be applied to seams with potential outburst risk.

One of the important utilisation of controlled blasting is deep-hole presplitting explosion. Cai *et al.* (2007) analysed the influence of the cracks generated in the process of deep-hole presplitting explosion and the performance of permeability improvement caused by the gap difference between explosive holes. A suitable gap (5−6 m) between explosive holes was proposed. It was concluded that cracks can be generated by the impacts of dynamic pressure, propagation and vibration superposition of stress waves, as well as crack developments by gas generated in the explosion process (Liu *et al.*, 2008; Wang and Xue, 2008). Deep-hole

presplitting explosion also provides an effective approach to improving the permeability of coal seam with high gas content and low permeability.

Static blasting technology and cumulative energy blasting technology are also used in the improvement of coal seam permeability. Static blasting technology is a technical method for increasing the gas migration channels and permeability of coal seam with Soundless Cracking Agent (SCA) in combination with a suitable borehole arrangement. In this process, there is no shake and no flame, which can ensure the safety of extracting coal seams in complicated conditions (Li *et al.*, 2011). Cumulative energy blasting had the apparent blasting wave unloading effect and directional blasting gas jet effect. Double stitching jet cumulative energy blasting can achieve directional fractures and good fracture surfaces. This technology can be applied to deep-hole presplitting explosion to improve the CSG drainage efficiency (Li *et al.*, 2010). Guo *et al.* (2008) reported that high kinetic energy generated by the cumulative energy blasting can penetrate through coal seams, and subsequently blasting gas enlarged the fracture range. The cumulative blasting was applied in the field trial, achieving the enhancement of gas concentration by 200-300 % with 5-6 m effective fracture radius in gas drainage.

Different technologies can be used together to achieve a better effect on increasing borehole surface area in underground gas drainage. Huang *et al.* (2011) suggested that hydraulic fracturing after controlled blasting was an efficient way to greatly increase the scale and range of cracks around the boreholes. By taking into considerations of the equipment, technology maturity, effectiveness, practicality, operational safety and cost, the most feasible gas drainage techniques in low permeability seams are cross measure boreholes and intensive parallel boreholes of large diameter (Wang and Xue, 2008). If the *in situ* condition is suitable, the hydraulic coal fracturing technique can significantly reduce drilling operations and the technique can be used to replace intensive parallel boreholes. The technique of controlled blasting in long boreholes has a similar effect with inter-crossing boreholes, although this technique is more complicated due to the drilling process and operation of placing explosive charges in boreholes and blasting. As the borehole becomes longer, the chance of successful blasting decreases, and the safety risk of the whole operation increases. Technique of hydraulic coal fracturing requires the assembly of sophisticated and heavy equipment, and there are still issues to be resolved in the control of inseam fracture generation and the type of materials to support the fractures (Wang and Xue, 2008).

2.5.4.2 In-seam directional drilling technology

Directional drilling has given the mining industry the ability to place boreholes in designed locations to achieve specific goals such as gas drainage, exploration, barrier proving and water drainage (Thomson, 1998; Thomson and Adam, 2007; Black, 2012; Hungerford *et al.*, 2012a). Figure 2.13 shows that a schematic layout of the directional drilling system. The first in-seam directional long-hole was drilled in Australia at Appin Colliery in 1987 to drain gas from the adjacent coal seam located 18 m below the working seam (Lunarzewski, 2001). Guided long-holes were used for pre-drainage of longwall panels and post-drainage of goafs, with the main part of drilling being in the targeted seam. Since then, more research and practical applications were established for hole stability protection and lead time for various geological, mining and gas conditions (Lunarzewski, 2001).

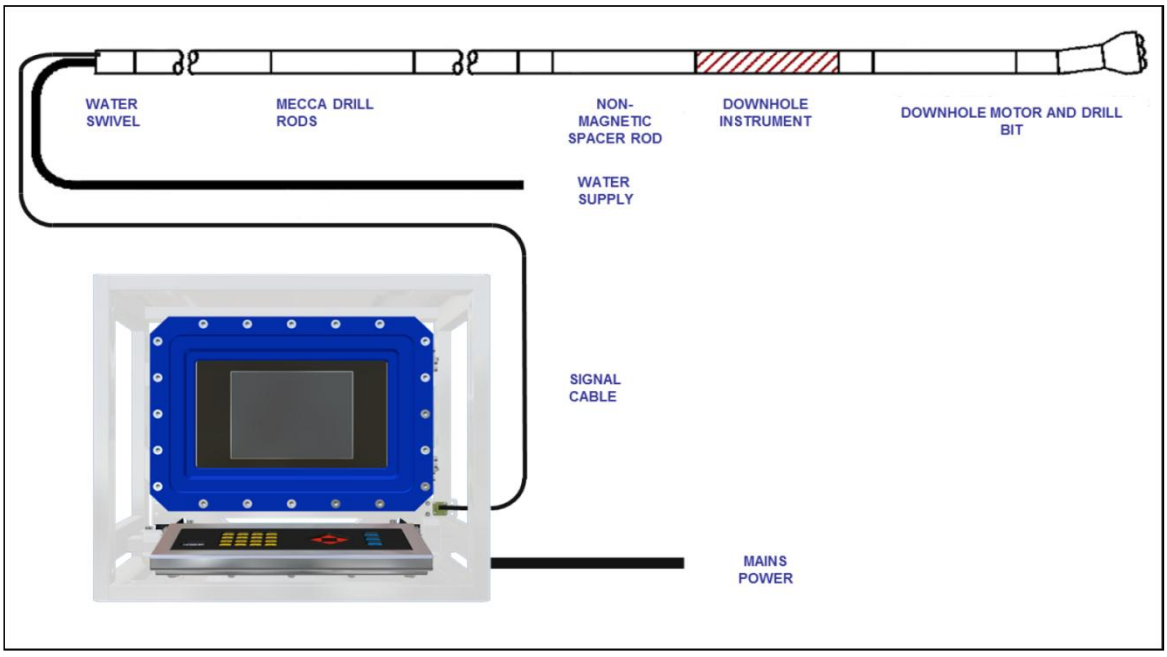

Figure 2.13: Directional drilling system schematic layout (after Hungerford *et al.*, 2012b)

Considerable success was achieved with inseam long-hole drilling using down-hole motors (DHM) and hole trajectory control techniques and equipment such as Directional Drill Monitor utilising Modular Electrically-Connected Cable Assembly (DDM-MECCA) and Drill Guidance System (DGS) survey tools. The system provides rapid and easy underground hole survey measurements whilst drilling, including computer monitoring if required. It measures the earth's magnetic field and gravity in all three directions (x, y and z) with borehole placement accuracy of ± 0.1 degree inclination and ± 0.5 degrees azimuth. The instruments and connections are intrinsically safe, which allows for their application in

underground gassy coal mines as well as giving fast and reliable data transmission irrespective of hole depth (Lunarzewski, 2001).

The use of DHM drilling provides the ability to off-set the direction of drilling and surveying to accurately locate the borehole and orient the DHM for steering. The off-set provided by the configuration of DHM bend and bit diameter has to be matched with the drilling environment to provide the ability to control the borehole trajectory and azimuth. Because of the variety of drilling environments likely to be experienced when drilling any long hole within a coal seam, proper configuration is set to manage the most adverse environment (Hungerford *et al.*, 2012a).

Surveying and drilling practices have evolved to suit the requirements at each mine. The ability to drill long holes becomes an exercise in directional control with drilling practices to limit the in-hole friction which increases as a borehole increases in depth. Reviewing these practices and resultant frictional effects is intended to refine driller's skills and practices to improve borehole drilling efficiency and depth capacity (Hungerford *et al.*, 2012a).

Drill patterns for coal mine gas drainage typically involve inseam boreholes drilled from exposed roadways and across blocks ahead of future mine development. The angle and spacing between boreholes are usually determined based on planner's experience and data related to coal seam permeability, available drainage time and gas content. The decision on which drill pattern to use is often based on available access for the drill rig, logistics and efficiencies associated with relocation and site establishment (Thomson, 1998).

Figure 2.14 shows the typical drill patterns used in underground gas drainage. These include a regular pattern of parallel boreholes drilled from a separate site requiring regular rig relocation (Type A); separate boreholes drilled in a fan pattern from a common drill site (Type B); multiple branches drilled from a common parent borehole (Type C), long boreholes drilled parallel to future mine development panels (Type D), and long exploration boreholes (Type E) (Thomson, 1998). When using long boreholes, such as in Type D, allowance should be made in the mine design and production schedule for increased drainage time, providing an opportunity to drain more gas and offset the increased drilling time and cost (Black, 2012).

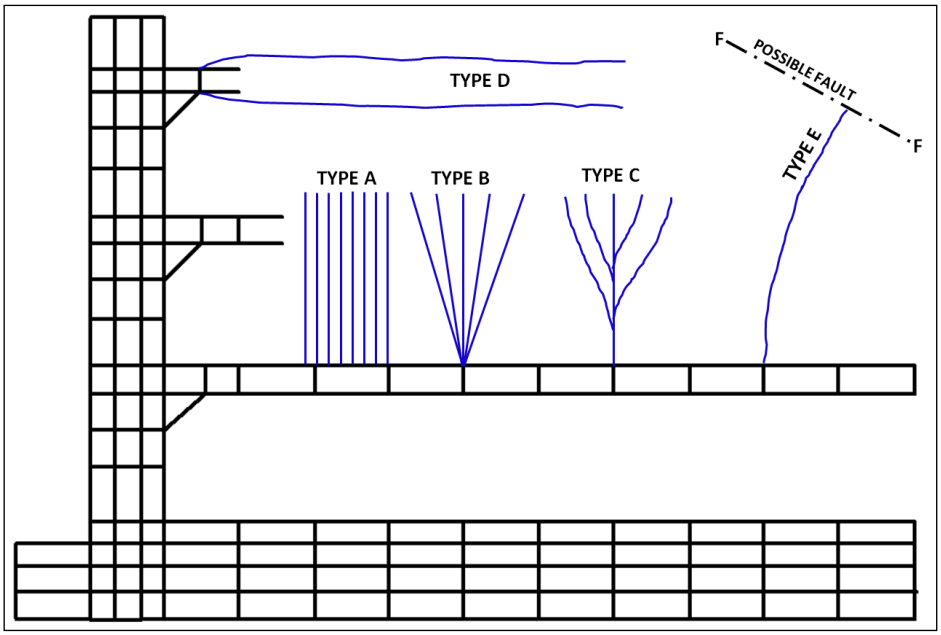

Figure 2.14: Inseam drilling patterns available for CSG drainage (after Thomson, 1998)

2.5.4.3 Underground ventilation and gas drainage strategy

Gas related disasters have long been recognised as one of the most serious threats to mine safety in underground coal mines in China, especially for those extracting multi-seams where gas migration from adjacent seam and gas bearing strata may result in unexpected or uncontrolled gas issues. China is rich in coal resources with most of its coal mines are associated with multi-seam conditions. A number of gas drainage techniques have been developed and practiced in many coal mines of China mainly to minimize outburst risk and reduce gas emission. Dependent upon local geological and mining conditions, one or more techniques may be practiced in a coal mine (Wang and Xue, 2008).

Although gas control techniques have been widely improved worldwide either by ventilation or gas drainage, they may not suit some Chinese high gassy coal mines due to the complex site conditions characterised by low coal seam permeability, deep seam bearing and high geo-stress. Many coal mines in the east of China have developed at depth exceeding 1000 m. It is estimated that the mining depth will increase at a rate of 8~12 m annually, creating a great challenge to the existing gas drainage and safety techniques (Wang *et al.*, 2011). Figure 2.15 shows some of the gas control techniques used for multi-seam mining.

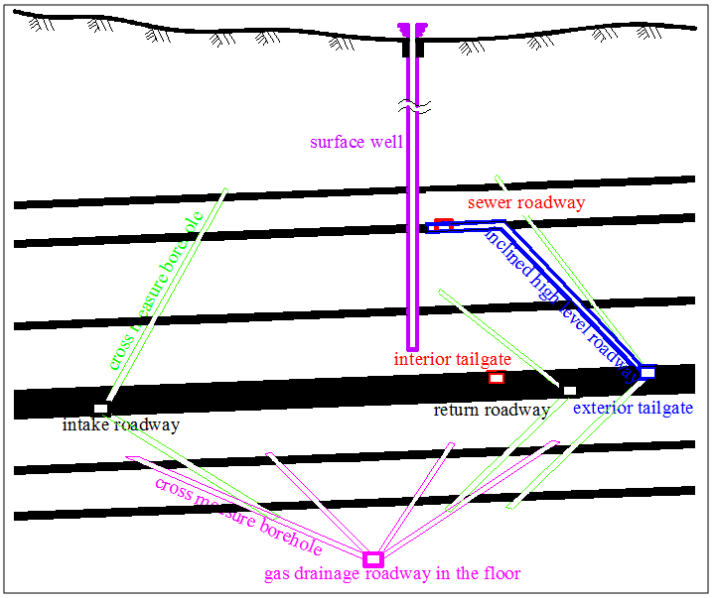

Figure 2.15: Gas control methods developed in Chinese coal mines for multi-seam mining with cross measure drilling (modified after Wang *et al.*, 2011)

'U+L' ventilation type

For longwall faces using the 'U+L' ventilation scheme, cross-measure boreholes can be drilled towards the fractured zone from the exterior tailgate (the second return roadway) at an interval of 15-35 m, as shown in Figure 2.16. Gas released from the underlying strata and coal left in the goaf, will flow through the cut through kept open behind working face, instead of flowing back to the face. This usually results in high gas concentration at the intersection of longwall face and the return roadway. This ventilation scheme mainly deals with goaf gas emitted from underlying seams, mined seam and overlying seams within the caving zone. The distance between cut throughs influences the performance of the exterior tailgate, as a result of recompaction in the goaf, large amounts of goaf gas may flow to the working face when the cut through behind the face is too far away.

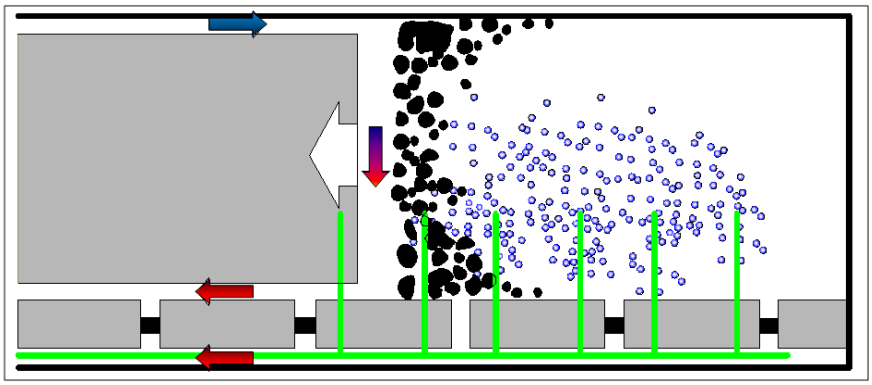

Figure 2.16: 'U+L' ventilation scheme combined with cross measure boreholes (after You *et al.*, 2008)

Compared with the general 'U' ventilation scheme, the 'U+L' ventilation scheme gas drainage technique is superior for the large dilution capacity of the exterior tailgate. The dilution amount could account for more than half of the total gas ventilation. Cross-measure boreholes or inclined high level roadway development and pipeline installation in the exterior tailgate can be used to drain CSG in this scheme. The field trial shows that the occurrence of gas concentrations exceeding the ventilation limit has been improved greatly around the intersection of longwall face and return roadway. However, a serious problem induced by this technique is the increasing oxidation risk in the goaf especially when cut-throughs behind the panel are not sealed tightly and timely (Wang *et al.*, 2011).

'U+I' ventilation type

To overcome the disadvantage of the 'U+L' ventilation scheme, the 'U+I' ventilation scheme is developed. A general layout of this technique is illustrated in Figure 2.17. For example, in the Yangquan mining area in China, an interior tailgate is developed in the top coal along the roof about 15-25 m away from the return roadway, and a sewer roadway parallel to the return roadway is developed in the fractured zone generally 40-60 m above the mined seam and about a third of the face length away from the return roadway horizontally (Zhu *et al.*, 1997).

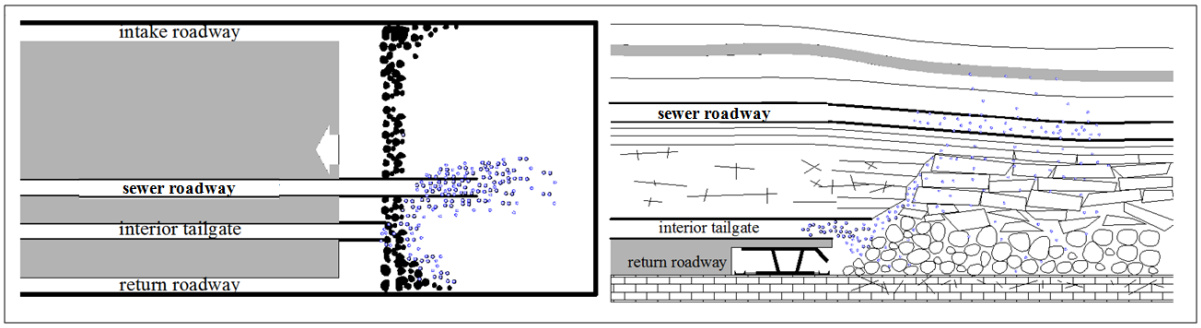

Figure 2.17: 'U+I' ventilation scheme based gas control technique (modified after You, 2008)

The interior tailgate provides a negative pressure outlet beside the return roadway along the panel, and takes advantage of the collapse with the panel advancing. The interior tailgate performs better in collecting gas emitted from the goaf compared with the return roadway and the exterior tailgate developed in the 'U+L' ventilation scheme (You *et al.*, 2008). In addition, the interior tailgate is easier to maintain than the exterior tailgate. The sewer roadway driven above the working seam along the length of the longwall blocks, has a cross-section of 4 to 5 m^2 and is superior to the inclined high level roadway for capturing gas

desorbed from the adjacent gassy strata as it works in a relatively stable and efficient condition during the panel retreat.

Numerous field trials have been carried out in the Yangquan mining area in China and this technique has now developed into a main strategy of coal and coalbed methane exploration for multi-seam mining in gassy seams. In these field trials, gas recovery of the above sewer roadway could be up to 80-90 %, and an average gas flow rate of 40-60 m^3/min could be achieved (Zhao, 1996). However, one limitation of this technique is that the interior tailgate will be difficult to maintain in soft or thin coal seams. Meanwhile, the mining height under the interior tailgate should be carefully controlled and the chock flipper should be extended in time to avoid collapse ahead of the working face. Other factors that should be taken into account including, gas issues encountered in development of the above sewer roadway, and the absence of a suitable adjacent seam where it can be developed. A challenge of this technique is the large rock roadway development operation that results in relatively high costs.

'Y' ventilation type

The gas drainage enhancement methods mentioned above may not be applicable in mining areas where coal and gas outbursts have become a major threat due to the high gas pressure and burial depth. Low permeability and high geo-stress greatly limits the effectiveness of a pre-drainage strategy, thus, other post-drainage techniques have to be developed. One of the most efficient and effective gas control methods was based on the 'Y' ventilation scheme without any coal pillars. From the perspective of outburst prevention, it is a protective mining method, in which a seam with low gas pressure and content is extracted in advance to provide stress relief for the outburst prone seams, thus enhance gas drainage and eventually lower the outburst risk of the protected seams (Yu, 1992).

It can be seen from Figure 2.18, that the 'Y' ventilation scheme is a modified version of the 'U' system, a roadway (bleeder) behind the panel is maintained for air return, and the other two roadways ahead of the panel act for air intake. Compared with the previously introduced 'U+L' and 'U+I' scheme, this method has its own advantages. Firstly, as there are two roadways for air intake, there is less air exchange between the goaf and working face, thus avoiding goaf gas from migrating into working face. Gas accumulation issues around the tailgate corner can be alleviated, which usually lead to production delay (Yuan, 2008);

secondly, as a result of lower ventilation pressure and the goaf gas buoyancy effect, large quantities of goaf gas accumulate along the retained roadway, benefiting high concentration gas drainage (Wei *et al*., 2011).

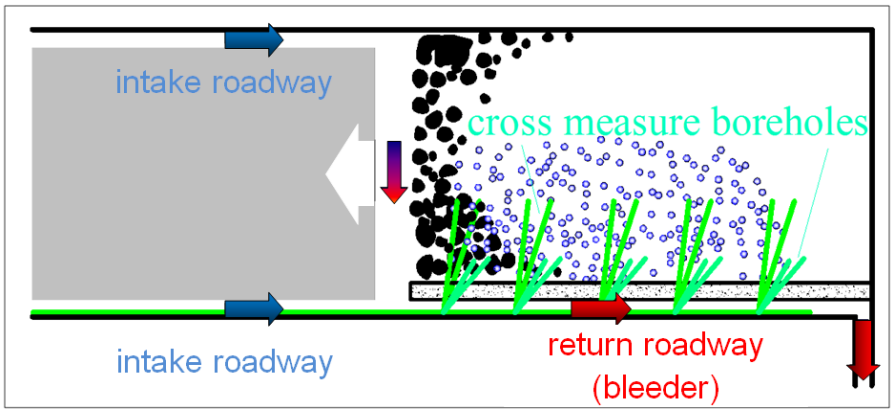

Figure 2.18: 'Y' ventilation scheme based gas control technique (modified after Yuan, 2008)

The retained roadway provides an access where cross-measure boreholes can be drilled to capture large quantity of desorbed gas. Two or three upward boreholes can be drilled in each drilling site to reach target seams where vertical fractures are not well developed in the bending zone. The borehole diameter is generally more than 90 mm, and the borehole spacing is around 20 m. Downward boreholes can also be drilled to drain gas desorbed from underlying seams; however, the stress relief effect may not be as good as that for overlying seams with the same distance from the mining seam. Field investigations show that the stress relief region in the Huainan mining area may extend up to 130-150 m above the roof and 80-100 m below the floor respectively (Yuan, 2008).

Based on various ventilation schemes, both cross measure boreholes and different roadway arrangement strategies are widely employed to capture gas desorbed from overlying and underlying seams in the underground coal mines in China. Continued improvement in underground drainage is an important and efficient strategy to enhance CSG capture. Selection of appropriate gas drainage techniques for a coal mine depends mainly on site specific geological and mining conditions, such as seam permeability, CSG content, seam hardness, gas emission source, as well as financial investment (Wang and Xue, 2008).

2.6 SUMMARY

This chapter reviewed the basic knowledge of the coalification process, generation of CSG and storage of CSG as well as gas transport in coal in terms of desorption from the coal

surface, diffusion in coal matrix and gas flow through the cleats. Different factors impacting on gas diffusion and gas flow in cleats are introduced. Additionally, different gas drainage technologies are reviewed according to the applications of gas drainage methods from surface and underground.

Many factors influence gas diffusion in coal. It was found that increasing temperature generally caused increasing sorption rates, while the gas diffusivity was decreased with coal moisture. Researchers confirmed that CO_2 adsorption on both dry and water-saturated coal was much more rapid than CH_4 adsorption. The decreasing sorption rate with increasing particle size and confining stress were also mentioned. Regarding different factors on gas flow through cleats, researchers found water produced steadily decreased, whereas the gas production rate steadily increased until it reached a plateau. Under low effective stress, the coal expanded and the permeability increased with temperature increase, while under high effective stress, the permeability decreased with temperature increase. The order of gas permeability in coal from high to low was N_2, CH_4, CH_4/CO_2 mixture and finally CO_2. The permeability of coal seams can be influenced by gas saturation and geological structure variations. Coal behaves differently in the process of gas adsorption, desorption and gas injection of CO_2 and N_2. Coal swells with gas adsorption and shrinks with desorption. Pore structure changes and coal permeability were also found to be affected with CO_2 and N_2 gas injection.

A variety of methods are available to increase the surface area of the natural fracture networks of the coal seam for gas drainage. The main technologies include open hole cavity completion, under-reaming and hydraulic fracturing. Secondary lateral drilling technology and stress relief can significantly enhance the CBM well production rate and methane recovery ratio in low permeability coal seams. Comparatively, various methods are also available to increase the surface area of the borehole with the natural fracture networks in underground coal mines. The main technologies include hydraulic fracturing, hydraulic water-jet cutting, hydraulic flushing, and controlled blasting. Directional drilling technology and underground drainage strategies can enhance gas capture in underground coal mines, reduce gas emissions and thus minimize outburst and explosion risks. Depending upon the local geological and mining conditions, different ventilation and drainage techniques may be practiced in a coal mine to achieve better and more effective gas management.

CHAPTER THREE – GAS SORPTION ISOTHERM TEST OF COAL

3.1 INTRODUCTION

Measurement of the volume of gas adsorbed per unit mass of coal with increasing pressure at a constant temperature produces an isotherm that describes the gas storage capacity of the tested coal type. The accurate testing and interpretation of coal sorption isotherms play an important role in the areas of coal mine methane drainage, CBM reservoir resource assessment, enhanced coalbed methane (ECBM) recovery, as well as the carbon dioxide sequestration in deep coal seams or similar geological formations, which has also been identified as an attractive option that may aid in mitigating GHG emissions.

Gas sorption in coal has been studied over the years by many researchers (Lama and Bartosiewicz, 1982; Aziz and Li, 1999; Clarkson and Bustin, 2000; Goodman *et al.*, 2004; Saghafi *et al*., 2007; Busch and Gensterblum, 2011; Chareonsuppanimit *et al*., 2012), and different types of apparatus are involved in isotherm tests. Correspondingly, different calculation methods are used to obtain coal sorption isotherms (Aziz and Li, 1999; Busch *et al*., 2003; Saghafi *et al*., 2007; Day *et al*., 2008; Pone *et al.*, 2009; Charriere *et al.*, 2010; Hol *et al.*, 2011). The general principle in determining the volume of gas being adsorbed by a particular type of coal is calculated by subtracting the void gas from the total gas. However, coal sorption isotherm apparatus and calculation methods vary significantly, depending on the limitations of the apparatus being used and the accuracy of the calculation procedures.

Busch and Gensterblum (2011) reviewed the CBM and CO_2-ECBM related sorption process in coal, in their study, the existing sorption methods were grouped into manometric, volumetric and gravimetric methods by separating the true volumetric approach with injection pump from the normal volumetric method with manometers. Actually the principle of the manometric and volumetric is similar, both methods require very accurate determination of cell and reference volumes as well as the injected gas volume either by injection pump or reference cell with pressure gauge. In the normal gravimetric method, the amount of sorbed gas is measured at constant pressure by means of a highly accurate balance.

The first inter-laboratory comparative study of carbon dioxide isotherms for coal samples was carried out by Goodman *et al.* (2004) and four independent laboratories involved in the

isotherm measurements on dry Argonne Premium coal samples. Goodman *et al.* (2004) pointed out that because no standard method or equipment was available for obtaining CO_2 isotherm data, the participating laboratories reported isotherms using their own, usually in-house built apparatus and procedures, as well as calculation methods. The research community recognises that several factors including the operator, the equipment and its calibration as well as the laboratory environment (i.e. temperature and humidity) could have had influence on the variability of their test results.

A critical study of the different methods that are used worldwide to test the coal sorption isotherms is presented. In general, these methods can be categorised into either volumetric or gravimetric methods. Test methods, based on these two approaches and associated apparatus as well as calculation methods, are introduced and compared. Based upon the indirect gravimetric method, a unique apparatus using only a sample cell, developed at the University of Wollongong is discussed. Its setup, operation procedures, absolute adsorption calculation theory and calculation methods with calibration curve or the Soave-Redlich-Kwong (SRK) equation are described.

3.2 ISOTHERM TESTING APPARATUS AND CALCULATION METHOD

3.2.1 Volumetric method

The volumetric method to determine coal sorption isotherms is widely used (Mohammad *et al.*, 2008; Chareonsuppanimit *et al.*, 2012; Krooss *et al.*, 2002 and Busch *et al.*, 2003), the method requires very accurate determination of cell and reference volumes as well as injected gas volume, either by injection pump or reference cell with pressure gauge. The volumetric method is categorised into two types, volumetric method with sample cell (equilibrium cell) and injection pumps, and the volumetric method with both sample cell and reference cell (or reference volume).

3.2.1.1 Sample cell (equilibrium cell) and injection pumps

Mohammad *et al.* (2008) and Chareonsuppanimit *et al.* (2012) reported a volumetric method with sample cell (equilibrium cell) and injection pump, as shown in Figure 3.1 and used in the adsorption laboratory in Oklahoma State University, Oklahoma, USA. This apparatus is based on the principle of mass balance, which requires accurate

measurements of volume, pressure and temperature. Because the displaced volume measurement at a constant pressure is involved in this system, it is also called the true volumetric method (Goodman *et al*., 2007). The entire apparatus is maintained in an air bath at constant temperature. 100 mesh size coal samples are put inside the equilibrium cell, and the cell is vacuumed before the gas injection.

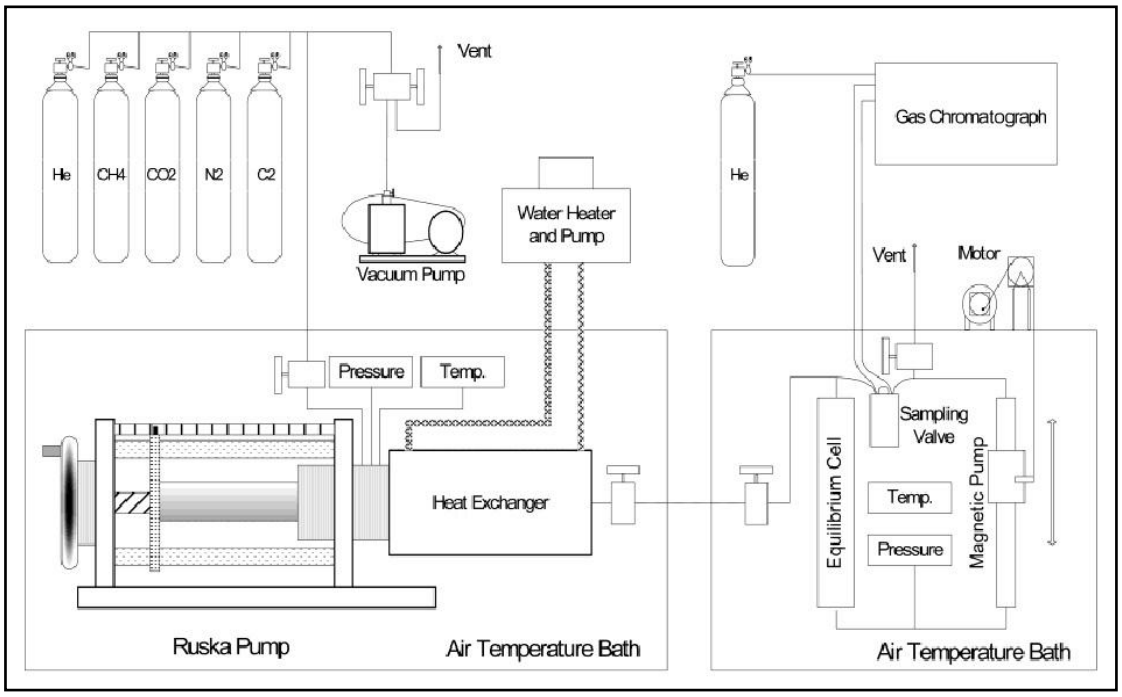

Figure 3.1: Schematic layout of volumetric method of gas sorption apparatus with injection pump (after Mohammad *et al.*, 2008)

A known amount of helium from a pump called Ruska which has been calibrated is injected to determine the void volume V_{void} of the equilibrium cell. Because helium is not significantly adsorbed by the coal sample, the void volume can therefore be determined from the measured values of the temperature, pressure, and the amount of helium injected into the cell. The mass balance equation (Mohammad *et al.*, 2008) is shown in the following:

$$V_{void} = \frac{\left(\frac{P\Delta V}{ZT}\right)_{pump}}{\left(\frac{P_2}{Z_2 T} - \frac{P_1}{Z_1 T}\right)_{sample\ cell}} \qquad (3\text{-}1)$$

Where ΔV represents the injected gas volume from the Ruska pump, Z represents the helium compressibility factor, P represents the pressure, T represents the temperature, subscripts "sample cell" and "pump" mean the apparatus part of the sample cell and pump and "1" and

"2" mean status before and after gas injection, respectively. The helium void volume measurements were carried out at the temperature which is the same as the isotherm test.

The Gibbs adsorption which is called the Excess adsorption as well, can be calculated from measured quantities directly in the experiment. A certain amount of gas $n_{injected}$ is injected into the sample cell from pump. The injected gas will be partially adsorbed, and the Gibbs n_{void} will exist in the equilibrium bulk (gas) phase. The amount of adsorbed gas can be calculated by using molar balance equation, Gibbs $n_{adsorbed}$ as:

$$n_{adsorbed} = n_{injected} - n_{void} \tag{3-2}$$

The injected amount can be calculated from temperature, pressure as well as volume data of the injection pump:

$$n_{injected} = \left(\frac{P\Delta V}{ZRT}\right)_{pump} \tag{3-3}$$

When equilibrium is achieved, the quantity of unadsorbed gas can be determined:

$$n_{void} = \left(\frac{PV_{void}}{ZRT}\right)_{sample\ cell} \tag{3-4}$$

Where the pressure P is measured after equilibrium is reached in the cell, which occurs when no further change in pressure is observed.

In Equation 3-3 and 3-4, Z represents the gas compressibility factor with a certain state of pressure and temperature. An adsorption isotherm is generated by repeating the mentioned steps at higher pressure with sequence. The amount of adsorbed gas is finally calculated by dividing Gibbs $n_{adsorbed}$ by the coal's mass in the cell.

3.2.1.2 Both sample cell and reference cell (or reference volume)

Krooss *et al.* (2002) and Busch *et al.* (2003) introduced the volumetric method with both sample cell and reference cell (or reference volume), also called the manometric method (Busch and Gensterblum, 2011; Gensterblum *et al.*, 2010) as shown in Figure 3.2 and used in Aachen University of Technology, Aachen, Germany. A schematic diagram of the experimental set-up including a stainless-steel sample cell, a series of valves and an accurate pressure transducer is shown in Figure 3.2 (A). The reference volume including the volume between valves V_2 and V_3 as well as the pressure transducer's dead volume is measured by

helium injection in the calibration process. The powdered coal sample is placed into the sample cell which has already been calibrated. An in line filter is adopted to avoid coal or other particles from entering the valves and charging and discharging pipes.

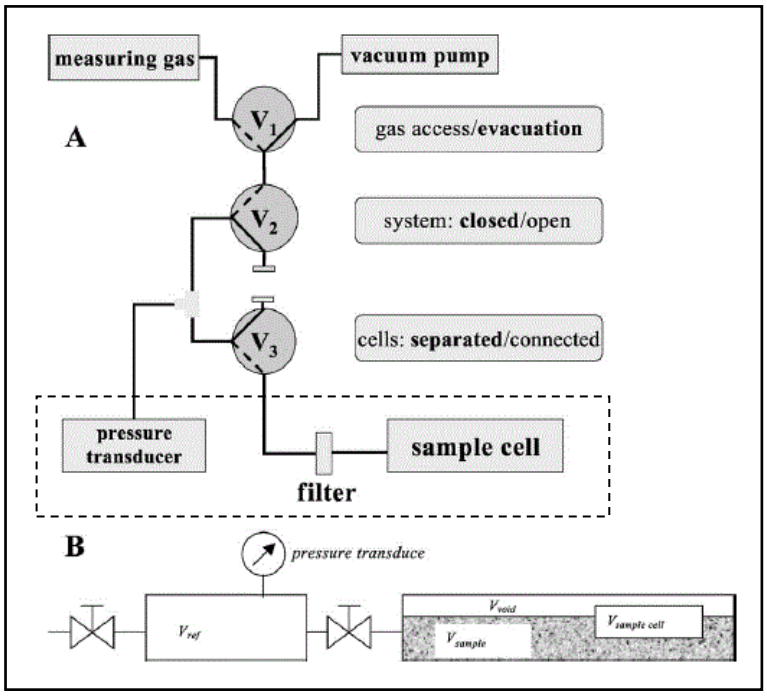

Figure 3.2: Schematic diagram of the experimental set-up for gas adsorption using; (a) stainless steel sample cell containing coal and a pressure transducer, and (b) sample cell volume and reference volume (after Krooss *et al.*, 2002)

The relevant volume relationships to measure and evaluate the Gibbs adsorption are shown in "B" section of Figure 3.2. The total amount of gas introduced into the system after charging to a certain pressure, is refer to the amount of gas released from the reference cell to the sample cell. The value of $n_{adsorbed,}$ which is the adsorbed gas volume, relies on the accurate calculation of the V_{coal} which can be calculated in the helium expansion process before the adsorption test. The void volume of sample cell V_{void} is calculated by:

$$V_{void} = V_{sample\ cell} - V_{coal} \qquad (3\text{-}5)$$

Where $V_{sample\ cell}$ is the total volume of the sample cell. The amount of adsorbed gas $n_{adsorbed}$ is calculated using Equation 3-6, $n_{adsorbed}$, which is the different value between the total gas n_{total} existing in the sample cell and the amount of the void volume V_{void} which is defined as the volume not occupied by the coal. V_{void} is calculated with c_{gas} which is the molar concentration of the gas phase and can be calculated from the gas Equation Of State (EOS) at a certain pressure and temperature condition:

$$n_{adsorbed} = n_{total} - c_{gas}V_{void} \quad (3\text{-}6)$$

As the same in the first method, the above steps are repeated with sequence to a higher pressure to form the whole isotherm and the amount of adsorbed gas is calculated by dividing Gibbs $n_{adsorbed}$ by the mass of coal tested in the experiment.

3.2.2 Gravimetric method

Apart from the volumetric method, the gravimetric method to determine coal sorption isotherms is also widely used (Charrière *et al.*, 2010; De Weireld *et al.*, 1999 and Saghafi *et al.*, 2007). In the normal gravimetric method, the amount of sorbed gas or the total injected gas is measured at constant pressure by means of an accurate balance. The gravimetric method can be divided into two types, gravimetric method with sample cell and suspension magnetic balance as well as gravimetric method with both sample cell and reference cell (or reference volume).

3.2.2.1 Sample cell and suspension magnetic balance

The gravimetric method with sample cell and suspension magnetic balance was introduced by Charriere *et al*. (2010) and Weireld *et al*. (1999). Figure 3.3 shows the schematic picture of the magnetic suspension balance. The basket contains the coal sample, which is unconnected to the balance directly; a magnetic force coupling between the electromagnet and the permanent magnet is used instead. An experimental apparatus combined with a sinker whose volume is calibrated is used to measure the density.

As shown in Figure 3.3, the suspension magnetic balance has three measuring status (pink coloured item refer to weighed part): In status 0, the permanent magnet is suspended and also weighed alone. In status 1, the sinker is at rest and the basket with coal is lifted. In status 2, basket and sinker are both lifted aiming to obtain the total weight of the whole system.

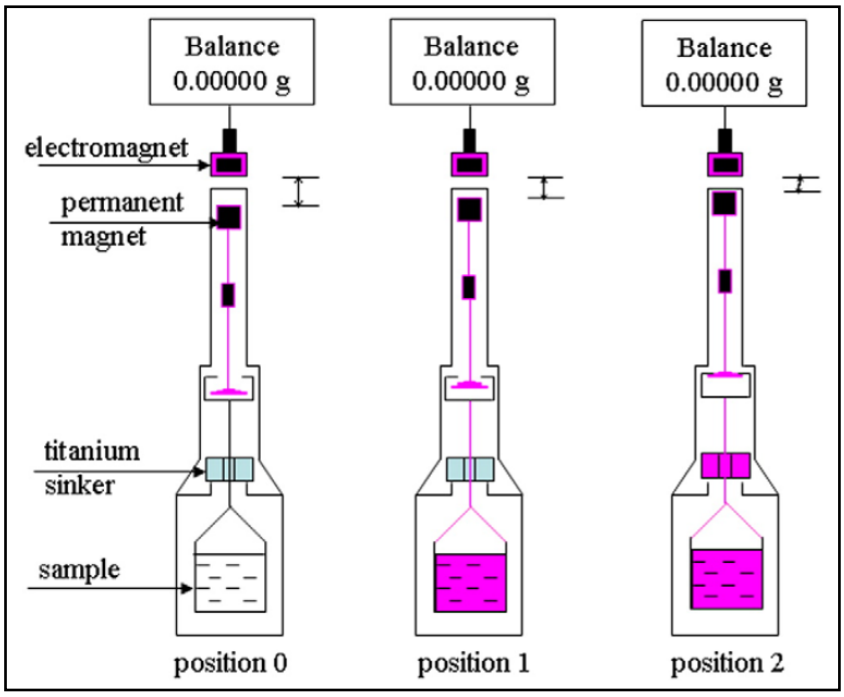

Figure 3.3: Schematic diagram of gravimetric method with sample cell and suspension magnetic balance (after Charriere *et al.*, 2010)

The weights of permanent magnet, basket and sinker can be weighed with the balance system (Figure 3.3). At the beginning, the balance is tarred and calibrated by the mass data of the permanent magnet. Secondly, buoyancy correction is calculated by measuring values of gas density d_{gas} determined by the balance and the system volume V_{system}, which accounts for the extra volumes of metal part and the coal. At a certain temperature and pressure condition, the mass of the adsorbed gas $M_{adsorbed}$ can be calculated by the following equation:

$$M_{adsorbed} = M_{total} - V_{system} d_{gas} - M_{coal} \quad (3\text{-}7)$$

Where M_{total} is the coal's total mass, d_{gas} is the gas density in the cell, V_{system} is the system volume and M_{coal} is the mass of the coal sample at vacuum.

All of the masses, including M_{total} and M_{coal}, can be measured directly by the balance with the precision of ±10 μg. d_{gas} can be calculated from the values of volume V_{system} and mass M_{sinker} of the sinker and the mass $(M_{sinker})_{P,T}$ with a fixed temperature and pressure condition, thus:

$$d_{gas} = \frac{M_{sinker} - (M_{sinker})_{P,T}}{V_{system}} \quad (3\text{-}8)$$

Where the mass $(M_{sinker})_{P,T}$ is the weight variation between status1 and in status 2 (Figure 3.3). The coal's volume can be calculated by the coal's density and the coal's mass. The volume of metal parts in the system needs to be measured using helium expansion method in the experiment process.

3.2.2.2 Both sample cell and reference cell (or reference volume)

The gravimetric method with both sample cell and reference cell shown in Figure 3.4 was introduced by Saghafi *et al*. (2007). This testing method can directly measure the weight increase of coal sample when the coal achieves adsorption equilibrium with the increase of gas pressure. The gas density of the free phase can be measured by the empty reference cell at the same time which owns the same temperature and pressure condition as the coal sample cell.

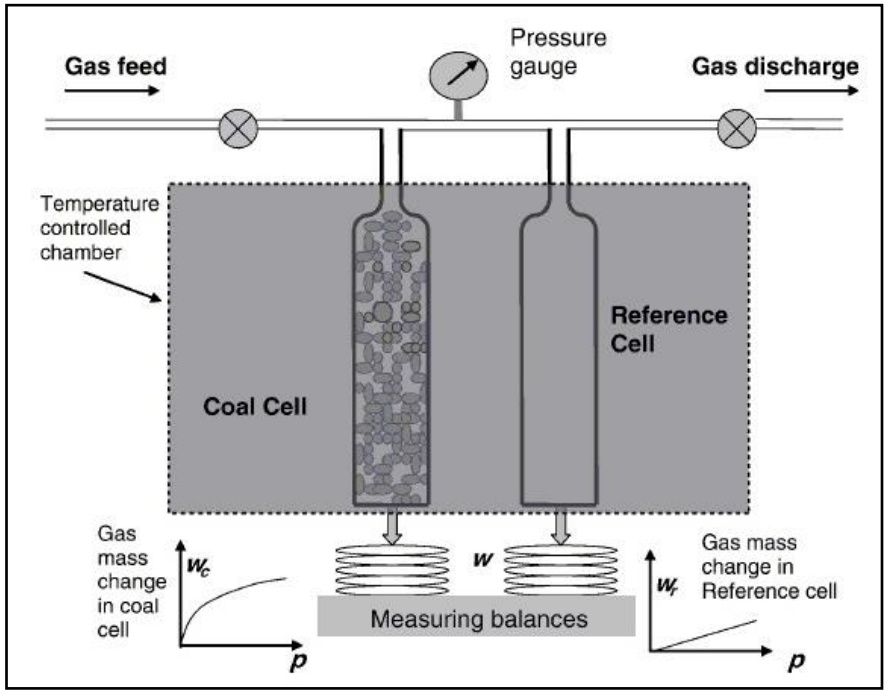

Figure 3.4: Schematic diagram of gravimetric method with both sample cell and reference cell (after Saghafi *et al.*, 2007)

In this gravimetric method, the weights increase of the empty reference cell and the cell with coal sample in it, are measured when two cells are connected to the charging gas at the same pressure condition. The density of gas at the testing pressure and temperature condition is calculated with the empty reference cell, the equation shows in the following equation:

$$d_{gas} = \frac{M_{reference\ cell}}{V_{reference\ cell}} \tag{3-9}$$

Where d_{gas} is the density of gas phase, $M_{reference\ cell}$ refers to the gas mass in the reference cell and $V_{reference\ cell}$ is the amount of volume inside the reference cell. The Gipps adsorption can be calculated by the equation:

$$M_{adsorbed} = M_{total} - V_{void} d_{gas} \quad (3\text{-}10)$$

Where M_{total} refers to the total mass of gas in the coal sample cell, V_{void} means the void volume, which is the total sample cell's volume subtracting the coal's volume. The repeating step from low to high pressure is used to get a complete isotherm and the amount of adsorbed gas is calculated by dividing Gibbs $M_{adsorbed}$ by the mass of coal tested. The amount of gas adsorbed in coal can also be expressed in volume per mass of coal by dividing the gas density.

3.2.3 OTHER METHODS

Other alternative test methods can also be used to record the coal sorption isotherms. Details of the under-confining stress sorption method and the sorption direct determining method are discussed in the following part.

3.2.3.1 Under-confining stress

Introduced by Pone *et al*. (2009), the sorption test method with confining stress, as shown in Figure 3.5, was used in Pennsylvania State University in USA. The diameter of 25 mm and length of 63 mm core sample is confined to represent the *in situ* condition. The diamond saw is used to cut and obtain the core coal samples to carry out sorption experiments with different confining stress conditions.

As shown in Figure 3.5, the sorption isotherm calculation method is the same as the volumetric method with both sample cell and reference cell, with the only difference of confining stress being applied during the sorption test.

The system consists of sample cell and reference cell, both of whose volume have already accurately determined. The cells are immersed inside a temperature controlled condition (±0.1 ℃). Two distinct apparatus system were set up to accommodate experimental tests with or without confining stress conditions. The void or dead volume in the sample cell is calculated by helium injection the same principle as the other methods.

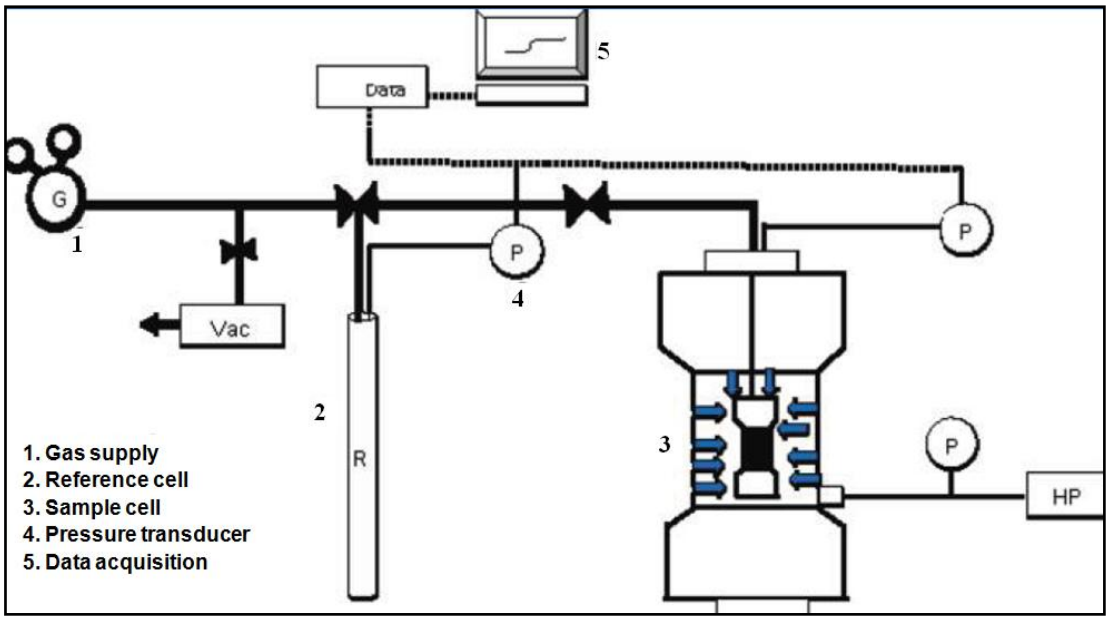

Figure 3.5: Schematic diagram of under-confining stress method (after Pone *et al.*, 2009)

3.2.3.2 Direct determining method

Introduced by Hol *et al*. (2011) as shown in Figure 3.6, this method was used in Utrecht University in Netherlands. A cylindrical coal sample, diameter of 4 mm and length of 4 mm, is jacketed inside a tightly fitted, annealed gold capsule which can be exposed to different gases at a constant temperature and pressure condition. The capsule has three main components, namely, (1) a cone and swage ring at the top of the capsule enabling the sealing the sample, (2) a ductile metal element (Au and In elements) wrapping material encapsulates the sample holder, allowing swelling to occur, and (3) an aluminium foil bag is attached to the capsule to capture the desorbed gas.

The swelling of coal in the sorption process can be obtained by the capsule's ductile deformation. As soon as the coal achieved the gas saturation, mechanical loading is used to seal the capsule and the external gas is discharged. This permits the gas to desorb from the sample and flow into the inflatable aluminium foil bag which is attached to the system of capsule. The volume of the bag, accounting for the gas amount stored in the coal, is obtained directly with the Archimedes method.

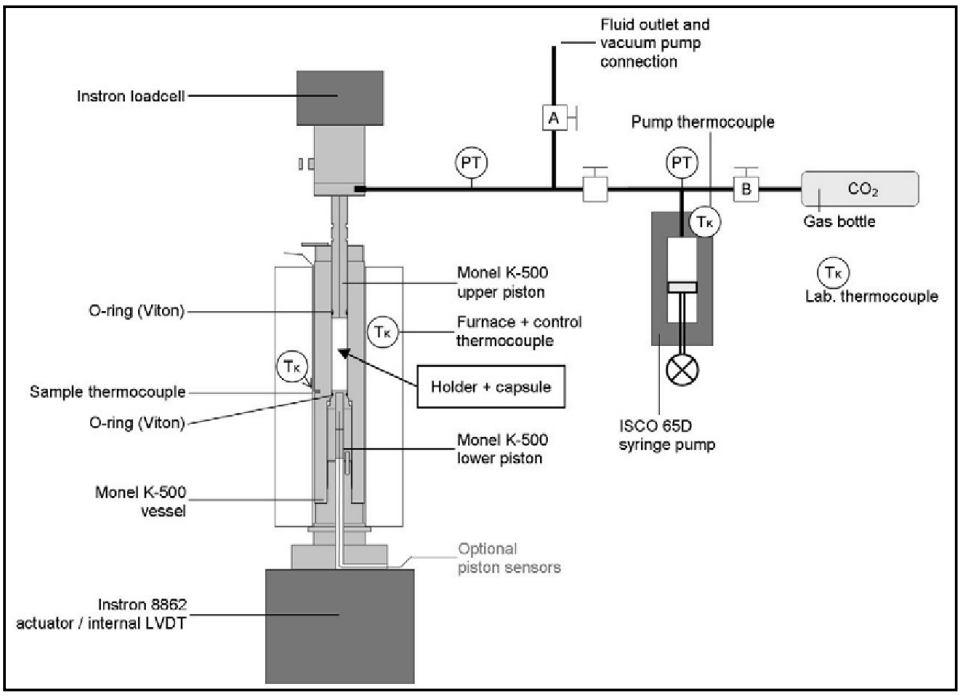

Figure 3.6: Schematic diagram of sorption direct determining method (after Hol *et al.*, 2011)

3.3 UNCERTAINTIES IN RECORDING SORPTION ISOTHERM

3.3.1 Helium as a reference gas

In the adsorption test, both the gravimetric and the volumetric methods use helium as reference gas to determine the total volume or the void volume of the sample cell or reference. Helium is commonly treated as an unadsorbing gas and it is assumed that the pore volume accessed by helium is the same as by sorbed gases CO_2 or CH_4. Actually, Gumma and Talu (2003) reported a method to modify sorption result for helium sorption, indicating that the helium sorption could contribute to an underestimation of the excess sorption capacity. As noted by Sakurovs *et al.* (2009), helium sorption is in the μmol/g range. If this degree of sorption capacity is compared with CH_4 or CO_2 gas, helium sorption is negligible. A small degree of helium sorption will lead to an underestimation of the sample volume for sorption tests.

3.3.2 Temperature

Inaccuracy in temperature measurement can also cause effects on sorption result. Busch and Gensterblum (2011) stated that temperature errors are commonly between 0.1 and 0.3 ℃ for experimental temperatures well above room temperature because it was typically harder to cool a system than to heat it and to maintain it at a constant temperature. As a result,

experimental temperature above room temperature was expected to have a less degree of uncertainty. A measurement performed in a project of the European Union, Busch and Gensterblum (2011) observed errors in excess sorption capacity calculations with an increase in temperature of 0.1 ℃. Evidently this effect can be neglected for CH_4 (<0.1 %), however for CO_2 it was quite significant and achieved a maximum close to the pressure of 7.39 MPa (critical pressure of CO_2) where small temperature changes could cause large variations in CO_2 density measurement.

3.3.3 Equations of state (EOS)

In most of the conventional sorption testing methods, an EOS is relied to estimate the density of the gases (He, CO_2, CH_4) at a certain condition of pressure and temperature, hence to calculate the gas or cell volumes. Innumerable different EOS for different gas are introduced, however the most commonly used ones are Span and Wagner (1996) and Setzmann and Wagner (1991) for CO_2 and CH_4 respectively, and the more universal EOS of Peng–Robinson (PR) and Soave–Redlich–Kwong (SRK) which can be used for a large range of gas species with variable interaction factors. Mavor *et al.* (2004) pointed out that these differences in EOS can also lead to variations of up to 20 % in the calculated sorption capacities. Actually, each EOS equation has its own precision limitation compared with the reality of gas state, indicating that every equation is just relatively accurate.

3.3.4 Volume calculation

The precise determination of the pump/reference volume or the void volume of the sample cell is indispensable for accurate calculation of the coal's sorption capacity in volumetric setup. Studies by Busch and Gensterblum (2011) showed the potential deviation from the originally calculated sorption result with the varying volumes of reference cell and void space in the sample cell could be by 0.5 %. In their study, as the volume of reference cell was constant and impacted directly on the void volume calculation of the sample cell, the error (0.5 %) remains constant within the entire pressure range. However, the variation of void volume of the sample cell led to an error which was larger than one order of magnitude. The error for CO_2 increased significantly close to the critical state and achieved an error of 12 % whilst the CH_4 result error increased linearly to 7 % at the final pressure in the experiment. The volume ratio of sample cell to the reference cell to sample cell had the effect on these errors. The inaccuracy of the EOS equation could also contribute to errors in volume calculation.

3.3.5 Impurity in the measurement gas

Small value of gas impurity in the void volume can result in inaccuracy of determining the gas density, thus to inaccurate sorption calculation. The cases of left residual gas in the coal can cause gas impurity, for example, sample cell is vacuumed or sample is degassed improperly, especially with larger coal particle samples. Also helium from void volume determination remaining in the pipe systems or impurity in the tested gas itself can influence the accuracy of sorption calculation. Gensterblum *et al.* (2010) suggested that the variation in CO_2 density at 10 MPa and 45 ℃ could be 0.1 % with various purities (0.9999 opposed to 0.999999), by using the EOS for mixture gas (Kunz *et al.*, 2007). If helium was not fully evacuated from the system prior to the CO_2 or CH_4 adsorption test, and with an assumption of a 0.1 MPa partial pressure of helium left, this could result in a much higher error of 6.1 %. The measurement gas contamination can also happen for sorption tests on coals containing water. Coal samples saturated at 30 ℃ and a relative humidity of 96–97 % under vacuum, can result in a certain partial pressure for water in the free gas phase, thus causing uncertainty in the gas density and the mass of sample (Busch and Gensterblum, 2011).

3.3.6 Gas dissolution in water and gas sorption on mineral matter

Gas sorption capacity is typically studied on a dry and ash free (daf) basis, with the assumption of no gas dissolving in water or sorption on mineral surface. Methane dissolving in water can be treated more or less negligible, however, CO_2 has proved to dissolve in water in different amount according to the coal's moisture content (Busch *et al.*, 2007). Gas sorbed on mineral surface (especially clay) has been claimed to be significant (Busch *et al.*, 2008; Weniger *et al.*, 2010; Wollenweber *et al.*, 2010). Although total amount of methane sorption on clay minerals is small, their CO_2 sorption capacity is in the same order as coal (Busch and Gensterblum, 2011). Consequently reporting CO_2 sorption capacity on a daf basis may be misleading to some extent, as dissolving in water and adsorption on clay mineral surface was apparent and can not be neglected in the sorption test.

3.3.7 Other sources of errors

A number of minor sources of error can occur in the sorption test (Busch and Gensterblum, 2011, van Hemert *et al.*, 2007). Cell contraction/expansion with thermal and mechanical reasons exists and this is mainly relevant when the volume calibration is carried out with large pressure difference between the reference cell charging and releasing into the sample

cell. The volume calibration or helium expansion performed at different temperatures compared with the sorption test can also cause this contraction/expansion problem. Cell volume changes with changes of gas pressure. Weight balances usually have a precision of 100 μg to ensure the mass is determined accurately. As sample mass larger than 1 g are typically used, this will pose a negligible error less than 0.01 %. It is unavoidable for each setup to have a certain leakage rate and if this rate is great, compared to the sorbed gas amount, then the apparatus should be modified and the operation process should be checked. Other sources of errors could also be attributed to the coal sample itself with moisture and volumetric effect, pressure gauge or transducer reading uncertainties or artificial operation induced errors.

3.4 COMPARISON OF DIFFERENT METHODS

For volumetric method with sample cell (equilibrium cell) and injection pump, the experimental method is based on the principle of mass balance, in which the accurate measurements of temperature, pressure and volume are required (Sudibandriyo *et al*., 2003). Pressure transducer and temperature gauge need to be calibrated regularly and cell volumes are usually estimated by Helium (He)-expansion method.

For volumetric method with both sample cell and reference cell (or reference volume), the pressure transducers needs to be calibrated in the range of studying pressure. Gensterblum *et al*. (2009) and Mohammed *et al*. (2009) confirmed that sorption isotherm measurement with volumetric devices requires highly accurate recording of pressures and temperatures. In addition, the volumetric method for gas adsorption measurement requires accurate calculation of the density of the free gas phase under certain temperature and pressure conditions in the experiment, thus an EOS is required for gas with better accuracy. The most widely used EOS equation is the Peng–Robinson or Redlich–Kwong equation (Krooss *et al*., 2002).

For gravimetric method with sample cell and suspension magnetic balance, the advantage is that the gas density at each pressure gradient can be determined without using an EOS equation and also allows measurements with condensable adsorbate. Particularly for gas mixtures where EOS is not available or of sufficient accuracy, this method offers more reasonable use (Busch and Gensterblum, 2011). The study of Weireld *et al*. (1999) shows the capability of their experimental device can achieve accurate adsorption isotherms with high temperature and high pressure conditions. This method also provides results which telly well with the volumetric method for a wide range of applicability. Nevertheless, two major issues,

i.e., the accurate volume evaluation of the coal sample and the gas density calculation, are commonly associated with the gravimetric method. Uncertainties relevant to the determination or calculation of the volume of coal can also result in significant error in the case of high gas density and low adsorbed mass.

For gravimetric method with both sample cell and reference cell (or reference volume), the advantage is that EOS can be obtained and checked from the density of the free gas phase and is measured at the same time in an empty reference cell maintained at the same temperature as well as pressure as the coal sample cell (Saghafi *et al*., 2007). This method is capable to directly measure the increase of the coal's weight when the sample is saturated with gas as gas pressure increases, thus needs a weighting balance with high accuracy measurement capacity.

Although the powdered coal samples prepared in the laboratory provide a fast indication of the sorption capacity of coal, compact coal monolith exists in the underground coal storage, thus it is essential to consider the *in situ* condition, especially confining stress, in order to get the meaningful estimate.

Sorption method testing result under-confining stress demonstrates that, 39 and 64 % CO_2 sorption capacity reduction occurs with the application of 6.9 and 13.8 MPa of confining stress respectively, similarly for CH_4 it amounted to 85 and 91 % reduction (Pone *et al.*, 2009). These findings emphasize it is essential to test coal at the representative *in situ* confining stress for reliable estimation of the adsorption capacity. This type of isotherm testing method is more suitable for laboratories with sophisticated equipment set up. The coal cores require a longer evacuation time and a prolonged period with adsorption compared with pulverised coal samples.

Unlike the conventional sorption isotherm testing methods, the direct sorption method can measure the absolute gas uptake in solid coal matrix cylinders directly, without the need of major volumetric corrections, assumptions related to the pore structure of coal, He-porosimetry, or the application of the EOS of gas. The technique makes use of a capsule consisting of ductile metals to jacket a coal sample, and traps the gas taken up in coal matrix directly. In comparison, this method is time-consuming and cannot differentiate between a free and an adsorbed phase, the absence of jumps around the critical pressure of CO_2 shows

that almost all of the CO_2 present in coal samples is adsorbed to the coal surface (Hol *et al*., 2011).

3.5 COMPARISON BETWEEN DIFFERENT LABORATORIES

Goodman *et al.* (2004) stated that although individual laboratories often determined their own intra-laboratory isotherm reproducibility, inter-laboratory isotherm reproducibility has not been reported. This made it difficult to compare the results obtained from different laboratories. Since no standard method or equipment for obtaining CO_2 isotherm data is available, laboratories reporting isotherms use their own, usually home-built, apparatus and procedures. Thus, it is possible that various laboratories report different storage capacities for the same coal samples.

Questions therefore arise concerning the extent to which differences in results can be attributed to the coal sample rather than to the details of the measurement technique. Goodman *et al.* (2004) also reported strict control must be placed on experimental methodology and variables in order to obtain reproducible results. Further, the research community recognised that several factors including the operator, the equipment, the calibration of the equipment, and the laboratory environment including temperature and humidity can influence the variability of a test result. This work provided guidance for estimating the reproducibility that might be expected when comparing published adsorption isotherms from different labs.

In the second inter-laboratory study, Goodman *et al.* (2007) compared the sorption isotherms of CO_2 on moisture-equilibrated Argonne coals at 55 ℃ and up to 15 MPa measured by six laboratories, which is also the first inter-laboratory comparison of carbon dioxide isotherm measurements for moisture-equilibrated coal. As received coal samples from the Argonne premium coal bank were moisture-equilibrated according to the modified standard procedure. The moisture-equilibrated values reported by the six laboratories for the same coals varied significantly among the laboratories and from the as-received moisture of the Argonne premium samples.

Goodman *et al.* (2007) also claimed the overall agreement between the laboratories was good up to 8 MPa with the exception of those instances where moisture content of the coals was either higher or lower than the as-received moisture threshold. At CO_2 pressures above 8 MPa, the reported sorption isotherms diverged significantly. This deviation was attributed to

substantial variations in equilibrium moisture contents. The fact that the laboratories followed essentially the same procedure indicates that the seemingly small modifications of the procedure had an unexpectedly large effect on the inter-laboratory reproducibility for coal moisture-equilibrated content.

In order to assess and improve the quality of high-pressure sorption isotherms of CO_2 on coals, an inter-laboratory study was conducted among three European research laboratories (Gensterblum *et al.*, 2009). Sorption experiments were performed at 45 ℃ and at pressures up to 16 MPa. A well-characterised activated carbon sample, Filtrasorb 400 (F400), was selected for the first series of measurements. This material was homogeneous, readily available and its chemical composition and micropore structure were similar to those of natural coal and facilitated the removal of moisture and attainment of a defined initial condition, which was one of the main sources of discrepancies in earlier inter-laboratory comparisons (Goodman *et al.*, 2007).

In their study (Gensterblum *et al.*, 2009), the isotherms determined by the participating laboratories on an F400 activated carbon sample showed good agreement with inter-laboratory deviations less than 5 % and a very good intra-laboratory reproducibility (variations <1 %). The direct comparison of manometric and gravimetric techniques indicated good agreement. The determination of accurate high-pressure sorption isotherms for CO_2 still represents a challenge. The study revealed, the manometric procedure, as a potential experimental problem and has identified strategies to avoid or minimise their impact on data quality. Careful adjustment of pressure steps during the measuring procedure and well-defined procedures for sample preparation were recommended.

Gensterblum *et al.* (2010) carried out the second European research laboratories comparison of high pressure CO_2 sorption isotherms on natural coals. The results showed that high-pressure CO_2 excess sorption isotherms on natural coals in the supercritical range can be determined accurately with both the gravimetric and manometric equipment. Methodological differences among the participating laboratories were negligible since the intra-laboratory comparison and the inter-laboratory comparison of the previous study with activated carbons were very good. In this study, a good agreement of the CO_2 excess sorption isotherms was observed for the low pressure range and larger deviations for the high pressure range.

The study of Gensterblum *et al.* (2010) reported the deviations between the CO_2 isotherms of the different laboratories are higher than the intra-laboratory deviations, indicating slight differences in procedures, in particular drying and sample preparation, but they could also be related to sample heterogeneity. For moderate-pressure CO_2 isotherms (up to 5 MPa), the intra-laboratory reproducibility is nearly equal to the difference between the different laboratories. For the high-pressure region, some improvements in the experimental procedure are still needed, especially the starting conditions.

Above all, inter-laboratory studies can help to identify and avoid errors and formulate standard procedures that improve overall data quality (Gensterblum *et al.*, 2009). Workshops and exchange of technical information among the member groups substantially contribute to an improvement of sample preparation and measuring procedures and the identification of potential errors in the determination of high-pressure gas sorption isotherms. The results confirm that sorption on natural coals in the supercritical range can be determined accurately with both gravimetric and volumetric method. As the need for inter-laboratory accuracy was well recognised by regulatory agencies and industry, this need will drive the development of standard methods (Goodman *et al.* 2004).

3.6 COAL SORPTION ISOTHERM TESTING IN UNIVERSITY OF WOLLONGONG

3.6.1 Apparatus

The gravimetric method with only sample cell, also referred to as the indirect gravimetric method, was first reported by Lama and Bartosiewicz (1982), and later by Aziz and Li (1999). Figure 3.7 shows the modified version of the apparatus currently being used in the gas laboratory, University of Wollongong, as reported also by Sereshki (2005) and Zhang *et al.* (2011). In this apparatus, each cell known as "bomb", has its own pressure transducer connected to the data logger so that the sorption process and pressure changes in the bomb can be readily determined. These bombs are immersed in the automatic temperature-controlled water bath, which allows the tests of coal isotherms at different temperatures. Approximately 200 g of coal ranging from powder size to standard coal core size can be used in the test. A high accuracy balance is used to weigh the bomb. The equipment has recently been modified to accommodate increases in temperature up to 100 ℃. The addition of a heat

isolation jacket outside the water bath as well as the insulation cover enabled the sample bombs to maintain the desired experimental temperature with an accuracy of 0.1 ℃.

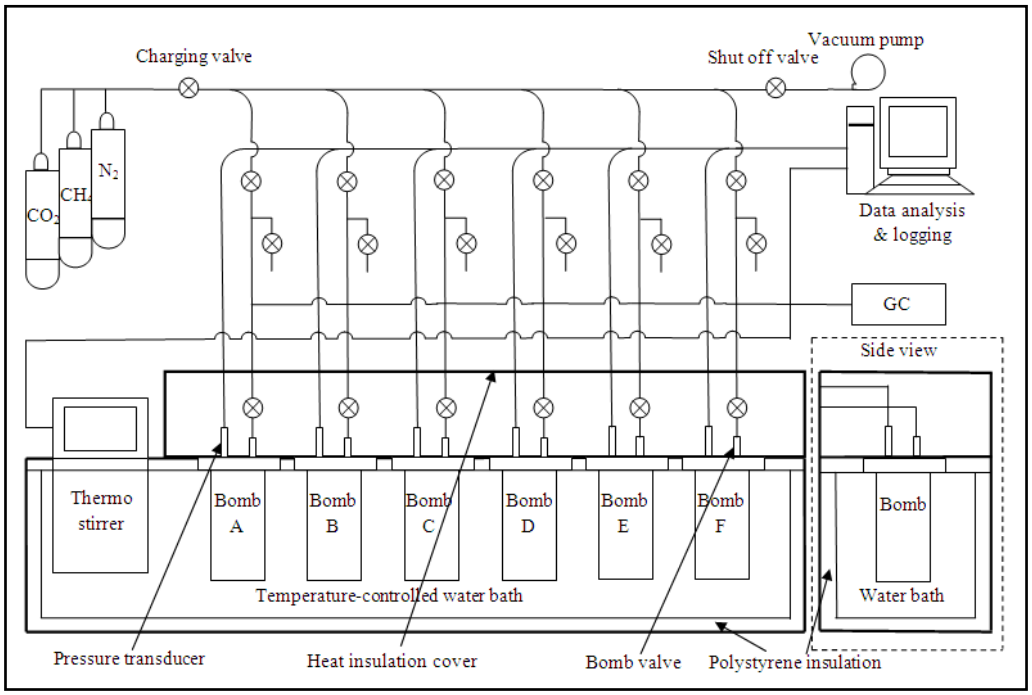

Figure 3.7: Schematic diagram of the modified gravimetric method with sample cells

3.6.2 Experimental procedure

The following experimental procedures are strictly followed for all the isotherm tests:

(1) Empty adsorption isotherm bomb is weighed;

(2) Coal sample is prepared and subsequently charged in the bomb and weighed;

(3) Bomb with coal sample is placed in the water bath and brought to the desired test temperature;

(4) Bomb is evacuated to make sure there is no air inside the bomb;

(5) Helium is introduced into the bomb and allowed to equilibrate until the pressure becomes constant;

(6) After equilibrium, the constant pressure is recorded and the bomb is weighed again;

(7) Repeat Steps 5 and 6, charging at different pressure steps of approximately 1, 2, 3, 4 MPa; this data is used to calculate the free volume (void volume) of the bomb and consequently the density of coal tested by helium;

(8) After determination of the void volume, the bomb is evacuated;

(9) The test gas is introduced into the bomb and allowed to equilibrate until the pressure becomes constant;

(10) After equilibrium, the constant pressure is recorded and the bomb is weighed again;

(11) Repeat steps 9 and 10 at different pressure steps to obtain final isotherm at approximate pressures of 0.5, 1, 2, 3, 4 MPa;

(12) The isotherm results are calculated as adsorbed volume per mass of coal at Normal Temperature and Pressure (NTP) condition which is 20 ℃ and 1 atm (101.325 kPa), the Australia standard condition.

3.6.3 Calculation method

3.6.3.1 SRK equation calculation

SRK equation is shown in Appendix B in detail. In the SRK equation calculation method (Appendix C), at each of the pressure steps, the total mass of gas in the bomb is directly weighed and the total gas in the bomb can be calculated by:

$$n_{total} = \frac{M_{total}}{M_{gas}} \tag{3-11}$$

Where n_{total} is the total amount-of-substance of gas, M_{total} is the total gas weight in bomb and M_{gas} is the mole mass of gas. The amount-of-substance of gas in the void space can thus be calculated using the following SRK equation:

$$PV_{void} = n_{void} Z_{SRK} RT \tag{3-12}$$

Where n_{void} is the void volume of the bomb, V_{void} is the void volume, calculated with the helium expansion, P is the equilibrium gas pressure inside the bomb, which can be measured with the transducer, T is the experiment temperature, R is universal gas constant, Z_{SRK} is the compressibility factor of the tested gas calculated with the SRK equation at the pressure P and temperature T. Using n_{total} and n_{void}, the Gibbs (Excess) amount of adsorbed gas can be calculated as:

$$n_{adsorbed} = n_{total} - n_{void} \tag{3-13}$$

The adsorption isotherm is expressed in terms of volume in NTP condition, hence the adsorbed volume is:

$$v_{adsorbed} = n_{adsorbed} V_m \tag{3-14}$$

Where $V_{adsorbed}$ is the adsorbed volume of gas and V_m is the mole volume of gas at NTP. For each of the pressure steps, the Gibbs adsorbed gas for the isotherm is calculated by dividing Gibbs $v_{adsorbed}$ by the mass of coal in the cell.

3.6.3.2 Calibration curve calculation

A modified calculation method called the calibration method with the real gas law is generated and used in this study (Appendix D). The method can be directly used to convert the volume of adsorbed gas from different conditions to NTP. The modified calibration method does not require the compressibility factor to be calculated with the EOS at every new pressure and temperature condition. The total volume of gas in the bomb at each of pressure level is calculated:

$$v_{total} = \frac{M_{total}}{d_{gas}} \tag{3-15}$$

Where v_{total} is the total volume of gas, M_{total} is the total mass of gas, accurately measured with a precise balance, d_{gas} is the gas density at NTP according to the real gas law, which takes into account the gas compressibility factor.

For each bomb at the tested temperature and at each pressure steps of 0.5, 1, 2, 3, 4MPa, the calibration of sorption gas carrying capacity of the empty bomb is evaluated, the volume from the calibration curve of gas carrying capacity of the bomb can be obtained:

$$v_{calibrated} = \frac{M_{calibrated}}{d_{gas}} \tag{3-16}$$

Where $v_{calibrated}$ is the calibrated volume of gas at NTP, $M_{calibrated}$ is the gas mass at each of the pressure step, d_{gas} is the tested gas density. Thus the unadsorbed volume of gas (v_{void}) can be calculated with the following equation:

$$v_{void} = \frac{V_{void}}{V_{bomb}} v_{calibrated} \tag{3-17}$$

Where v_{void} is the unadsorbed volume of gas at NTP, V_{void} is the void volume of bomb after the coal is placed inside the bomb which can be calculated with the helium expansion, V_{bomb} is the total bomb volume, $v_{calibtaed}$ is the volume of gas obtained from the volume calibration curve. Finally, the Gibbs (Excess) adsorbed volume of gas ($v_{adsorbed}$) can be calculated from the following equation:

$$v_{adsorbed} = v_{total} - v_{void} \quad (3\text{-}18)$$

The adsorbed gas for the isotherm is calculated by dividing Gibbs $v_{adsorbed}$ by the mass of coal in the cell.

3.6.3.3 Gibbs adsorbed volume and absolute adsorbed volume

As discussed by various researchers (Krooss *et al*., 2002; Busch *et al*., 2003; Goodman *et al*., 2007; Saghafi *et al*., 2007), the Gibbs sorption is based on the assumption of the constant ratio of void volume and condensed phase volume in the whole adsorption procedure. However, the gas adsorption by the coal can result in a non-uniform concentration in the vicinity of the coal's surface and an adsorbed phase is generated. At low gas pressure the adsorbed phase has a much higher specific density than gas phase, thus the volume of the adsorbed phase may be neglected compared with the sample cell's void volume. At high pressure the amount of adsorbed phase increases when the density difference between the free gas and the adsorbed gas decreases simultaneously. In order to obtain the "absolute sorption", the volume of the adsorbed phase has to be considered. Thus the bomb's volume is divided into the solid sample (coal) volume, the void volume and the volume of the adsorbed phase:

$$V_{bomb} = V_{coal} + (V_{void})_{corrected} + V_{adsorbed} \quad (3\text{-}19)$$

Where V_{coal} is the coal volume, $(V_{void})_{corrected}$ is the corrected void volume and $V_{adsorbed}$ is the volume of the adsorbed phase. The Gibbs excess adsorption quantity can be calculated with the following equation:

$$(M_{adsorbed})_{Gibbs} = M_{total} - V_{void} d_{gas} \quad (3\text{-}20)$$

Where M_{total} is the total mass of gas in the bomb, V_{void} is the uncorrected volume of void space, d_{gas} is the density of the gas phase at that temperature and pressure condition. The correct void volume can be calculated with the volume of the adsorbed phase subtracted from the uncorrected void volume:

$$(V_{void})_{corrected} = V_{void} - \frac{(M_{adsorbed})_{Absolute}}{d_{adsorbed}} \quad (3\text{-}21)$$

Where $(M_{adsorbed})_{Absolute}$ is the absolute adsorbed mass of gas, $d_{adsorbed}$ is the density of the adsorbed phase. The absolute adsorbed phase mass is:

$$(M_{adsorbed})_{Absolute} = M_{total} - (V_{void})_{corrected} d_{gas} \quad (3\text{-}22)$$

If the corrected void volume from Equation 3-21 is used in Equation 3-22, the adsorbed phase mass would be:

$$(M_{absorbed})_{Absolute} = \frac{d_{adsorbed}}{d_{adsorbed} - d_{gas}} (M_{adsorbed})_{Gibbs} \quad (3\text{-}23)$$

The adsorption isotherm is expressed in terms of volume, at NTP condition. So the absolute adsorbed volume of gas is:

$$(V_{adsorbed})_{Absolute} = \frac{(M_{adsorbed})_{Absolute}}{(d_{gas})_{NTP}} \quad (3\text{-}24)$$

Where $(v_{adsorbed})_{Absolute}$ is the absolute adsorbed volume of gas, $(d_{gas})_{NTP}$ is the gas density at NTP, the adsorbed gas for the isotherm is calculated by dividing $(V_{adsorbed})_{Absolute}$ by the mass of coal in the cell.

3.6.3.4 Discussion regarding the two calculation methods

In the sorption calculations with equation of real gas law, the amount-of-substance of gas in the void space is directly calculated by the more universal EOS of Soave–Redlich–Kwong (SRK) which can be used for a large suite of gas species, using different interaction parameters (Busch and Gensterblum, 2011). As a comparison, in the calibration curve method, the amount-of-substance of gas in the void space is determined by the existing calibrated curve, and the volume of adsorbed gas from different conditions to NTP is directly converted. This calculation does not require the EOS calculation at every pressure and temperature condition. Actually, coal sorption isotherm apparatus in the University of Wollongong is the combination of the gravimetric and volumetric methods, it utilises the gravimetric principle to calculate the total gas amount in the bomb and the volumetric principle to calculate the gas amount in the void space.

In general, the experiment operating procedure is the same for the two calculation methods, and both the calculation methods need to determine the density of coal tested by helium to calculate the void volume of the bomb before charging the sorption gas. The main difference of the two methods is how to calculate the gas amount in the void volume, either by SRK equation or calibration curve. In the calibration method, the gas density still needs to be calculated, usually it can be referred to published accurate gas density at different

temperature and pressure state; if the gas density is also determined by the SRK equation, the principle of the two methods will be the same as well as the accuracy of the results.

3.7 SUMMARY

Different methods have been used to obtain coal sorption isotherms, and according to their experimental setup and calculation principle, these can be broadly grouped into volumetric and gravimetric methods. The volumetric methods can be subdivided into those with sample cell (equilibrium cell) and injection pump and those with both sample cell and reference cell (or reference volume). The gravimetric methods include experimental apparatus with sample cell and suspension magnetic balance, as well as those with both sample cell and reference cell (or reference volume). The apparatus set up and the calculation method and the uncertainties in the sorption test are also introduced. Based upon the indirect gravimetric method, the modified coal sorption isotherm test at the University of Wollongong offers the advantage of directly converting the volume of adsorbed gas from different conditions to NTP condition, using the calibration curves.

Normal volumetric method requires precise measurements of pressure, volume, and temperature. Pressure transducer and temperature gauges need to be calibrated and cell volumes are usually estimated by the He-expansion method. EOS is required for gas with good precision as well. For the normal gravimetric method, the advantage is the gas density at each reference pressure can be determined without relying on an EOS. This method involves direct measurement of the increase in weight of charged gas or coal as it is saturated with gas at increasing gas pressures, this needs a precise measurement capacity of the balance.

Although the powdered coal samples provide a good indication of the gas sorption capacity, observations emphasize that it is necessary to use coal samples confined at representative *in situ* confining stress for reliable evaluation of the sorption capacities. Apart from the conventional sorption isotherm testing methods, another type of sorption test called the sorption direct determining method can directly measure the absolute gas uptake of solid coal matrix cylinders.

Studies have identified that there are different testing results existing with inter and intra laboratories, because of the different sample preparation and measuring procedures and the potential errors in the determination of high-pressure gas sorption isotherms. The need for

inter-laboratory accuracy was well recognised by regulatory agencies and industry, which will drive the development of standard methods.

Different factors such as temperature, moisture and coal particle size play a significant role in coal sorption characteristics. Accordingly, a series of experimental studies were undertaken to examine the relationship between various factors and coal surface free energy theory that will be discussed in the next chapter.

CHAPTER FOUR – FACTORS INFLUENCING SORPTION CHARACTERISTICS AND SURFACE FREE ENERGY OF COAL

4.1 INTRODUCTION

Gas sorption in coal has been studied over the years by many researchers (Briggs and Sinha, 1933; Moffat and Weale, 1955; Joubert *et al.*, 1973; Lingard *et al.*, 1984; Wu, 1994; Gode and Pehlivan, 2005; Zhang *et al.*, 2011), The coal sorption characteristics of moist coal at higher temperatures (>25 ℃) is recognised as being an attractive option for *in situ* sorption study. With the improvement in coal production, mines are facing the operational realities of underground workings with increased risk of gas explosion or outburst. Accurately identifying coal's sorption characteristics in changing environmental conditions will shed light on the behaviour of gas sorption and desorption from *in situ* coal, especially when mining is taking place in deeper coal deposits.

The testing apparatus of coal sorption, ash content and helium density testing as well as coal sample preparations in the gas laboratory at the University of Wollongong are introduced in this chapter. The influence of different factors on coal sorption characteristics with coal samples from hard-to-drain Bulli seams are discussed with particular reference to temperature, moisture, ash content and coal particle size. The coal surface free energy theory is introduced and used to analysis the experimental data. The theory of coal surface free energy tallies well with the experimental results and which can be used to explain both dry and moist coal sorption characteristics with CO_2, CH_4 and N_2 at higher temperatures.

4.2 EXPERIMENTAL SET UP AND SAMPLE PREPARATION

4.2.1 Coal sorption apparatus and coal samples

The indirect gravimetric method is used to calculate the quantity (by mass or volume) of gas adsorbed in and desorbed from coal. The gas sorption apparatus used in this study and shown in Figure 4.1 was described previously by Lama and Bartosiewicz (1982), Aziz and Ming-Li (1999) and Zhang *et al.* (2011). In this apparatus, each vessel, known as "bomb", has its own pressure transducer so that the sorption process and changes in bomb pressure can be readily determined. The equipment has been modified to accommodate increases in temperature up

to 100 ℃. The addition of a heat insulation jacket surrounding the water bath help to maintain the bombs at the desired experiment temperature with an accuracy of 0.1 ℃. An example of isotherm calculations with SRK equation and calibration curve (including calibration curve for the bomb) are shown in the Appendix C and D, respectively.

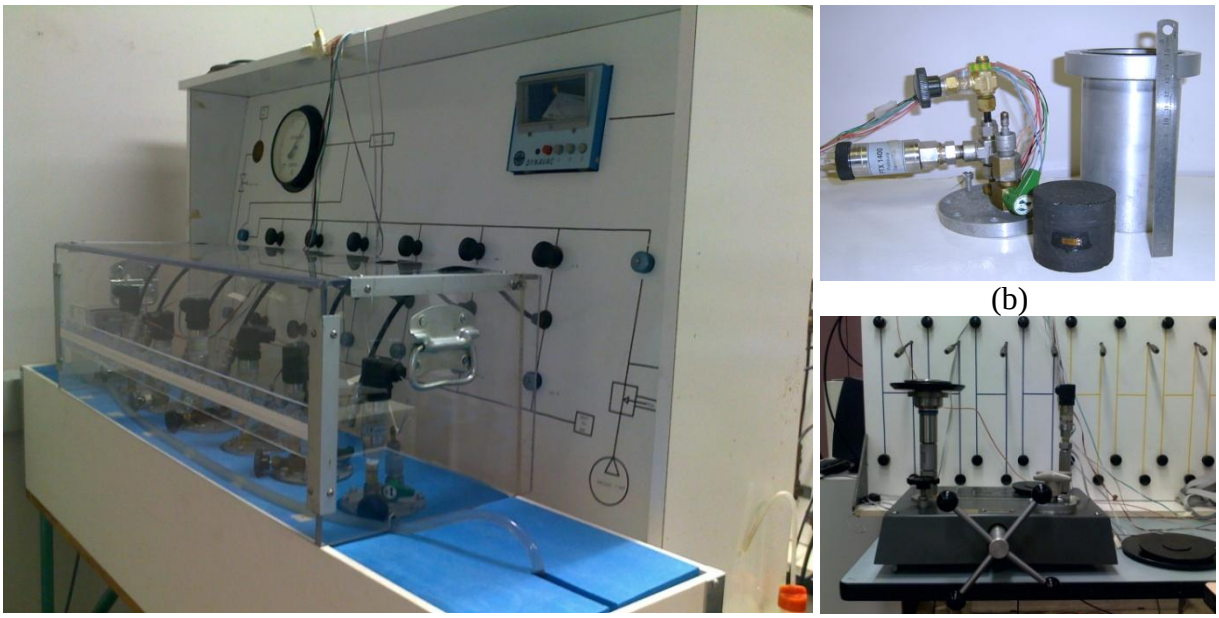

(a) (b) (c)

Figure 4.1: Schematic diagram of the gas sorption apparatus (a) sorption apparatus including bombs, water bath and charging board, (b) sorption bomb, (c) pressure calibration apparatus for pressure transducer

4.2.2 Coal sample retrieval and preparation for testing

The coal samples used in this chapter were collected from hard-to-drain areas in the Bulli seam, specifically from longwall panel 520, Area 5, West Cliff Colliery, as shown in Figure 4.2.

The coal samples used in the study consisted of the borehole cores as well as core samples prepared from coring of large coal lumps freshly collected the development headings. The retrieved large coal samples were wrapped in plastic sheet and taken to the laboratory, where they were immersed in water tanks to minimise oxidation and adverse environmental effects. Besides cores, fragments of coal were also used for the study. The fragments were crushed and sieved to obtain the appropriate particle sizes for the test. Coal particle sizes of 2.36-3.35 mm (2.4 mm), 8-9.5 mm (8 mm), 16-19 mm (16 mm) and coal powder 150-212 µm (150 µm) were used in this study.

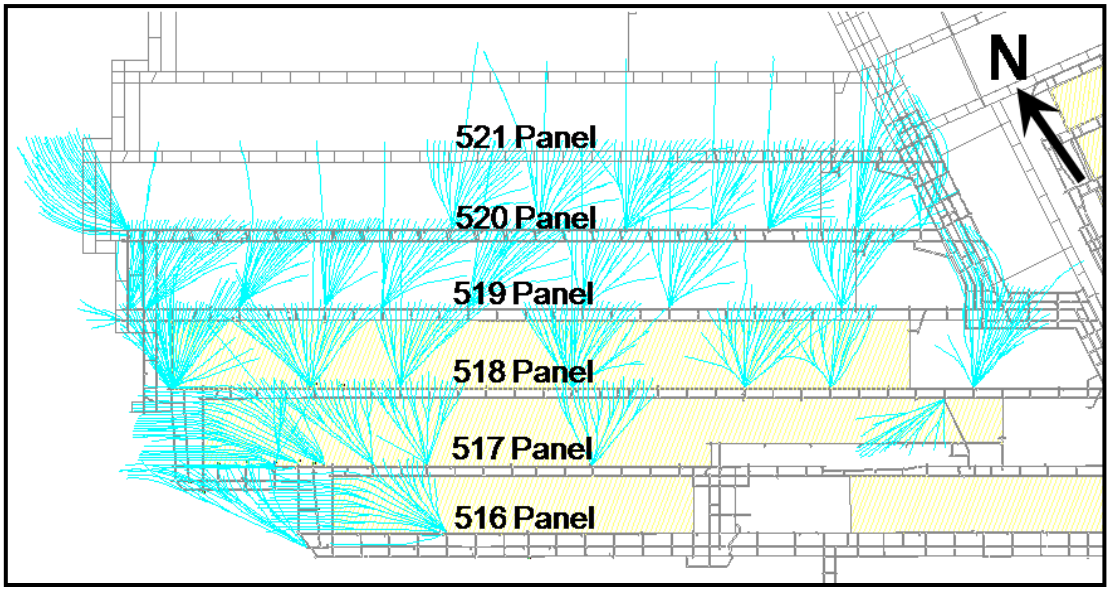

Figure 4.2: Mine plan showing the location of longwall panel 520, Area 5, West Cliff Colliery (blue lines represent the underground gas drainage boreholes) (after Black, 2012)

The preliminary information about the coal properties was sourced from the CSIRO report by Saghafi and Roberts (2008), shown in Table 4.1 and Table 4.2.

Table 4.1: Coal density and proximate analysis (after Saghafi and Roberts, 2008)

Sample Code	Depth (m)	Moisture (%)	Volatile Matter(%)	Fixed Carbon(%)	Volatile Matter(%,daf)	Coal Density (g/cm^3)
520	450	1.3	21.7	71.4	23.3	1.43

Table 4.2: Coal Petrography (after Saghafi and Roberts, 2008)

Sample Code	Vitrinite Reflectance (%)	Maceral (%)			Maceral (%, mineral free)			
		Vitrinite	Liptinite	Inertinite	Mineral	Vitrinite	Liptinite	Inertinite
520	1.28	41.6	0.1	55.3	3.0	42.9	0.1	57.0

The coal samples tested for sorption isotherms were crushed and sieved to obtain different particle sizes. Prior to sorption testing, the coal samples were dried in a desiccator containing water sorbing material. The desiccator was kept in a 60 ºC heated oven as show in Figure 4.3 (a, b). The purpose of vacuuming was to keep the coal from the air and prevent coal sample oxidation. The coal sample moisture content was checked regularly to achieve a total dry condition (zero moisture content).

(a) (b) (c)

Figure 4.3: Coal sample preparation (a) temperature controlled oven, (b) coal sample with water-sorbing silicon, (c) coal sample with saturated solution of potassium sulphate

A number of studies reported on the moisture adding processes to the coal (Joubert *et al.*, 1974; Clarkson and Bustin, 2000; Busch *et al.*, 2003; Day *et al.*, 2008). The method of adding moisture to the coal sample as reported by Day, *et al,* (2008), was subsequently used in this study. The dry coal samples were vacuumed in the desiccator containing the saturated solution of potassium sulphate at 25 ℃. The objective was to achieve 97 % relative humidity. The consistency of maintaining sample humidity was monitored by repeated weighing till the weight was constant indicating the moisture equilibrium, as shown in Figure 4.3(a, c).

Figure 4.4 shows the moisture content equilibrium test in terms of different coal particle size. It can be seen that the moisture content added to the sample was influenced by the sample fragment size. The 150 µm particle size achieved the highest level of moisture content at 2.12 % and the largest particle size of 16 mm had the lowest at 1.40 %. The coal samples with 2.12 % equilibrium moisture content were used in the following isotherm tests.

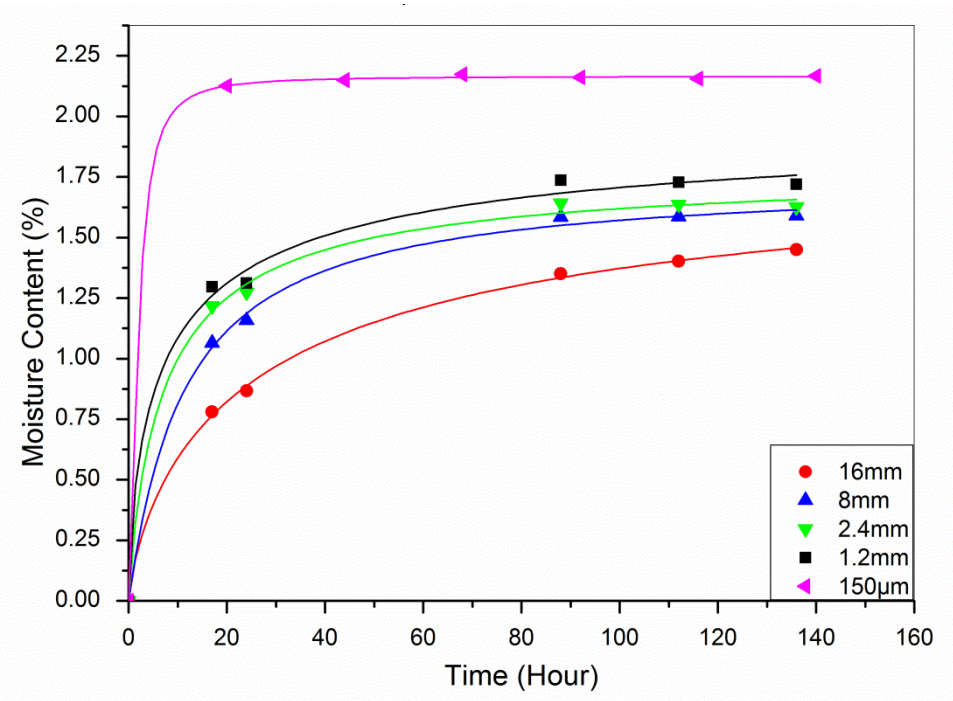

Figure 4.4: Moisture content equilibrium in coal samples at different particle size

In comparison, to obtain higher moisture content coal samples, the following steps were followed: at first different particle size coal samples were prepared, using a crusher and then oven dried. The sample was then immersed in distilled water for two hours to saturate it. Finally the mixture was filter drained. Table 4.3 shows the moisture content of coal samples at different coal particle sizes. The higher moisture content added to the coal samples related strongly to the sample size.

Table 4.3: Moisture content of coal samples at different particle size

Coal Size	54mm	16mm	8mm	2.4mm	1.2mm	150 µm
Moisture Content	3.45%	3.97%	4.53%	7.78%	10.95%	35%

It was found through both sample preparation tests that the water molecule is firstly adsorbed on the surface of coal and remained near the surface of the particle, rather than penetrating deep into the coal structure. This is clearly evident from the high rate of moisture content in fine particles in comparison with coarse samples. Actually, the interaction of carbon materials like natural coal with water is more complex than with nonpolar gases like helium, argon, nitrogen, methane, or carbon dioxide (Busch and Gensterblum, 2011). This complexity is due to the weak dispersion interaction of water with coal, the tendency of water to form hydrogen

bonds with other sorbed water molecules and surface chemical species, and the chemisorptive interaction with the coal mineral matter. Busch and Gensterblum (2011) also stated that up to a sample-specific limit additional water is only present as free water on the surface coal without occupying sorption sites.

4.2.3 Ash content test

Ash content of coal was carried out using a dedicated furnace and in accordance with the Australian Standard, methods for the analysis and testing of coal and coke (AS 1038.3-1989) for the determination of the ash content of coal. Figure 4.5(a) shows the Furnace apparatus, Figure 4.5(b, c) shows the micron coal sample in the crucible before and after incineration, respectively. Before the ash test, the coal samples are dried in a vacuumed desiccator containing water sorbing material and kept in the oven at 60 ºC for 24 hours.

A known mass of sample was heated in air to 500 ºC for 30 min, maintained at this temperature for another 30 min and further heated to 815 ºC until the sample was constant in mass. The percentage of ash was calculated from the mass of residue remaining after incineration. Results of the ash content test of different coal particle size are shown in Section 4.5.

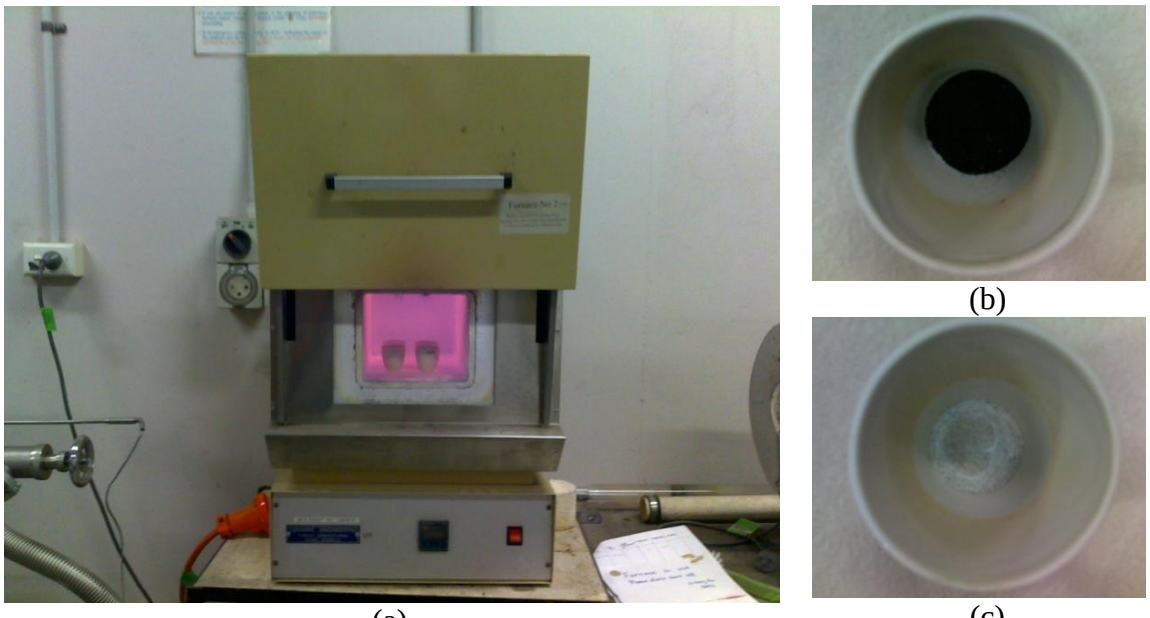

(a) (b) (c)

Figure 4.5: Ash content test (a) furnace, (b) coal sample before incineration, (c) coal sample after incineration

4.3 INFLUENCE OF TEMPERATURE ON COAL ADSORPTION ISOTHERMS

Lama and Bodziony (1996) reported that the term "sorption" consists of two parts: adsorption and absorption. Adsorption refers to the accumulation of gas on the surfaces of pores and cracks and absorption means the penetration of gas into the internal structure of coal. A summary of the various adsorption measurements in recent years are provided in Table 4.4. Siemons and Busch (2007) measured CO_2 sorption isotherms on both dry and moist coals of various ranks from coal basins from around the world and these measurements were made at temperature of 45 ℃. Day *et al.* (2008) carried out experiments on supercritical gas sorption of carbon dioxide on moist coals at temperatures of 21 ℃ and 55 ℃ and pressures up to 20 MPa. The difference of gas content due to different temperatures were not compared and the samples for the experiment were prepared by crushing and screening fresh air-dried lumps of coal to a particle size range of 0.5-1.0 mm.

Table 4.4: Sorption experiments performed by various authors (h.v.b, m.v.b. and l.v.b are high, medium and low volatile bituminous coals.) (after Busch and Gensterblum, 2011)

Author	Gas	Location	Coal rank	Method	Grain size (mm)	dry/moist	T (°C)	P (MPa)
Gruszkiewicz	CO_2, CH_4, CO_2/CH_4	Black Warrior Basin, USA	h.v.b.	Manometric	0.045–0.15; 1–2; 5–10	Dry, moist	35, 40	1.4–6.9
Busch	CO_2, CH_4	Upper Silesian Basin, Poland	h.v.b.	Manometric	<0.063; 0.063–0.177; 0.177–0.354; 0.354–0.707; 0.707–2; ~3	Dry, moist	32, 45	CO_2 <6; CH_4<10
Charriere	CO_2, CH_4	Loraine Basin, France	l.v.b.	Gravimetric	0.5–1	Dry	10–60	<5
Li	CO_2, CH_4	Inner Mongolia, Henan, Shanxi, China	subbituminous, m.v.b., anthracite	Manometric	0.354–1	Dry	35, 45, 55	<5
Pone	CO_2, CH_4	Western Kentucky Coalfield, USA	h.v.b.	Manometric	<0.25; cylindrical: d 2.5, l 6.2	Moist	20	3.1
Pan	CO_2, CH_4	Sydney Basin, Aus	m.v.b.	Flow experiment	cylindrical: d 25.4; l 82.6	dry, Moist	26	<4
Marecka	CO_2, CH_4	n.a.	semi-anthracite	Volumetric	<0.032; 0.30–0.10; 0.75–0.49; 1.50–1.00	n.a.	20, 30	n.a.
Ciembroniewicz	CO_2	Poland	anthracite	Manometric	0.49–0.75	n.a.	16–35	<0.065
Siemons	CO_2	Great Britain	h.v.b.; semi-anthracite	Manometric	0.04–0.06; 0.06–0.18; 0.35–0.71; 0.71–2.0	Dry, moist	45	<12
Clarkson	CO_2, CH_4	Lower Cretaceous Gates Formation, Canada	m.v.b.	Volumetric	<0.25; <4.76	CH_4 dry, moist; CO_2 dry	30	<2
Cui	CO_2, CH_4, N_2	–	h.v.b.	Manometric	<0.25	Moist	30	<7
Seewald	CH_4	Ruhr Basin, Germany	h.v.b.; m.v.b.; anthracite	Volumetric	0.04 to 1 in 9 fractions	Dry, moist	0, 15, 50	<0.1
Kelemen	CO_2, CH_4	Argonne Coals, US	h.v.b., l.v.b.	Gravimetric	~7mm^3	Dry	30, 75	1.8

4.3.1 Coal adsorption isotherm

Prior to sorption tests, the moisture content of the coal samples was determined in accordance with the Australian standard (AS 1038.25-2002) for the determination of the moisture content of coal. The testing procedure followed in the sorption study was according to the detailed procedure which was introduced previously in Chapter Three, Section 3.6. All samples were enclosed in bombs and systematically subjected to CO_2 and CH_4 gas pressurisation at various temperatures of 35 ℃, 45 ℃ and 55 ℃ respectively. The level of gas pressurisation of the samples was carried out initially at 500 kPa steps until reaching 1000 kPa and later it increased at 1000 kPa steps until reaching a maximum of 4000 kPa. Some of the important operational procedures were specially noted, for both dry and moist samples, the same coal sample was tested at 35 ℃, 45 ℃ and 55 ℃ at each of the pressure step, in order to avoid the samples' variation and extra errors. The equilibrium at different temperatures (35 ℃, 45 ℃ and 55 ℃) was achieved by changing the water bath temperature to avoid possible hysteresis due to repeated high pressure charging processes.

Figure 4.6 and Figure 4.7 show the adsorption isotherm at three temperatures for dry and moist coals (2.12 % moisture content). For both dry and moist coals, at every pressure step, from 0 to 4 MPa, the adsorbed volume of CO_2 and CH_4 is decreased with the increasing temperature step. The sorbed volume achieved the highest level at 35 ℃ and the lowest at 55 ℃. The results indicate clearly the exothermic nature of the adsorption process; higher temperature has a negative influence on the surface tension and results in decreased adsorption capacity of coal samples.

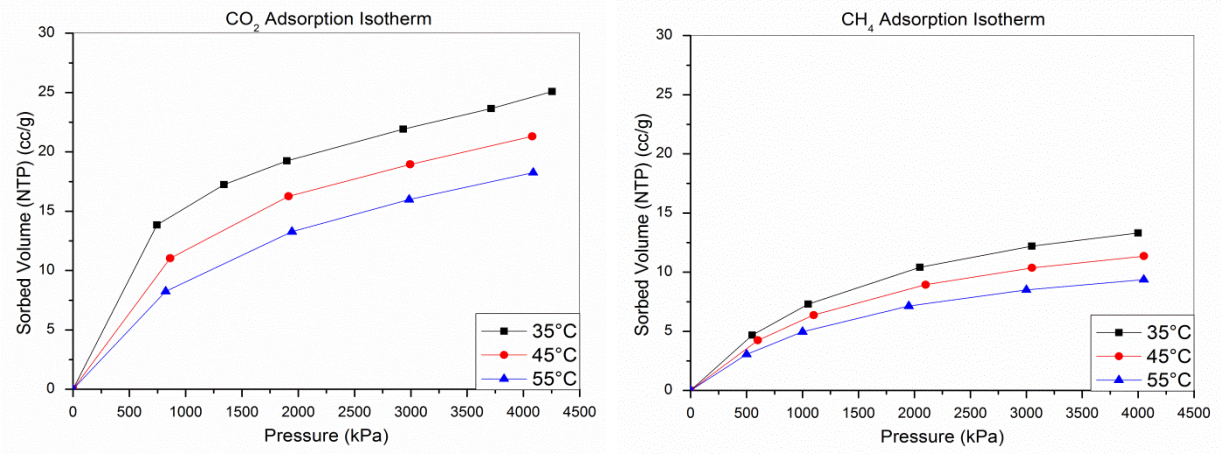

(a) (b)

Figure 4.6: CO_2 and CH_4 adsorption isotherms at different temperature (Dry samples)

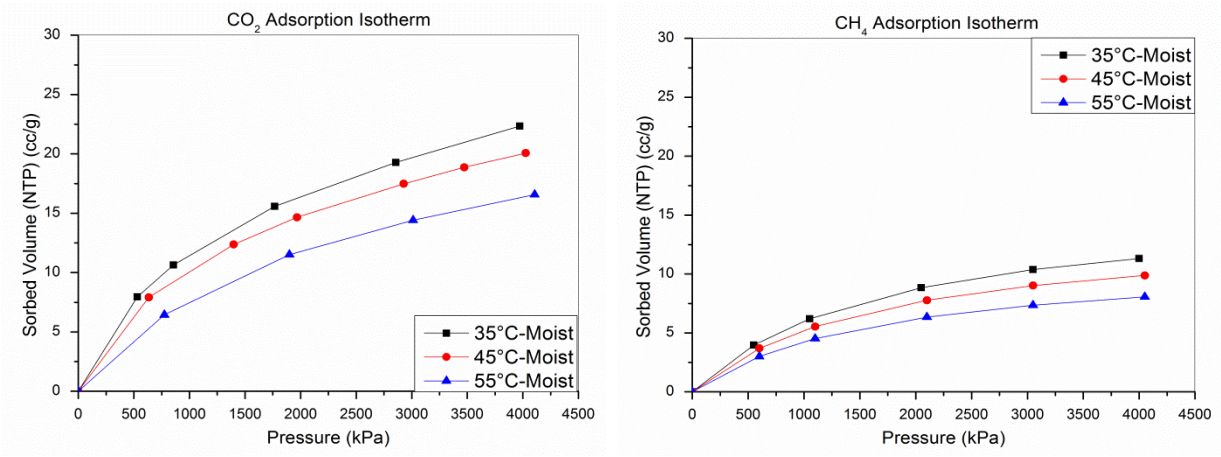

(a) (b)

Figure 4.7: CO_2 and CH_4 adsorption isotherms at different temperature (Moist samples)

4.3.2 Coal adsorption capacity

As already shown in Chapter Two (also Appendix A), in the Langmuir equation (Equation 4-1), the inverse of the slope of the Langmuir plot provided the Langmuir volume (V_L). The product of the Langmuir volume within the Y intercept gave the Langmuir pressure P_L. When the sorbed volume is half of the Langmuir volume, the pressure value is referred to as the Langmuir pressure P_L. Both V_L and P_L are important parameters for economic assessment of CBM resources. While V_L is the maximum sorption capacity of the coal, which is the value of gas content at high pressure, P_L represents the pressure to which the coalbed reservoir has to be depleted to obtain a 50 % recovery (Harpalani *et al.*, 2006).

$$\frac{P}{V} = \frac{1}{V_L} \times P + \frac{P_L}{V_L} \qquad (4\text{-}1)$$

Figure 4.8 shows that the CO_2 and CH_4 adsorption capacity analysis of dry and moist coals (2.12 % moisture content) at different temperatures are represented by their Langmuir volume (V_L). It is apparent that the Langmuir volume for CO_2 and CH_4 adsorption decreases with increasing temperature. The decreasing coal sorption capability of CO_2 and CH_4 with increasing temperature was confirmed by other researchers (Sakurovs *et al.*, 2008; He *et al.*, 2010; Busch and Gensterblum, 2011). Langmuir volume of CO_2 adsorption for dry coal follows the trend line: y = -0.5449x+54.3400 (R^2 = 0.894), and for CH_4 y = -0.2818x+ 28.3890 (R^2=0.908). The Langmuir volume of CO_2 adsorption for moist coal follows the trend line y = -0.4529x+ 46.7810 (R^2= 0.936), and for CH_4 y= -0.2329x+ 23.9340 (R^2= 0.916). The adsorption capacity of coal shows a linear decrease with increasing temperature.

For both the dry and moist coal samples tested, the decreasing rate of adsorption capacity was greater for CO_2 than CH_4, and for each gas test, the decreasing rate was higher for dry coals.

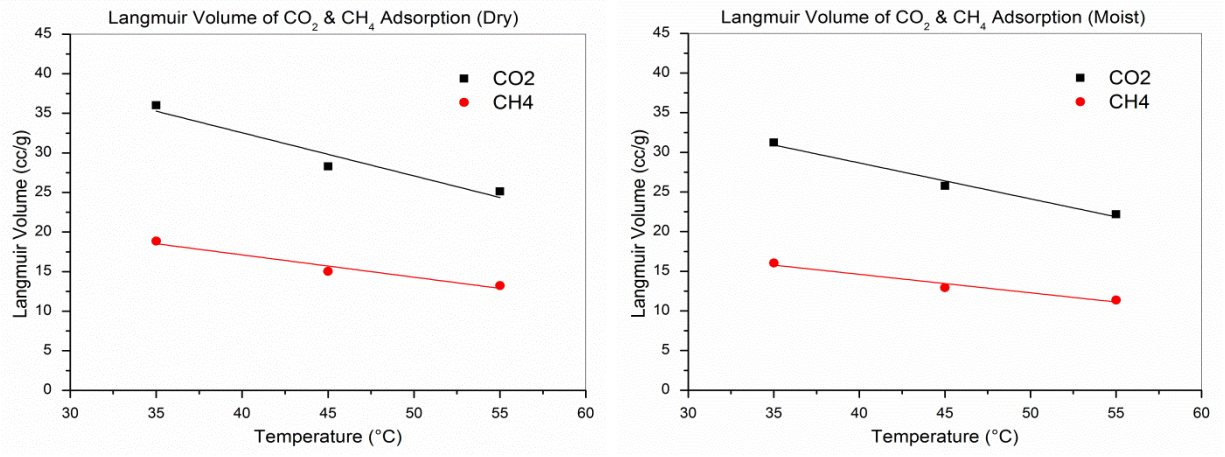

(a) (b)

Figure 4.8: CO_2 and CH_4 adsorption capacity of dry and moist at different temperature

For the tested coals at three temperature levels, the average adsorption capacity for dry coal for CO_2 reduced by 5.45 cc/g with temperature increase of every 10 ℃. The coal adsorption capacity of CO_2 in moist coal reduced by 4.53 cc/g. However, under similar situation the adsorption reduction capacity for CH_4 was in the order of 2.82 cc/g for dry coal and 2.33 cc/g for moist coal. It is indicated clearly greater reduction value for CO_2 than CH_4 is observed with increasing temperature on the adsorption capacity of coal.

Regarding the issue of CO_2 versus CH_4 sorption, several studies reported on sorption of both CO_2 and CH_4 using the same coal sample under different moisture conditions, in order to obtain information on the selectivity of the coal for either gas species (Busch *et al.*, 2003; Harpalani *et al.*, 2006; Day *et al.*, 2008; Li *et al.*, 2010). Higher CO_2 sorption values were observed as compared to CH_4, while the CO_2/CH_4 sorption ratio varied from 1.1 to 9.1 (Figure 4.9). A relative decrease in sorption ratio with coal rank was observed for moist coal, with a ratio of around 9 for low coal rank, decreasing to 1.2-1.5 for anthracite coals (Busch and Gensterblum, 2011). Busch and Gensterblum (2011) explained that the high CO_2/CH_4 sorption ratios for low coal maturity could (partly) be due to a much high solubility of CO_2 in water as compared with CH_4, considering the large moisture content for low rank coal (Figure 4.9). For dry coal such a relationship with coal rank was not observed and the data scatter for CO_2/CH_4 varied around 1-3 for different coals maturities (Busch and Gensterblum, 2011). It should be noted that some coal samples sorption measurements for pure CH_4, CO_2

indicate that some Sydney Basin coals can store twice as much CO_2 as CH_4 (Saghafi *et al.*, 2007).

In this study, the adsorption ratio of CO_2 versus CH_4 is 1.90 for dry coal and 1.96 for moist coal, which indicates for the medium volatile bituminous coal (m.v.b), CO_2/CH_4 ratio is higher for moist coal than dry coal and no apparent difference is found between CO_2/CH_4 sorption ratio and temperature increase.

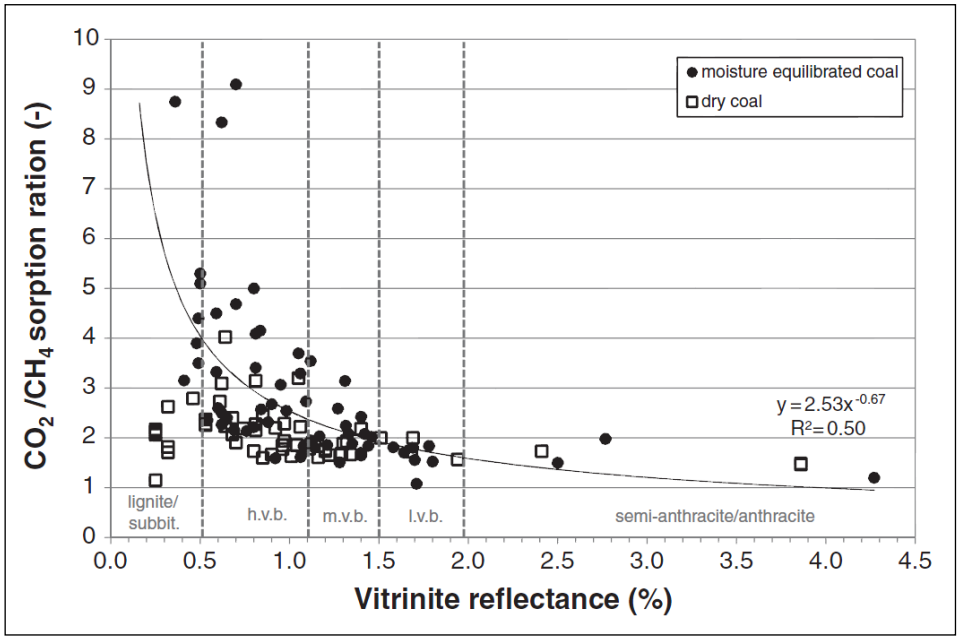

Figure 4.9: CO_2/CH_4 sorption ratio for different moist and dry coal samples at various temperatures as a function of coal rank. Values were picked between 1 and 5 MPa. Data fit for moist samples only (after Busch and Gensterblum, 2011)

4.4 INFLUENCE OF MOISTURE ON COAL ADSORPTION ISOTHERMS

4.4.1 Coal adsorption isotherm

Figure 4.10 shows that the isotherm curves at 35 ℃, 45 ℃ and 55 ℃ of moist 150 µm coal sample with a moisture content of 2.12 %. It is apparent from Figure 4.10 that the moist coal sample isotherms for both CO_2 and CH_4 have a much lower sorption capacity. This clearly indicates that the moisture in the coal reduces the adsorption capacity of coal.

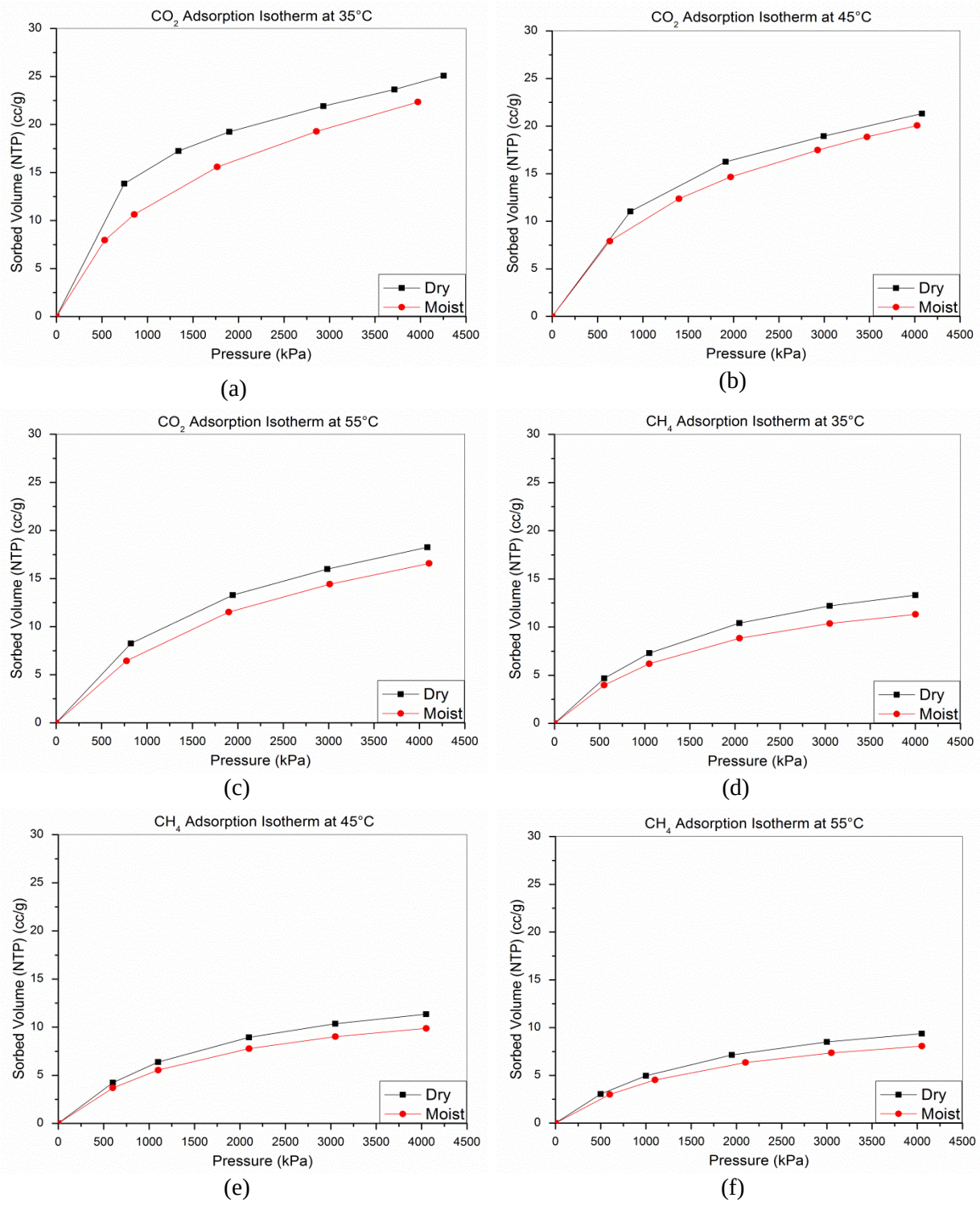

Figure 4.10: Dry and moist adsorption isotherms in terms of different temperature: (a), (b) and (c) is CO_2 at 35 ℃, 45 ℃ and 55 ℃ respectively; (d), (e) and (f) is CH_4 at 35 ℃, 45 ℃ and 55 ℃ respectively

This is in agreement with the previous study carried out by Mohammad *et al.* (2008), inferring that water was treated as "pacifying" the coal matrix; i.e., water occupies part of the coal pore surfaces, thus limiting the accessible space for adsorbing gases. In actuality, the adsorption on wet coal was less than that on dry coal, partly because water competes with gas

molecules for the available coal surface, impeding gas molecules from accessing this surface. Based on the study of Mohammad *et al.* (2008), the model parameter "gas surface area" for wet coal was considerably less than the area accessed by gas on the dry coal. The reduction of coal's adsorption capacity in this experiment reflects the effect of water on gas adsorption on wet coals, implicitly assuming that the water is strongly adsorbed that it denies access by CO_2 or CH_4 to a constant portion of the surface area throughout the pressure range of the measurements.

4.4.2 Coal adsorption capacity

Figure 4.11 shows the CO_2 and CH_4 adsorption capacity of dry and moist coals (2.12 % moisture content) in terms of different temperature. It is apparent that the Langmuir volume for CO_2 and CH_4 adsorption decreases with the moisture content. The decreasing coal sorption capability with the moisture content was confirmed by recent researchers (Day *et al.*, 2008; Mohammad *et al.*, 2008; He *et al.*, 2010; Busch and Gensterblum, 2011).

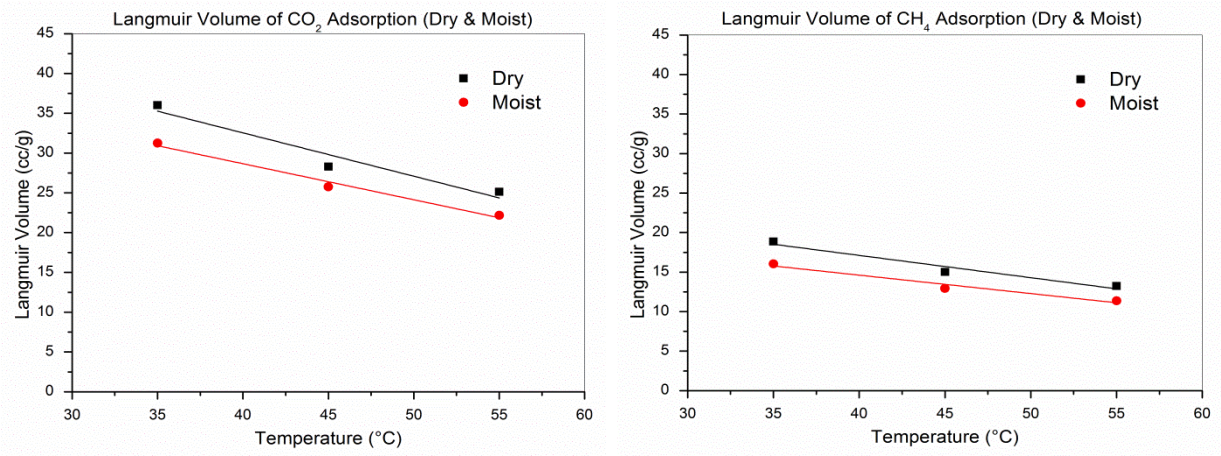

(a) (b)

Figure 4.11: CO_2 and CH_4 adsorption capacity of dry and moist coal at different temperature

The average value of coal adsorption capacity of CO_2 reduces 3.42 cc/g from dry samples to moist samples, while the average value of coal adsorption capacity of CH_4 reduces 2.26 cc/g. For the tested three temperatures, the average reduction ratio of coal adsorption capacity of CO_2 is 11.3 % from dry samples to moist samples, while the average reduction ratio of coal adsorption capacity of CH_4 is 14.3 %.

Moist coal had a variously lower maximum sorption capacity for both CO_2 and CH_4 than dry coal (Joubert *et al.*, 1974; Levy *et al.*, 1997; Clarkson and Bustin, 2000; Mohammad *et al.*, 2008), ranging from 15 % (Joubert *et al.*, 1974) to 60 % (Levy *et al.*, 1997), however, the

extent to which the capacity was reduced was dependent upon the rank of the coal (Day *et al.*, 2008; He *et al.*, 2010). Higher rank coals were less affected by the presence of moisture than low rank coals and all coals exhibited a certain moisture content beyond which further moisture did not affect the sorption capacity (Day *et al.*, 2008; Joubert *et al.*, 1973, 1974). Day *et al.* (2008) reported that in the case of the Illawarra coal, no further reduction in sorption capacity occurred beyond about 0.9 % moisture.

The experimental result also shows that the equilibrium moisture content of 2.12 % in coal has more effect on CH_4 than CO_2, indicating a significant competition for the sorption sites between methane and water molecules. As confirmed by other researchers (Day *et al.*, 2008; Busch and Gensterblum, 2011), although the general trend of reducing CH_4 capacity was similar to that for CO_2, in relative terms, the effect was greater for methane and the effect was less pronounced in higher rank Illawarra coal but the CH_4 capacity was still more affected than CO_2. Alcaniz-Mongue *et al.* (2002) found the process of water sorption was due to both physical sorption and chemical interaction with surface groups. In accordance with this process, micropore filling was progressive: the narrow micropores were filled first, and subsequently, water was sorbed in the remaining greater range of microporosity.

Figure 4.12 shows schematically the total set of sorption sites for CO_2, CH_4 and water on coal at constant temperature and pressure. CO_2 has the highest amount of sorption sites, followed by CH_4 and water (Busch and Gensterblum, 2011). The ratio of sorption capacity or sorption sites of CO_2 and CH_4 is in the range of 1 to 9 and changes strongly to lower ratios when moisture content decreases or coal rank increases (Busch *et al.*, 2003; Harpalani *et al.*, 2006; Day *et al.*, 2008; Li *et al.*, 2010). The intersection area of water and methane (γ) is smaller than the intersection area of water and CO_2 (β), as illustrated in Figure 4.12. Intersection δ represents the primary sorption sites of water. If there is water present in the system, these sorption sites will be occupied by water molecules because of its higher heat of sorption.

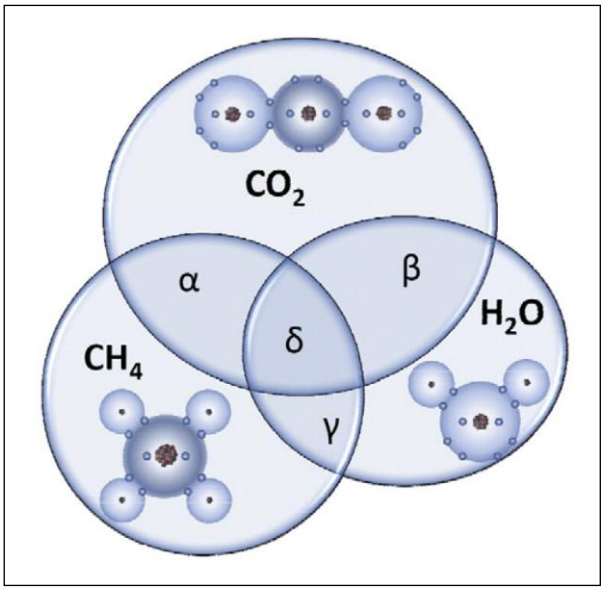

Figure 4.12: Sorption sites of each gas at one given fixed surface coverage (fixed P,T) and the intersection for multi-component sorption isotherms (after Busch and Gensterblum, 2011)

According to the above isotherm results in the experiment the gas adsorption isotherms are in general less sensitive to changes in temperature than to variations in moisture content, also confirmed by others' studies (Joubert *et al.*, 1974; Day *et al.*, 2008; Ozdemir and Schroeder, 2009). However, in the *in situ* condition, an increase in temperature results in a decrease in moisture-saturation. Lower equilibrium moisture contents will increase the gas sorption capacity; higher temperature will decrease the sorption capacity (Joubert *et al.*, 1974; Day *et al.*, 2008; Ozdemir and Schroeder, 2009), which is shown in Figure 4.13(a).

The results of this study also indicate that coal sorption capacity decrease with the increasing temperature and moist content, confirming with common expectation (Figure 4.13(a, b) Case 1). However, Crosdale *et al.* (2008) found no significant temperature dependence for CH_4 sorption capacity with low-rank coals at constant moisture content (Figure 4.13(b) Case 2). It is explained that, due to the high displacement ratios, it is possible that the release of water sorption sites could be able to compensate the decrease in CH_4 total sorption sites at higher temperatures.

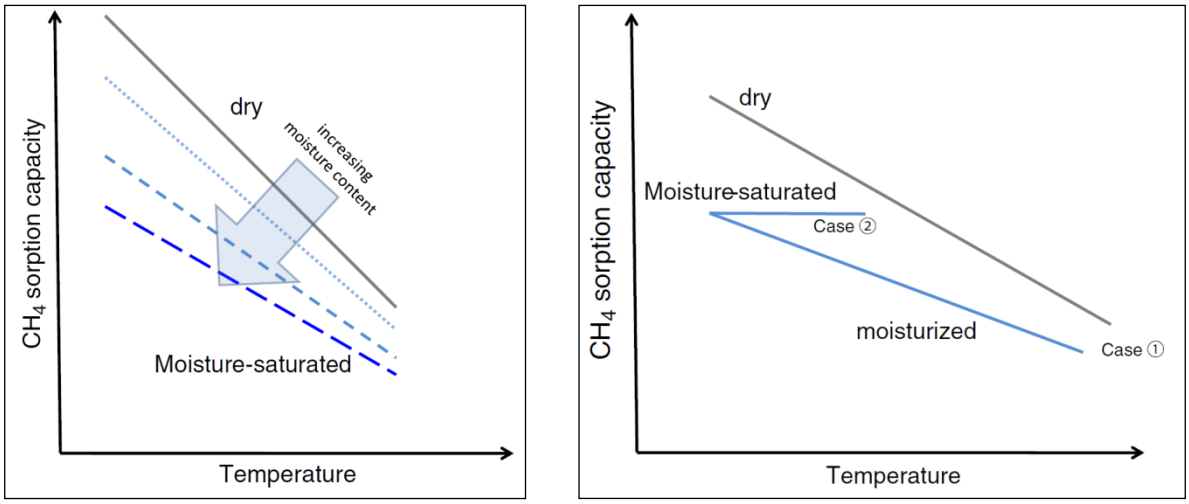

(a) (b)

Figure 4.13: (a) Schematic diagram of sorption capacity of coals at different moisture contents and as a function of temperature; (b) schematic plot of the sorption capacity in the dry and moisturized state as a function of temperature (after Busch and Gensterblum, 2011)

4.5 INFLUENCES OF COAL PARTICLE SIZE ON COAL ADSORPTION AND DESORPTION ISOTHERMS

The Bulli seam coal samples from West Cliff Colliery were next examined. Coal samples at 2.36-3.35 mm (2.4 mm), 8-9.5 mm (8 mm) and 16-19 mm (16 mm) particle size and pulverized samples at 150-212 μm (150 μm) were used in the study.

4.5.1 Coal ash content and helium density

For each of the coal samples tested with the isotherm, the ash content test was carried out in accordance with the Australian Standard (AS 1038.3-1989). The only variation from this standard was that different particle size coal samples were directly used in the ash content test, instead that usually powder coal sample was used in the standard. The relationship of different analytical bases to various coal components is shown in Figure 4.14. The percentage of ash was calculated from the mass of residue remaining after incineration. For the larger particle size sample ash content test, the heating time at 815 ℃ took longer to achieve the constant mass to ensure that the coal samples were totally incinerated. It should be noted that in this study all the residual material for each particle size tests which were not incinerated in the above condition could be treated as ash content.

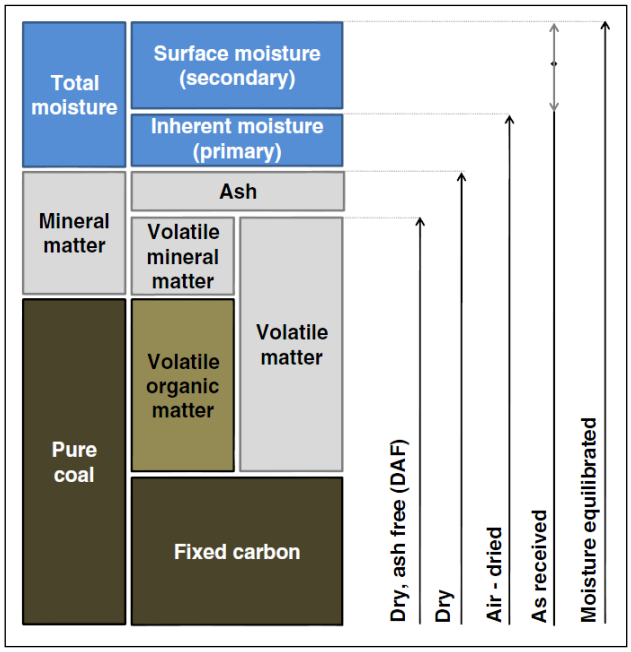

Figure 4.14: Relationship of different analytical bases to various coal components (after Busch and Gensterblum, 2011)

Before commencing the sorption isotherm experiments, the moisture content, ash content and helium tests for the different particle size coal samples were carried out to fully understand the basic parameters of tested coal samples. The moisture content of tested coal samples at different particle size was nearly zero to make sure the samples were totally dry. The ash content of coal was treated as a key parameter in the sorption experiment especially with different particle size samples and isotherms calculated on dry basis. This is confirmed by the results from Massarotto *et al.* (2010) who recommended measuring the ash content of the chosen particle size range to represent the original coal block. Figure 4.15 and Figure 4.16 show coal ash content test samples before and after incineration.

(a) (b) (c) (d)

Figure 4.15: Coal samples before the ash content test (a) 16 mm, (b) 8mm, (c) 2.4mm, (d) 150 µm

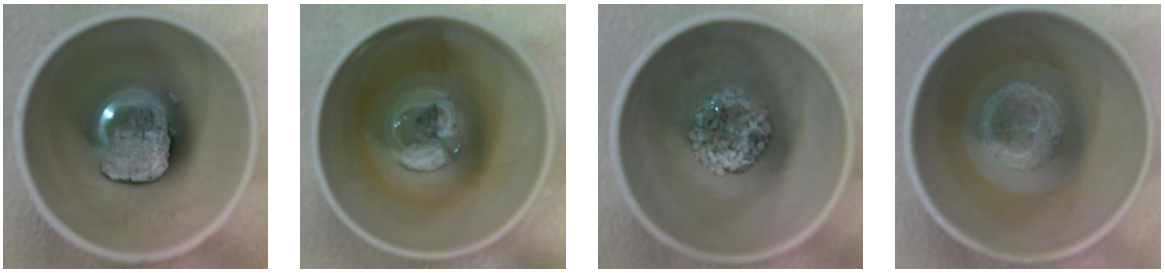

(a) (b) (c) (d)

Figure 4.16: Coal samples after the ash content test (a) 16 mm, (b) 8mm, (c) 2.4mm, (d) 150 µm

As shown in Figure 4.17, ash content of coal samples increased with increasing coal particle size. The ash content was 27.0 % for the 16 mm particle size while the ash content of the 150 µm was around 11.3 %. With linear fitting of the ash content results, the relationship between the ash content and coal particle size is y_1=0.9525x+10.7870 with R^2=0.866. The ash contents of cube samples of 15 mm were apparently larger than finer particle samples (200 µm). The difference in the ash content with particle size indicates that some ash content materials were lost during the powder sample preparation as some pore and matrix is the storage space for the mineral matter which is opened in the grinding process.

As shown in Figure 4.17(a), the helium density of coal also increases with the increasing coal particle size. The helium density of 16 mm sample achieves 1.39 g/cm^3 while the helium density of 150 µm is lowest which is 1.30 g/cm^3 and the linear relationship between them is y_2=0.0054x+1.2992 with R^2=0.882. One of the reasons why larger particle size coal samples have higher helium density is because they have higher ash content, which contains higher mineral matters with higher density than organic matters (i.e. macerals). In the process of grinding, coal is likely to lose the higher density material component and concurently increase the pore accessibility indicating that when coal is being ground, coal mass relatively decreases and coal volume increases resulting in the helium density decrease.

The linear relationship between the helium density of tested coal and the ash content is y_2=0.0057y_1+1.2380, coal helium density increases with the increasing ash content. As there is an apparent difference in the ash content between the different coal particle samples, it is important to report the ash content of the particle size range that is used for determining accurate adsorption measurements.

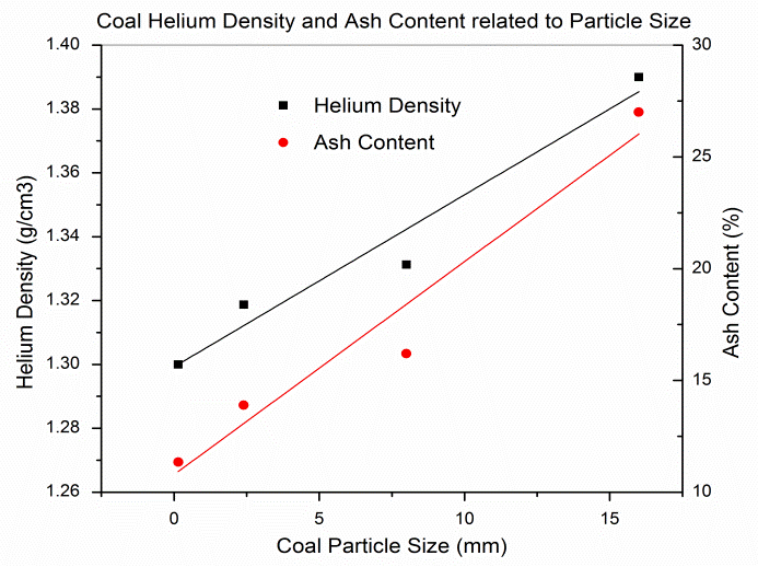

Figure 4.17: Coal helium density and ash content test results

4.5.2 Coal adsorption isotherms

The CO_2 adsorption isotherm in Figure 4.18 shows coal sorbed volume decreases with increasing coal particle size, both on a dry basis and on a dry ash free basis. This is similar to the results reported by Bae and Bhatia (2006), the fact that the larger particle size coal samples are ground down to finer particles, which possibly opens some otherwise closed pores, thus leading to an increased pore accessibility and consequently an increase in the CO_2 amount adsorbed. Another possible reason is that larger particle size samples need much longer time period for diffusion process to achieve complete saturation. By comparison of Figure 4.18(a) with Figure 4.18(b), the difference of CO_2 adsorption isotherms of different particle size coal sample calculated on a dry ash free basis is smaller than on a dry basis.

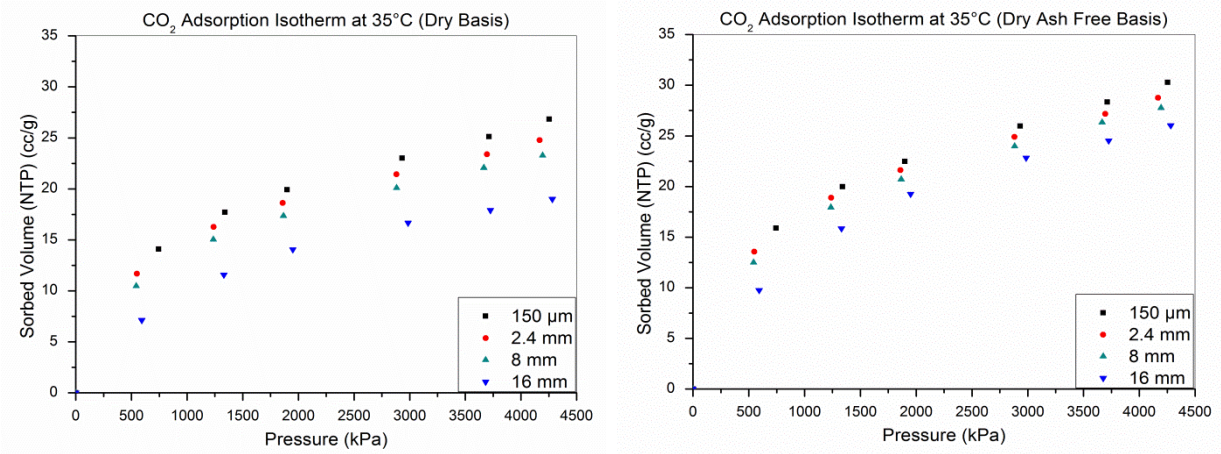

(a) (b)

Figure 4.18: Coal adsorption isotherm results with CO_2

CH_4 adsorption isotherms in Figure 4.19 follow the same trend as the CO_2 isotherms, showing the coal sorbed volume decreases with increasing coal particle size, both on a dry basis and dry ash free basis and the isotherm difference is smaller with dry ash free basis than dry basis. Results are similar to Beamish and O'Donnell (1992) who researched particle size on gas sorption capacity and claimed that reducing coal particle size to speed up the sorption process has often been confused as a possible source of falsely increasing storage capacity (Perkins and Cervik, 1969; Beamish and O'Donnell, 1992; Gamson and Beamish, 1992). A constant difference of isotherm with coal particle size results is also observed (Busch *et al.*, 2004). Busch *et al.* (2004) found that obvious variations existed in the isotherms for different particle size coal samples, but no specific trend was claimed in terms of shape or maximum sorption capacity.

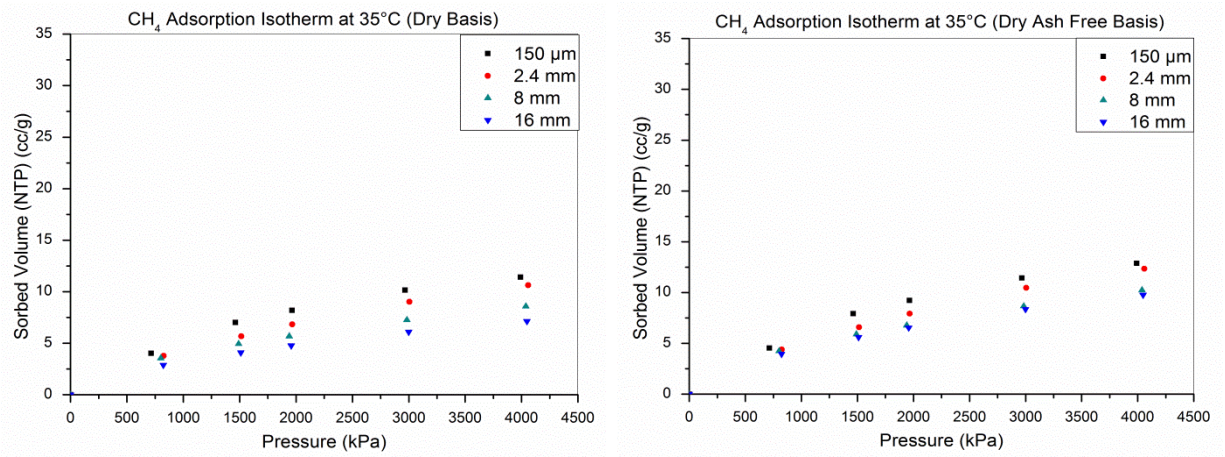

(a) (b)

Figure 4.19: Coal adsorption isotherm results with CH_4

4.5.3 Coal adsorption capacity

After the Langmuir parameters for each isotherm are calculated, the average Langmuir pressure is used to recalculate the Langmuir volume, ensuring that Langmuir volume for each isotherm is estimated under the same Langmuir pressure. As shown in Figure 4.20, the Langmuir volume decreases with the increasing coal particle size. The Langmuir volume of CO_2 adsorption follows the trend line: y= -0.3911x+35.9134 (R^2=0.929) for dry ash free basis and y= -0.6238x+31.8565 (R^2=0.917) for dry basis. The Langmuir volume of CH_4 adsorption follows the trend line: y= -0.2969x+18.3335 (R^2=0.696) for dry ash free basis and y= -0.3964x+16.2932 for dry basis (R^2=0.849). It can be seen that the Langmuir volume difference becomes larger between dry ash free basis and dry basis with the increasing coal particle size, especially for the CO_2 adsorption isotherm. The CO_2 adsorption capacity of this

bituminous coal with 150 µm coal size is 1.85 times larger than the CH_4 adsorption capacity (daf).

Beamish and O'Donnell (1992) calculated the percentage change in the increasing surface area by crushing a bituminous coal to 250 µm is of the order of 0.02 %, which indicated the sum of external surface area of coal particles is progressively smaller as compared to the internal surface area of the pores available for sorption. Thus increased accessibility to the new opened pore space is a more important reason than the increased coal surface area. It can also be concluded to some extent, that removing some of the ash content creates extra gas adsorption capacity. Different results are obtained between the results from this study and some other researchers, as referring to the low degree of statistical difference results of testing by Bielicki *et al.* (1972) and Ruppel *et al.* (1974) with the storage capacities of coals tested at particle sizes ranging from 3.36 mm - 44 µm and 12.7 mm - 74 µm respectively.

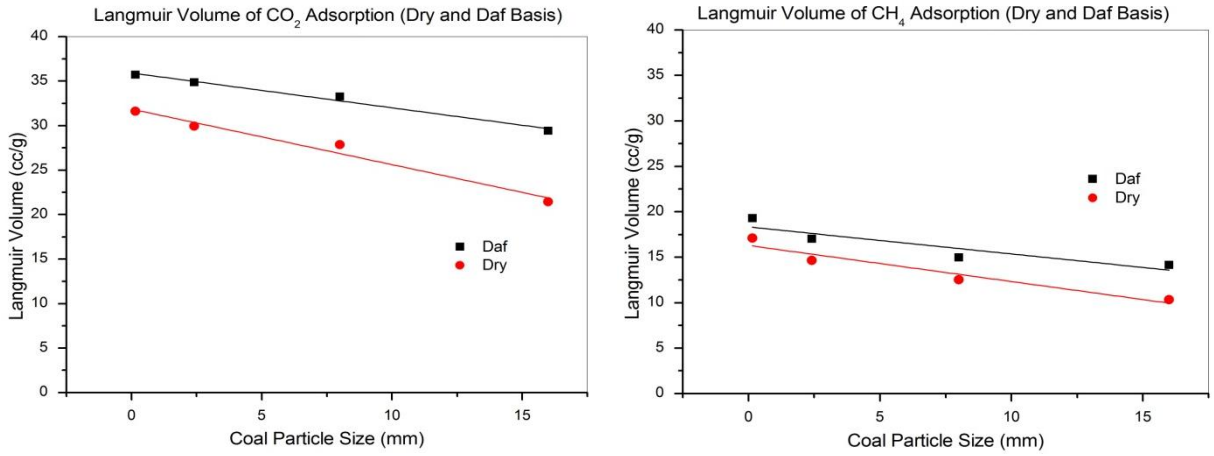

(a) (b)

Figure 4.20: Langmuir volume of adsorption isotherm with CO_2 and CH_4

4.5.4 Coal desorption isotherms

Figure 4.21shows the tested coal isotherms have apparent hysteresis for both CO_2 and CH_4 at all coal particle sizes. The phenomenon that desorption isotherms generally lie above the sorption isotherms represents the sorption hysteresis which is associated with the sorption/desorption process. Coal as a sorbate, when coal adsorbs and desorbs the sorbent, it has the hysteresis, which not only happens with gas which is widely observed (Goodman *et al.*, 2004; Medek *et al.*, 2006; He *et al.*, 2010), but also with water (McCutcheon and Barton, 1998; McCutcheon *et al.*, 2002; Charrière and Behra, 2010). The hysteresis effect indicates that the sorbent/ sorbate system is in a metastable state and at decreasing pressure the gas is

not readily released to the extent corresponding to the thermodynamic equilibrium value (Busch *et al.*, 2003).

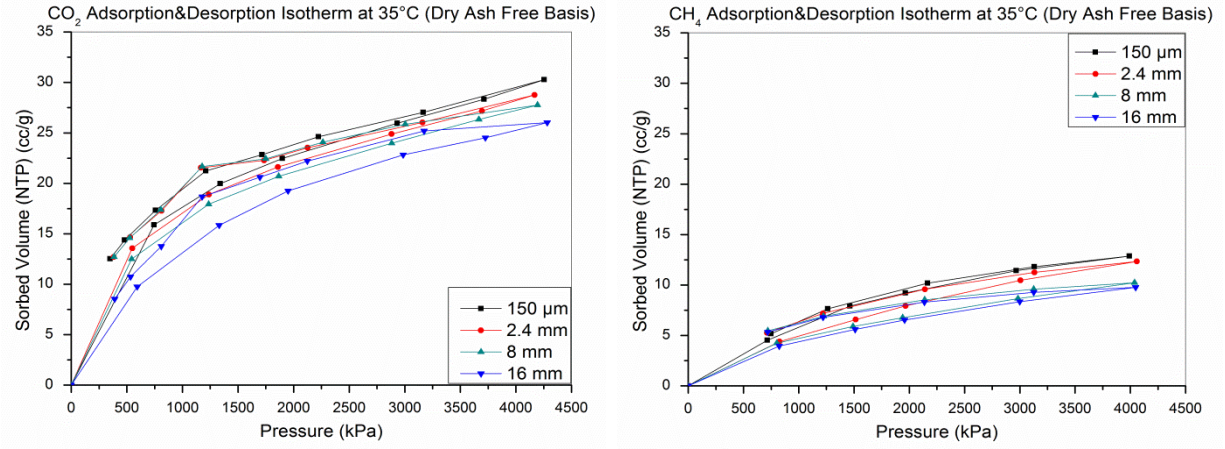

(a) (b)

Figure 4.21: Coal desorption isotherm results with CO_2 and CH_4

The study from Dutta *et al.* (2011), indicated that there were explanations other than those cited above for adsorption/desorption hysteresis, the nature of sorption of CO_2 molecules on coal may well be a reason for the hysteresis. The hysteresis due to this reason may get relatively smaller with a longer term desorption process. As shown in Figure 4.21(a), larger particle size coals show a larger hysteresis, CO_2 may also be absorbed/dissolved into the coal structure and during desorption, only the adsorbed molecules come out of the pore-spaces leaving behind the dissolved molecules in the coal structure. This was also confirmed by Ozdemir *et al.* (2004), where the positive deviation of CO_2 desorption was attributed to the swelling of the coal matrix. Shrinkage/swelling of the coal matrix is believed to be associated with the desorption/adsorption process. Coal with larger particle size has a better chance to trap the gas molecules as it has more pore system and longer path distances for gas to desorb from the internal surface.

The desorption hysteresis on coal or any adsorbent may occur due to two different reasons, which are the changes in the adsorbent properties/structures and/or the capillary condensation in the adsorbent micropores (Harpalani *et al.*, 2006). Tang *et al.* (2005) postulated that the surface geometry heterogeneity may account for the adsorption–desorption hysteresis. They mentioned the work of Seri-Levy and Avnir (1993) who used Monte-Carlo simulations of gas-solid systems to examine gas adsorption on rough surfaces of various geometries and computed significant hysteresis in equilibrium isotherms as a result of path dependent configurations of adsorbed molecules.

4.5.5 Coal desorption capacity

As the same calculation procedure with adsorption analysis, the Langmuir volume is recalculated with the average Langmuir pressure. As shown in Figure 4.22, Langmuir volume decreases with the increasing coal particle size. The Langmuir volume of CO_2 desorption follows the trend line: y= -0.4387x+39.9164 (R^2=0.755) for dry ash free basis and the Langmuir volume of CH_4 adsorption follows the trend line: y= -0.1725x+19.9469 (R^2=0.797) for dry ash free basis. It can be seen that the Langmuir volume difference becomes larger between adsorption and desorption isotherms with the increasing coal particle size, especially for CH_4 tests.

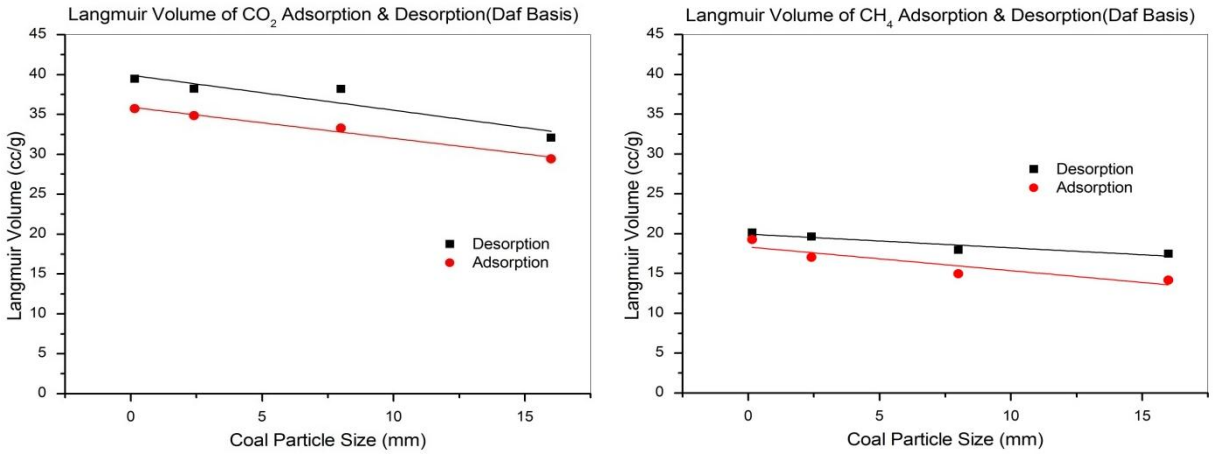

(a) (b)

Figure 4.22: Langmuir volume of desorption isotherm with CO_2 and CH_4

4.6 COAL SURFACE FREE ENERGY THEORY

The amount of adsorbed gas phase in coal depends both on the available surface area and the equilibrium state of surface attraction and repulsion forces (van der Waals forces). Equilibrium is reached when the total gas-solid surface potential energy is minimised. Adsorption of gas onto coal is a long-range weak interaction and the phenomenon is therefore a physisorption or physical adsorption process. In the process of physisorption, molecules of gas lose their kinetic energy and adhere to the coal surface. The amount of energy released is an indication of the strength of adsorption (Saghafi *et al.*, 2007).

The change of surface free energy of coal was the most important reason why different ranks of coal sorbed different quantities of gas (Wu, 1994). Based on the principle of surface chemistry, the coal surface free energy, which indicates the interaction capacity between the

coal surface and gas molecules, can be calculated. In his study, Wu (1994) found that the coal surface free energy related to the rank of coal.

Nie *et al.* (2000) examined the characteristics of coal surface free energy and found that the reduced value of surface tension is the key point to explain coal sorption characteristics. The reduced value of surface tension is affected by coal rank, temperature and gas type, that is, when the temperature and pressure are the same, the reduced value of surface tension for CH_4 is relatively smaller than CO_2 and for a certain gas the reduced value is decreased with increasing temperatures (i.e., step of 20 ℃, 30 ℃ and 40 ℃).

Adsorption of methane on coal at normal temperature and coal surface free energy was studied by Xie *et al.* (2004). The reduced value of surface tension decreased in accordance with the gas type and in the order of high CO_2, followed by CH_4 and N_2 in sequence. This explains why coal sorption capacity decreased in the same sequence. All their studies shed light on the principle that coal sorption behaviour with different gases can be better explained based on the coal surface free energy and the results can be adapted in the areas of coalbed methane reservoir resource assessment, enhanced gas drainage for gas recovery applications as well as carbon dioxide sequestration in coal seams.

4.6.1 Calculation

The theory of coal surface free energy has been studied for some time by several researchers (Wu, 1994; Nie *et al.*, 2000; Xie *et al.*, 2004), and according to surface chemistry theory, when gas is adsorbed on the coal surface, the concentration of adsorbed gas on the surface area of coal is larger than the concentration in the coal structure (absorbed gas), this difference is called the surface excess Γ:

$$\Gamma = \frac{V}{V_0 S} \tag{4-2}$$

Where Γ is the surface excess, V is the adsorbed volume, V_0 is the molar volume of gas, which is 22.4 L/mol at standard condition and S is the specific surface area of coal. When the coal sorbs the gas, the coal surface tension ($\boldsymbol{\gamma}$) will decrease. $\boldsymbol{\gamma}$ can be calculated from Gibbs equation:

$$-\mathrm{d}\gamma = RT\Gamma \mathrm{d}(\ln p) \tag{4-3}$$

Where $\boldsymbol{\gamma}$ is surface tension, R is universal gas constant which is 8.3143 J/mol· K, T is the absolute temperature and p is the gas pressure. Combining Equations 4-2 and 4-3 and by integrating the pressure from 0 to p, then the reduced value of surface tension can be calculated:

$$\Delta\gamma = \gamma_0 - \gamma = \frac{RT}{V_0 S}\int_0^p \frac{V}{p}\,dp \tag{4-4}$$

Where $\Delta\,\boldsymbol{\gamma}$ is the reduced value of surface tension, $\boldsymbol{\gamma}_0$ is the surface tension at vacuumed condition and $\boldsymbol{\gamma}$ is the surface tension. The Langmuir model used to calculate the adsorbed volume V is given by:

$$V = \frac{pV_L}{p + P_L} \tag{4-5}$$

Where V_L is the Langmuir volume and P_L is the Langmuir pressure. Then substituting for adsorbed volume V from Equation 4-5 into Equation 4-4, the reduced value of surface tension ($\Delta\boldsymbol{\gamma}$) can be simplified as:

$$\Delta\gamma = \frac{RT}{V_0 S}\int_0^p \frac{V_L}{p + P_L}\,dp = \frac{V_L RT}{V_0 S}\ln\left(1 + \frac{p}{P_L}\right) \tag{4-6}$$

From Equation 4-6, it can be concluded that the reduced value of surface tension ($\Delta\boldsymbol{\gamma}$) can be determined from the gas adsorbed volume, coal surface structure, sorption system temperature and gas pressure. According to surface chemistry theory, the sorption capacity is determined by the reduced value of surface tension, the larger the reduced value of surface tension, the stronger will be the sorption capacity.

4.6.2 Result analysis

4.6.2.1 Dry coal sample test analysis

The isotherm results of the 150 μm size dry coal samples with CO_2 has been analysed and the surface free energy was calculated as shown in Figure 4.23. Figure 4.23(b) shows the CO_2 surface free energy calculation results at different temperatures. In the adsorption process, at predetermined test temperatures, the reduced value of surface tension increased with the increasing pressure steps. As confirmed in Figure 4.23(a), the adsorption capacity of coal has increased with increasing gas pressure, in accordance with the surface chemistry theory. At

the same pressure point, the reduced value of surface tension ($\Delta\boldsymbol{\gamma}$) decreased with increasing temperature steps of 35 ℃, 45 ℃ and 55 ℃ respectively, which is in line with the adsorption isotherm. This indicates the exothermic nature of the adsorption process, in which higher temperature atmosphere will cause the negative influence on the surface tension and results in the decrease in the adsorption capacity of coal samples.

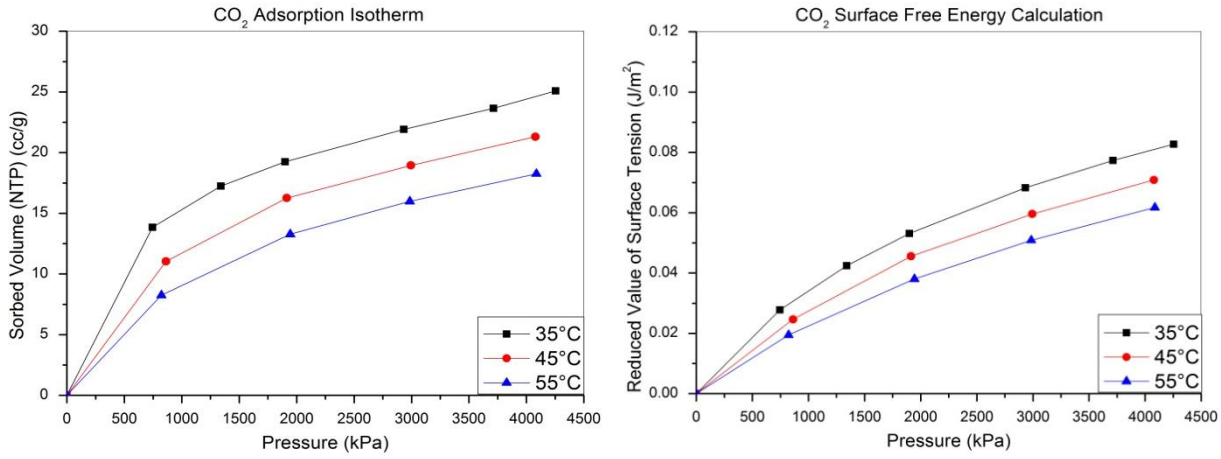

(a) (b)

Figure 4.23: CO_2 adsorption isotherm and surface free energy calculation at different temperature (Dry sample)

Figure 4.24(a) shows the adsorption and desorption isotherms of a 150 µm dry coal sample. The desorption hysteresis of CO_2 in coals is clear and the desorption isotherms lie above the adsorption isotherms. Adsorption is an exothermic process and is opposite to desorption, which is endothermic (Moffat and Weale, 1955; Yang and Saunders, 1985; Stevenson *et al.*, 1991). Figure 4.24(b) shows the CO_2 surface free energy calculation results corresponding to the adsorption and desorption processes, it is apparent that for each of the desorption gas pressure steps, the reduced value of surface tension ($\Delta\boldsymbol{\gamma}$) decreases with increasing pressure. More importantly, at each pressure step, the reduced value of the surface tension at desorption is relatively greater than adsorption, which explains the reason why coal adsorbs more gas in the desorption process. This also explains the desorption hysteresis in accordance with the principle of the surface chemistry.

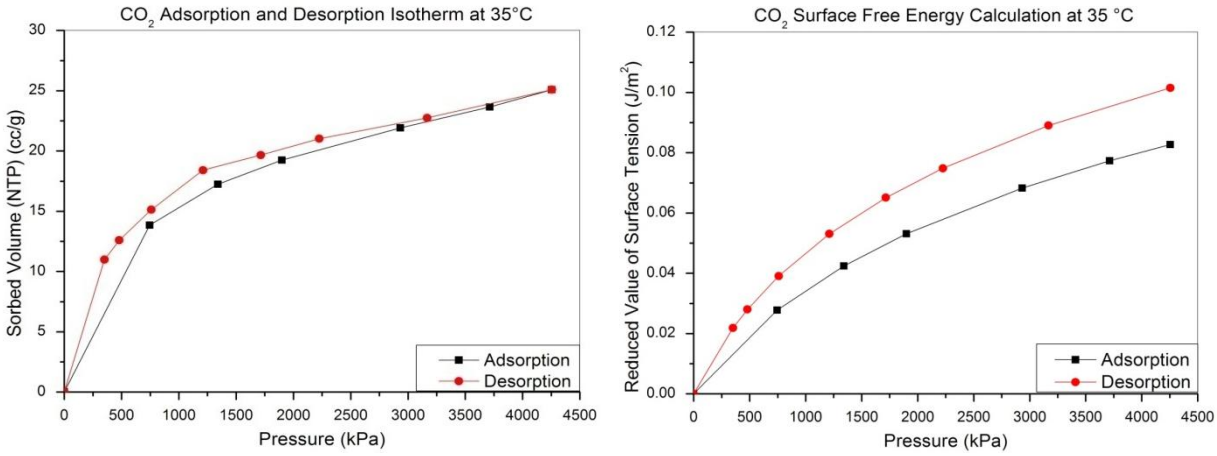

(a) (b)

Figure 4.24: CO_2 isotherm and surface free energy calculation in terms of adsorption and desorption (Dry sample)

The adsorption results of dry coal samples with different types of gases in terms of CO_2, CH_4 and N_2 were shown as an example in Figure 4.25(a), where the adsorption capacity of coal for various tested gases decreased in the order of CO_2, CH_4 and N_2. A preferential varying adsorption capacity of CO_2 to CH_4 and N_2 has been widely reported in the literature (Busch *et al.*, 2003; Harpalani *et al.*, 2006; Prusty, 2008).

Figure 4.25(b) shows the calculation results of the reduced surface tension of coal adsorption with CO_2, CH_4 and N_2. As expected, the value of surface tension increases with increasing pressure. For CO_2, CH_4 and N_2 at the same pressure point, the CO_2 value is larger than the CH_4 followed by N_2 which explains the decreasing adsorption capacity of coal with CO_2, CH_4 and N_2.

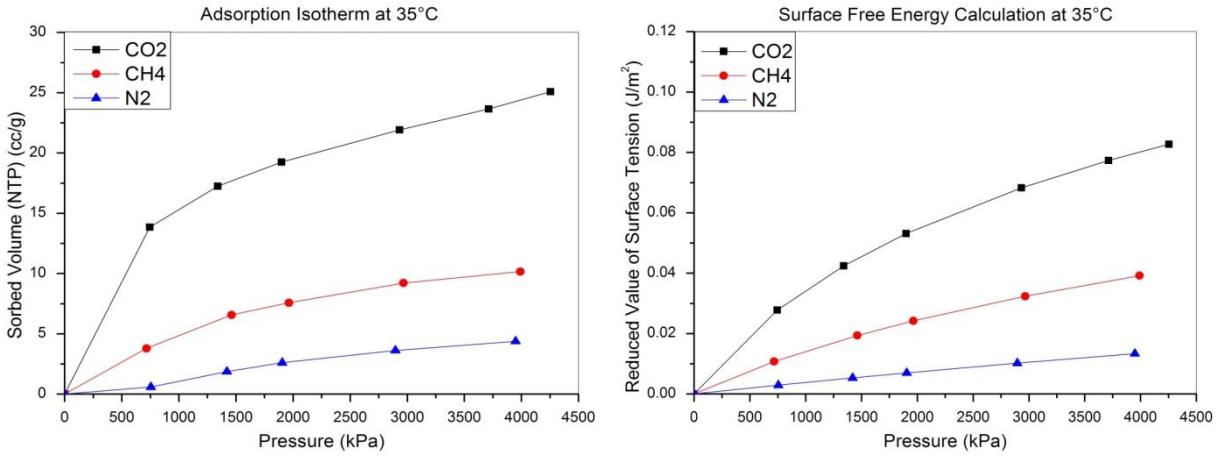

(a) (b)

Figure 4.25: Adsorption isotherm and surface free energy calculation in terms of CO_2, CH_4 and N_2 (Dry sample)

4.6.2.2 Moist coal sample test analysis

The adsorption and desorption test results of 150 μm size coal samples with 2.12 % equilibrium moisture content were analysed with surface free energy. Compared with the reducing influence on the adsorption with increasing temperature from Figure 4.26(a), Figure 4.26(b) shows the reduced surface tension value for the moist samples at different temperatures, the same general trend was found as for the dry samples calculation. The value of surface tension also decreased at increasing temperature.

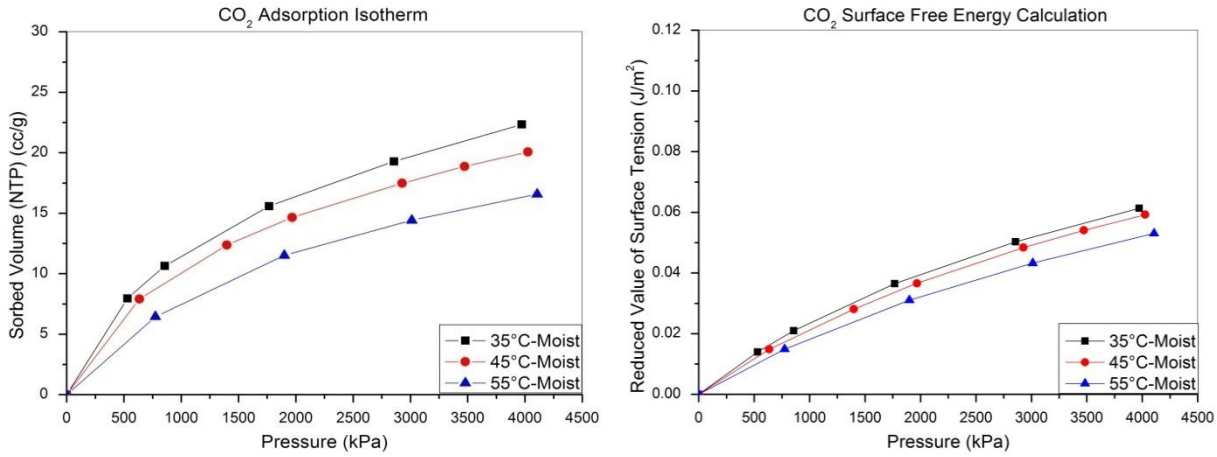

(a) (b)

Figure 4.26: CO_2 adsorption isotherm and surface free energy calculation at different temperature (moist sample)

Figure 4.27(a) shows the CO_2 surface free energy calculation results for moist coal samples in terms of the adsorption and desorption processes, in which the phenomenon of desorption hysteresis was observed with moist samples. The result shows that the equilibrium moisture content of 2.12 % minimises the desorption hysteresis, when compared with dry sample tests. Possible reasons include: firstly the most attractive surface sorption positions are already occupied by the large amount of water molecules; secondly, the water molecule, may result in gas molecules being sorbed in the easy-desorbing surface areas. Both processes will result in the easier gas desorption from the micron size coal samples and further explains the smaller hysteresis phenomenon for the moist coal samples.

The surface free energy calculation results for the desorption test of moist samples are shown in Figure 4.27(b). At each pressure step, the reduced value of surface tension of desorption is relatively larger than the adsorption, which also confirms the results with the dry samples. Thus, irrespective of the coal being dry or moist, coal retains more gas during the desorption process.

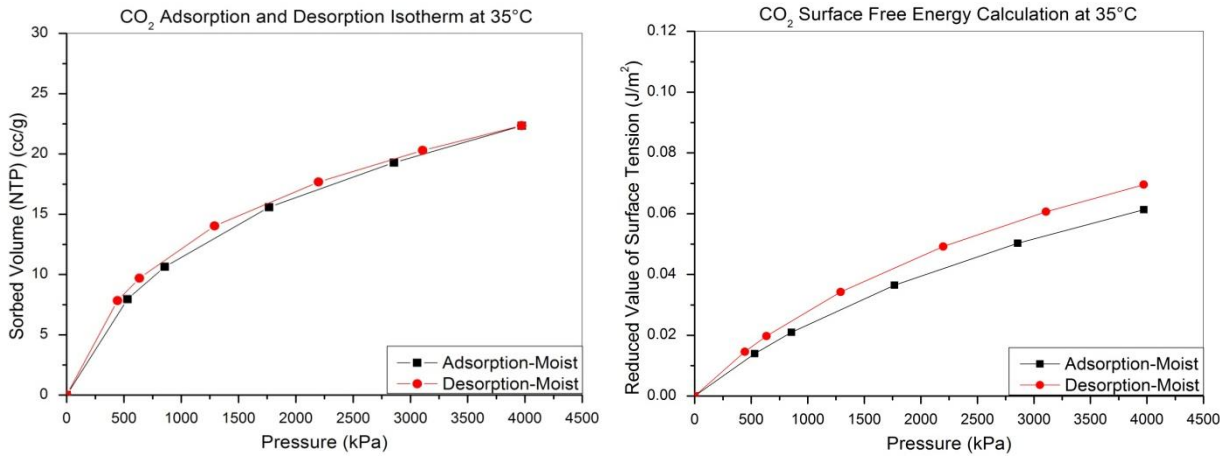

(a) (b)

Figure 4.27: CO_2 isotherm and surface free energy calculation in terms of adsorption and desorption (moist sample)

Figure 4.28(b) shows the surface free energy calculation for comparing the adsorption of moist and dry samples. It can be seen that the reduced value of surface tension curve of moist samples lies under the dry sample curve. That explains why the adsorption capacity for the moist samples is reduced by the moisture inside the coal samples. Through the surface chemistry theory, the water molecules are already first adsorbed on the surface of coal, the coal surface tension has already been decreased by the existing water molecules which then decrease the coal surface tension reduction potential and finally cause the decreasing adsorption capacity of the moist coal samples.

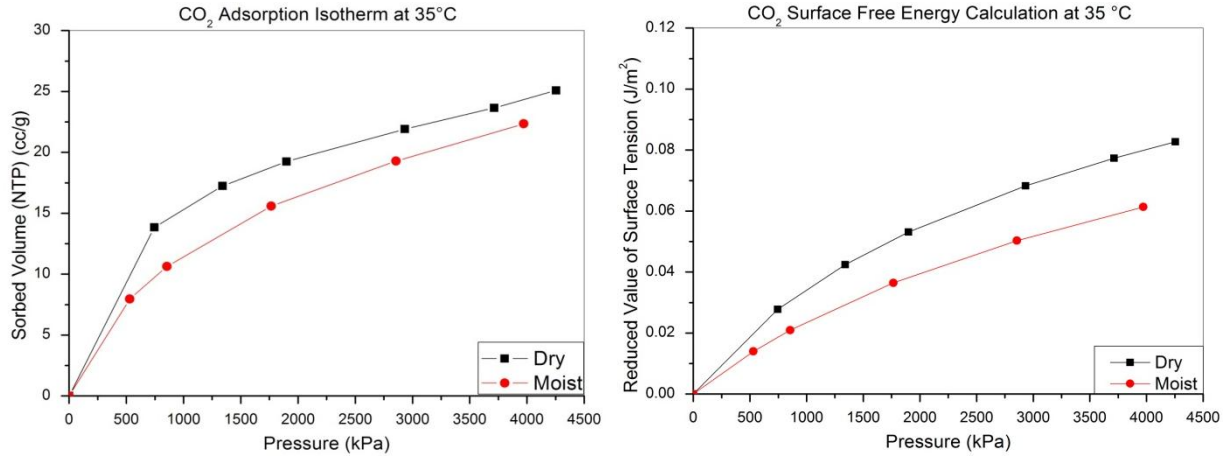

(a) (b)

Figure 4.28: CO_2 adsorption isotherm and surface free energy calculation in terms of dry and moist samples

4. 7 SUMMARY

Based on the testing method and calculation principle in Chapter Three, isotherm tests were carried out at 35 ℃, 45 ℃ and 55 ℃ on dry and moist coals obtained from the Bulli seam of the Sydney Basin. It was considered as a valid approach in order to avoid the samples difference causing extra errors and at each of the pressure step, that equilibrium at these three temperatures was achieved by changing the water bath temperature to avoid the apparent hysteresis caused in a repeated high pressure charging process.

For both dry and moist coals tests, the adsorption capacity of coal shows a linear decrease with increasing temperature. For both the dry and moist coal samples tested, the decreasing rate of adsorption capacity is greater for CO_2 than CH_4, and for each gas test, the decreasing rate is higher for dry coals. Greater reduction value for CO_2 than CH_4 is observed with increasing temperature on the adsorption capacity of coal.

The moist coal sample isotherm for both CO_2 and CH_4 demonstrated a much lower sorption capacity. This clearly indicates that the moisture in the coal reduces the adsorption capacity. For the coal sample tested at these temperatures (35 ℃, 45 ℃ and 55 ℃), the average reduction ratio of coal adsorption capacity with moisture of CO_2 and CH_4 is 11.1 % and 14.0 %, respectively. The experimental result shows that moisture content in coal has more effect on CH_4 than on CO_2.

The helium density of coal increases with increasing coal particle size and ash content. In the process of grinding, coal loses the higher density component and at the same time the pore accessibility increases, finally resulting in coal volume relatively increasing and with the helium density decreasing. Coal sorbed volume decreases with increasing coal particle size, both in dry and on a dry ash free basis. The difference of CO_2 and CH_4 adsorption isotherms for different particle size coal samples calculated on a dry ash free basis is smaller than dry basis. Langmuir volume decreases with the increasing coal particle size for CO_2 and CH_4 adsorption and desorption. Langmuir volume difference becomes larger between dry ash free and dry basis with increasing coal particle size, especially for CO_2 adsorption isotherms.

The tested coal isotherms of different coal particle sizes have apparent hysteresis for both CO_2 and CH_4. Larger particle size coals show a greater hysteresis. Langmuir volume decreases with increasing coal particle size. Langmuir volume differences become larger

between adsorption and desorption with the increasing coal particle size, especially for CH_4 adsorption and desorption isotherms.

The reduced surface tension value reduces with increasing coal temperature and moisture and this value decreases with gas type and in the order of CO_2, CH_4 and N_2 respectively. The reduced surface tension value is relatively greater in the desorption process than in adsorption for both dry and moist coal samples. The experimental results showed that the theory of coal surface free energy tallied well with the experimental results and this can be used to explain both dry and moist coal sorption characteristics with CO_2, CH_4 and N_2 at higher temperatures.

CHAPTER FIVE – STUDY OF GEOLOGICAL VARIATION AND COAL MICROSTRUCTURE

5.1 INTRODUCTION

Coal seams in Australia often contain large volumes of gas with geological variations and in many cases mixed gas conditions prevail where CSG consists of a mixture of CO_2 and CH_4. Metropolitan Colliery in the Southern Sydney Basin has experienced difficulty in reducing gas content within the available drainage lead time in an area of MG 22, as the seam in this area would not drain even with additional drainage boreholes. Research was therefore carried out to identify the main reasons contributing to "difficult-to-drain" areas between 8-11 c/t of MG 22 (Figure 5.1), establish the fingerprints of coals that are able to give early warning signs for future drainage process, and develop a new method based on nitrogen flushing to help drain off the coal seam gas.

Geological variation, mineralisation and coal seam cleat system were found to influence gas drainage borehole arrangements especially the direction of the borehole for efficient gas drainage. The geological variation could be the source of cleat system variations as well as the permeability changes along the different directions. It is also believed that gas concentration variations of CO_2 and CH_4 gases were usually associated with geological variations.

This chapter presents the studies of geological variations related to gas drainage and the use of Scanning Electron Microscopy (SEM) to characterise microstructures of coal samples from both easy-to-drain and hard-to-drain areas. The field geological conditions and observations of coal cleat systems in the laboratory are introduced. Coal microstructure results based upon SEM imaging technology for coal samples from both hard-to-drain and easy-to-drain areas are examined and compared to establish correlations between the geological variation, cleat system, coal microstructures and gas drainability.

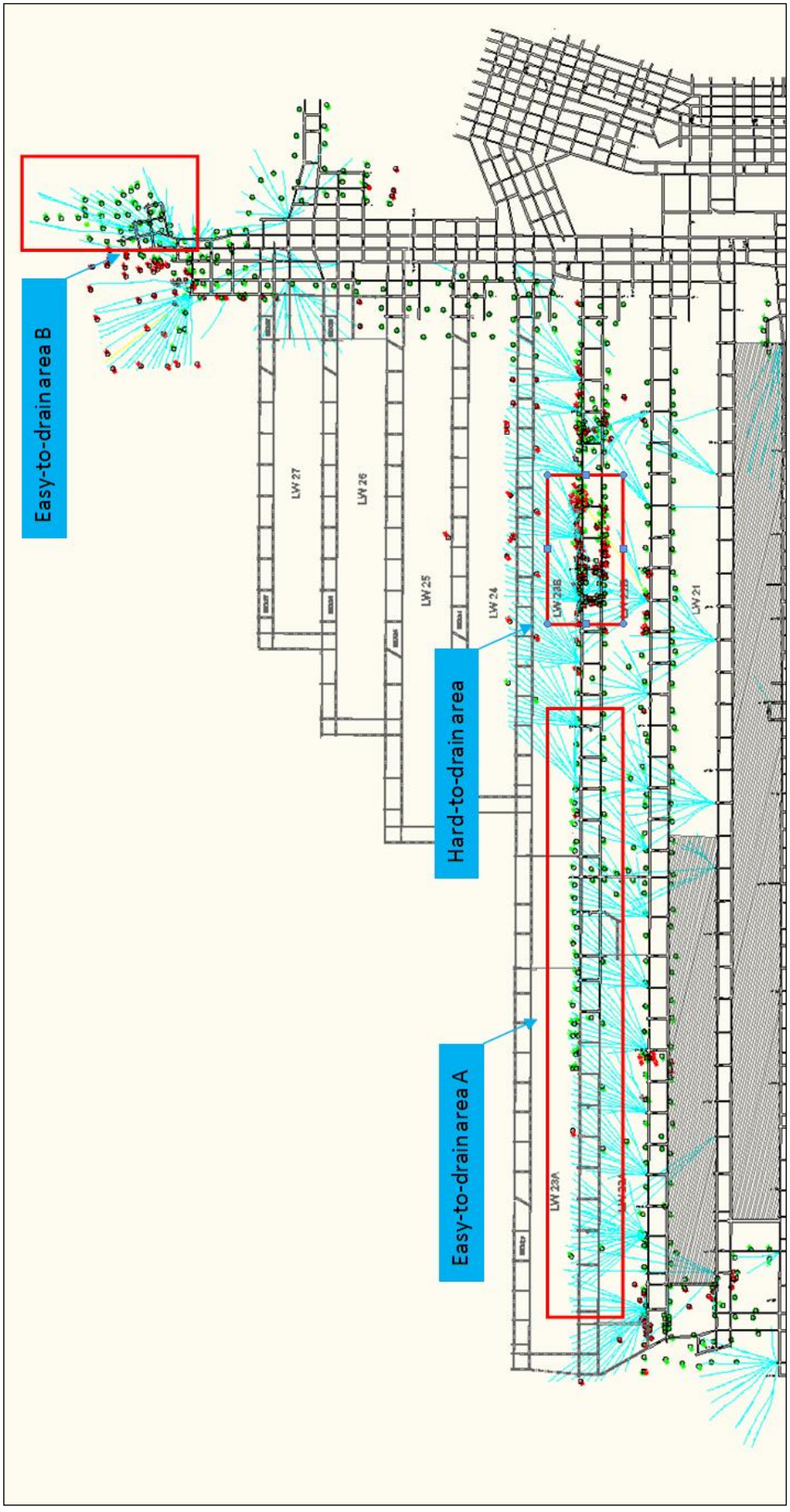

Figure 5.1: Metropolitan mine plan showing the hard-to-drain and easy-to-drain areas

5.2 GEOLOGICAL VARIATION

5.2.1 Geological background

Metropolitan Colliery is located in the Southern Sydney Basin, currently exploring the Bulli seam of Illawarra Coal Measures, which is the main coal bearing sequence of the Late Permian Illawarra Coal Measures (Figure 5.2). The coal varies in rank, from high volatile bituminous to low volatile bituminous with maximum vitrinite reflectance values ranging from about 0.9 to 2.0 % (Faiz, 1993). The coal measures comprise 11 named coal seams of which the Bulli and Wongawilli coals are the most extensively developed and mined. Other coals of potential economic value include the Balgownie, American Creek and Tongarra seams (Faiz *et al.*, 2007).

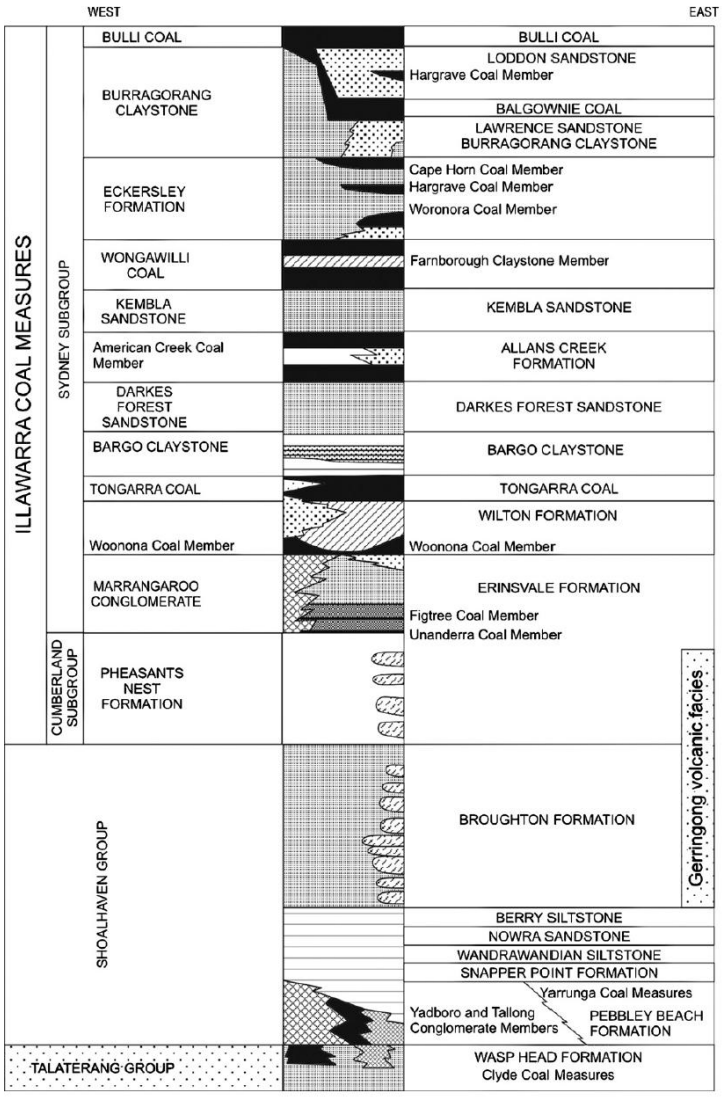

Figure 5.2: Generalised Permian stratigraphy for the southern Sydney Basin (after Faiz *et al.*, 2007)

The coal measure sequence includes numerous igneous intrusions (Figure 5.3) ranging from Permian to Tertiary. Radiometric dating indicates that igneous activities occurred periodically with three peak episodes: at 250, 180 and 50 million years ago (Facer and Carr, 1979; Embleton *et al.*, 1985).

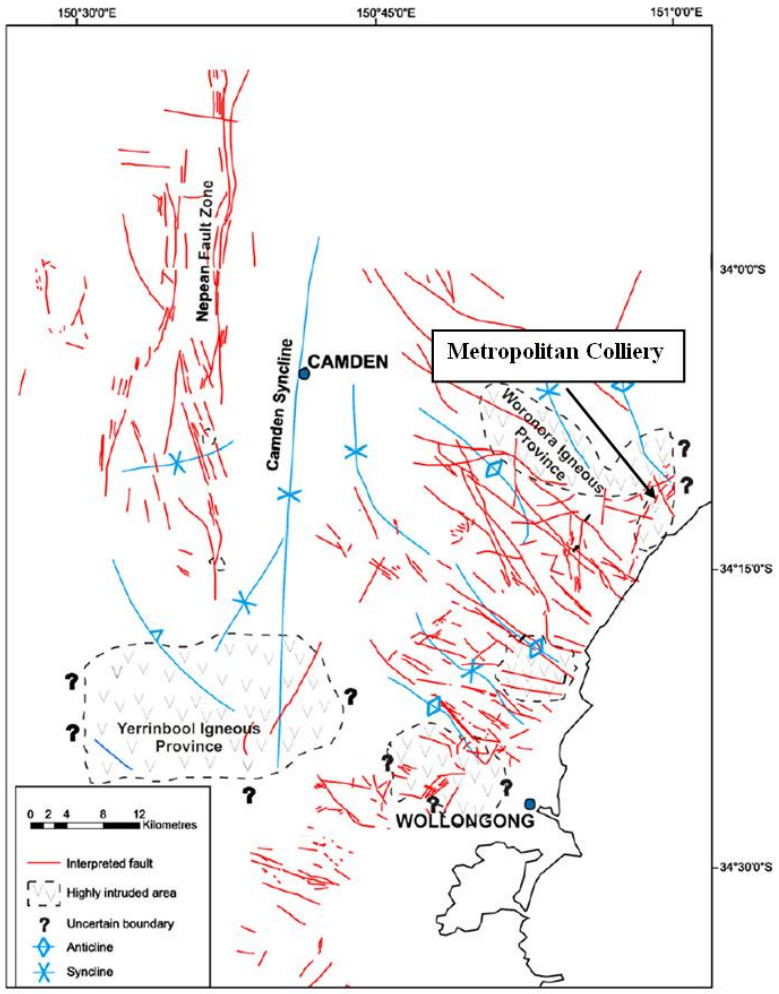

Figure 5.3: Map showing major geological structures and regions of igneous intrusions in the Illawarra Coal Measures (after Faiz *et al.*, 2007)

As shown from the geological survey around this typical hard-to-drain area of the Bulli seam in Metropolitan Colliery (Figure 5.4), there is a strike/slip fault and mylonite existing in the typical hard-to-drain area (8-11 c/t of MG 22). It has been reported that no stress driven roof failure was observed in MG 22 Panel and the faulting intersecting MG 22 panel is characterised by: vertical displacement (0.1 m); mylonite band of approximately 20-30 mm thick; slickensides; and jointing parallel and sub-parallel to the main structure. As the permeability of coal seams and CSG variation can be influenced by geological structures, gas

drainage can also be influenced. This fault may become the source of cleat system variations, causing CO_2 and CH_4 variations in this area and thus a possible high concentration of CO_2.

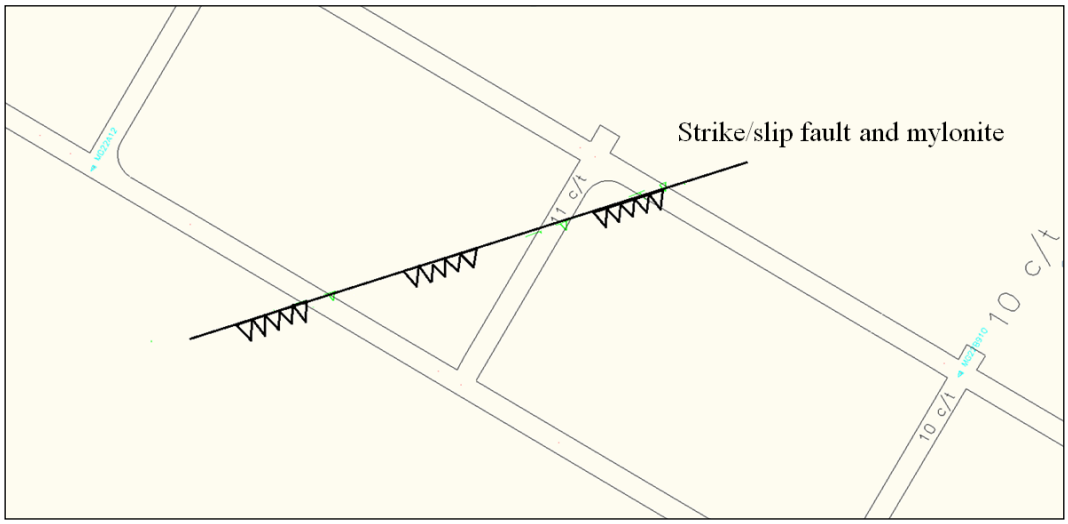

Figure 5.4: Typical hard-to-drain area with fault structure and mylonite presence

5.2.2 Mineralisation

There are some differences between low and high permeability in the coal seam. These differences can be related to the presence of some specific pore and cleat fillings such as mylonite, the development of cleats and their mineralisation, and the mode of occurrence of minerals in coal macerals. Successful drainage and a suitable rate of gas flow through the coal can be influenced by coal microstructures, especially micro-cleat openings and mineral matter. In good drainage and high permeability coal seams, the micro-cleats are mostly empty, or only partly mineralised (Sereshki, 2005).

Based on microscopic studies of Australian coal samples, Gurba (2002a) found that the Bulli seam had two different sets of cleats; open and the mineralised cleats. Microscopic studies on coal samples from West Cliff Colliery showed micro-cleats totally mineralised by carbonates and siderite nodules (iron carbonate). Those filled cleats were observed to cause difficulty in drilling and gas drainage. Mylonite is also present in West Cliff coal samples, and mylonitic type coal could be prone to outbursts (Gurba, 2002b).

Additionally, microscopic examination of the coal samples from difficult drainage areas has shown that the mylonite filling in micro-cleats is a possible factor causing difficulty in gas drainage. As studied by electron microprobe analysis, the mylonite in micro-cleats is cemented by calcite, dolomite or kaolinite. Coal samples from Central Colliery in the Bowen

Basin that were collected from a low permeability area and outburst prone zone showed, the cleats were totally filled with calcite. Coal samples collected in Appin Colliery also showed that both carbonates and mylonite were present in the cleats, blocking the pores with not much space left for gas flow (Sereshki, 2005).

5.2.3 Coal cleat system

Generally, a coal seam is characterized by the natural fracture network which is commonly referred to as cleat. The cleat system consists of two perpendicular sets of fissures; the more predominant cleat is called the face cleat. The butt cleat has less continuous individual fractures often ending at intersections with face cleats. The angle between the face and butt cleats is around 90° (McCulloch *et al.*, 1974; Cui *et al.*, 2004). Gregory *et al.* (1986) noted that cleat space accounts for less than 2 percent of the seam bulk volume, and the mechanism of gas storage is the same as in conventional reservoirs where flow of gas is governed by Darcy's law.

The mechanism of the coal cleat system has been discussed extensively by many researchers, and a common understanding is that cleats are formed due to the effects of the intrinsic tensile force, fluid pressure, and tectonic stress (Laubach *et al.*, 1998; Su *et al.*, 2001). The intrinsic tensile force arises from matrix shrinkage of coal, and the fluid pressure arises from hydrocarbons within the coal. These two factors are considered to be intrinsic reasons for cleat formation. The tectonic stress is regarded as extrinsic to cleat formation and is the major factor controlling the geometric pattern of cleats. Face cleats extend in the direction of maximum *in situ* stress, and butt cleats extend in the direction of minimum *in situ* stress. This is why regular cleats are formed in face and butt pairs.

Figures 5.5 and 5.6 show the cleat system found in Metropolitan lump coal samples. Generally the coal bedding direction, face and butt cleats can be clearly identified. It can be observed that this type of coal is really tight with small cleat spacings and narrow apertures. The SEM analysis in the later part of this chapter will show the cleat system observation with magnification.

Optimal gas production is usually achieved from coal seams characterised by highly fractured coal and cleat networks with wide cleat apertures, great cleat density and intermediate cleat spacing (Dabbous *et al.* 1974; Lingard *et al.*, 1984; Cui and Bustin, 2006; Solano-Acosta *et al.*, 2007). Coal seams with high cleat permeability and low cleat porosity are expected to

have a short time to achieve peak production and a high production rate during the main stage of production.

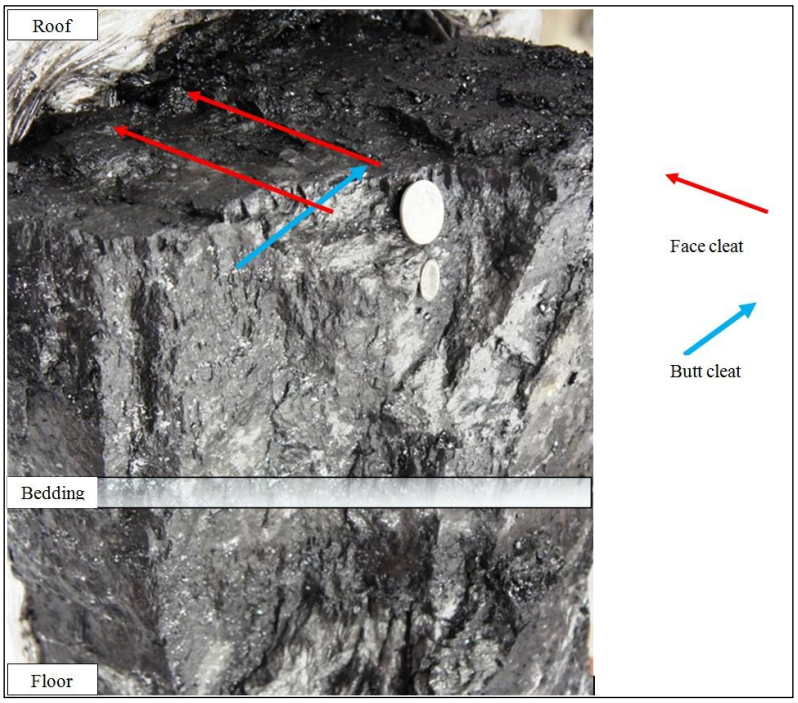

Figure 5.5: Picture of the lump coal sample showing the cleat systems relative to the coal bedding direction

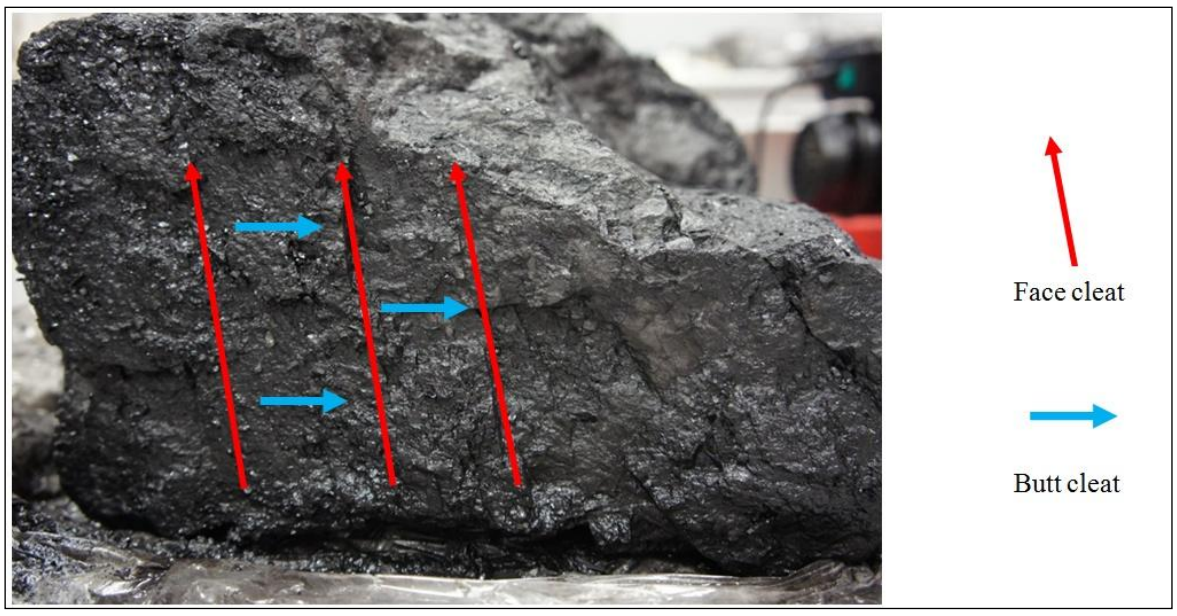

Figure 5.6: Picture of the lump coal sample showing the face cleat and butt cleat from roof side of the lump coal sample

5.2.4 Geological variation induced permeability change

As discussed in Chapter Two, the permeability of coal seams can be influenced by geological structure variations. Generally, favourable areas for coalbed methane drainage are likely to have a relatively simple geological structure that ensures the continuity of reservoirs (Sereshki, 2005). Wallace (1990) reported that gently folded areas in coal seams tended to have higher permeability than steeply folded and faulted areas. Gas pressure increase and permeability decrease occur around the region of intrusions (Sereshki, 2005). Cleat orientation has been reported to be an important parameter for the permeability of coal, it is therefore generally accepted that boreholes drilled perpendicular to face cleat tend to be more productive than boreholes drilled otherwise (Hayes, 1982; Hargraves, 1983 and Osisanya and Schaffitzel, 1996). Battino and Hargraves (1982) reported that, testing in the Castor seam at Cook Colliery, using a 21 m long, 43 mm diameter borehole, measured gas flow rates ranging from 85 to 175 L/min from boreholes drilled perpendicular to the major cleat, this was marginally higher than the flow rates from boreholes drilled parallel to the major cleat, which were up to 75 L/min.

To understand the cleat system, field visits were carried out to examine the coal seams and geo-stress conditions in relation to borehole drilling direction in the hard-to-drain area of MG 22 at Metropolitan Colliery. Figure 5.7 shows the drainage borehole layout and the residual gas content after six-months drainage (red points are the “Fail” drainage samples while green points are the “Pass” drainage samples) in the typical hard-to-drain area. The “Pass” or “Fail” sample is determined by the measured gas content and composition compared with outburst threshold limit shown in later paragraphs in Figure 5.11.

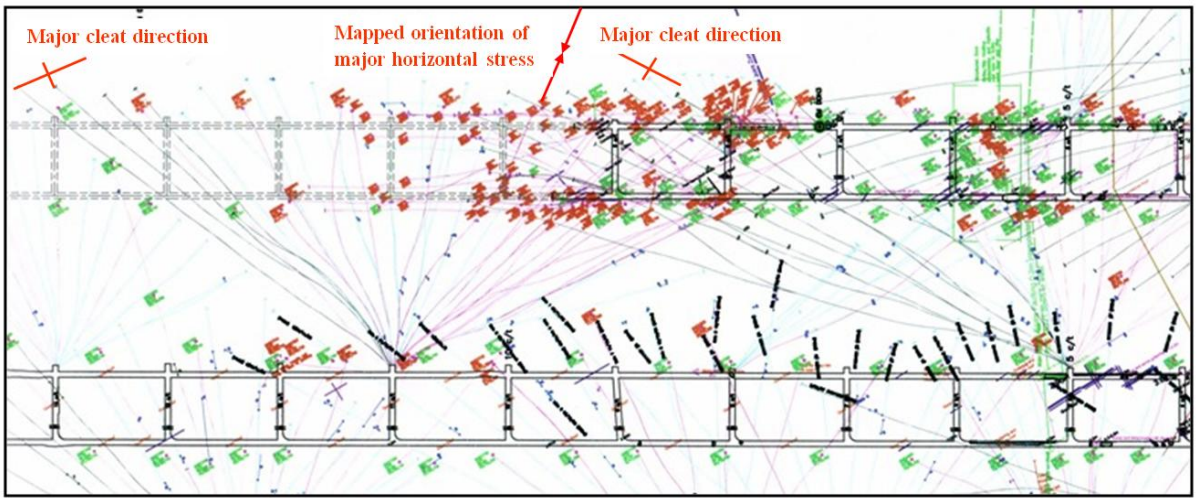

Figure 5.7: Mine plan picture of typical hard-to-drain area showing the drainage borehole layout

As shown in Figure 5.7, some boreholes are relatively more productive than others drilled in different directions in this area. By relating this field observation with the field observed cleat system, some boreholes drilled perpendicular to the major cleat system (from drilling stub towards Mains or outbye) could be more productive; whilst boreholes drilled inbye would be less effective for degassing. Regarding the mapped orientation of major horizontal stress, it seems that the major stress direction is perpendicular to the major cleat direction, hence sealing the major cleat and likely causing the closure of boreholes orientated inbye. This may also contribute to the less effective gas drainage of the hard-to-drain area. Figure 5.8 shows the gas drainage borehole location underground along the roadway in Metropolitan Colliery.

Figure 5.8: Field observation of gas drainage borehole location

5.2.5 Geological variations inducing high CO_2 concentration

In situ gas contents of coal in the Illawarra Coal Measures range from less than 1 to 20 m^3/t with the highest contents occurring at depths between 600 and 800 m. The desorbed gas often comprises CH_4, CO_2, N_2, C_2H_6 and other higher hydrocarbons (Faiz *et al.*, 2007). The two most abundant gases are CO_2 and CH_4, accounting for greater than 90 % of the total gas in most areas of the Sydney Basin. Thermal history modelling indicates that most of the hydrocarbon gases were generated as a result of coalification during the Jurassic and Early Cretaceous (Faiz *et al.*, 2003); additional CH_4 was apparently generated from post-Cretaceous microbial activity (Smith and Pallasser, 1996; Faiz *et al.*, 2003).

Faiz *et al.* (2007) stated that isotope carbon-13 ($\delta^{13}C$) values for CO_2 from coal seams of the Illawarra Coal Measures vary between -25 and +15 ‰ (IAEA international standard defining

Vienna Peedee Belemnite, VPDB), indicating various sources (Figure 5.9). These sources include thermogenic gas from coal/microbial oxidation of hydrocarbons ($\delta^{13}C$ -25 ± 5 ‰), magmatic activity ($\delta^{13}C$ -7 ± 3 ‰) and residual CO_2 after microbial reduction of CO_2 to CH_4 (0 to +15 ‰).

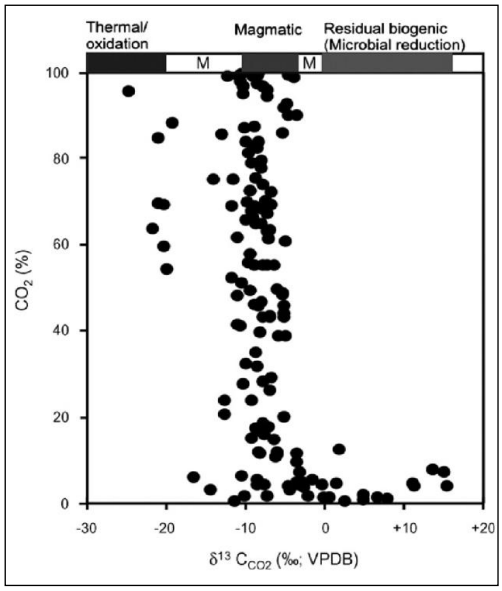

Figure 5.9: Carbon dioxide concentrations and δ13C CO_2 (VPDB) values for coal seam gases from the southern Sydney Basin (after Faiz *et al.*, 2007)

Most of the $\delta^{13}C$ values ranging between -5 and -10 ‰ suggest mainly magmatic sources, which was probably associated with the main episodes of igneous activity in the Permian, Jurassic and Tertiary. The majority of CO_2 currently present in the coal seams was probably sourced during the Tertiary period, replacing the CH_4 generated during the main phase of coalification in the late Jurassic-early Cretaceous periods (Faiz *et al.*, 2007) (Figure 5.10).

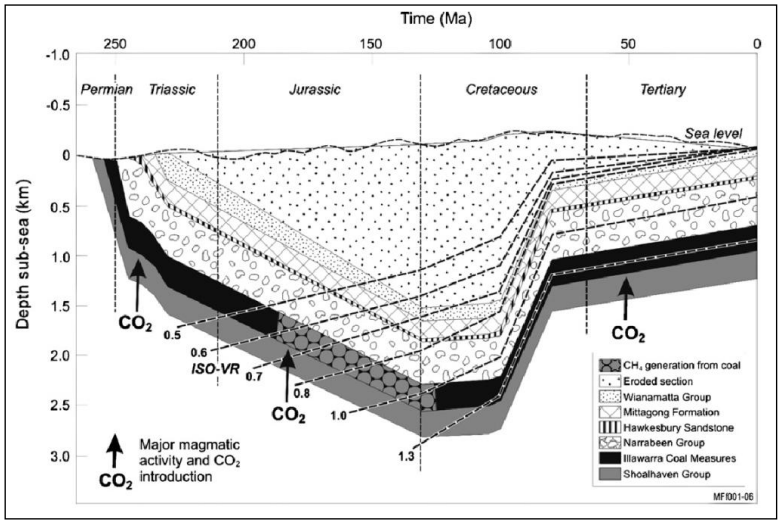

Figure 5.10: Burial and thermal history reconstruction for the southern Sydney Basin based on data from Bootleg-8 well ('iso-VR' signifies lines of equal vitrinite reflectance) (after Faiz *et al.*, 2007)

As previously discussed in the Chapter Two, the variations of CO_2 and CH_4 are mainly related to the geological structure and depth. The variations in the gas composition have no clear relationship with coal composition or rank but show well-defined relationships with geological structure and stratigraphy. High proportions of CH_4 occur in the synclinal structures, whereas the CO_2 content increases towards structural highs. Extensive areas of pure CO_2 gas occur on anticlines and domes. In structural lows, high CO_2 concentrations are found near some dykes and related faults (Faiz and Hutton, 1995). Actually, confirmed within the typical hard-to-drain area of this study, there appeared to be a fault feature existing.

It is also confirmed that this area is a high CO_2 concentration area, according to the gas content and composition analysis of the coal within the typical hard-to-drain area (MG 22, 8-11 c/t) with 94 sample test results. As shown in Figure 5.11, the scatter of typical hard-to-drain area is concentrated almost entirely in the CO_2 rich area. Among the 94 samples, 63 samples are "Fail" samples, accounting for 67.0 %, which directly indicates the area is a typically hard-to-drain area. The average values of CO_2 in both "Pass" and "fail" samples are 87.6 % and 84.5 % respectively, all the gas content and composition detailed information will be discussed in the next chapter.

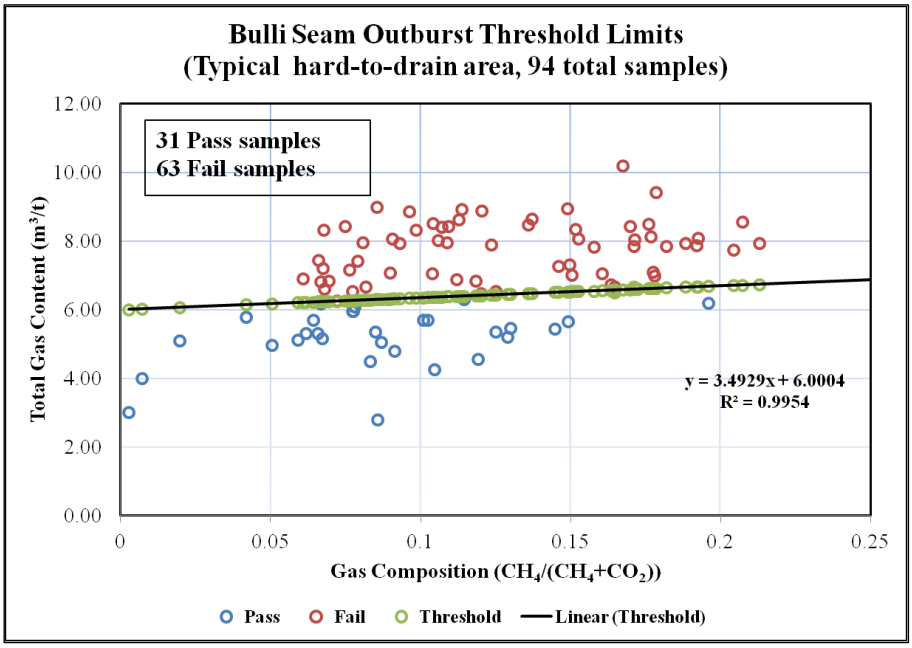

Figure 5.11: Bulli Seam outburst threshold limits (Typical hard-to-drain area)

5.3 COAL MICROSTRUCTURE STUDY

Better understanding of gas drainage production characteristics from coal seams requires detailed and reliable information on gas sorption and fluid transport as well as their inter-dependent interaction. An understanding of these processes relies on an improved understanding of coal structure from the macroscopic to the microscopic. Commonly, gas transport in coal is considered to occur in two ways (shown in Figure 5.12): (I) diffusion and sorption in the coal matrix, and (II) laminar flow through the cleat system. Gas storage by physical sorption occurs mainly in the coal matrix (Harpalani and Chen, 1997).

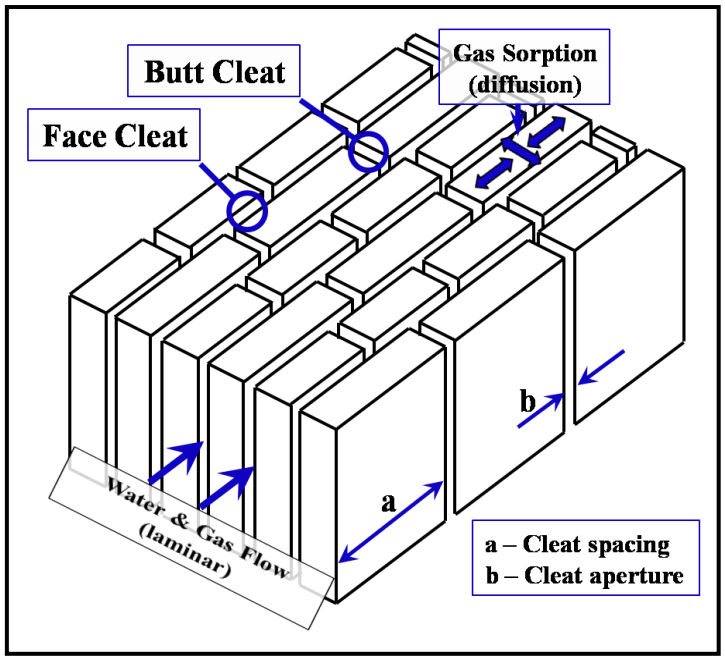

Figure 5.12: Illustration showing coal matrix blocks and cleat system of a coal (after Black, 2012)

Generally in a gas drainage process, coal seam gas molecules need to first desorb from the coal surface, diffuse from the coal matrix into the cleat system, then move out of the coal structure by pressure drawdown towards a production hole. Thus higher gas production rates may be expected from highly fractured coal with reduced spacing between fracture surfaces and cleats, which are characterised with increased pore system for the gas to travel by diffusion before exiting from the coal matrix and entering cleat and fracture systems.

5.3.1 Scanning Electron Microscopy (SEM) test

Coal samples that appear to be tighter and less porous may contribute to the problem of poor gas drainage. To improve the current understanding of micro-fracture patterns of the hard-to-

drain seam, SEM technology was used to analyse the coal structures of coal samples from both the easy-to-drain and hard-to-drain areas in the Bulli seam.

SEM tests were undertaken by using an analytical instrument JSM-6490 LV Scanning Electron Microscope, as shown in Figure 5.13. The JSM-6490LV is a high-performance, scanning electron microscope with a high resolution of 3.0 nm. The low vacuum mode, allows for observation of specimens which cannot be viewed at high vacuum due to excessive water content or due to a non-conductive surface. Its asynchronous five-axis mechanically eucentric stage with compeucentric rotation and tilt can accommodate a specimen of up to 200 mm in diameter. Standard automated features include Auto Focus/Auto Stigmator, Auto Gun (saturation, bias and alignment), and Automatic Contrast and Brightness. Table 5.1 shows the key product features of the JSM-6490 LV Scanning Electron Microscope.

In this study, coal samples from 11-12 c/t, MG 22 and 9-10 c/t, MG 22 (shown in Figure 5.1, hard-to-drain area) and GME 2193 (Figure 5.1, easy-to-drain area B) and GME 2237 (Figure 5.1, easy-to-drain area A) of Metropolitan Colliery were prepared and analysed. For each of the coal samples, two pieces were prepared according to the surface directions of coal, including perpendicular to bedding and parallel to bedding. A total of eight samples were prepared by cutting roughly 10 mm thick coal from both surfaces of perpendicular and parallel directions to cleat orientations. Then each coal piece was mounted on a 40 mm diameter aluminium stub with carbon tape, as shown in Figure 5.14.

All the SEM images were taken with the Secondary Electron (SE) mode, which is the most important as these electrons can be collected easily by means of a positively biased collector grid placed on one side of the specimen, because of their low exit energy of a few electronvolts. The SE dependence yield on the tilt angle of a surface element, the enhanced emission at the edges and small particles and the shadow contrast that results from incomplete collection can all be used to image the surface topography. The SE is retarded by a positive bias and repelled by a negative bias of the specimen and is influenced by the electrostatic field between regions at different biases. These effects generated voltage contrast, with negatively biased areas appearing bright and positively biased regions, appearing dark (Reimer, 1998).

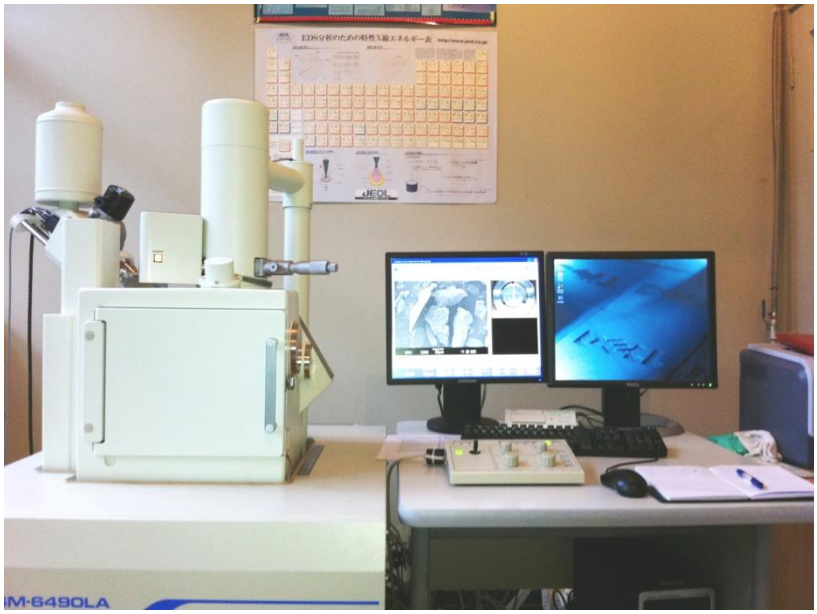

Figure 5.13: The diagram of SEM equipment

Table 5.1: JSM-6490 LV Key Product Features (after JEOL, 2012)

Resolution	High Vacuum mode: 3.0 nm (30kV) Low Vacuum mode: 4.0 nm (30kV)
Accelerating Voltage	0.3 to 30 kV
Magnification	×5 to 300,000
Filament	Pre-centred W hairpin filament (with continuous auto bias)
Objective Lens	Super conical lens
Objective Lens Apertures	Click-stop type (3-step variable) Fine position controllable in X/Y directions
Maximum Specimen Size	200 mm coverage, 300 mm specimen can be loaded
Specimen Stage	5 axis computer controlled Eucentric goniometer X=125mm, Y=100mm, Z=5 to 80mm T= -10 to 90°, R=360° (endless)
Display LCD	500 mm, high resolution FPD
Vacuum Mode Changeover	Automatic (PC interface controlled)

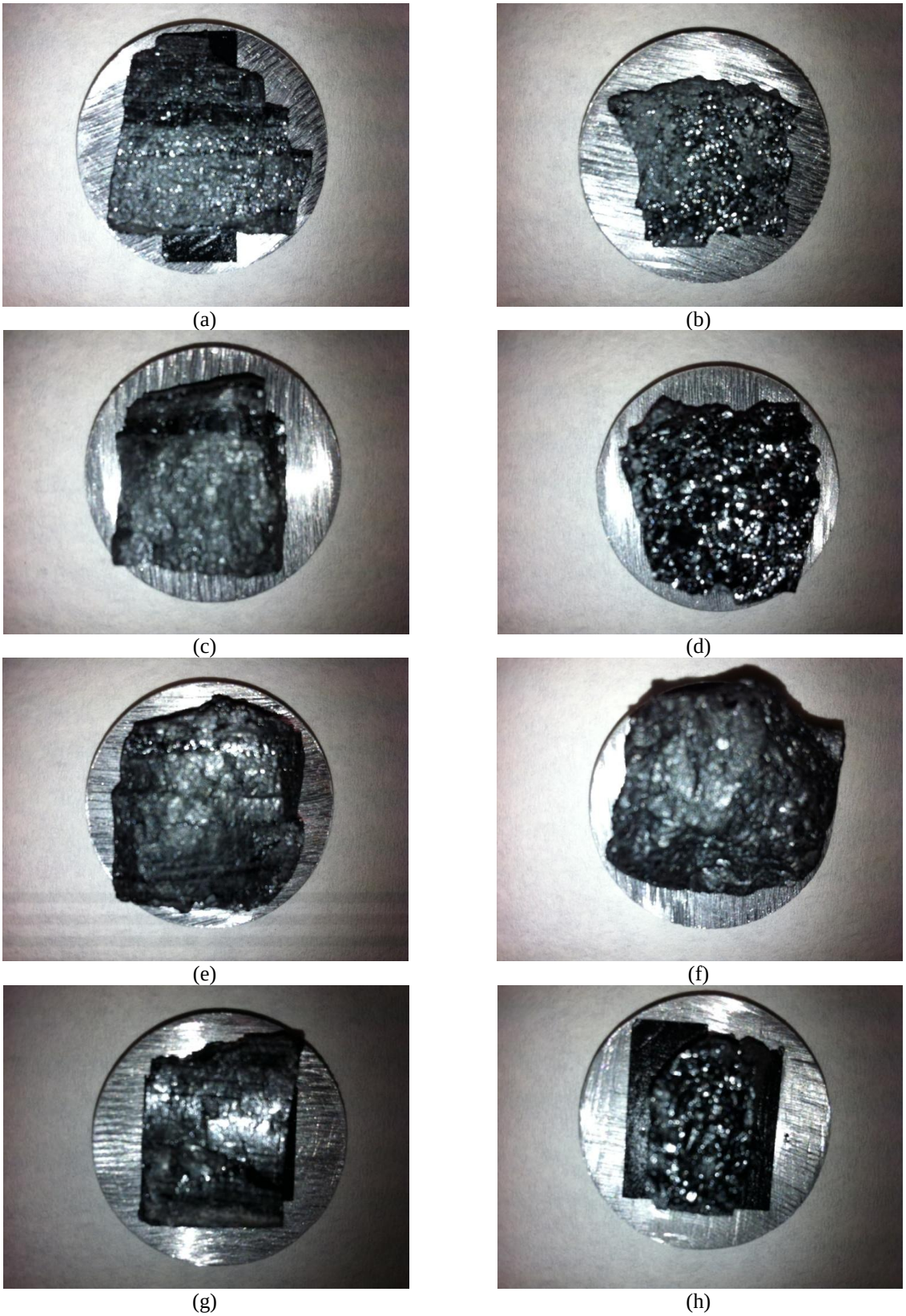

Figure 5.14: Pictures of sample piece in SEM test, (a) 11-12 c/t, MG 22 (perpendicular to bedding), (b) 11-12 c/t, MG 22 (parallel to bedding), (c) 9-10 c/t, MG 22 (perpendicular to bedding), (d) 9-10 c/t, MG 22 (parallel to bedding), (e) GME 2193 (perpendicular to bedding), (f) GME 2193 (parallel to bedding), (g) GME 2237 (perpendicular to bedding), (h) GME 2237 (parallel to bedding)

5.3.2 SEM analysis of coal samples from hard-to-drain area

Cuttings of coal samples of the hard-to-drain area from 11-12 c/t, MG 22 and 9-10 c/t, MG 22 were tested. SEM images of these samples generally have solid surface being the dominant feature. Figure 5.15 shows the SEM image of coal face and butt cleat systems (from 11-12 c/t, MG 22, perpendicular to bedding). With higher magnification, generally two types of cleat were observed, open cleat and closed cleat (Figure 5.16). Thus, the micro magnitude cleat spacing of less than 10 micron indicated the coal is really tight coal type, compared with some other Australian coals (Massarotto *et al*., 2000).

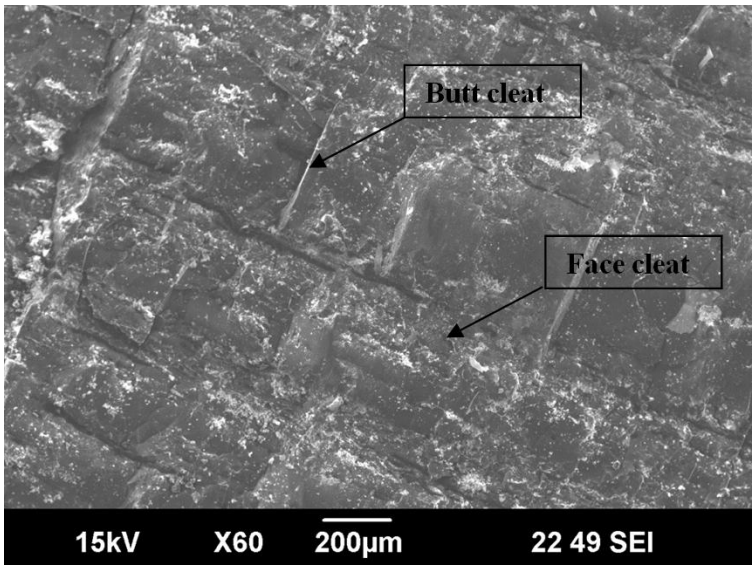

Figure 5.15: SEM image showing the coal face and butt cleat system (from 11-12 c/t, MG 22, perpendicular to bedding)

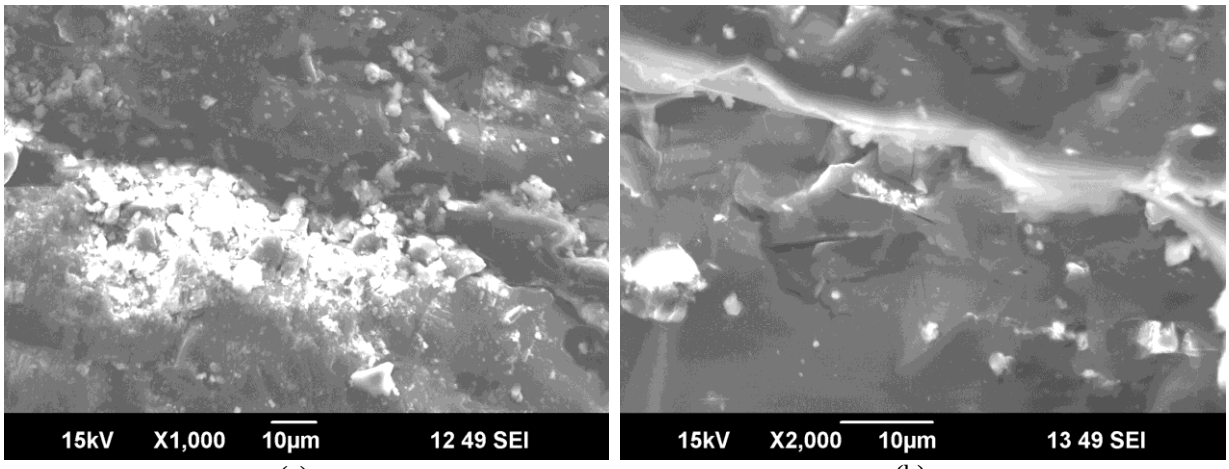

(a) (b)

Figure 5.16: SEM images showing the coal face cleat, (a) open face cleat, (b) close face cleat (from 11-12 c/t, MG 22, perpendicular to bedding)

Figure 5.17 and Figure 5.18 shows the coal solid surfaces being observed for samples from 11-12 c/t, MG 22. This feature was found from scale 10 to 100 µm, both from perpendicular and parallel directions to the bedding. Figure 5.19 shows the microstructure of coal with solid surface which was also easily observed for sample 9-10 c/t, MG 22.

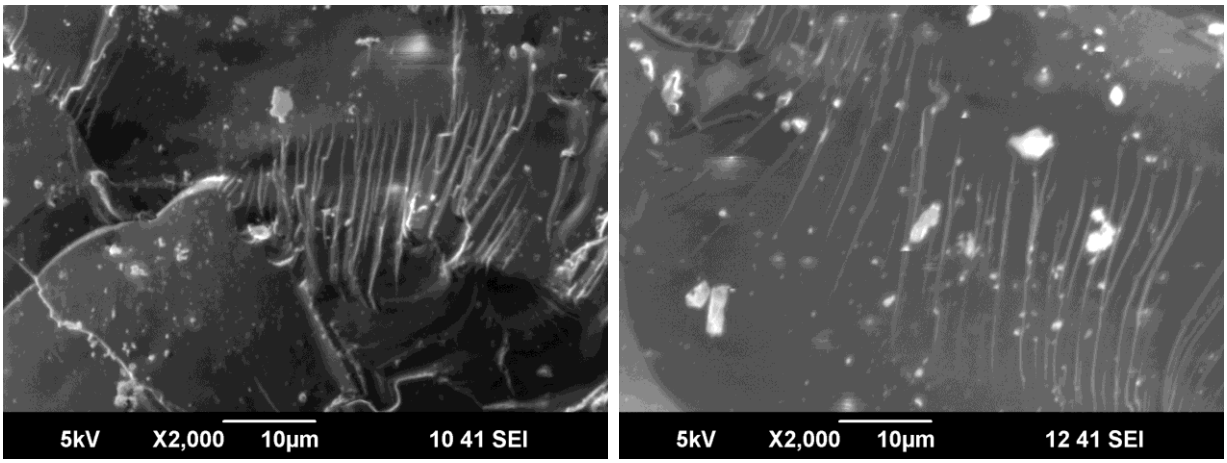

Figure 5.17:SEM images showing the coal solid surface(from 11-12 c/t, MG 22, perpendicular to bedding)

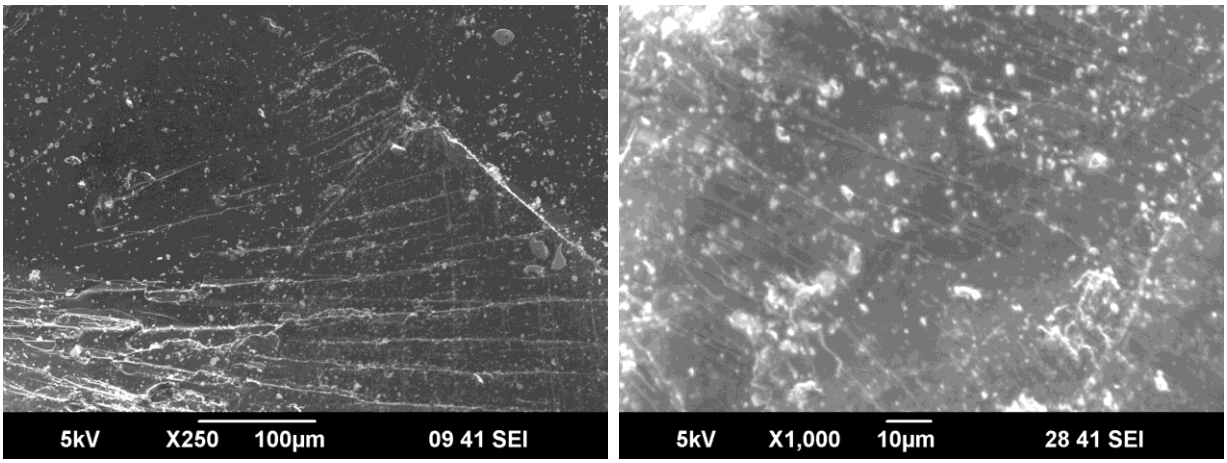

Figure 5.18: SEM images showing the coal solid surface (from 11-12 c/t, MG 22, parallel to bedding)

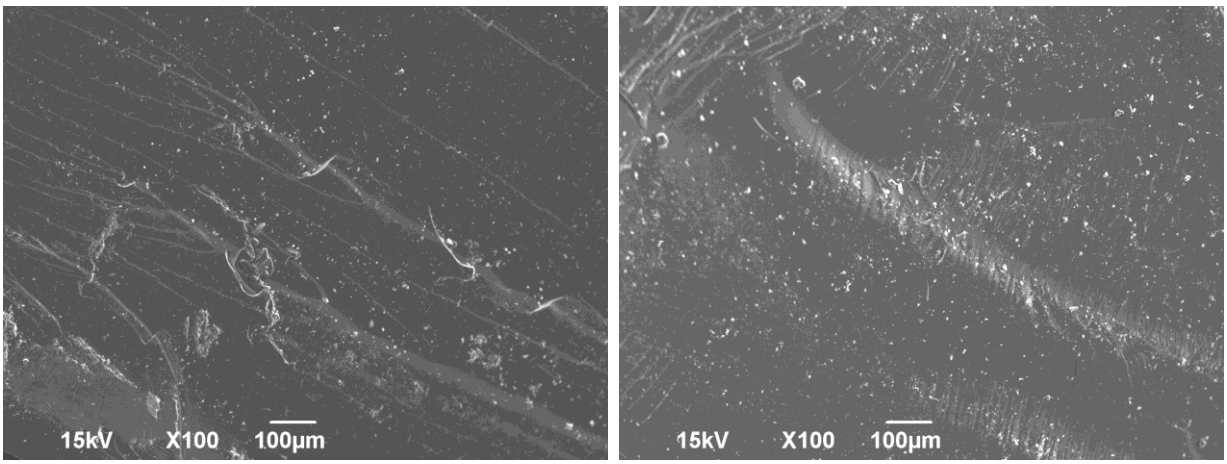

Figure 5.19: SEM images showing the solid surface (from 9-10 c/t, MG 22, parallel to bedding)

In the SEM test of the hard-to-drain samples, ten micron size porous structures were observed for sample from 11-12 c/t, MG 22 parallel to bedding direction. As shown in Figure 5.20, some of the coal pores were filled with coal particles and mineral matter. Speight (1983) showed that mineral matter usually filled macropores and as consequence the porosity of coal could be decreased, causing a reduction in coal permeability. Furthermore, mineral matter was found to impede the gases from leaving by affecting gas desorption and shrinkage property of the coal matrix (Sereshki, 2005).

Gamson *et al.* (1993) in an extensive study on Australian coals found that the amount of fracture infilling with minerals was one of the factors which influenced the effectiveness of methane flow through the coal matrix. They noted that mineral matters such as clay, calcite and quartz block the methane flow path through cleats and interconnected pores by forming a compact amorphous or crystalline structure. The size of infilling influences gas diffusion as well as laminar flow in the coal matrix.

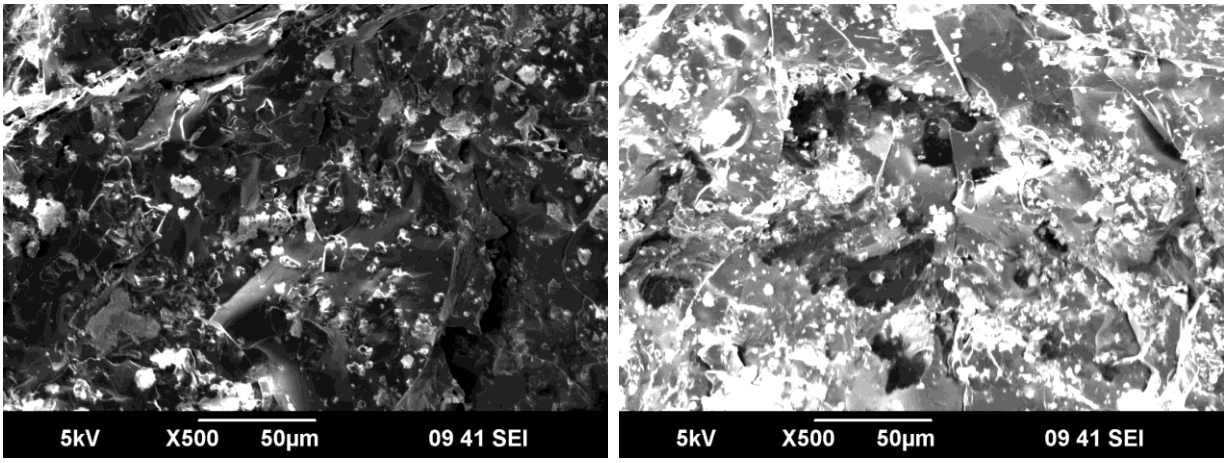

Figure 5.20: SEM images showing the coal porous structure (from 11-12 c/t, MG 22, parallel to bedding)

Intrusions were also captured in the SEM test of hard-to-drain area (Figure 5.21). Circumstances of low permeability can occur *in situ* as a result of geological anomalies such as intrusions, i.e. it was known that gas pressure increase and permeability decrease occur around the region of intrusions (Sereshki, 2005). Clayton (1998) reported that mineral reactions such as thermal decomposition or dissolution of carbonates or other metamorphic reactions and magmatic intrusions can be very important sources for CO_2 gas in coal seams, which confirmed the high CO_2 concentration in this typical hard-to-drain area.

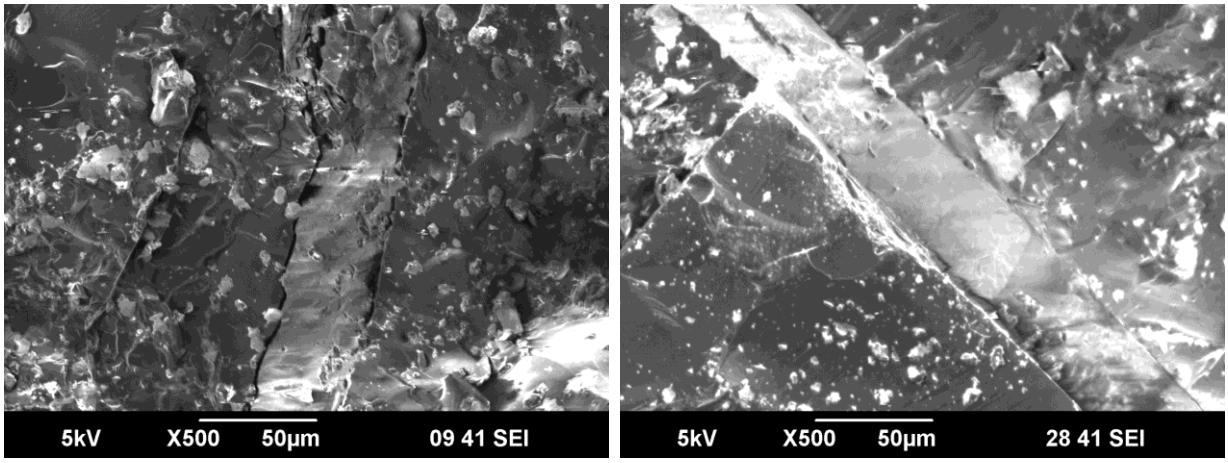

Figure 5.21: SEM images showing the intrusion filling the coal cleat (11-12 c/t, MG 22, parallel to bedding)

5.3.3 SEM analysis of coal samples from easy-to-drain area

Coal samples collected from the easy-to-drain areas of GME2193 and GME2237 were tested next. Generally pore structure was easily captured in the SEM test of these two samples, both from perpendicular and parallel directions, as shown in Figure 5.22 and Figure 5.23. Successful drainage and a suitable rate of gas flow through the coal can be influenced by coal microstructures, especially micro-cleat openings and mineral matter. In good drainage and high permeability coal seams, the micro-cleats are mostly empty, or only partly mineralised (Sereshki, 2005).

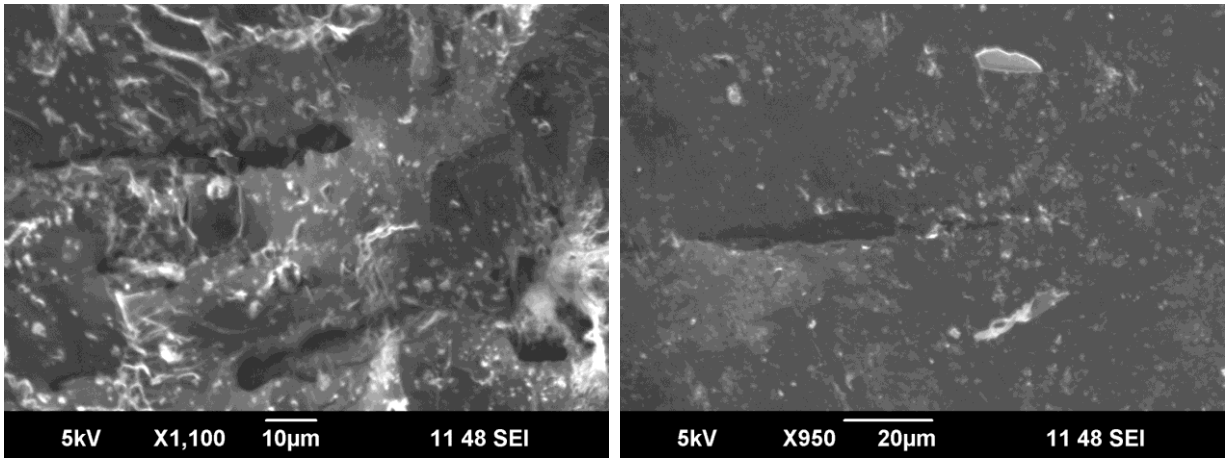

Figure 5.22: SEM images showing porous structure (from GME2193, perpendicular to bedding)

For coal samples from the easy-to-drain area of GME2193, it was found that the micron size pores system was relatively well generated parallel to the bedding direction. Pores were observed from 100 µm, 20 µm and 10 µm scale images respectively as shown in Figure 5.23.

Figure 5.24 shows that a similar pore structure was observed in the GME 2237 coal sample perpendicular to the bedding direction.

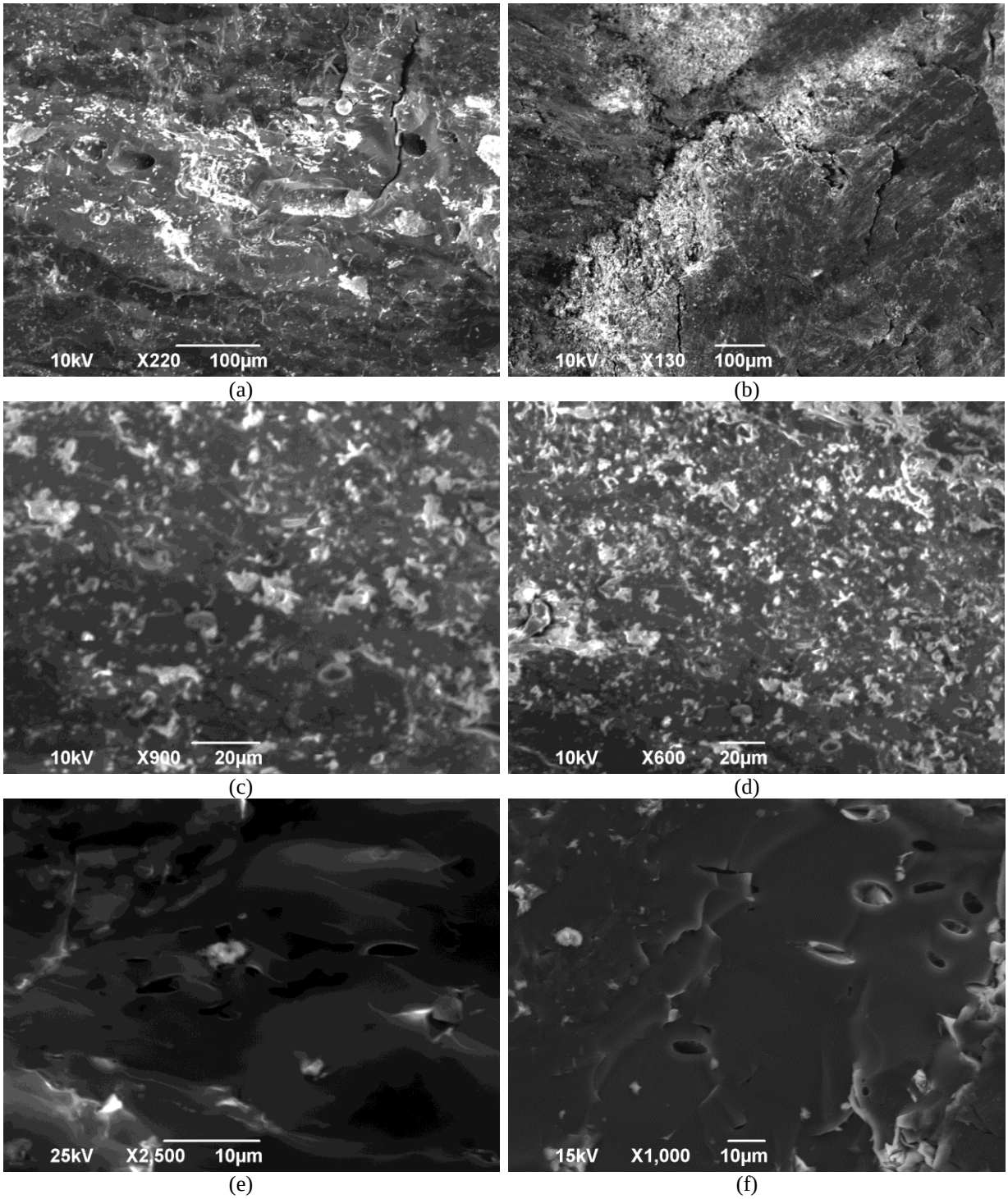

Figure 5.23: SEM images showing porous structure (from GME2193, parallel to bedding)

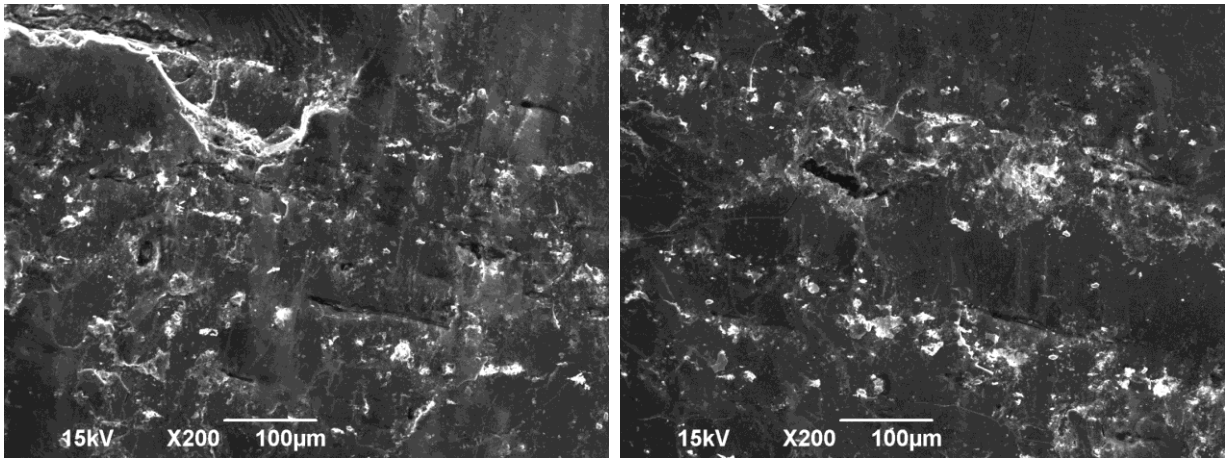

Figure 5.24: SEM images showing porous structure (from GME2237, perpendicular to bedding)

Figure 5.25 shows the coal solid surfaces observed for samples from the easy-to-drain area (GME2237, parallel to bedding). This slide was similar to the feature of the hard-to-drain area. Fracture structures were also observed in this sample, as shown in Figure 5.26.

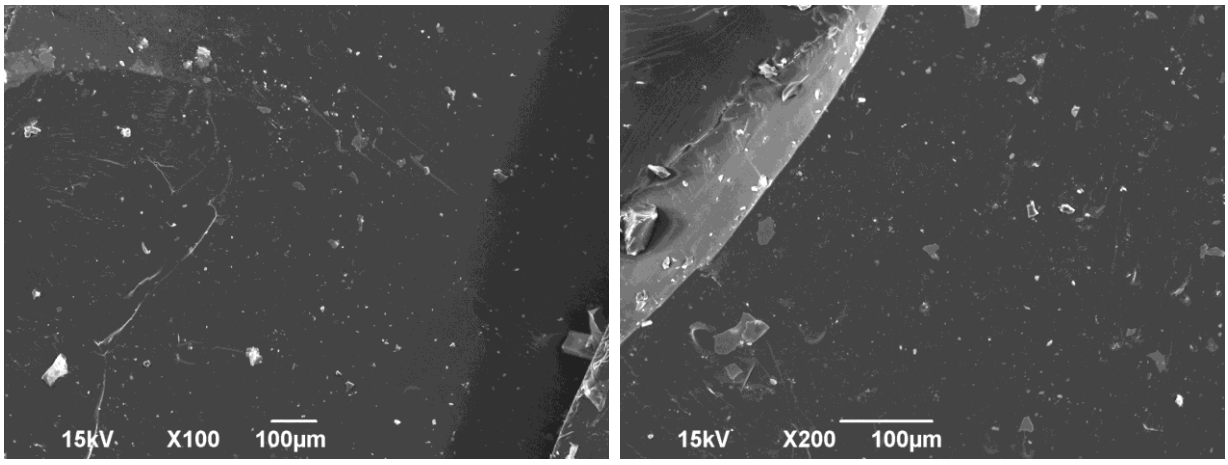

Figure 5.25: SEM images showing solid surface (from GME2237, parallel to bedding)

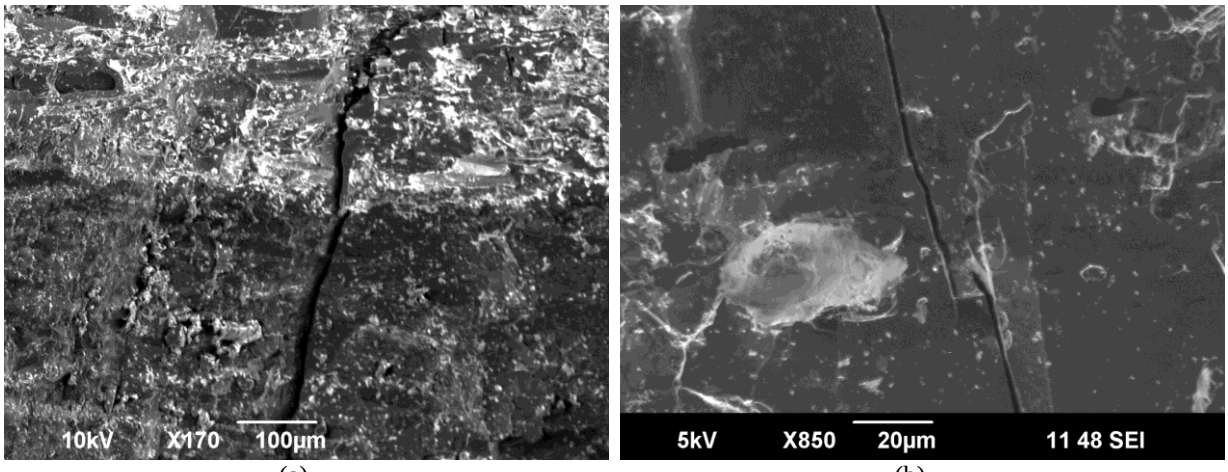

(a) (b)

Figure 5.26: SEM images showing coal fracture, (a) from GME2193, parallel to bedding, (b) from GME2193, perpendicular to bedding

5.3.4 Identification of coal porous structure

As a part of this research, the element mapping technology was used to identify the coal porous structure. As shown in Figure 5.27, the same image area was both taken with SE and BSE modes, the coal pore structure features were apparent with SE and BSE mode. Unlike SE, BSE moves on straight trajectories and is not affected by electrostatic collection fields. Since the BSE emission depends on the surface tilt, the surface topography was imaged at lower magnifications with better shadow effect than with SE, owing to the straight trajectories.

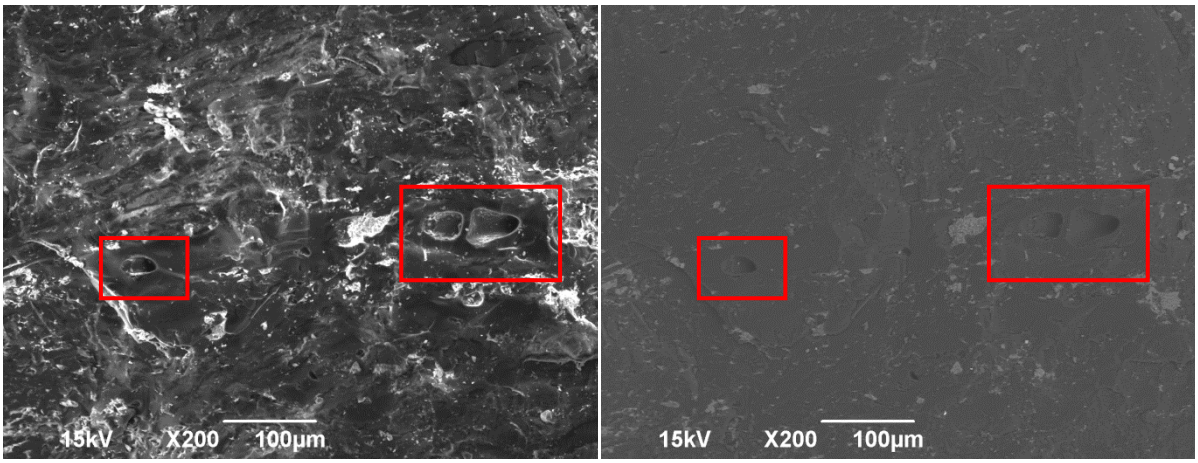

(a) SE mode (b) BES mode

Figure 5.27: SEM images showing coal porous structure, (a) with SE mode, (b) with BSE mode (from GME 2193, parallel to bedding)

Figure 5.28 shows the element mapping results of this area which consistently showed a typical porous morphology, confirming the SE and BSE mode images. The correction procedures developed for X-ray microprobes and normal incidence can be used for quantitative analysis in SEM by comparing the number of counts from an element in the specimen with the number of counts from a standard of known composition. However, quantitative analysis becomes more uncertain for inhomogeneous composition.

As shown in Figure 5.28, the area of porous structure (red square in each figure) appears to be dark black, indicating there is no element existence. Table 5.2 shows that the percentage of the four top elements in this mapping area, C (carbon) element is the dominating component, followed with O (oxygen) element. Usually the Si (silicon), S (sulphur), H (hydrogen) elements and mineral elements like Al (aluminium), Fe (iron), Ga (gallium) can be found in the element mapping figures.

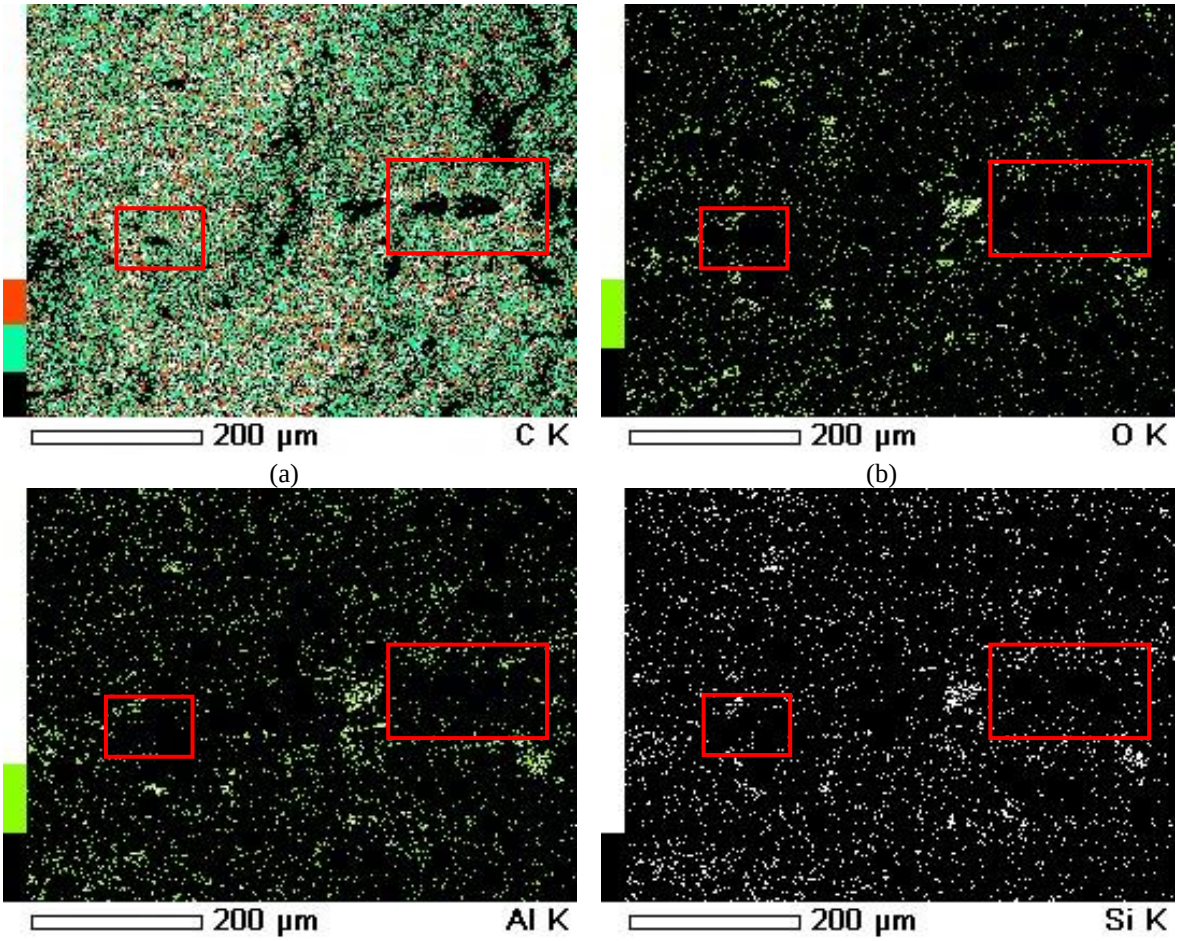

Figure 5.28: Element mapping images, (a) element C mapping, (b) element O mapping, (c) element Al mapping, (d) element Si mapping

Table 5.2: Top 4 elements percentage in the mapping area

Element	keV	Mass%	Atom%	Error%
Carbon	0.277	87.62	91.05	0.10
Oxygen	0.525	10.22	7.97	1.18
Aluminium	1.486	1.09	0.51	0.36
Silicon	1.739	1.07	0.47	0.39

5.4 SUMMARY

Geological variations can lead to changes in seam gas compositions as well as impact on the performance of gas drainage. Geological survey of the Bulli seam in Metropolitan Colliery showed that there is a strike/slip fault and mylonite existing in the typical hard-to-drain area (8-11 c/t, MG 22). This fault may be responsible for cleat system variations, CO_2 and CH_4 variations in this area and the high concentration of CO_2.

Field observation of cleat system and gas drainage borehole arrangements were carried out and face and butt cleat systems can be clearly observed on the lump coal sample provided, which appears to support field observations that boreholes drilled perpendicular to the face cleat (from drilling stub towards Mains or outbye) tend to be more productive, whilst boreholes drilled inbye were less effective for degassing.

The SEM technology is used to analyse the coal microstructures of coal samples from both easy-to-drain and hard-to-drain areas. It is observed that the microstructures of the hard-to-drain coal samples appear to be tighter and less porous compared with the easy-to-drain samples. In particular, coal samples from 11-12 c/t, MG 22 (hard-to-drain area) appears to have dominant solid surface feature both from the perpendicular and parallel to bedding directions. More coal porous structures are found with GME2193 (easy-to-drain area), especially in the direction parallel to bedding.

As the porous structure acts as the main gas flow and transport channel, coals with less porous structures will have the problem of poor gas drainage, particularly for the hard-to-drain areas of the Bulli seam, where the coal structure is less fractured. SEM technology shows a good method to indentify the coal surface features, operated with SE and BES signal mode and combined with element mapping technologies.

CHAPTER SIX – DRAINABLITY ASSESSMENT OF THE BULLI SEAM AT METROPOLITAN COLLIERY

6.1 INTRODUCTION

Metropolitan Colliery has experienced difficulty in reducing gas content within the available drainage lead time in an area of MG 22, as the seam in this area would not drain even with additional drainage boreholes. Metropolitan Colliery has supported the University of Wollongong to conduct a fundamental study into the problem of hard-to-drain areas in the Bulli coal seam. Apart from the geological variation, cleat system analysis and SEM based microstructure studies, laboratory tests on the permeability and sorption capacity of coal samples from hard-to-drain areas in Metropolitan Colliery were conducted. A critical examination of the gas database provided by Metropolitan was also carried out to evaluate the impact of gas content and gas composition on the drainability of the Bulli Seam. The detailed results are shown in this chapter.

Permeability is considered by many researchers to have a significant impact on the ability of a coal seam to produce gas (Jones *et al.*, 1982; Osisanya and Schaffitzel, 1996; Zutshi and Harpalani, 2005 and Lamarre, 2007). A recent study by Black (2012), examining factors contributing to effective drainage of gas from coal, found significant lack of information or insufficient data on coal permeability in comparison with other parameters such as gas content estimation and proximate analysis values. Difficulties associated with permeability determination in the laboratory or in the field, are mainly due to the fact that both the laboratory and field tests raise concerns about the test method. Permeability tests of Metropolitan samples were conducted with both normal triaxial permeability apparatus and a unique permeability apparatus, called the Multi Function Outburst Research Rig (MFORR), to understand the relationship between axial stress, gas pressure and permeability.

Gas sorption capacity, gas content and gas composition are believed to be related to gas drainage performance. The average gas composition value of CO_2 of whole database samples indicates the seam in this area is CO_2 rich. Through the systemic analysis of the whole gas database and typical hard-to-drain area, the gas components Q_1, Q_2 and Q_3 and their ratio in response to increasing measured total gas content Q_M and CH_4 gas composition were studied.

A comparative analysis of the three groups including whole database (CH_4<20 %), whole database (CH_4≥20 %) and the typical hard-to-drain area was carried out.

6.2 COAL PERMEABILITY

Permeability refers to the ability of coal to transmit gas when a pressure or concentration gradient exists across it. Permeability can vary significantly with stress condition (Lama, 1995 and Sereshki, 2005), and also fluid pressure changes during the gas production process (Cui and Busten, 2006) as well as gas type and gas pressure (Somerton *et al.*, 1975; Xue and Thomas, 1995; Sereshki, 2005). It has a strong effect on the gas production profile and gas well performance.

Generally, three types of approaches can be used to evaluate the permeability of coal: (1) the field test approach, where formation permeability is measured with *in situ* condition; (2) the experimental approach, where absolute permeability is directly measured in a controlled laboratory setting; (3) the theoretical modelling approach, where fracture width can be calculated according to the principles of rock mechanics. Each approach has its own advantages and disadvantages. The measured core sample permeability can be different from bulk permeability along the cleat tested *in situ* (Gray, 1982). The absolute permeability test in the laboratory is better able to discern and verify subtle changes compared with the precision and the accuracy of field measurements. Large permeability changes might potentially be measurable by field tests, however, these may intrude on a mine's operation and production.

A number of different laboratory permeability testing apparatus have been reported. They are basically triaxial cells and used to simulate the *in situ* conditions. Some apparatus consists of a conventional triaxial cell, modified to provide gas inlet and exit ports through the upper and lower platens (Harpalani and Schraufnagel, 1990), while others are more elaborate in design, such as those reported by Lingard *et al*. (1984), Lama (1995), Gillies *et al.* (1995) and Nakajima *et al.* (1995). The mode of permeability testing, using these different apparatus however, can vary with respect to the way and role of confinement pressure application.

In order to obtain representative permeability values with respect to effective gas drainability from the difficult to drain zone as well as provide a better understanding of the potential gas recovery through the nitrogen injection and displacement process, a laboratory permeability test program was conducted in this study. The laboratory test program consisted of duplicate testing of coal samples using two different permeability testing apparatus.

Both tests were carried out under triaxial test conditions. The first permeability testing method was carried out using a MFORR which was previously reported by Lama (1995), Aziz and Li (1999) and Sereshki (2005). In this test, the sample was enclosed in a triaxial gas chamber. The coal sample was subjected directly to gas as the confining pressure. The pressurised gas was allowed to filter through the coal sample while it was being loaded axially. A centrally drilled hole in the coal sample allowed the gas to flow out of the chamber in a controlled manner. The second permeability testing apparatus used in this study was a high pressure triaxial cell, initially built for determining the relative permeability of coal measure rocks under two-phase flow conditions (Indraratna and Haque, 1999; Jasinge *et al*., 2011; Perera *et al*., 2011). Both methods of testing and the results obtained are the subject of discussion in this chapter.

6.2.1 Multi Function Outburst Research Rig test

6.2.1.1 Multi Function Outburst Research Rig

The MFORR shown in Figure 6.1, was used to study the permeability of coal parallel to its stratification. MFORR comprises a number of components which can be utilised for permeability testing with the confining pressure being provided by the applied gas pressure which filters through the coal being tested. As a multifunction apparatus the MFORR has various components:

- The main apparatus support frame
- A precision drill
- A high pressure chamber which has a load cell for measuring the load applied to the samples of coal
- A pressure transducer for measuring the pressure inside the chamber
- Flow meters for measuring the gas flow rate
- Two strain gauges for measuring the vertical and horizontal strains of the coal sample
- A universal socket for loading a sample of coal vertically into the gas pressure chamber
- A gas chromatograph (GC)
- A data acquisition system

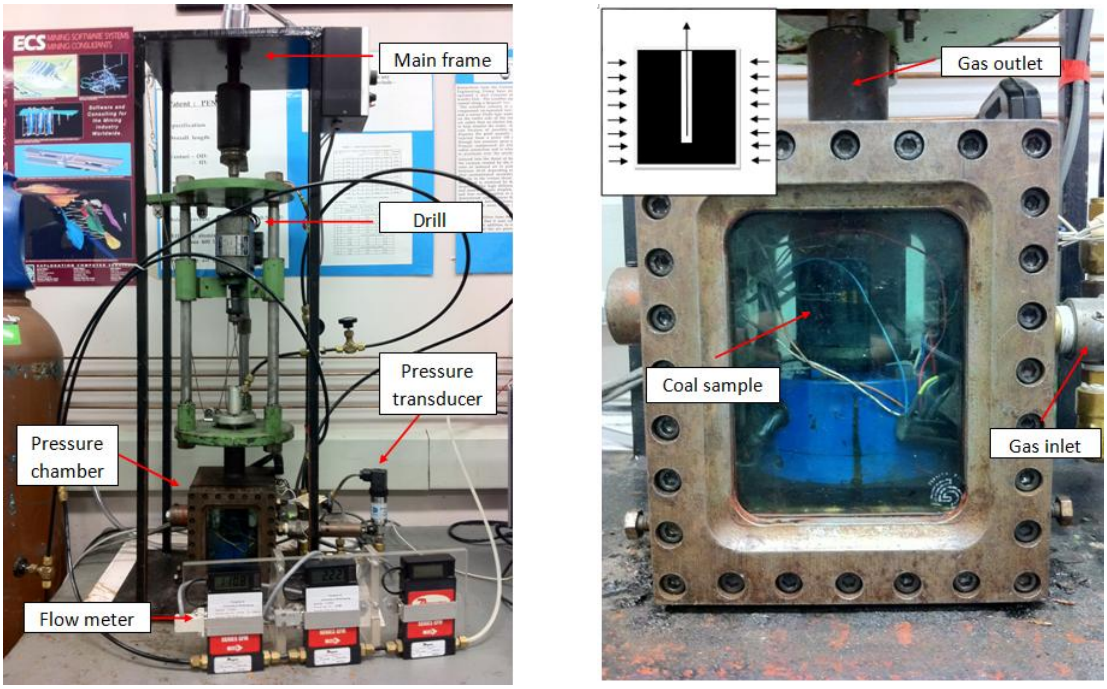

(a) (b)

Figure 6.1: Multi Function Outburst Research Rig (MFORR)

The gas pressure chamber containing the coal sample is a hollow rectangular prism of cast iron with removable front and back viewing plates. The dimensions of the box are 110 mm x 110 mm x 140 mm. The viewing windows are made of 20 mm thick glass in a cast iron frame. Housed in the chamber is a 1210-BF interfaced load cell with a capacity of 40 kN for monitoring the load applied.

6.2.1.2 Coal sample preparation

A lump of coal sample was collected from panel MG 22 hard-to-drain area. Prior to coring, the coal sample was cast in concrete to form a uniform block for easy coring. A standard core sample with dimension of 54 mm in diameter and 50 mm in height was cored out of the block. A 2 mm diameter hole was drilled in the middle of the cored coal sample to measure the permeability of this apparatus. Prior to testing, both ends of the prepared specimen were sealed with an adhesive 1 mm thick rubber layer to ensure effective gas flow along radius in the coal. Figure 6.2 shows a snapshot of the prepared test sample.

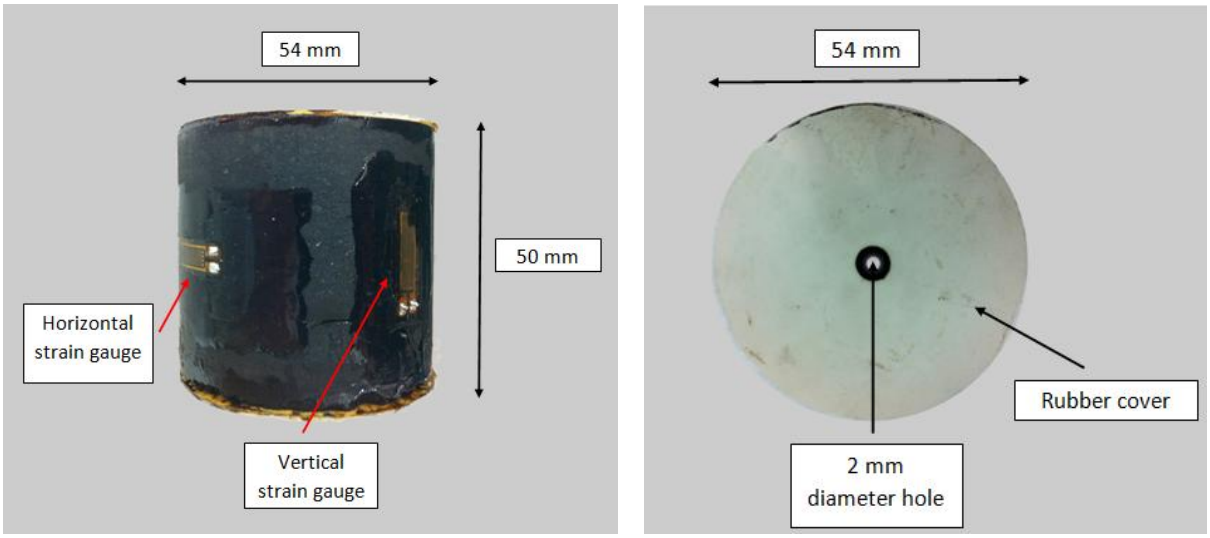

Figure 6.2: Coal samples for permeability test with MFORR

6.2.1.3 Testing procedure

The procedure adopted for permeability testing consisted of each sample being first mounted in the pressure chamber. The chamber was then sealed, the system then evacuated to remove air and subsequently repressurised to a predetermined level and maintained at that level. The N_2 gas was allowed to permeate the coal sample and flow out through the central hole. The released gas from the coal flows through a measuring system, consisting of a vacuum pressure sensor and a line of gas flow meters of 0-2 L/min and 0-15 L/min measurement ranges respectively.

The test sequence was followed in steps of varying vertical stress of 1, 2, 3 and 4 MPa, for the consideration that if the highest applied load was greater than the mechanical strength of the coal, the coal could be crushed, and this resulted in higher permeability. For each selected vertical loading, confining gas pressures varying between 0.2 to 3 MPa were applied. The load cell, flow meters, pressure transducer and strain gauges were connected to a PC through a data logger for data collection.

6.2.1.4 Results and analysis

The permeability of the sample was calculated using the following Darcy's equation:

$$K = \frac{\mu Q ln(\frac{r_0}{r_i})}{\pi h({P_1}^2 - {P_2}^2)} \qquad (6\text{-}1)$$

where K is the permeability of coal, μ is viscosity of gas, Q is the flow rate of gas, h is the height of the sample, r_o and r_i are the external radius and internal radius of sample, P_1 and P_2 are absolute gas pressure inside and outside the chamber, respectively.

Figure 6.3 shows the permeability test result with the MFORR apparatus, which is being pressurised by N_2 gas, at different applied vertical stress levels. For each of the vertical stress levels, the coal sample permeability decreases with increasing gas pressure and at higher gas pressure, the coal permeability starts to stabilise just below 1 mD with little variations, under different vertical stresses. Test results show that the permeability values stay below 1 mD when the applied confining gas pressures become greater than 0.5 MPa. The results of MFORR tests are shown in Appendix E in detail.

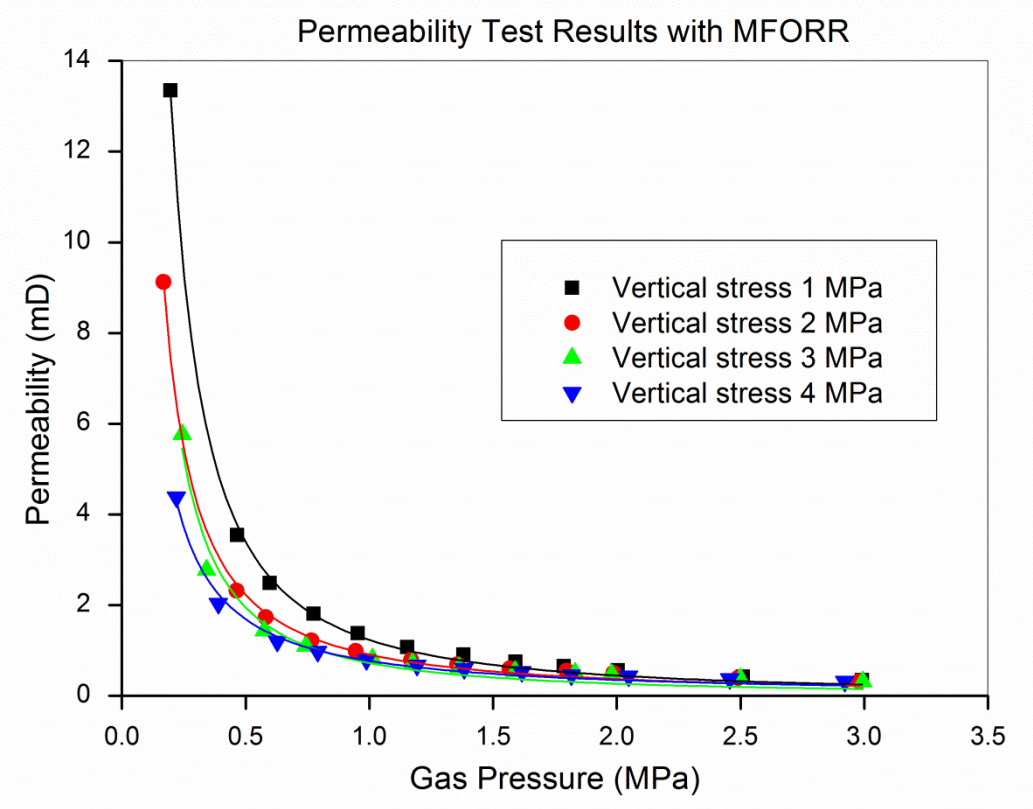

Figure 6.3: Coal permeability test result with MFORR

Figure 6.4 shows coal strain behaviour in the MFORR permeability test. Test results show that the degree of strain, both axially and laterally, is influenced by the level of pressure that the sample is subjected to under triaxial environment.

There is an increased compaction of the coal layers parallel to bedding with increased vertical stress due to applied axial loads perpendicular to layering. The degree of axial shrinkage

increases with increasing axial stress as demonstrated in Figure 6.4(a). Also, the level of vertical or axial strain has reduced with the increase of the applied lateral gas confining pressure. The level of lateral/horizontal strain is affected by the level of the applied axial load as well as the confining gas pressure, this time in reverse order. That is, at high vertical stress of 4 MPa, the confining lateral stress is the greatest, while the least applied axial stress contributes to increased maximum lateral strain. Also and irrespective of the level of the axial stress, the horizontal stain gradually decreases with gradual increase of the applied confining gas pressure, as demonstrated in Figure 6.4(b).

These results clearly demonstrate that the coal samples undergo negative volumetric changes or shrinkage with increased confinement pressures axially and laterally, and that the degree of the volumetric changes is dependent on the level of the applied axial and lateral pressures or stresses.

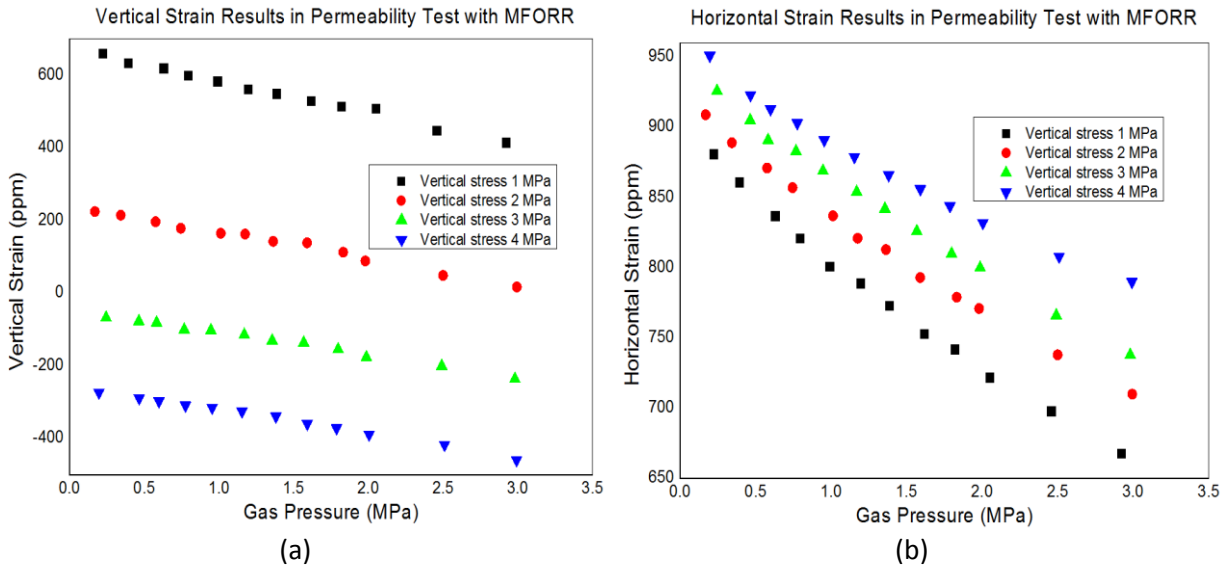

Figure 6.4: Coal strain behaviour in the permeability test with MFORR (ppm refers to part per million, dimensionless unit)

6.2.2 Triaxial Compression Apparatus test

6.2.2.1 Triaxial Compression Apparatus

The Triaxial Compression Apparatus is shown in Figure 6.5. This test rig comprises a number of components which can be utilised in normal triaxial permeability tests of coal. Major components of the apparatus include:

- A main apparatus loading system for holding and loading the pressure cell

- High pressure cell for holding the coal sample in triaxial permeability test
- An axial loading and measuring device
- Oil pump generating and maintaining the confining pressure applied to the coal sample
- A pressure transducer for measuring the pressure inside the cell
- A pressure transducer for measuring the pore pressure
- Flow meters for measuring the gas flow rate
- A data acquisition system

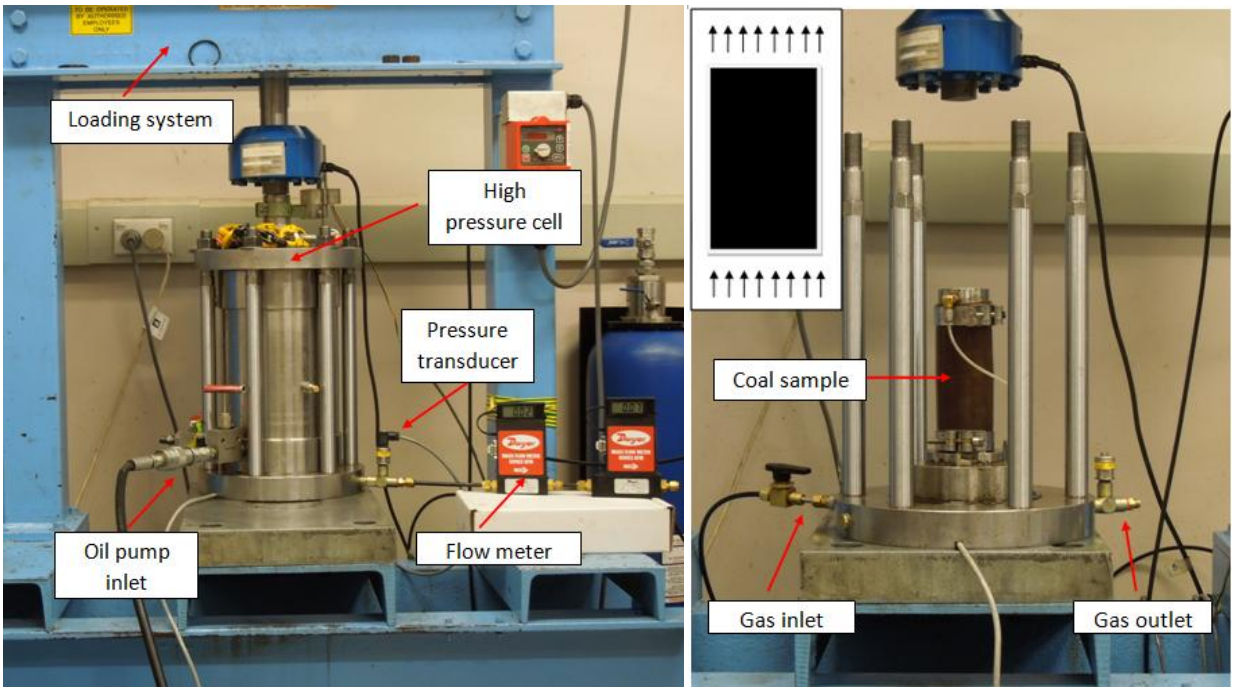

(a) (b)

Figure 6.5: Triaxial Compression Apparatus

In this apparatus, the cell pressure is controlled manually by a hydraulic jack and a pressure transducer, which is mounted on the cell to ensure the required confining pressure. The cell is made of high-yield steel and it can withstand a maximum pressure of 150 MPa with a safety factor of 2. The cell is capable of carrying out high confining pressure tests, making it suitable to simulate a high *in situ* stress environment in coal measure rocks. The axial load is applied by a servo-controlled compression test machine with a maximum force of 250 kN.

6.2.2.2 Coal sample preparation

The standard core samples with a dimension of 54 mm in diameter and 100 mm in height were drilled from the same lump coal sample as the MFORR permeability test samples which

were also collected from MG22 from Metropolitan coal mine. Figure 6.6 shows a snapshot of the sample.

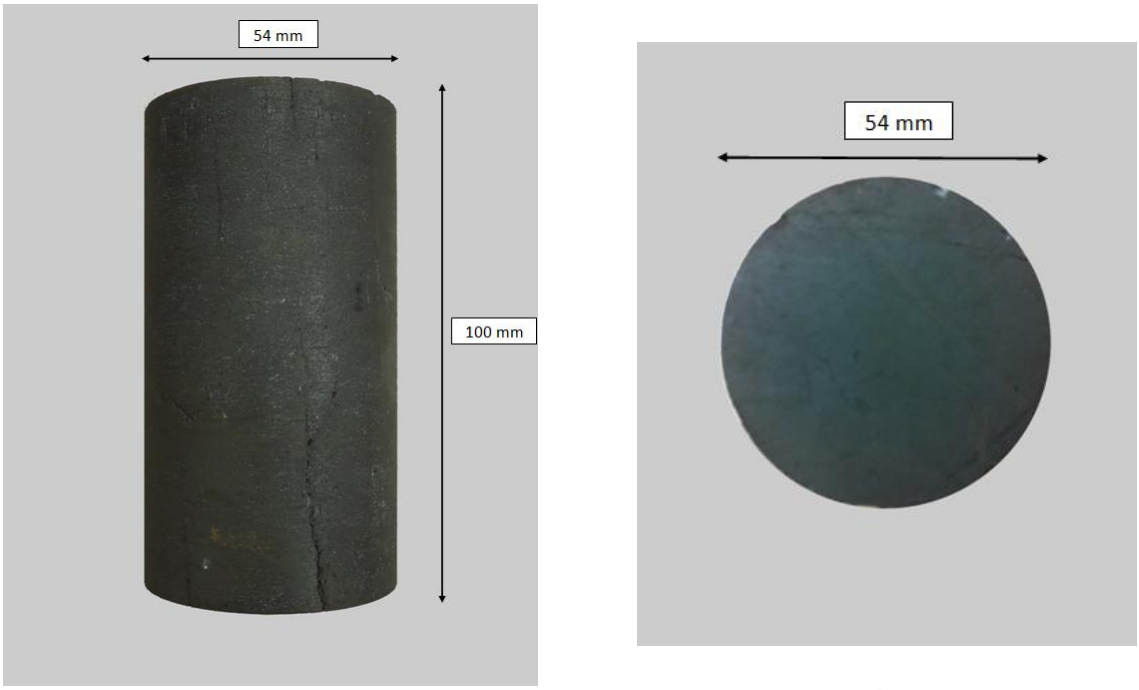

(a) (b)

Figure 6.6: Coal samples for triaxial permeability test with Triaxial Compression Apparatus

6.2.2.3 Testing procedure

The procedure for conducting each test consisted of the sample being correctly installed inside a membrane. The specimen was placed into the high pressure cell where a small axial load was applied firstly to keep it stable. Then oil was pumped into the cell until the cell was filled with oil with both the axial load and confining pressure applied to predesigned values. Subsequently, N_2 gas pressure was applied at a predetermined level and maintained at that level. The released gas from the coal flowed through a monitoring system consisting of gas flow meters with 0-2 L/min and 0-15 L/min measurement ranges.

The test sequence was followed in steps, with different vertical stress of 3, 4, 6 and 8 MPa applied respectively. The gas pressure was charged from 0.2 MPa to higher pressure around 3 MPa. The load cell, flow meters and pressure transducer were all connected to a PC through a data logger for data collection.

6.2.1.4 Results and analysis

The permeability of the sample was calculated using the following Darcy's equation:

$$K = \frac{2Q\mu LP_2}{A(P_1^2 - P_2^2)} \quad (6\text{-}2)$$

where K is the permeability of coal, μ is viscosity of gas, Q is the flow rate of gas, L is the length of the sample, A is the cross section of specimen, P_1 and P_2 are the inlet and outlet absolute gas pressure, respectively.

Figure 6.7 shows the triaxial permeability test results with N_2 at different vertical stresses. Tests with a vertical stress of 3, 4, 6 and 8 MPa were examined. For each vertical stress, two horizontal stresses were examined, coal sample permeability decreased with the increasing gas pressure. The results of the triaxial tests are shown in Appendix F in detail.

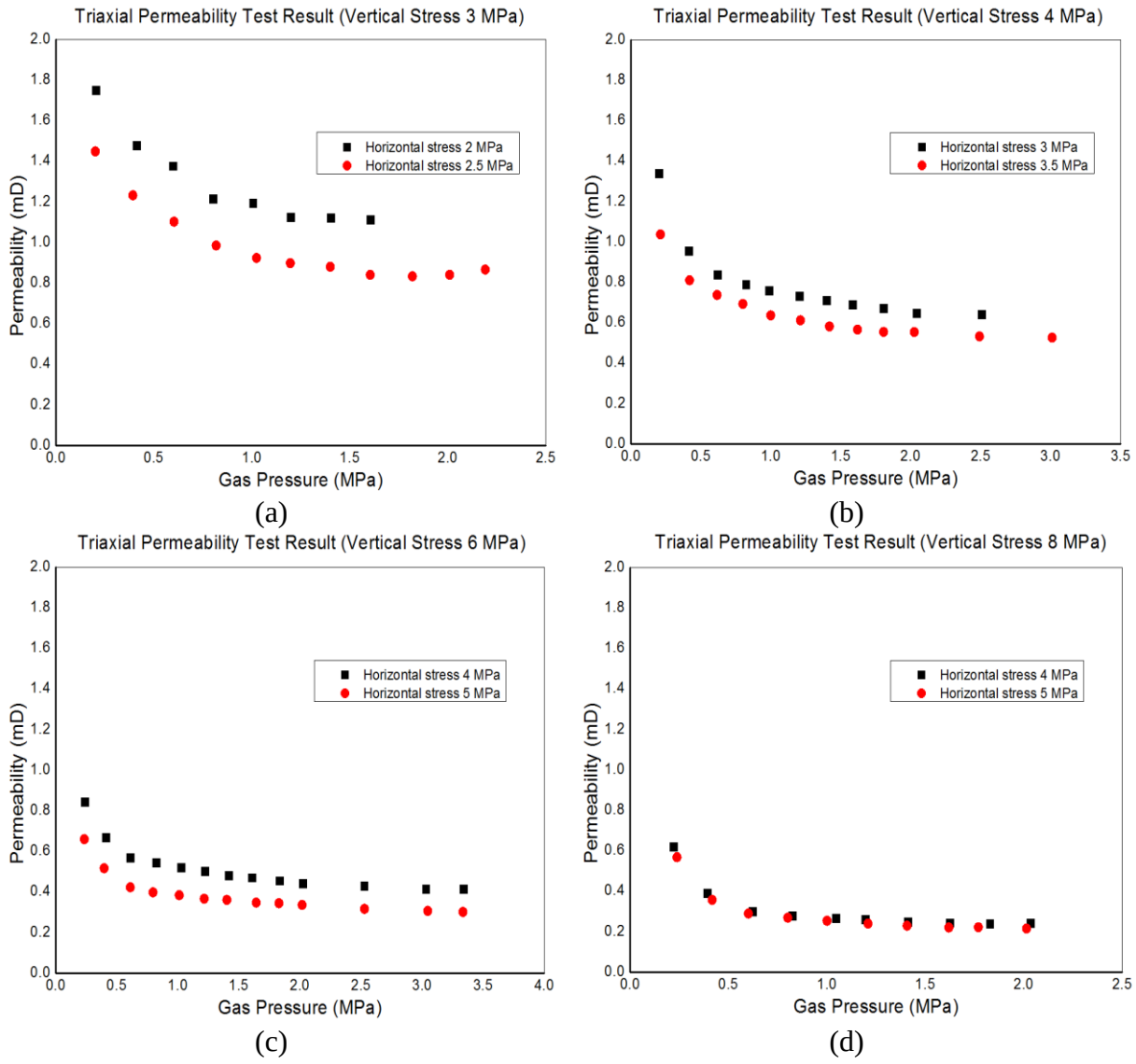

Figure 6.7: Coal triaxial permeability test with a certain vertical stress

As shown in Figure 6.7, at higher gas pressures, the value of coal permeability stayed almost constant, following a similar trend as the permeability results with MFORR. At each vertical stress, coal permeability decreases with increasing horizontal stress.

Figure 6.8 shows the triaxial permeability test results at various horizontal stresses. Tests at horizontal stress of 4 and 5 MPa are analysed in this study. At each of the horizontal stress, coal sample permeability decreases with increasing vertical stress. It can be observed from the tests that the permeability values converge below 1 mD under higher triaxial stress conditions.

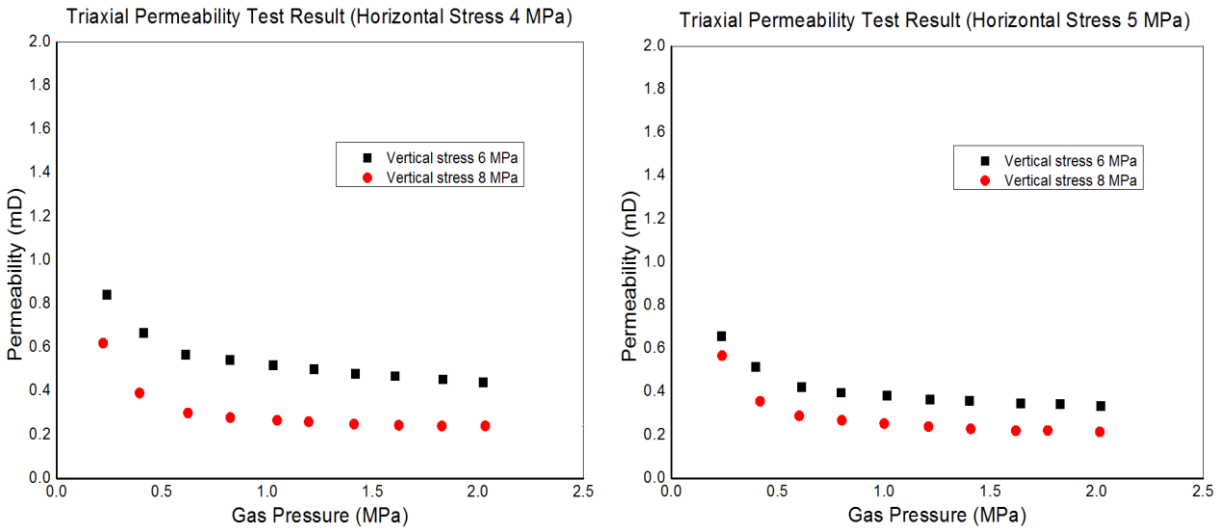

(a) (b)

Figure 6.8: Coal triaxial permeability test with a certain horizontal stress

6.2.3 Comparative analysis of MFORR and Triaxial Compression Apparatus test results

Figure 6.9 shows a comparison of the permeability results between the MFORR and normal triaxial tests at various vertical stress levels. Although the results show some significant difference in permeability values at lower confining gas pressure, the permeability converges to a steady level below 1 mD under high triaxial stress conditions, portraying the near *in situ* conditions of the Bulli seam.

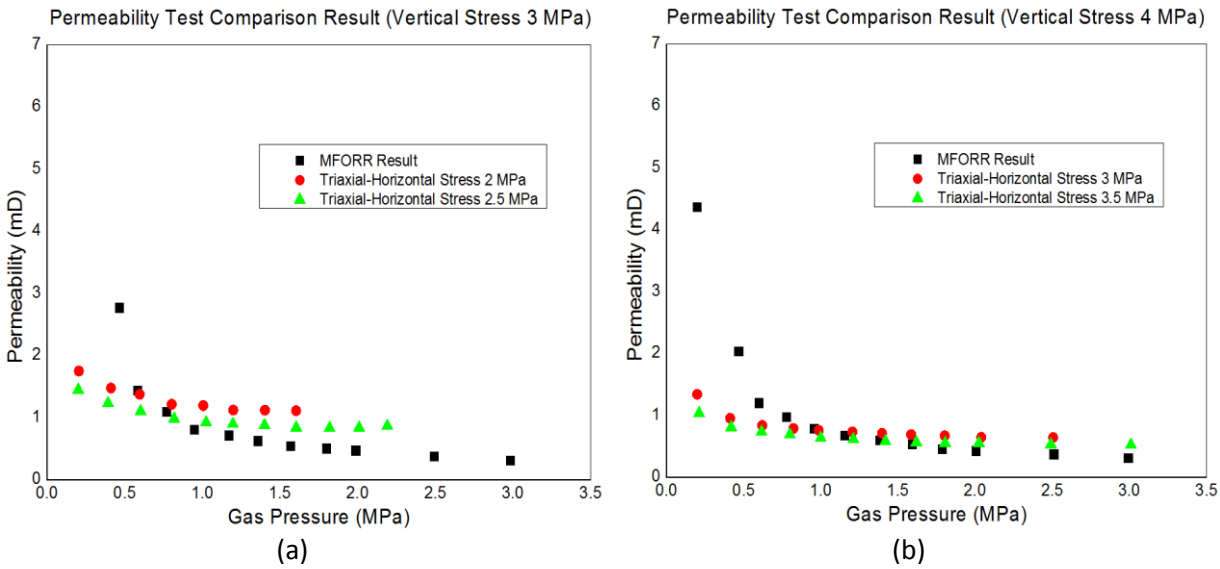

Figure 6.9: MFORR permeability and triaxial permeability test results comparison

Similar results were reported by other researchers; Hayes (1982) reported that the Bulli seam coal permeability was considerably less than 1 mD. Lingard *et al.* (1984) reported permeability of Australian coals from Appin, West Cliff and Leichhardt collieries that varied from less than 0.1 mD to 100 mD. Recently the Bulli seam coal permeability was measured using a combination of injection / falloff and step-rate testing methods (Jackson, 2004) and the results from 31 locations of the Bulli seam at West Cliff Colliery (Fredericks, 2008 and Black, 2012) showed the average *in situ* permeability of coal was 2.2 mD, with the range extending from a low of 0.005 mD to a high of 5.8 mD.

6.2.4 Permeability classification of coalbeds

The permeability of coal plays an important role in the entire process of gas drainage in coal mines and CBM production. Santillan (2004) classified coalbeds into four groups based on their *in situ* permeability (Figure 6.10). An assignment of CBM well completions based on permeability is shown in Figure 6.11 (Palmer, 2010). The study by Palmer (2010) stated the especially important role of coal permeability measurement in development of a CBM play, which may be underestimated (or even ignored) by many operators.

Hughes and Logan (1990) stated that the minimum required permeability of coal for coalbed gas drainage is generally greater than 1 mD. However for Australian coals, Thomson and MacDonald (2003), referring to the work by Williams (1999), indicated that the Australian coal seams suitable for drainage (medium radius drill method) should have a gas content of

more than 6 m^3/t gas and permeability greater than 2 mD at a depth of 150 to 500 m as illustrated in Figure 6.12.

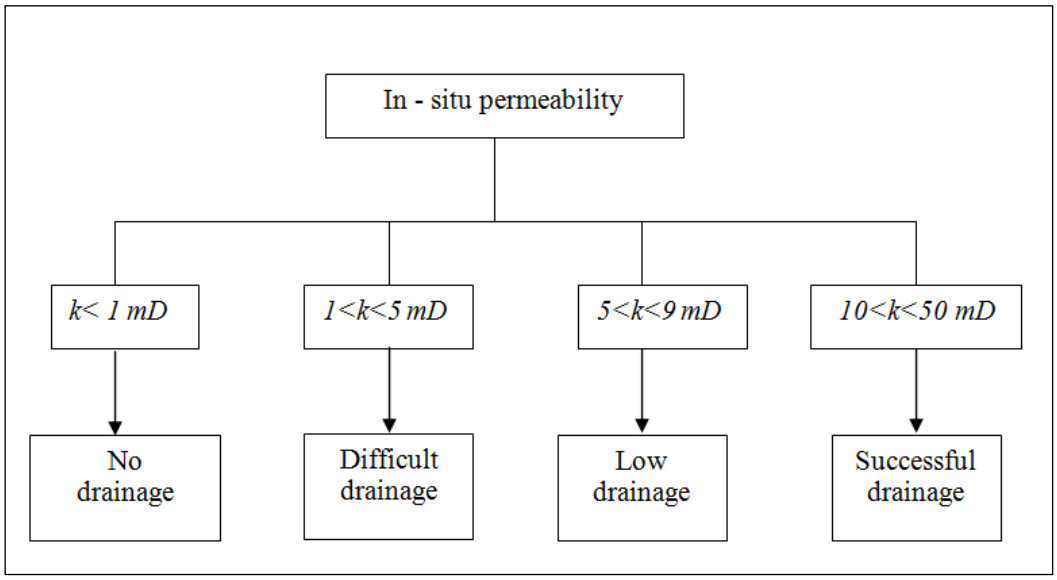

Figure 6.10: Classification of coal-beds based on their permeability (after Santillan, 2004 and Sereshki, 2005)

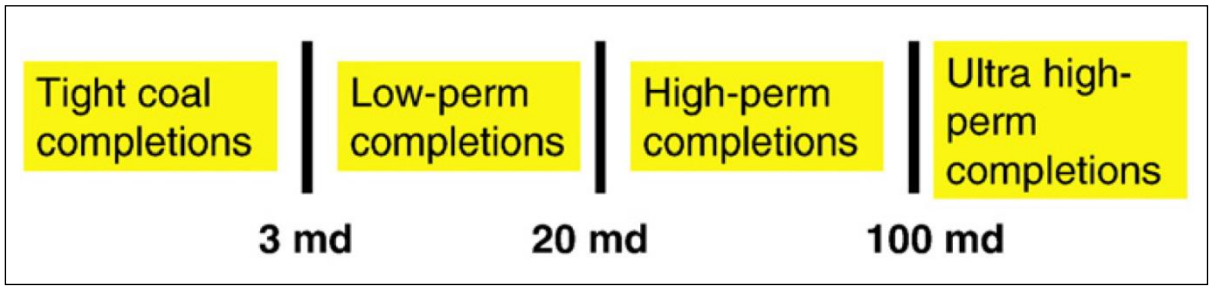

Figure 6.11: Permeability bands for CBM well completions (after Palmer, 2010)

As the permeability test is carried out with N_2 gas and dry coal samples, the *in situ* permeability should be lower than the lab tested permeability result. Due to Metropolitan Colliery's *in situ* situation, high concentration of CO_2 and CH_4 mixture gas and water in the coal matrix and borehole, the *in situ* permeability should be less than 1 mD, and with the coal seam depth of more than 400 m and gas content of 7.76 m^3/t in the typical hard-to-drain area, gas drainage in these areas will be of poor performance if no other enhancement techniques are employed.

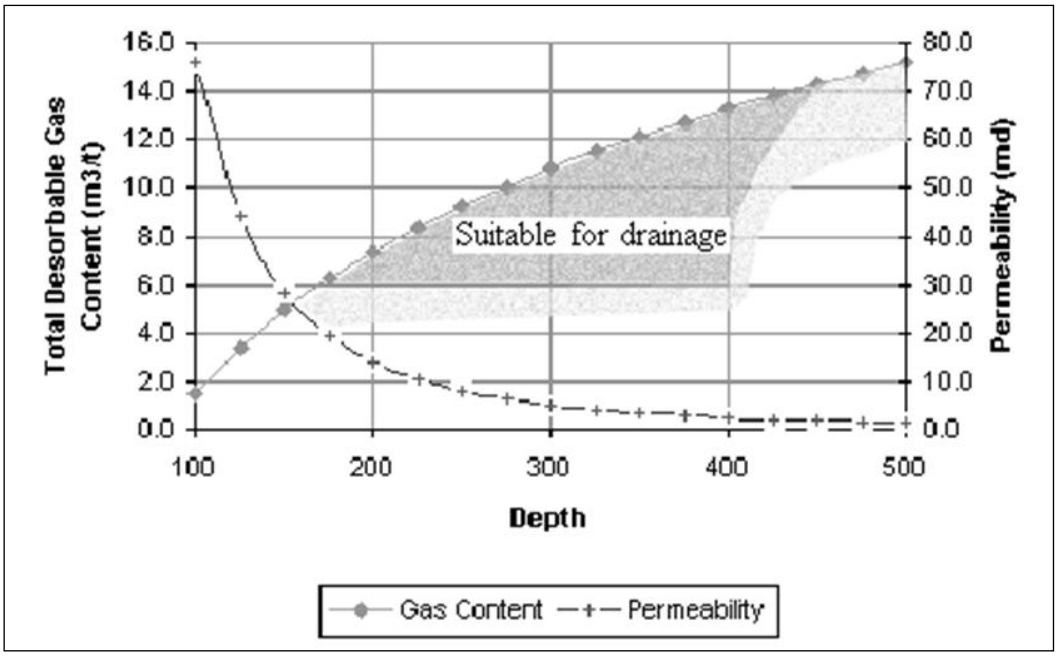

Figure 6.12: Permeability and gas content relationship with depth (after Thomson and MacDonald, 2003)

6.3 COAL SORPTION CAPACITY

6.3.1 Ash content test

The coal samples used in the ash content test are from the core samples after the fast desorption gas content test. Before the test, the coal samples are crushed to -212 μm and dried in a vacuum desiccator containing water sorbing material and kept in the oven at 60 ºC for 24 hours. The ash content test of coal follows the Australian Standard, methods for the analysis and testing of coal and coke (AS 1038.3-1989).

The test results show that the ash content of Metropolitan coal is around 7 %, which can be regarded as relatively low ash content coal. Generally speaking, low ash content coal has larger gas adsorbing capacity than high ash content coal, which also explains why this type of coal has a strong gas adsorbing capacity and therefore requires longer drainage lead time to reduce gas content below a threshold limit.

Ash content correlates strongly to gas adsorption capacity of coal as shown in Figure 6.13 (Laxminarayana and Crosdale, 1999). The Langmuir volume parameter represents coal sorption capacity and with increasing ash (mineral matter) content related to a reduction in the Langmuir volume of the raw coal. Linear decrease in adsorption capacity with increasing ash content indicates that the ash (mineral matter) acts as a simple diluent, thereby reducing the storage capacity. For the Metropolitan coal sample, the ash content is very low, which

could be another important reason why the coal has a strong sorption capacity (and therefore hard-to-drain).

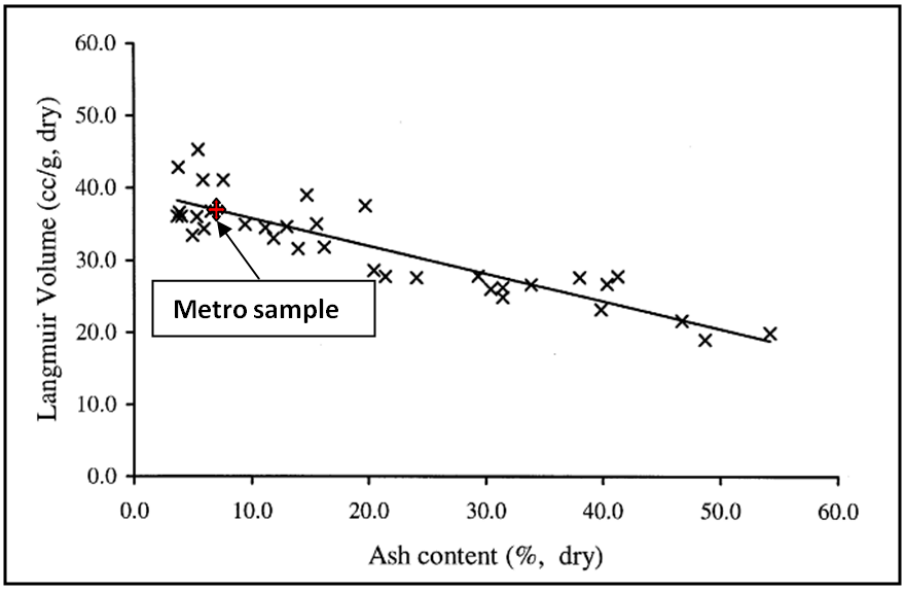

Figure 6.13: Relationship between Langmuir Volume representing coal sorption capacity and ash content (after Laxminarayana and Crosdale, 1999)

6.3.2 Adsorption isotherm test

Samples from both the hard-to-drain and easy-to-drain areas were tested. Sample GME 2126, GME 2127, GME 2128 and GME 2130 were from the typical hard-to-drain area (from c/t 8-11 along MG 22). Sample GME 2233 (from c/t 17-18 along MG 22), GME 2192 (from c/t 26-27 along MG22) and GME 2238 (from c/t 31-32 along MG22) were from easy-to-drain area A, and sample GME 2198, GME 2203, GME 2213, GME 2218 and GME 2225 were from easy-to-drain area B. The location of typical hard-to-drain area and easy-to-drain area A and B are previously shown in Figure 5.1 in Chapter Five.

The indirect gravimetric method was used to calculate the volume of gas adsorbed and desorbed from coal in the gas laboratory at the University of Wollongong. The gas adsorption apparatus has been shown in chapter four and the calculation method has been shown in chapter three. In this apparatus, each vessel, known as a "Bomb", has its own pressure transducer so that the sorption process and changes in bomb pressure can be readily determined. All samples were prepared by crushing to powder size of -212μm. Prior to testing, the coal samples were placed in a vacuum in a desiccator containing water sorbing material and put into the oven at 60 ºC for 24 hours.

All samples were enclosed in pressure bombs and subjected systematically to CO_2 and CH_4 gas pressurisation at the temperature of 25 °C. The first step is using the helium expansion method to determine the void volume of the bomb for each sample, and then each of the bombs is charged with the test gases, the level of charging gas pressure of the sorption test is carried out initially at 1000 kPa and then 1500 kPa, 2000 kPa, 3000 kPa until reaching the maximum of 4000 kPa. Finally the isotherms are obtained with the equilibrium point of pressure and adsorbed gas volume.

Figure 6.14 shows the test results for four samples from the typical hard-to-drain area and Figure 6.15 shows the test results for eight samples from easy-to-drain areas A and B. Figure 6.16 shows the straight coal adsorption isotherm comparisons at 25 °C for both CO_2 adsorption isotherm and CH_4 adsorption isotherm. It can also be observed there is no apparent variations and group trend for hard-to-drain and easy-to-drain coals (more details can be seen in Appendix G).

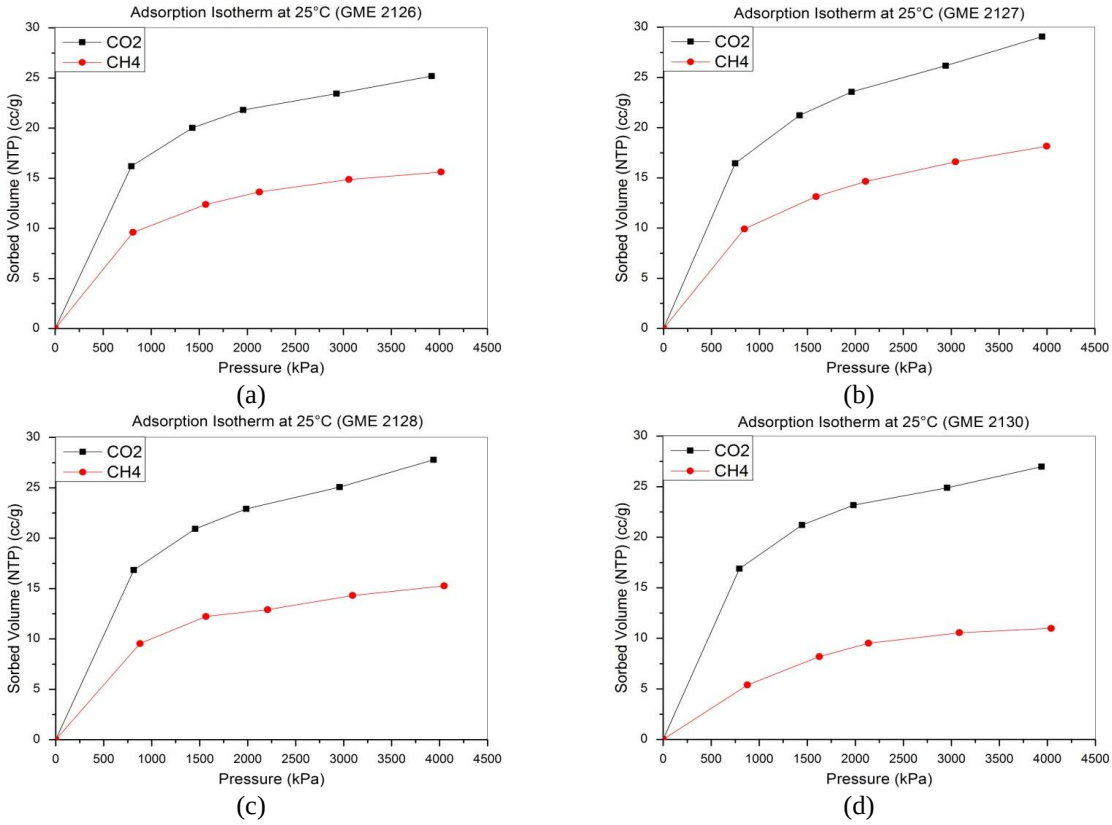

Figure 6.14: Coal adsorption isotherms at 25 °C (pictures a, b, c are from typical hard-to-drain area)

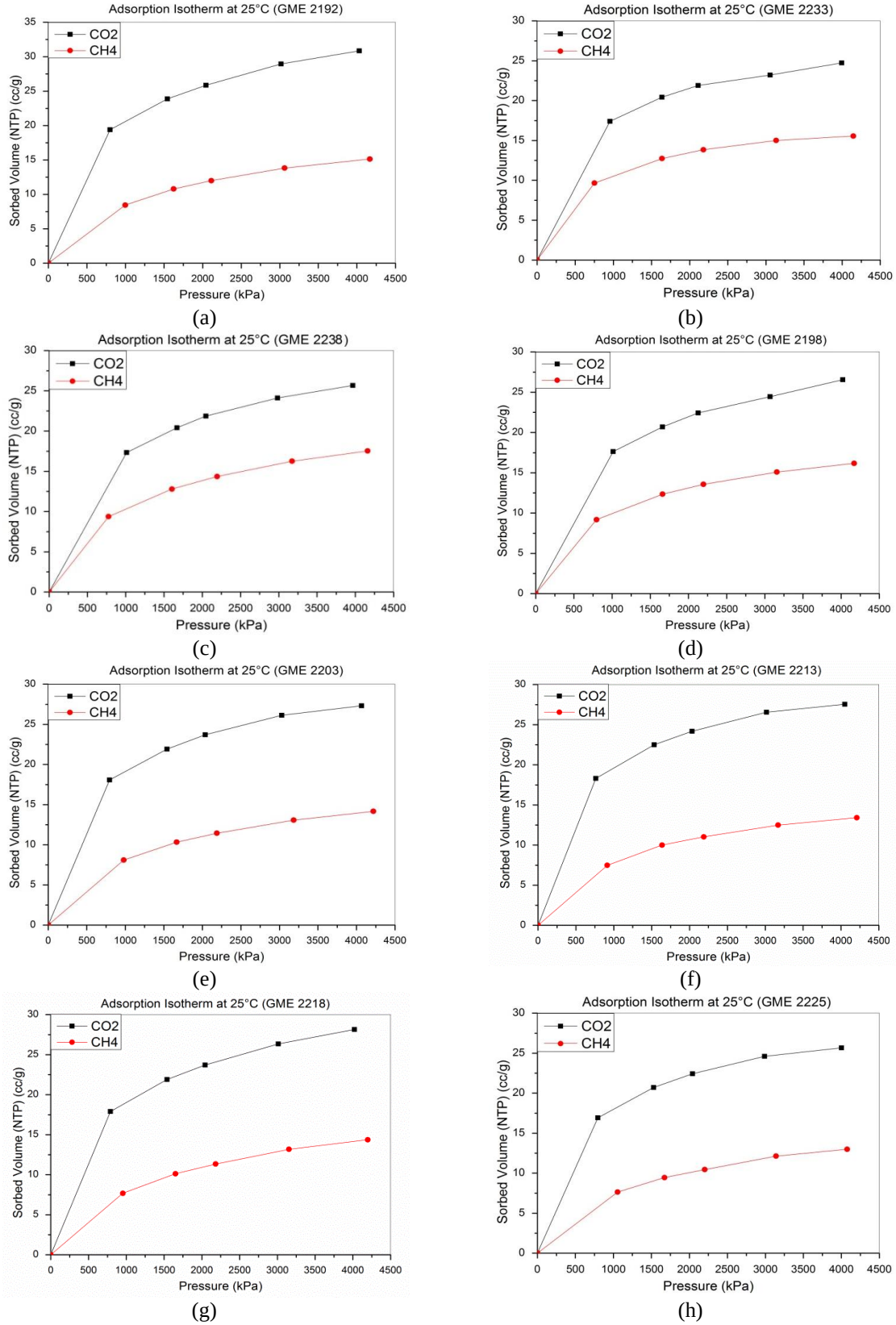

Figure 6.15: Coal adsorption isotherms at 25 °C (pictures a, b and c are from easy-to-drain area A, pictures d, e, f, g and h are from easy-to-drain area B)

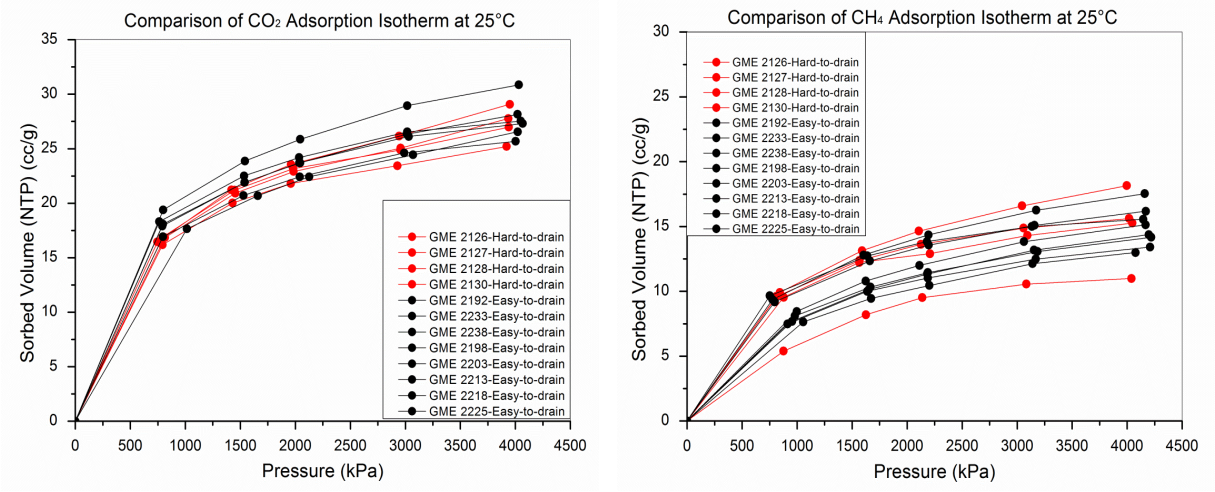

(a) (b)

Figure 6.16: Coal adsorption isotherm comparisons at 25 °C (picture a is for CO_2 adsorption isotherm, picture b is for CH_4 adsorption isotherm)

As the mine site is CO_2 rich, the CO_2 isotherm should affect the gas drainage more than the CH_4 isotherm. Table 6.1 shows the Langmuir volume of CO_2 and CH_4 for hard-to-drain area sample. Compared with the results from the easy-to-drain area test results (Table 6.2), the Langmuir volume of CO_2 and CH_4 for easy-to-drain area had no larger difference with both of the easy-to-drain areas.

Figure 6.17 indicates the critical desorption point of a typical Bulli seam sample, based on isotherms representing the adsorption capacity for both pure CH_4 and CO_2 (Black and Aziz, 2010). Considering the same initial *in situ* gas condition, gas content (10.5 m^3/t) and pressure (3.5 MPa), it can be seen that a CO_2 rich coal requires far larger reservoir pressure reduction to reach the critical desorption point than does an equivalent CH_4 rich sample.

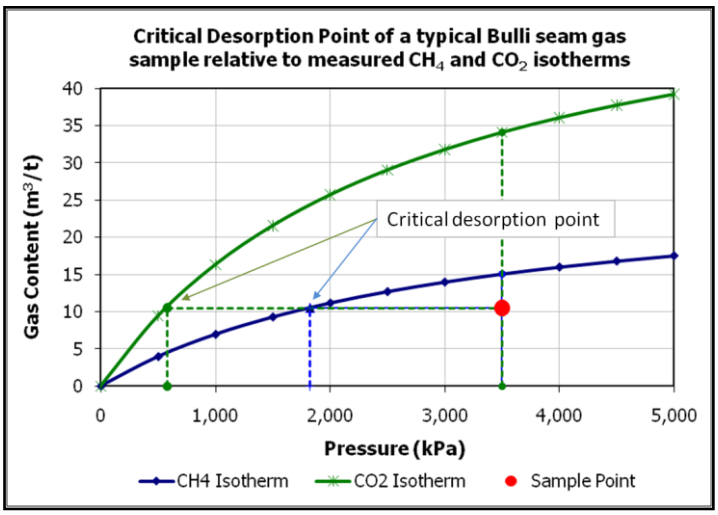

Figure 6.17: Critical desorption point of a typical CO_2 and CH_4 rich Bulli seam coal sample. (after Black and Aziz, 2010)

Table 6.1: Langmuir parameters for the tested samples in terms of CO_2 and CH_4 (hard-to-drain area)

Langmuir parameters	GME 2126	GME 2127	GME 2128	GME 2130
Drainage area	Hard-to-drain	Hard-to-drain	Hard-to-drain	Hard-to-drain
Langmuir volume for CO_2 (cc/g)	29.2	35.2	33.1	31.4
Average Langmuir volume for CO_2 (cc/g)	32.2			
Langmuir pressure for CO_2 (kPa)	653.4	992.1	845.0	704.4
Langmuir volume for CH_4 (cc/g)	18.6	23.4	18.2	15.3
Average Langmuir volume for CH_4 (cc/g)	18.9			
Langmuir pressure for CH_4 (kPa)	774.4	1213.5	812.8	1457.5

Table 6.2: Langmuir parameters for the tested samples in terms of CO_2 and CH_4 (easy-to-drain area)

Langmuir parameters	GME 2192	GME 2233	GME 2238	GME 2198	GME 2203	GME 2213	GME 2218	GME 2225
Drainage area	Easy-to-drain A	Easy-to-drain A	Easy-to-drain A	Easy-to-drain B	Easy-to-drain B	Easy-to-drain B	Easy-to-drain B	Easy-to-drain B
Langmuir volume for CO_2 (cc/g)	36.5	28.4	30.9	32.0	31.5	31.5	33.0	29.7
Average Langmuir volume for CO_2 (cc/g)	31.9			31.54				
Langmuir pressure for CO_2 (kPa)	776.9	626.1	827.3	878.9	636.4	582.7	741.0	635.7
Langmuir volume for CH_4 (cc/g)	20.2	18.1	22.1	19.8	18.4	17.2	19.5	17.4
Average Langmuir volume for CH_4 (cc/g)	20.1			18.5				
Langmuir pressure for CH_4 (kPa)	1415.8	667.5	1120.7	971.4	1288.3	1194.8	1508.5	1396.9

6.4 STUDY OF GAS CONTENT AND GAS COMPOSITION

Gas content and gas composition are the important factors in relation to coal mine operation and safety, and currently they have become more important in coalbed methane resource assessment and recovery operations for CBM industries. These data can be used in evaluation of coal seam gas control options in underground coal mining and the gas resource calculation and reservoir modelling. To prevent outburst events, the outburst threshold limit, which is the stipulation of limits on seam gas content prior to mining, has to be established. The parameters of coal seam gas content and composition are the two key parameters to determine the limitation values for safe mining. The study of gas content of each gas component as well as its ratio with measured total gas content was carried out by Black (2012), who claimed that there was a certain relationship between them.

The results of fast desorption gas testing conducted at the BHP Billiton Illawarra Coal Gas Laboratory were gathered for 519 core samples collected from underground at Metropolitan Colliery. From each gas test report the following data was extracted and collated for analysis:

- Core sample reference;
- Outburst threshold limit value;
- Measured total gas content Q_M;
- Gas content components, including Q_1, Q_2 and Q_3 (m^3/t);
- Gas composition of desorbed gas, including CH_4, CO_2 and $CH_4/(CH_4+CO_2)$ (%).

The result trends are generally in agreement with the study of Black (2012), however, some minor variations are due to the number of samples tested and seam regions. Black (2012) conducted the research with 4785 coal samples across the Bulli, Wynn, Piercefield and Kayuga seams in NSW as well as Goonyella Middle and German Creek seams in QLD. Comparatively, the study in this chapter focused on:

- Whole sample database from the same coal seam and mine site;
- Separate analysis and comparison for “Pass” and “Fail” samples;
- Special analysis for typical hard-to-drain area coal samples;
- Comparison between the whole database and hard-to-drain area database.

6.4.1 Measurement of coal seam gas content and gas composition

Generally, two types of method are used to estimate the coal seam gas content, namely, the direct method and the indirect method. The direct method directly measures the total volume

of gas contained in a coal sample. While the indirect method is estimated with the sorption isotherm under given temperature and pressure conditions, or calculated from empirical correlations. Australian Standard AS3980:1999 groups the direct method into fast and slow desorption methods by the time allowed for gas to desorb from the intact core prior to final crushing. The fast desorption test is taken over a period of time less than five days and typically less than one day and the slow desorption method requires a much longer time equal to or greater than five days (AS3980:1999). The fast direct desorption method is used by BHP Billiton Illawarra Coal Gas Laboratory to test the gas content. Gas composition is determined by a Varian CP4900 Four Channel Micro Gas Chromatograph. Different methods can be used to sample gas, including methods using glass gas burettes, gas bags and syringes.

6.4.1.1 Lost gas component

The lost gas component (Q_1) is the part of gas that escapes from the coal sample during its collection, prior to being sealed into a desorption canister. Q_1 needs to be estimated from gas emission data collected subsequent to the sample being sealed into the desorption canister. It is generally accepted that during initial desorption the volume of gas released is proportional to the square root of the desorption time, which is described in detail in Australian Standard AS3980:1999. Projecting the line of best fit representing initial gas emission from the time the core was sealed into the gas desorption canister to the time midway between the commencement and completion of coring the sample gives a measure of the gas volume lost during core sample recovery.

6.4.1.2 Desorbed gas component

The desorbed gas component (Q_2) is a measure of the volume of gas released from a coal sample whilst contained in a desorption canister. The duration of the fast desorption test is taken over a period of time less than five days and typically less than one day. Typically, gas released from a core sample is measured by water displacement using a graduated glass or plastic measuring flask. As shown in Figure 6.18 the measurement apparatus may be setup such that the gas liberated from the core sample within the desorption canister enters the measuring flask via a tube connected to the bottom or top of the measuring flask. Gas entering the top of the cylinder is preferred as the desorbed gas does not bubble through the water column thereby reducing the risk of gas loss through dissolving, particularly in the case of seam gas containing high concentration of CO_2 (AS3980:1999).

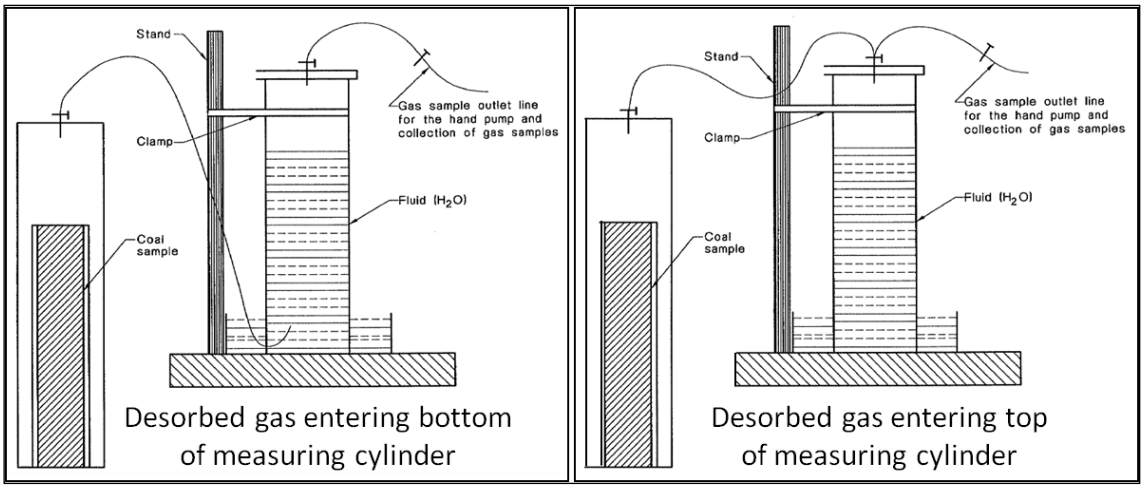

Figure 6.18: Desorbed gas volume measurement apparatus (after AS3980:1999)

6.4.1.3 Residual gas component

The residual gas component (Q_3) is a measure of the gas liberated from a coal sample following crushing. Following completion of the desorbed gas test the coal core is removed and a representative sub-sample collected and sealed into a crushing or grinding mill. The coal is crushed to micron size which 95 % of coal is less than 212µm. The volume of gas liberated from the coal sample is measured volumetrically with a water column similar to that used in the desorbed gas measurement.

6.4.1.4 Measured total gas Content

The calculation of total gas content is by sum of the three gas component, as shown in Equation 6-3, and the measured result is corrected to 20°C at 101.325 kPa.

$$Q_M = Q_1 + Q_2 + Q_3 \tag{6-3}$$

6.4.2 Analysis of whole gas database

6.4.2.1 Bulli Seam outburst threshold limits (TLV)

The outburst threshold limits varied linearly based on gas composition, increasing from a minimum in CO_2 rich conditions to a maximum in CH_4 rich conditions. According to the test results from BHP Gas Lab, the whole database of Metropolitan Colliery containing 519 sample results was studied. The gas database of this study is shown in Appendix H and Appendix I in detail. From the mining level values in the database, the threshold limits were generated. As shown in Figure 6.19, the gas content was 6.0 m^3/t for pure CO_2 and 9.5 m^3/t

for pure CH_4. Thus if the test gas content for coal sample is under the TLV limit, the sample will be marked as "Pass", otherwise it will be marked as "Fail".

Figure 6.19 shows the whole gas composition data scatter, ranging from CO_2 rich to CH_4 rich. From 519 samples tested, 325 samples are "Pass" samples, accounting for 62.6 %, while 194 samples are "Fail" samples, accounting for 37.4 %. The value of total gas content of "Fail" samples ranges from 6.14 m^3/t to 25.44 m^3/t. The average value of measured total gas content Q_M of "Pass" samples is 4.4 m^3/t and is 9.2 m^3/t for "Fail" samples. The average gas composition value of CH_4 of "Pass" samples is 17.1 % and 14.0 % for "Fail" samples, while the average values of CO_2 of "Pass" samples is 73.5 % and 82.6 % for "Fail" samples, which indicates the seam of this area is in a CO_2 rich condition. The zone with CH_4/ (CH_4+CO_2) ratio less than 0.2 includes 171 "Fail" samples, accounting for 88.1 % of total "Fail" samples. Including the "Pass" samples, 41.0 % of samples in the zone with CH_4/ (CH_4+CO_2) ratio less than 0.2 are failed, compared with 22.5 % in the zone with CH_4/ (CH_4+CO_2) ratio more than 0.2.

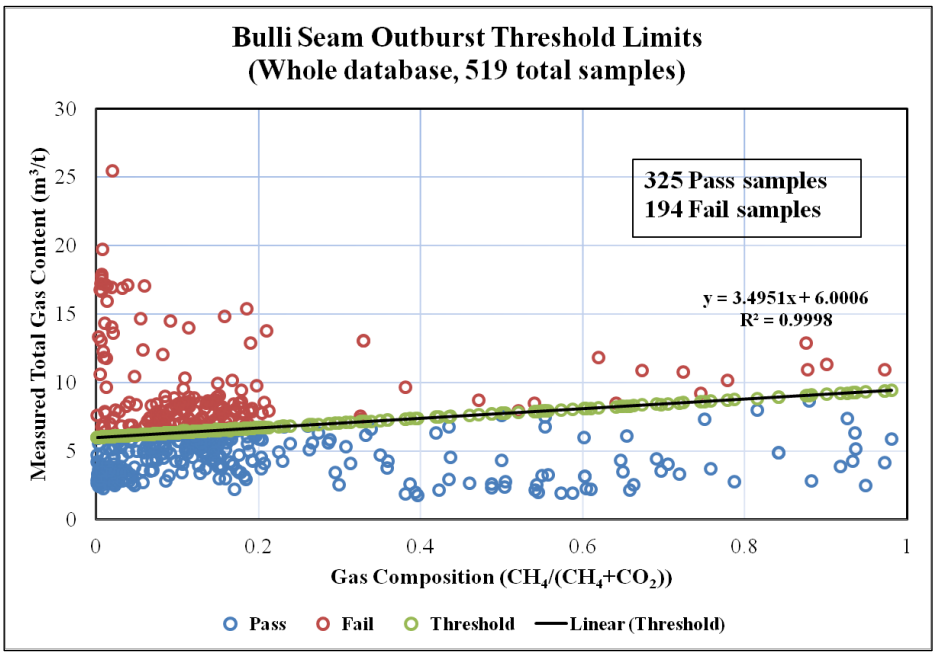

Figure 6.19: Bulli Seam outburst threshold limits (whole data base)

6.4.2.2 Q_1 gas content component

The Q_1 component of measured total gas content (Q_M) represents the lost gas from a coal sample, during core recovery, prior to being sealed in a gas desorption canister. Figure 6.20(a) shows the distribution of Q_1 gas content data relative to Q_M. The average Q_1 gas

content is 0.5 m^3/t for the whole database, 0.2 m^3/t for "Pass" samples and 1.0 m^3/t for "Fail" samples. Q_1 increased in response to increasing Q_M. Figure 6.20(b) shows the distribution of Q_1:Q_M ratio data relative to Q_M. Although a high degree of scatter was evident, statistical analysis confirmed an increase in the Q_1:Q_M ratio corresponding to increased Q_M. The average Q_1:Q_M ratio is 6.0 % for the whole database, 4.0 % for "Pass" samples and 9.5 % for "Fail" samples.

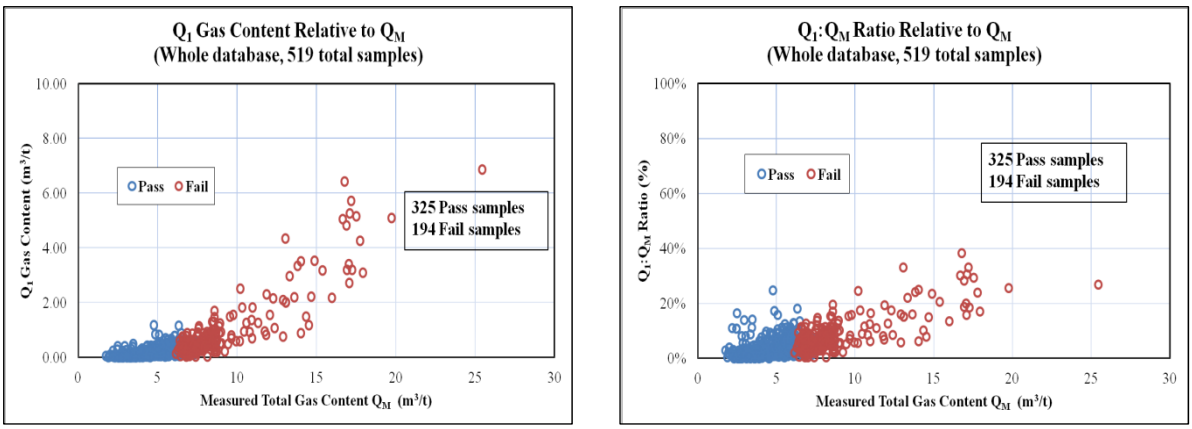

(a) (b)

Figure 6.20: Distribution of Q_1 gas content and Q_1:Q_M ratio relative to Q_M (whole data base)

Figure 6.21(a) shows the distribution of Q_1 data relative to the gas composition (CH_4 %) of each sample. In the 0-20 % CH_4 gas composition zone the average Q_1 gas content is 0.6 m^3/t for all the samples, 0.2 m^3/t for "Pass" samples and 1.1 m^3/t for "Fail" samples, while in the 20-80 % CH_4 gas composition zone the average Q_1 gas content is 0.3 m^3/t for all the samples, 0.2 m^3/t for "Pass" samples and 0.9 m^3/t for "Fail" samples. Figure 6.21(b) shows the distribution of the Q_1:Q_M ratio data relative to gas composition. In the 0-20 % CH_4 gas composition zone the average Q_1:Q_M ratio is 6.3 % for all the samples, 4.1 % for "Pass" samples and 9.5 % for "Fail" samples, while in the 20-80 % CH_4 gas composition zone the average ratio is 4.7 % for all the samples, 3.5 % for "Pass" samples and 8.7 % for "Fail" samples.

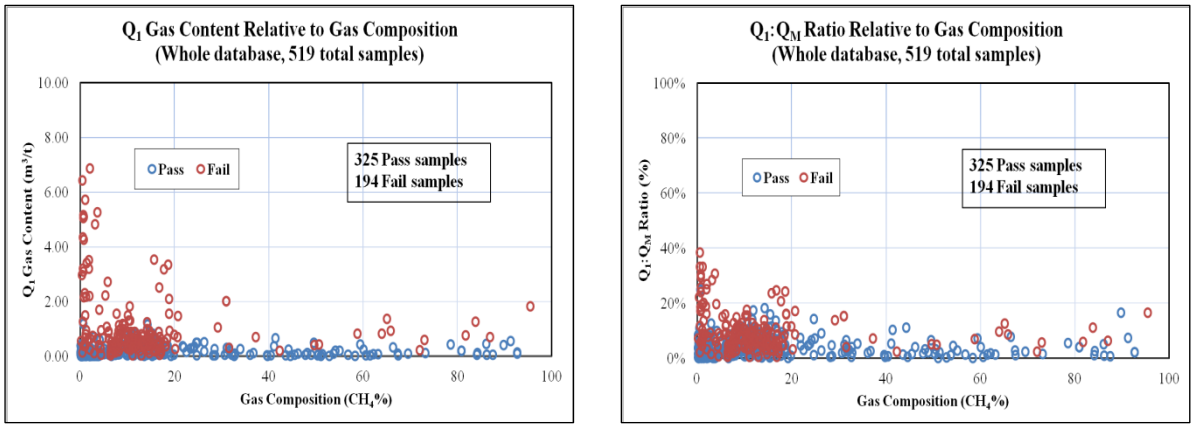

(a) (b)

Figure 6.21: Distribution of Q_1 gas content and Q_1:Q_M ratio relative to gas composition (whole data base)

6.4.2.3 Q_2 gas content component

The Q_2 component of measured total gas content (Q_M) represents the measurable gas desorbed from an as-received coal sample during the laboratory gas emission testing at atmospheric pressure. Figure 6.22(a) shows the distribution of Q_2 gas content data relative to Q_M. The average Q_2 gas content is 1.2 m^3/t for the whole database, 0.6 m^3/t for "Pass" samples and 2.2 m^3/t for "Fail" samples. Q_2 increased in response to increasing Q_M. Figure 6.22(b) shows the distribution of Q_2:Q_M ratio data relative to Q_M. Although a high degree of scatter was evident, statistical analysis confirmed an increase in the Q_2:Q_M ratio corresponding to increased Q_M. The average Q_2:Q_M ratio is 17.1 % for the whole database, 14.1 % for "Pass" samples and 22.0 % for "Fail" samples.

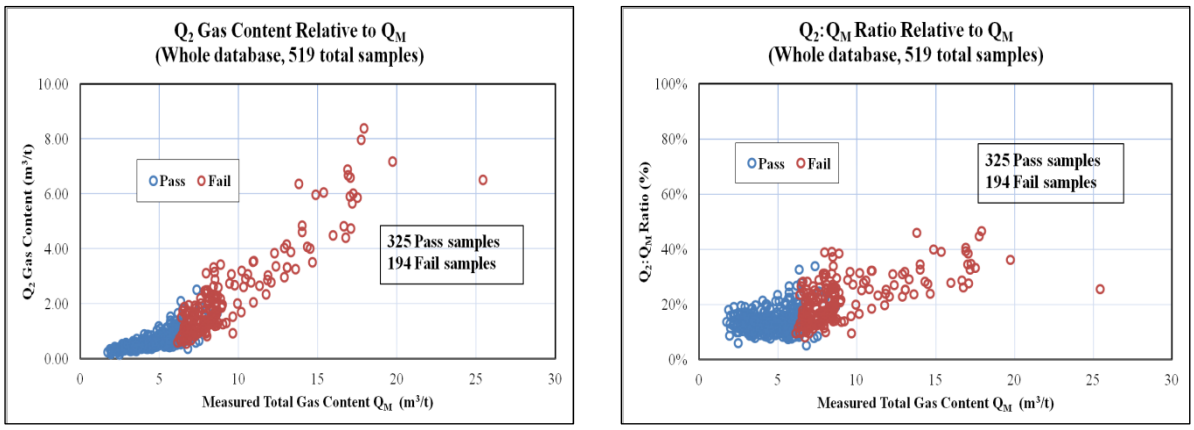

(a) (b)

Figure 6.22: Distribution of Q_2 gas content and Q_2:Q_M ratio relative to Q_M (whole data base)

Figure 6.23(a) shows the distribution of Q_2 data relative to the gas composition (CH_4 %) of each sample. In the 0-20 % CH_4 gas composition zone the average Q_2 gas content is 1.3 m^3/t

for all the samples, 0.6 m^3/t for "Pass" samples and 2.2 m^3/t for "Fail" samples, while in the 20-80 % CH_4 gas composition zone the average Q_2 gas content is 0.9 m^3/t for all the samples, 0.6 m^3/t for "Pass" samples and 2.1 m^3/t for "Fail" samples. Figure 6.23(b) shows the distribution of the Q_2:Q_M ratio data relative to gas composition. In the 0-20 % CH_4 gas composition zone the average Q_2:Q_M ratio is 17.5 % for all the samples, 14.3 % for "Pass" samples and 22.2 % for "Fail" samples, while in the 20-80 % CH_4 gas composition zone the average Q_2:Q_M ratio is 15.1 % for all the samples, 13.5 % for "Pass" samples and 20.7 % for "Fail" samples.

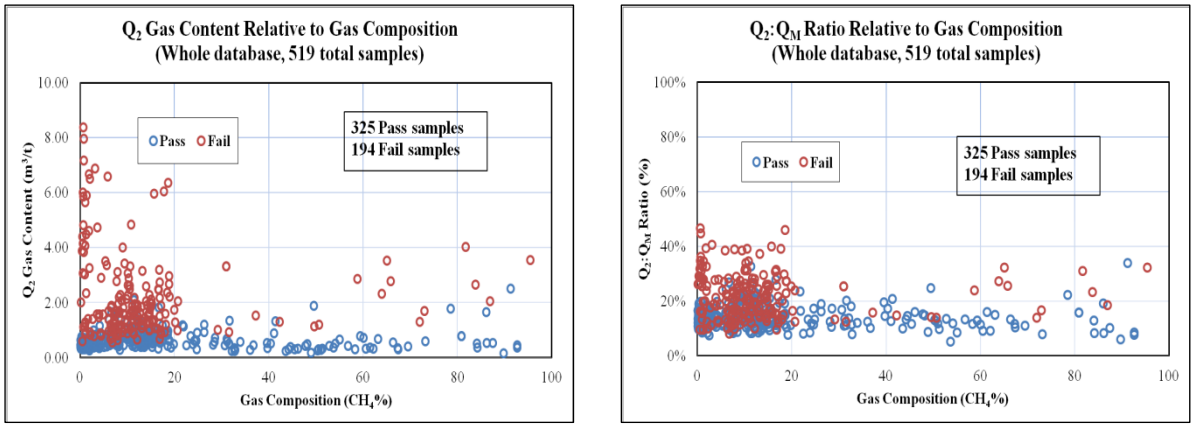

(a) (b)

Figure 6.23: Distribution of Q_2 gas content and Q_2:Q_M ratio relative to gas composition (whole data base)

6.4.2.4 Q_3 gas content component

The Q_3 component of total gas content (Q_M) represents the gas released from a coal sample following crushing to less than 212 µm. Figure 6.24(a) shows the distribution of Q_3 gas content data relative to Q_M. The average of Q_3 gas content is 4.5 m^3/t for the whole database, 3.6 m^3/t for "Pass" samples and 6.0 m^3/t for "Fail" samples. Q_3 increased in response to increasing Q_M. Figure 6.24(b) shows the distribution of Q_3:Q_M ratio data relative to Q_M. Although a high degree of scatter was evident, statistical analysis confirmed a decrease in the Q_3:Q_M ratio, corresponding to increased Q_M. The average Q_3:Q_M ratio is 76.9 % for the whole database, 81.9 % for "Pass" samples and 68.5 % for "Fail" samples.

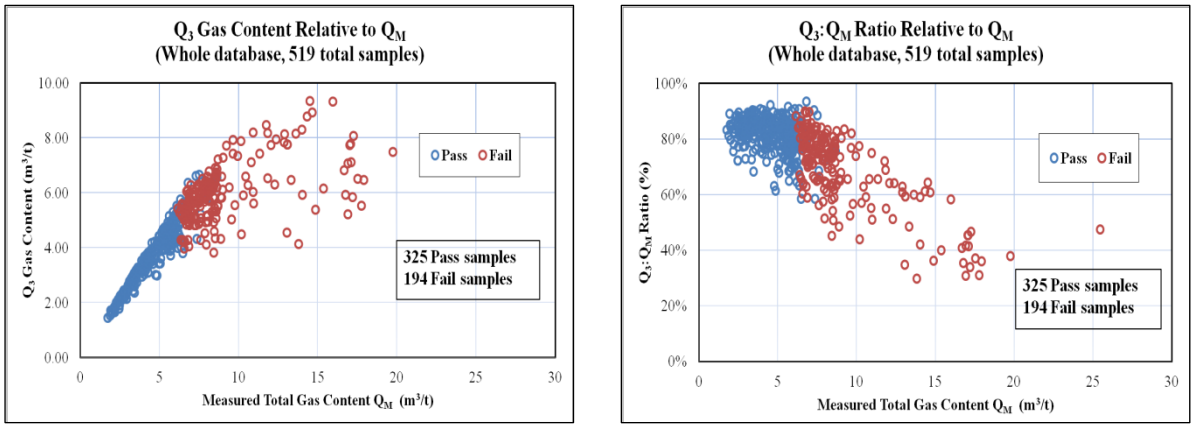

(a) (b)

Figure 6.24: Distribution of Q_3 gas content and Q_3:Q_M ratio relative to Q_M (whole data base)

Figure 6.25(a) shows the distribution of Q_3 data relative to the gas composition (CH_4 %) of each sample. In the 0-20 % CH_4 gas composition zone the average Q_3 gas content is 4.5 m^3/t for all the samples, 3.6 m^3/t for "Pass" samples and 5.9 m^3/t for "Fail" samples, while in the 20-80 % CH_4 gas composition zone the average Q_3 gas content is 4.3 m^3/t for all the samples, 3.5 m^3/t for "Pass" samples and 6.9 m^3/t for "Fail" samples. Figure 6.25(b) shows the distribution of the Q_3:Q_M ratio data relative to gas composition. In the 0-20 % CH_4 gas composition zone the average Q_3:Q_M ratio is 76.2 % for all the samples, 81.6 % for "Pass" samples and 68.3 % for "Fail" samples, while in the 20-80 % CH_4 gas composition zone the average Q_3:Q_M ratio is 80.2 % for all the samples, 83.0 % for "Pass" samples and 70.6 % for "Fail" samples.

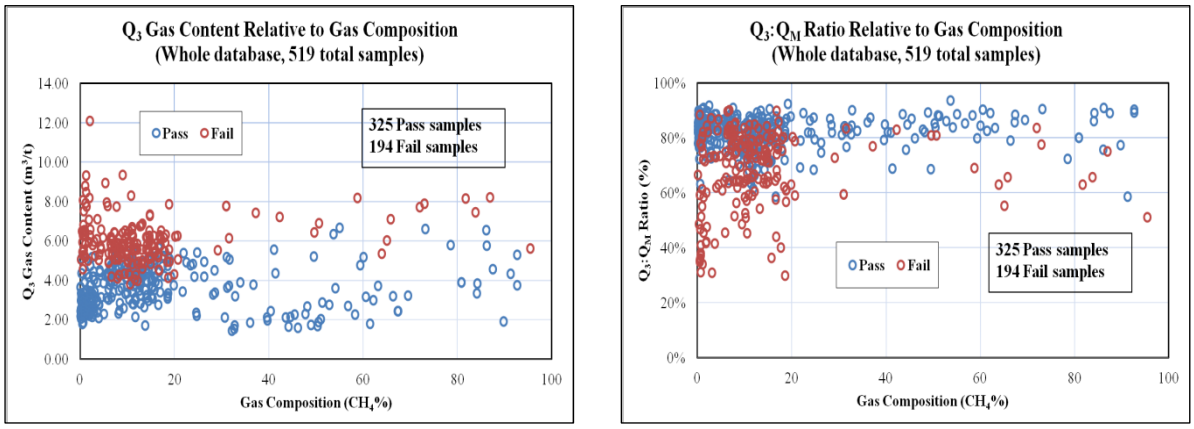

(a) (b)

Figure 6.25: Distribution of Q_3 gas content and Q_3:Q_M ratio relative to gas composition (whole data base)

6.4.2.5 Gas content component summary

Figure 6.26 shows the results of the gas content component values Q_1, Q_2 and Q_3, plotted relative to Q_M for each sample of the whole database. A linear trend line was plotted to represent the average relationship of each gas content component relative to Q_M. As shown in Figure 6.26(a), for "Pass" samples, $Q_1 = 0.047Q_M$, $Q_2 = 0.1469Q_M$ and $Q_3 = 0.8062Q_M$. The statistical correlation is greater for the Q_3 gas component, which indicates a better linear relationship between Q_3 and Q_M for "Pass" samples. As shown in Figure 6.26(b), for "Fail" samples, $Q_1 = 0.1384Q_M$, $Q_2 = 0.2599Q_M$ and $Q_3 = 0.6017Q_M$. The statistical correlation is small for the Q_3 gas component, which indicates a non linear relationship between Q_3 and Q_M for "Fail" samples.

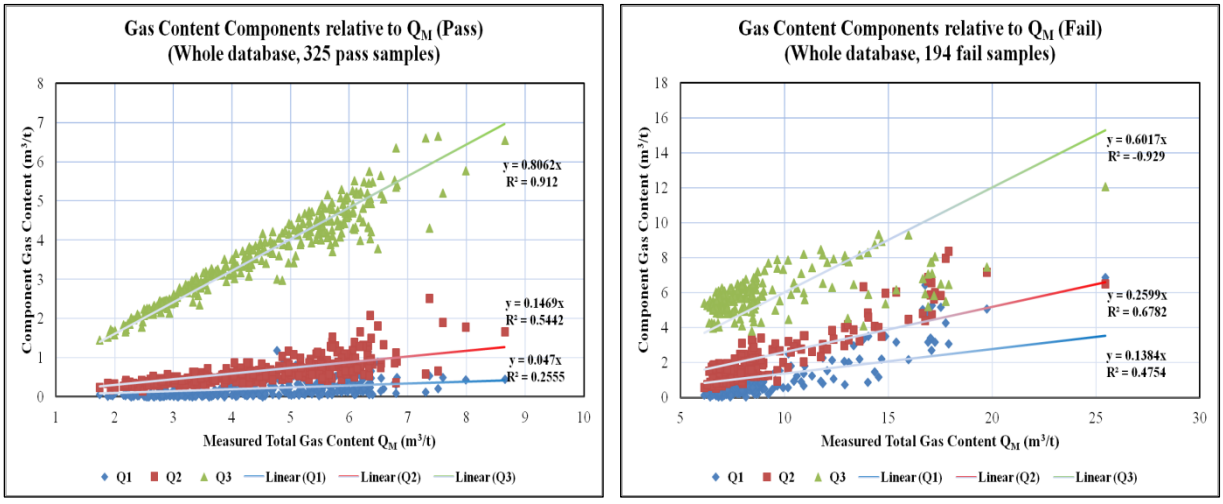

(a) (b)

Figure 6.26: Gas content component relative to Q_M (whole data base, linear relationship)

Figure 6.27 shows the results of the gas content component values, Q_1, Q_2 and Q_3, plotted relative to Q_M for each sample with the power trend line. As shown in Figure 6.27(a), for "Pass" samples, $Q_1 = 0.0029Q_M^{2.4819}$, $Q_2 = 0.1172Q_M^{1.1046}$ and $Q_3 = 0.9102Q_M^{0.9241}$. For "Fail" samples, shown in Figure 6.27(b), $Q_1 = 0.0017Q_M^{2.7218}$, $Q_2 = 0.0365Q_M^{1.7947}$ and $Q_3 = 2.642Q_M^{0.3686}$. The statistical correlation is greater for the power trend line than the linear trend line, which indicates a power relationship was considered to more accurately represent the average of each gas content component relative to Q_M. Figure 6.27(b) shows that the Q_1 and Q_2 gas component increases sharply with the increasing total gas content Q_M.

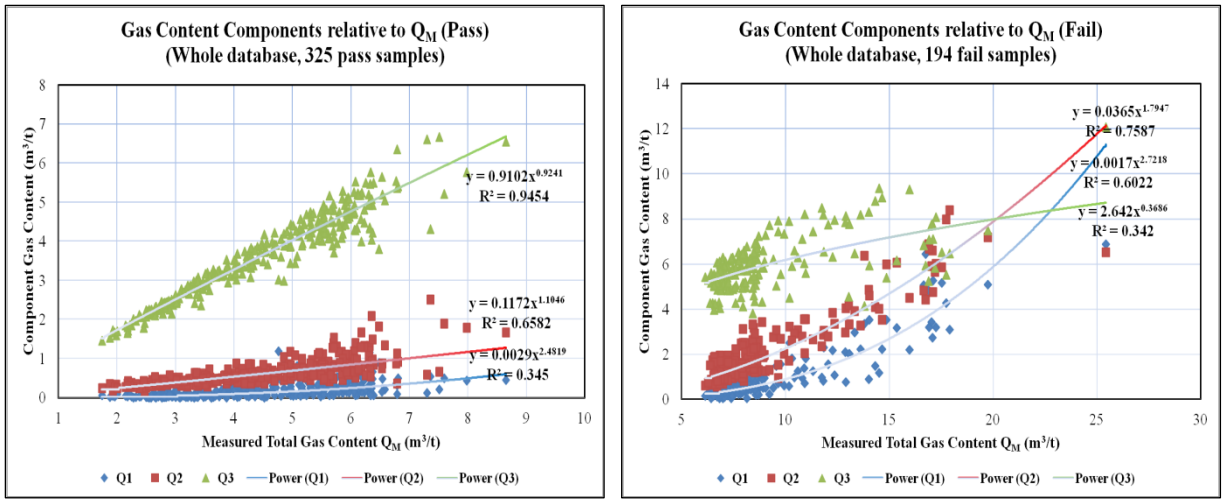

(a) (b)

Figure 6.27: Gas content component relative to Q_M (whole data base, power relationship)

6.4.3 Analysis of the hard-to-drain area

6.4.3.1 Bulli Seam outburst threshold limits (TLV)

In order to better understand the coal drainage capacity, the gas content and composition of the coal within the typical hard-to-drain area (8-11 c/t, MG 22), a total of 94 sample results were studied. The gas database of this study is shown in Appendix J in detail. As shown in Figure 6.28, unlike the whole data scatter, the scatter of typical hard-to-drain area concentrates almost entirely in the CO_2 rich area, with the highest CH_4/ (CH_4+CO_2) ratio being 0.21. Among the 94 samples, 31 samples are "Pass" samples, accounting for 33.0 %, while 63 samples are "Fail" samples, accounting for 67.0 %. The value of the total gas content of "Fail" samples ranges from 6.27 m^3/t to 10.19 m^3/t. The average value of the measured total gas content Q_M of "Pass" samples is 5.2 m^3/t and 7.8 m^3/t for "Fail" samples. The average values of CH_4 of "Pass" and "Fail" samples are 8.5 % and 12.5 % respectively, while the average values of CO_2 of both "Pass" and "fail" samples are 87.6 % and 84.5 % respectively. The zone with CH_4/ (CH_4+CO_2) ratio less than 0.2 includes 60 "Fail" samples, accounting for 93.8 % of total "Fail" samples. Including the "Pass" samples, 65.9 % of samples in the zone with CH_4/ (CH_4+CO_2) ratio less than 0.2 are failed.

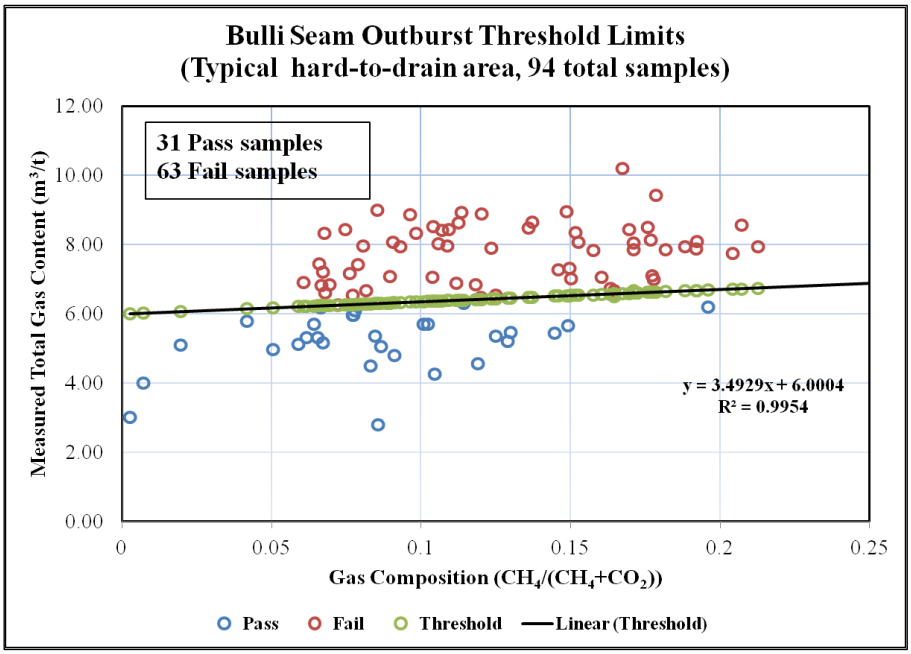

Figure 6.28: Bulli Seam outburst threshold limits (Typical hard-to-drain area)

6.4.3.2 Q_1 gas content component

Figure 6.29(a) shows the distribution of Q_1 gas content data relative to Q_M in the typical hard-to-drain area. The average Q_1 gas content is 0.5 m^3/t for all the samples, 0.2 m^3/t for "Pass" samples and 0.6 m^3/t for "Fail" samples. Figure 6.29(b) shows the distribution of Q_1:Q_M ratio data relative to Q_M in this area. The average Q_1:Q_M ratio is 6.0 % for all the samples, 3.9 % for "Pass" samples and 7.1 % for "Fail" samples. Figure 6.30(a) and Figure 6.30(b) shows the distribution of Q_1 and Q_1:Q_M ratio data relative to the gas composition (CH_4 %) of each sample in the hard-to-drain area.

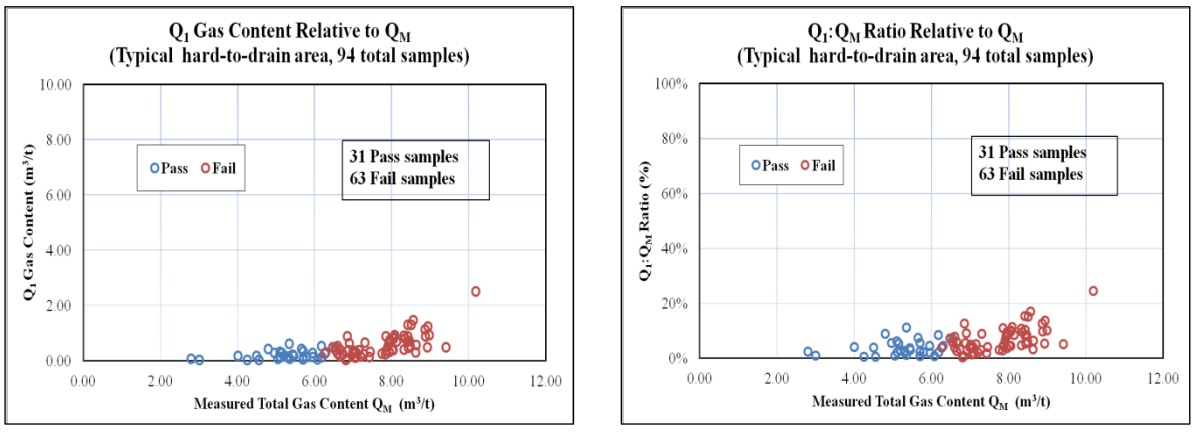

(a) (b)

Figure 6.29: Distribution of Q_1 gas content and Q_1:Q_M ratio relative to Q_M (Typical hard-to-drain area)

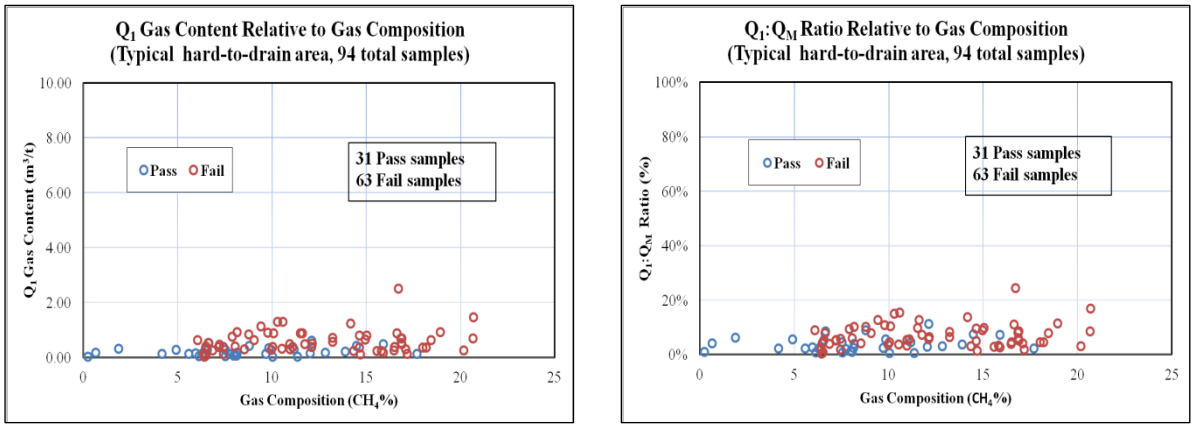

(a) (b)

Figure 6.30: Distribution of Q_1 gas content and Q_1:Q_M ratio relative to gas composition (Typical hard-to-drain area)

6.4.3.3 Q_2 gas content component

Figure 6.31(a) shows the distribution of Q_2 gas content data relative to Q_M in the typical hard-to-drain area. The average Q_2 gas content is 1.4 m^3/t for all the samples, 0.8 m^3/t for "Pass" samples and 1.7 m^3/t for "Fail" samples. Figure 6.31(b) shows the distribution of Q_2:Q_M ratio data relative to Q_M in this area. The average Q_2:Q_M ratio is 19.6 % for all the samples, 15.6 % for "Pass" samples and 21.5 % for "Fail" samples. Figure 6.32(a) and Figure 6.32(b) shows the distribution of Q_2 and Q_2:Q_M ratio data relative to the gas composition (CH_4 %) of each sample in the typical hard-to-drain area.

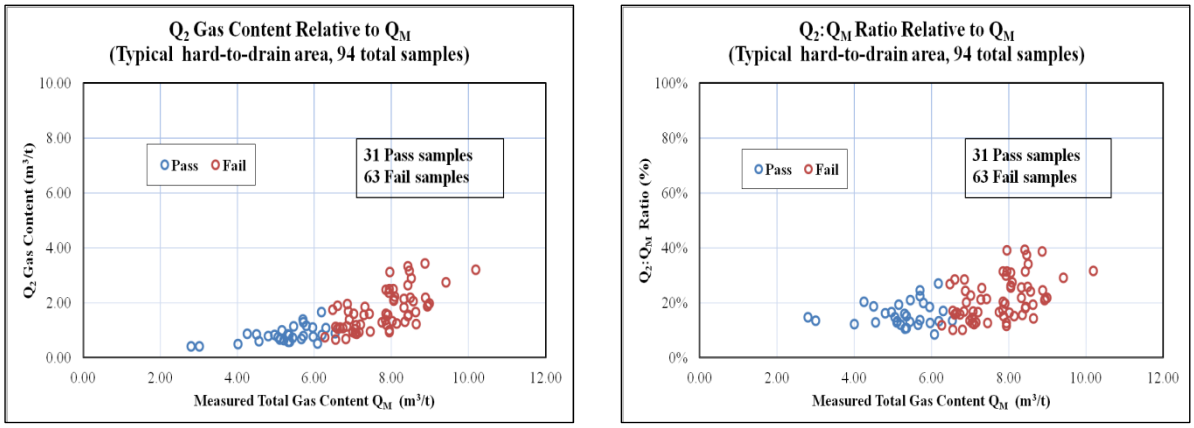

(a) (b)

Figure 6.31: Distribution of Q_2 gas content and Q_2:Q_M ratio relative to Q_M (Typical hard-to-drain area)

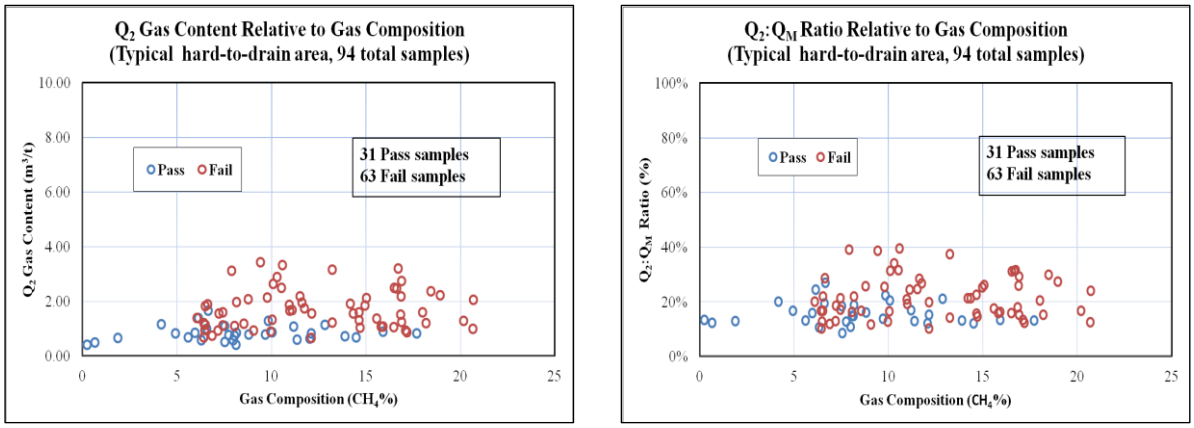

(a) (b)

Figure 6.32: Distribution of Q_2 gas content and Q_2:Q_M ratio relative to gas composition (Typical hard-to-drain area)

6.4.3.4 Q_3 gas content component

Figure 6.33(a) shows the distribution of Q_3 gas content data relative to Q_M in the typical hard-to-drain area. The average Q_3 gas content is 5.1 m^3/t for all the samples, 4.2 m^3/t for "Pass" samples and 5.5 m^3/t for "Fail" samples. Figure 6.33(b) shows the distribution of Q_3:Q_M ratio data relative to Q_M in this area. The average Q_3:Q_M ratio is 74.4 % for all the samples, 80.5 % for "Pass" samples and 71.4 % for "Fail" samples. Figure 6.34(a) and Figure 6.34(b) shows the distribution of Q_3 and Q_3:Q_M ratio data relative to the gas composition (CH_4 %) of each sample in the typical hard-to-drain area.

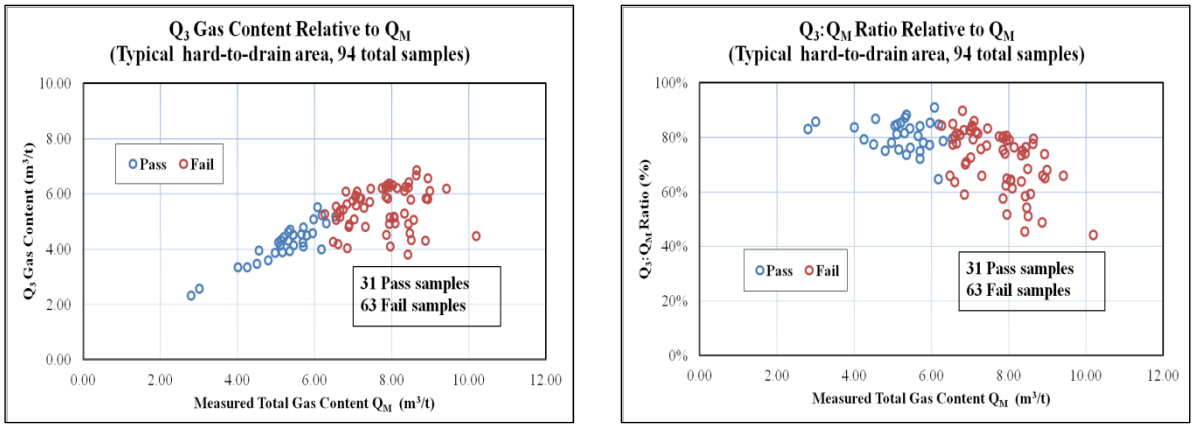

(a) (b)

Figure 6.33: Distribution of Q_3 gas content and Q_3:Q_M ratio relative to Q_M (Typical hard-to-drain area)

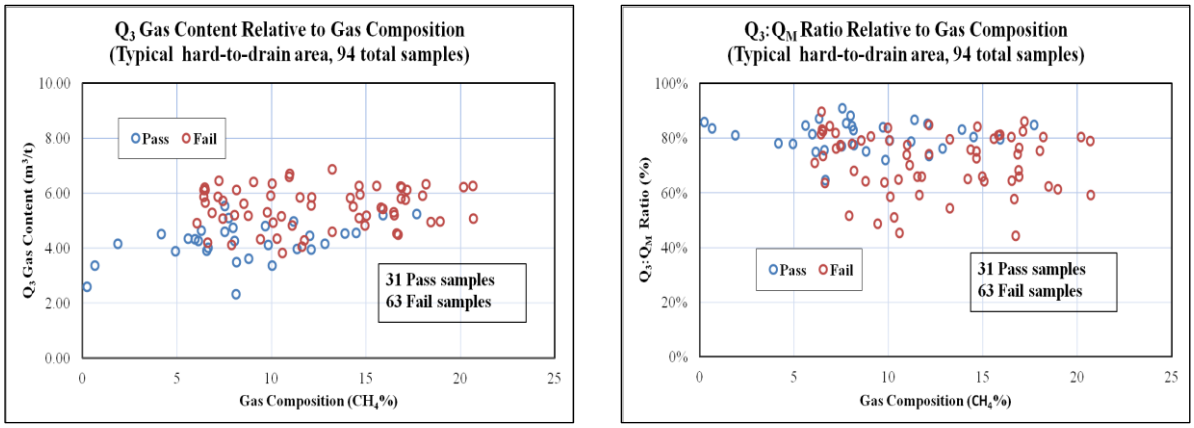

(a) (b)

Figure 6.34: Distribution of Q_3 gas content and Q_3:Q_M ratio relative to gas composition (Typical hard-to-drain area)

6.4.3.5 Gas content component summary

Figure 6.35 shows the results of the gas content component values Q_1, Q_2 and Q_3, plotted relative to Q_M for each sample of the typical hard-to-drain area. A linear trend line was plotted to represent the average relationship of each gas content component relative to Q_M. As shown in Figure 6.35(a), for "Pass" samples, $Q_1 = 0.0406Q_M$, $Q_2 = 0.1574Q_M$ and $Q_3 = 0.802Q_M$. The statistical correlation is greater for Q_3 gas component, which indicates a better linear relationship between Q_3 and Q_M for "Pass" samples. As shown in Figure 6.35(b), for "Fail" samples, $Q_1 = 0.0765Q_M$, $Q_2 = 0.2225Q_M$ and $Q_3 = 0.7012Q_M$. The statistical correlation is small for the Q_3 gas component, which indicates a non linear relationship between Q_3 and Q_M for "Fail" samples.

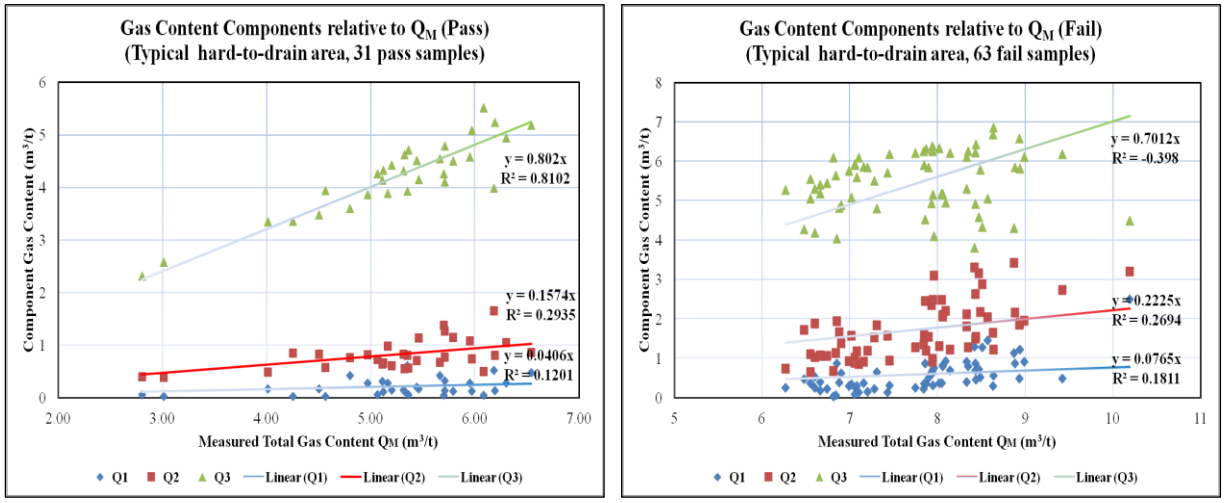

(a) (b)

Figure 6.35: Gas content component relative to Q_M (typical hard-to-drain area, linear relationship)

Figure 6.36 shows the results of the gas content component values, Q_1, Q_2 and Q_3, plotted relative to Q_M for each sample with the power trend line. As shown in Figure 6.36(a), for "Pass" samples, $Q_1 = 0.0049Q_M^{2.0895}$, $Q_2 = 0.1262Q_M^{1.1081}$ and $Q_3 = 0.9186Q_M^{0.9183}$. As shown in Figure 6.36(b), for "Fail" samples, $Q_1 = 0.00007Q_M^{4.3083}$, $Q_2 = 0.009Q_M^{2.5229}$ and $Q_3 = 3.7074Q_M^{0.1878}$. The statistical correlation is greater for the power trend line than the linear trend line, which indicates a power relationship was considered to more accurately represent the average of each gas content component relative to Q_M and a similar trend of different gas components with increasing total gas content is observed.

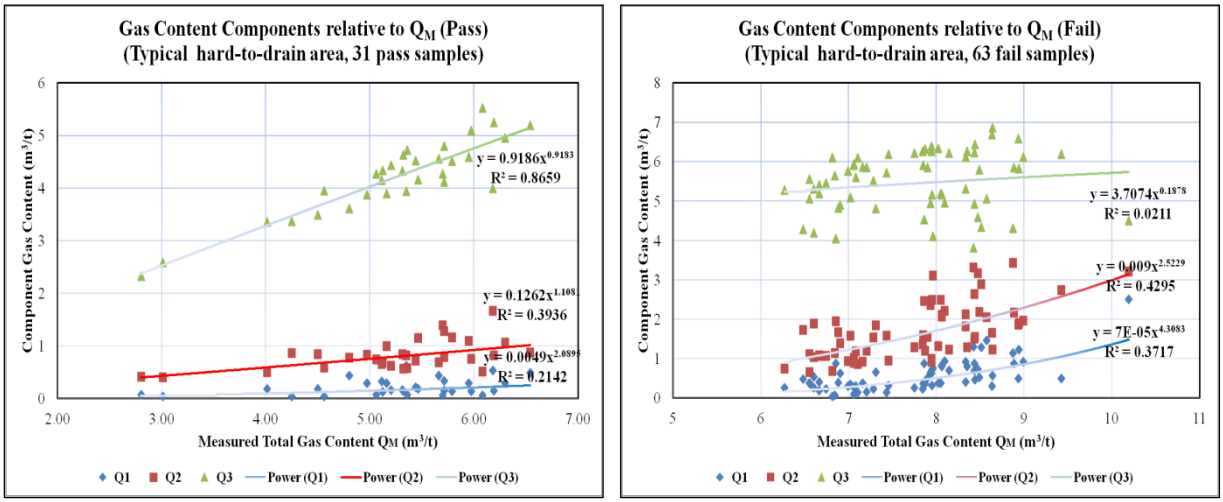

(a) (b)

Figure 6.36: Gas content component relative to Q_M (typical hard-to-drain area, power relationship)

6.4.4 Comparative analysis of gas content and composition between the whole gas database and the hard-to-drain area

Table 6.3 presents a summary of the average value of each gas analysis measure of the whole database and the typical hard-to-drain area. The data of the whole database separates into two categories, that are less than 20 % CH_4 and greater than 20 % CH_4. According to the data in Table 6.3, gas components Q_1, Q_2 and Q_3 as well as their ratio to Q_M are plotted in bar charts to compare.

Table 6.3: Average gas analysis data summary

Category	Whole database				Typical hard-to-drain	
	Pass		Fail		Pass	Fail
Gas composition of CH_4	<20 %	≥20 %	< 20 %	≥20 %		
Sample Number	325		194		94	
Sample Number	252	73	173	21	31	63
Q_1 (m^3/t)	0.19		1.05		0.45	
Q_1 (m^3/t)	0.20	0.17	1.07	0.89	0.21	0.57
Q_1:Q_M (%)	4.0 %		9.5 %		6.0 %	
Q_1:Q_M (%)	4.1 %	3.5 %	9.5 %	8.7 %	3.9 %	7.1 %
Q_2 (m^3/t)	0.64		2.20		1.41	
Q_2 (m^3/t)	0.65	0.60	2.21	2.13	0.82	1.70
Q_2:Q_M (%)	14.1 %		22.0 %		19.6 %	
Q_2:Q_M (%)	14.3 %	13.5 %	22.2 %	20.7 %	15.6 %	21.5 %
Q_3 (m^3/t)	3.59		5.99		5.07	
Q_3 (m^3/t)	3.61	3.53	5.89	6.87	4.21	5.49
Q_3:Q_M(%)	81.9 %		68.5 %		74.4 %	
Q_3:Q_M (%)	81.6 %	83.0 %	68.3 %	70.6 %	80.5 %	71.4 %
Q_M (m^3/t)	4.42		9.24		6.93	
Q_M (m^3/t)	4.45	4.30	9.16	9.89	5.24	7.76

Figure 6.37(a) shows the comparative analysis of gas content component Q_1 and Q_1:Q_M ratio. The largest value of gas content component Q_1 for "Fail" samples is 1.07 m^3/t of group CH_4<20 % (whole database), followed by 0.89 m^3/t of group CH_4≥20 % (whole database) and 0.57 m^3/t of the typical hard-to-drain area. The same order was followed for Q_1:Q_M ratio for "Fail" samples as shown in Figure 6.37(b). The value of Q_1 gas content and Q_1:Q_M ratio for "Pass" samples varies relatively less among the three groups, Q_1 content is around 0.2 m^3/t and Q_1:Q_M ratio is around 4 %.

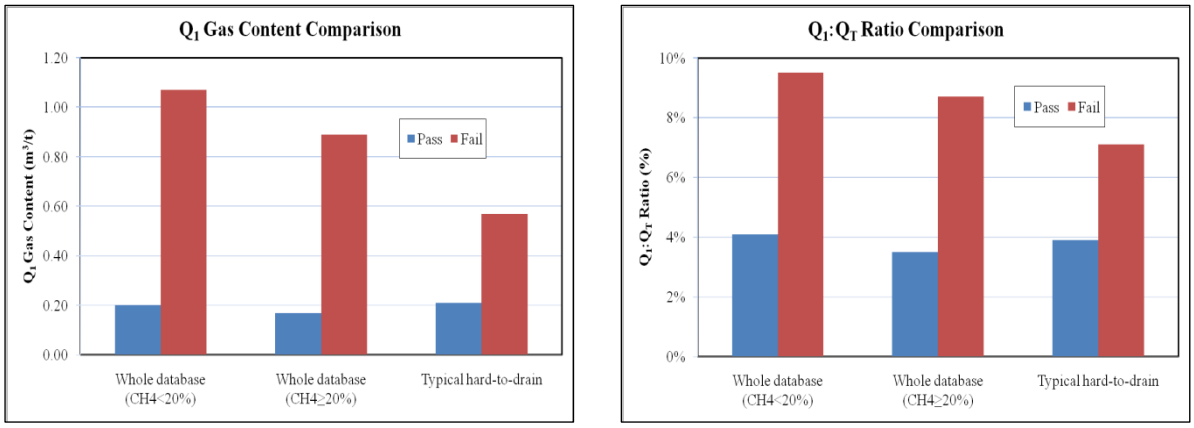

(a) (b)

Figure 6.37: Comparative analysis of gas content component Q_1 and Q_1:Q_M ratio

Figure 6.38(a) shows the comparative analysis of gas content component Q_2 and Q_2:Q_M ratio. The largest value of gas content component Q_1 for "Fail" samples is 2.21 m^3/t of group CH_4<20 % (whole database), followed by 2.13 m^3/t of group CH_4≥20 % (whole database) and 1.70 m^3/t of the typical hard-to-drain area. The Q_1:Q_M ratio for "Fail" samples is around 20 % (Figure 6.38(b)). The value of Q_2 gas content and Q_2:Q_M ratio for "Pass" samples varies relatively less among the three groups, Q_2 content and Q_2:Q_M ratio is 0.82 m^3/t and 15.6 % of the typical hard-to-drain area, higher than 0.64 m^3/t and 14.1 % of whole database.

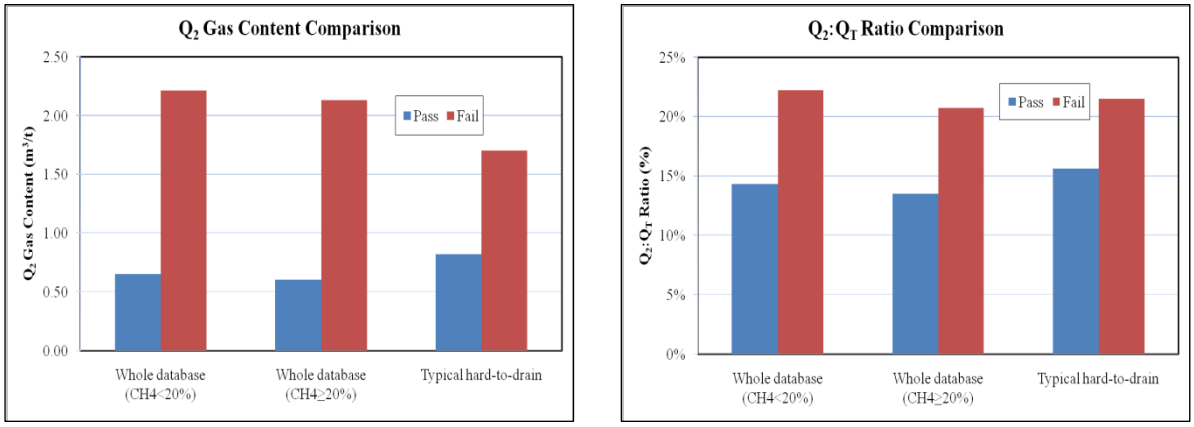

(a) (b)

Figure 6.38: Comparative analysis of gas content component Q_2 and Q_2:Q_M ratio

Figure 6.39(a) shows the comparative analysis of gas content component Q_3 and Q_3:Q_M ratio. The largest value of gas content component Q_3 for "Fail" samples is 6.87 m^3/t of group CH_4≥20 % (whole database), followed with 5.89 m^3/t of group CH_4<20 % (whole database) and 5.49 m^3/t of the typical hard-to-drain area. The value of Q_3 gas content for "Pass" samples varies relatively less among the three groups, Q_3 content is 4.21 m^3/t of the typical

hard-to-drain area, higher than 3.59 m^3/t of whole database. Among the three groups, the Q_3:Q_M ratio is stable for "Fail" and "Pass" samples, it is around 70 % for "Fail" samples and 80 % for "Pass" samples (Figure 6.39(b)).

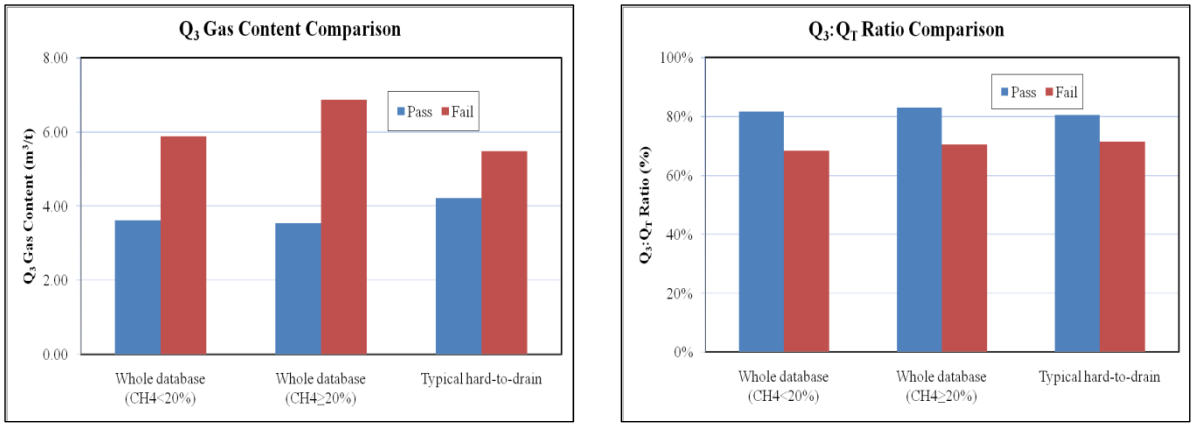

(a) (b)

Figure 6.39: Comparative analysis of gas content component Q_3 and Q_3:Q_M ratio

Above all, the value of gas component Q_1, Q_2 and Q_3 for "Fail" samples of the typical hard-to-drain area maintains the smallest compared with the other two groups. However, the value of gas component Q_1, Q_2 and Q_3 for "Pass" samples of the typical hard-to-drain area maintains the largest compared with the other two groups. As the main component of the total gas content, Q_3:Q_M ratio is stable among the three groups, for "Fail" and "Pass" samples, it is around 70 % for "Fail" samples and 80 % for "Pass" samples.

Figure 6.40 shows the comparative analysis of measured total gas content Q_M. The largest value of total gas content Q_M for "Fail" samples is 9.89 m^3/t of group CH_4≥20 % (whole database), followed with 9.16 m^3/t of group CH_4<20 % (whole database) and 7.76 m^3/t of typical hard-to-drain area. However, the value of total gas content Q_M for "Pass" samples is 5.24 m^3/t of typical hard-to-drain area, which is higher than 4.45 m^3/t of group CH_4<20 % (whole database), and 4.30 m^3/t of group CH_4≥20 % (whole database). This indicates that the typical hard-to-drain area is a relatively lower total gas content area with the smallest difference between the "Fail" and "Pass" samples.

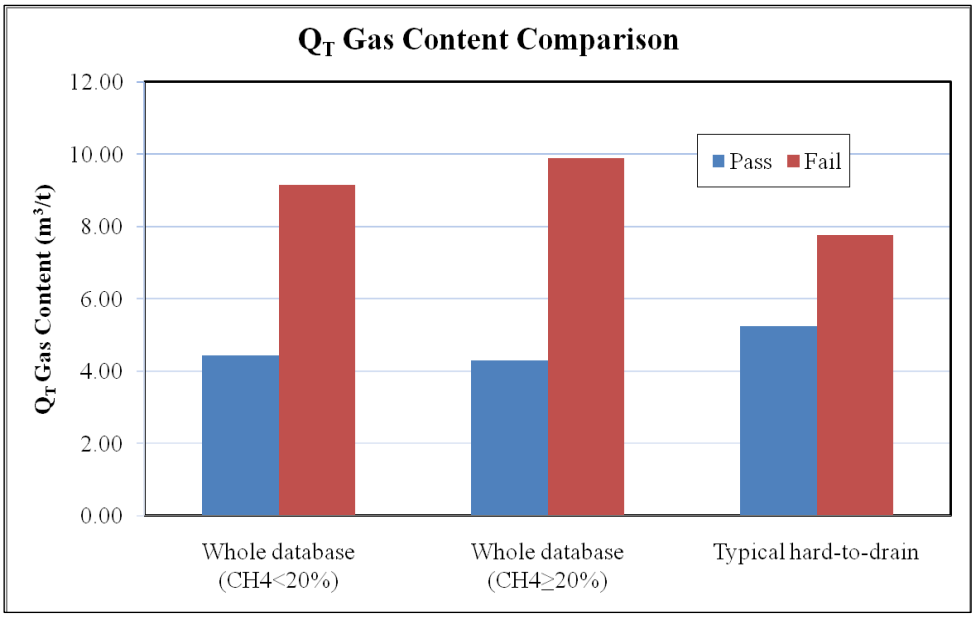

Figure 6.40: Comparative analysis of gas content component Q_M

6.5 SUMMARY

Permeability of coal samples from MG22 of Metropolitan mine was tested with the MFORR and Triaxial Compression Apparatus. Tests show at each of the vertical stress level that coal sample permeability decreases with increasing gas pressure and at higher gas pressure, coal permeability stays stable and undergoes minor changes under different vertical stress.

It is concluded that there is no significant mathematical difference between the two types of testing apparatus and calculation methods. Both the permeability tests are comparable and tally well with the Bulli coal seam tests result calculation from the *in situ* condition. A permeability of <1 mD should be adopted under high triaxial stress conditions, which is a relative low permeability explaining the possible reason causing the problem of hard to drain. Strain gauge results from the MFORR test clearly demonstrate the coal samples experienced negative volumetric changes or shrinkage with increased confinement pressures axially and laterally. The degree of the volumetric changes is found to be dependent on the level of the applied axial and lateral pressures or stresses.

Ash content of this type of coal is about 7% which is relatively low, and this may contribute to higher gas adsorption capacity, and hence lead to poor drainage. Gas adsorption tests and Langmuir modelling demonstrate that the average value of Langmuir volume of CO_2 and CH_4 for the hard-to-drain area had no larger difference with both of the easy-to-drain areas. The Langmuir volume for CO_2 is much higher than for CH_4 which indicates the larger

adsorption capacity for coal seams and higher undersaturation potential with higher gas composition value of CO_2 which is the case at Metropolitan Colliery.

An analysis of the whole gas database found that the Q_1, Q_2 and Q_3 components increased in response to increasing measured total gas content Q_M. Statistical analysis also shows an increasing trend in the Q_1:Q_M and Q_2:Q_M ratio corresponding to increased Q_M, but a decreasing trend in the Q_3:Q_M ratio corresponding to increased Q_M. No clear correlation is found between the gas components and their ratio corresponding to the gas composition.

The statistical correlation shows a better linear trend line fitting for "Pass" samples than "Fail" samples especially for the Q_3 gas component. The greater statistical correlation indicates a power equation is considered to more accurately represent the relationship between each gas content component and Q_M especially for "Fail" samples. Analysis also shows that the Q_1 and Q_2 gas components increased more sharply than Q_3 with the increase of Q_M especially for "Fail" samples.

According to the analysis of the whole database (519 samples) and typical hard-to-drain area (94 samples), "Fail" samples always appear with the higher CO_2 concentration. The zone of the whole database with $CH_4/(CH_4+CO_2)$ ratio less than 0.2 includes 171 "Fail" samples, accounting for 88.1 % of total "Fail" samples. The zone of typical hard-to-drain area with $CH_4/(CH_4+CO_2)$ ratio less than 0.2 includes 60 "Fail" samples, accounting for 93.8 % of total "Fail" samples. Including the "Pass" samples, 65.9 % of samples in the zone with $CH_4/(CH_4+CO_2)$ ratio less than 0.2 are failed.

Comparative analysis among the three groups including whole database (CH_4<20 %), whole database ($CH_4\geq$20 %) and the typical hard-to-drain area, shows that the value of gas component Q_1, Q_2, Q_3 and Q_M for "Fail" samples of typical hard-to-drain area remains the smallest compared with the other two groups; whilst, the value of gas component Q_1, Q_2, Q_3 and Q_M for "Pass" samples of the typical hard-to-drain area is the highest compared with the other two groups. The measured total gas content (Q_M) in the typical hard-to-drain area is relatively lower and the difference of Q_M between the "Fail" and "Pass" samples is marginal. The Q_3:Q_M ratio remains constant among the three groups, for "Fail" and "Pass" samples, i.e., around 70 % for "Fail" samples and 80 % for "Pass" samples.

Apparently, the gas content and composition, in conjunction with other parameters, can be used as important indicators for identifying the hard-to-drain areas. A warning index for the

hard-to-drain area can include relatively lower gas content (6-10 m^3/t), high gas composition of CO_2 (CO_2>80 %, CH_4<20 % or $CH_4/(CH_4+CO_2)$<0.2) and other geological variations. If the gas samples have all the above features then the mine should be cautious with their gas drainage in the area from where the samples are taken.

CHAPTER SEVEN – GAS INJECTION TO FLUSH COAL SEAM GAS

7.1 INTRODUCTION

Results from the geological and cleat system studies, SEM based coal microstructure imaging, coal permeability tests and a systematic analysis of gas database have confirmed that coal seams having similar features to longwall block near MG 22 of Bulli seam at Metropolitan Colliery will be in the hard-to-drain category. Therefore there is a need to develop a novel technique based on N_2 injection technique to flush coal seam gas and enhance gas recovery.

There is growing interest in gas injection to enhance CSG recovery. The utilisation of N_2 injection has been found to help CSG recovery (Reeves and Oudinot, 2004; Reeves and Oudinot, 2005; Kiyama *et al.*, 2011; Packham *et al.*, 2012; Florentin, 2012; Zhang *et al.*, 2012). It was found that incremental increase in methane recovery of approximately 10-20 % of original gas in place was achieved with N_2 injection. The future N_2 injection was forecast to add another 25-40 % of original gas in place to the total recovery. The future N_2 injection at Tiffany was also forecast to be economic (Reeves and Oudinot, 2005).

Packham *et al*. (2012) reported the results from a field trial conducted with SIS pre-drainage wells and concluded that the enhanced drainage could provide the means for both accelerating methane drainage and reducing residual gas content. Packham *et al*. (2011) provided the background to this field trial including details of the reservoir characteristics, well geometry and installations. Packham *et al*. (2011) also described how history matching of the reservoir and simulation of the effects of nitrogen injection indicated that accelerated drainage was likely.

Kiyama *et al.* (2011) found that the core coal permeability decreases after supercritical CO_2 injection, showing that adsorption-induced swelling has a significant impact on coal permeability. Subsequent N_2 flooding tests following CO_2 injection showed slow strain recovery, suggesting that N_2 displaces the adsorbed CO_2 in the coal matrix and the permeability of the coal core also recovered to a certain degree after N_2 injection. Similarly, Pan *et al.* (2010) confirmed that coal swells with gas adsorption, and shrinks with gas desorption and as coal permeability is highly sensitive to stress, the permeability decline with

pore pressure is a direct result of adsorption-induced coal swelling and under reservoir conditions these strain changes affect the cleat porosity and thus permeability.

All this indicates that N_2 gas injection can be used to enhance the gas drainage of CSG and gas injection will cause a significant impact on coal behaviour and further influence the gas transport in coal when performing gas drainage. An experiment was conducted to further understand the mechanism of N_2 gas flushing to enhance the recovery of CSG, such as CO_2 and CH_4. The relationships between flushing time and N_2 as well as CO_2 and CH_4 concentration, N_2 charging volume and CO_2 and CH_4 recovery volume, coal behaviour and flushing process were analysed in this experiment.

7.2 HARD-TO-DRAIN SEAMS

In order to understand the gas drainage problem, various investigations including field visits, laboratory tests and gas data analysis were carried out in this study. The cleat system was observed both from the underground field trials and lump coal samples. The coal sorption capacity was tested with ash content and isotherm tests with well modified apparatus and calibration. Coal microstructures were observed by SEM technology under SE and BSE mode with element mapping technology. Regarding to the permeability investigation, two different types of test equipment were used under triaxial conditions. The *in situ* gas content and composition data were systemically analysed in terms of whole gas database and the hard-to-drain area. These general results were found:

- Geological variation inducing cleat system variation, permeability change and high CO_2 concentration in the typical hard-to-drain area is believed to be related to the gas drainage problem.
- SEM technology shows the microstructures of the hard-to-drain coal samples seem to be less apparent and fractured than the easy-to-drain samples.
- Coal ash content and isotherm test results showed coal samples from Metropolitan Colliery has a high gas storage capacity especially for CO_2.
- Both of the permeability tests show that the Bulli coal seam will have a low permeability of <1 mD under *in situ* condition.
- Coal with high sorption capacity, relatively low gas content and high CO_2 concentration ($CH_4/(CH_4+CO_2)$ <0.2) will result in low saturation degree and thus poor gas drainage.

The comparative result between hard-to-drain and easy-to-drain areas is summarised in Table 7.1:

Table 7.1: The comparative result between hard-to-drain and easy-to-drain area

Category	Hard-to-drain area	Easy-to-drain area
Geology	Geological variation, including fault presence and cleat system variation	No large geological variation or cleat system variation
	Coal mineralisation, mylonite presence	Coal with less mineralisation
Coal microstructure	Close face and butt cleat system observation, also with mineral matter and particles	Open face and butt cleat system observation
	Coal solid surface with less porous structure system generation observation	Coal with more porous structure and fracture system generation observation
	Coal with mineralisation and intrusion observation	Coal with less mineralisation and coal particles in the porous structure
Coal permeability	Geological variation induced coal permeability direction and value changes, low permeability of <1 mD	Constant or relatively higher coal permeability without large geological variation
Coal sorption capacity, gas composition and gas content	High sorption capacity especially with CO_2 gas, with high CO_2 concentration area, low gas saturation.	Low CO_2 concentration area with high gas saturation
	Gas composition of CO_2 > 80 %	Gas composition of CH_4 > 80 %
	Relatively lower gas content 6-10 m^3/t with low gas saturation	Relatively higher gas content with high gas saturation
	Relatively smaller Q_M margin between the "Fail" and "Pass" samples	Relatively larger Q_M margin between the "Fail" and "Pass" samples

The investigation of hard-to-drain coal is summarised and shown in Figure 7.1, it can be seen:

- Coal sorption capacity is influenced by environmental conditions, such as temperature and moisture.
- High gas storage capacity, low gas content and high CO_2 concentration results in low gas saturation of coal.
- Geological variation and geo-stress affect coal micro-structure and coal permeability, low permeability is also related to poor porous structure.

- Low gas saturation, poor porous structure, low permeability and geological variation directly cause the gas hard-to-drain problem.
- Actually, the indirect reasons causing the hard-to-drain problem also influence each other. *In situ* environmental conditions such as moisture and temperature also affect coal permeability and can also be induced by geological variations.
- High CO_2 concentration will also result in low permeability in coal and can also be induced by geological variation and geological stress.
- The hard-to-drain problem is caused by a combination of these factors, especially when most of the features appear within a particular coal seam area.

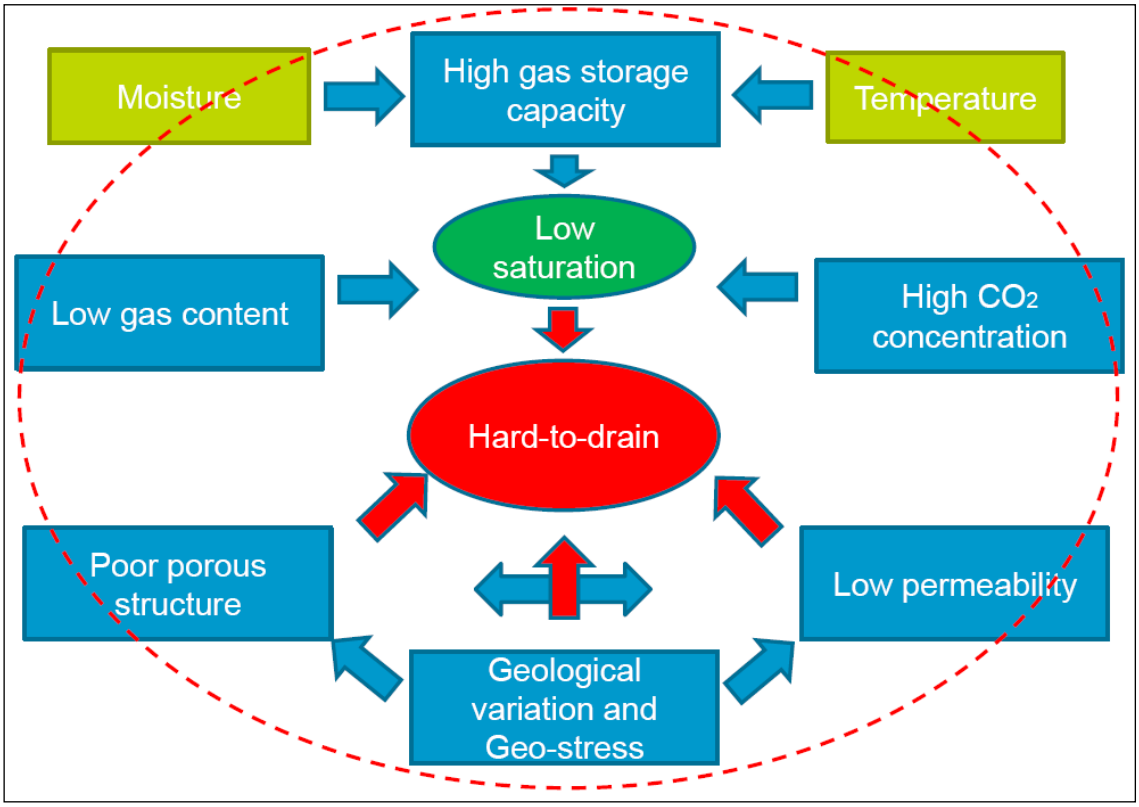

Figure 7.1: Summary of investigation of hard-to-drain

7.3 STUDY OF GAS INJECTION TO FLUSH COAL SEAM GAS

Gas content and gas composition results are the important factors in relation to mine operation and safety for mine sites, and currently they become more important in coalbed methane resource assessment and recovery operations for the CBM industries. These data can be used in evaluation of coal seam gas control options in underground coal mining and the

gas resource calculation and reservoir modelling. To prevent outburst occurrences, outburst threshold limits were established. The parameters of coal seam gas content and composition are the two key parameters to determine the limitation values for safe mining.

Florentin (2012) did a laboratory study of research of stored gas in coal recovery by nitrogen injection. It is reported that nitrogen appeared to replace both carbon dioxide and methane and also found that nitrogen gas appeared to displace more CO_2 than CH_4. Injection of N_2 gas also caused changes in coal volume both perpendicular and parallel to coal bedding. The current laboratory study is considered to further research into N_2 injection to enhance/flush coal seam gas. Modifications are made in terms of different injection direction, a specially separated flushing stage arrangement, an accountable set-up of flushing gas volume and consuming N_2 volume, a further mathematical determination of the CO_2/CH_4 gas in coal based on the experimental result. Specifically this study has improved the test by:

- A more meaningful injection direction from the central hole of the coal sample to simulate the *in situ* borehole;
- Separation of the whole flushing test into three stages, i.e., gas sorption stage, N_2 injection stage, desorption stage after the injection;
- Gas pressure, vertical and horizontal strain was continuously logged in the different stages, and more importantly the flushed gas CO_2/CH_4 and N_2 flushing gas was consistently collected;
- Vertical and horizontal strain, flushing gas volume and N_2 consumed volume was collected and compared between the different stages and the different gas injection test; and
- A further mathematical determination of the CO_2/CH_4 gas in coal was generated based on the experimental result, to calculate the adsorbed CO_2/CH_4 gas in coal in the N_2 injection and gas desorption stages.

7.4 LABORATORY TEST OF INJECTION WITH MULTI FUNCTION OUTBURST RESEARCH RIG

7.4.1 Multi Function Outburst Research Rig (MFORR) and Gas Chromatograph

The combined set up of the MFORR and Gas Chromatograph (GC) used in this test is shown in Figure 7.2, introduced in the study by Zhang *et al.* (2012). The MFORR comprises a number of components which can be utilised for various coals and gas behaviour testing, which was previously reported in Chapter Six.

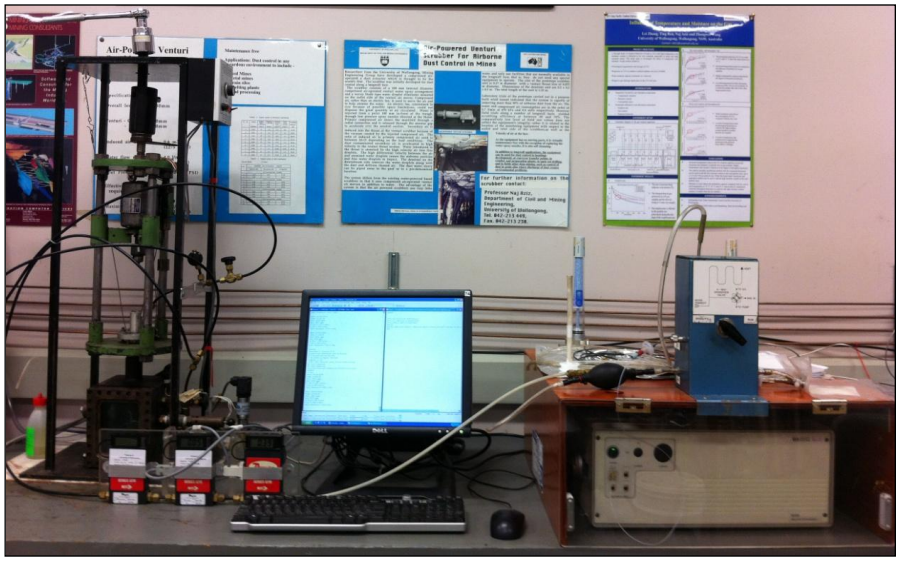

Figure 7.2: A combination set up of MFORR and GC

Generally, the MFORR has various key components. These include the main apparatus support frame and a precision drill, a high pressure chamber which contains a load cell for measuring the load applied to the samples of coal, a pressure transducer for measuring the pressure inside the chamber, several flow meters set in series for measuring the gas flow rate, two strain gauges for measuring volumetric changes of the coal sample vertically and horizontally, a universal socket for loading a sample of coal vertically into the gas pressure chamber and a data acquisition system and a GC for the analysis of the gases discharged from the chamber. Figure 7.3 shows the schematic view of the experimental set up.

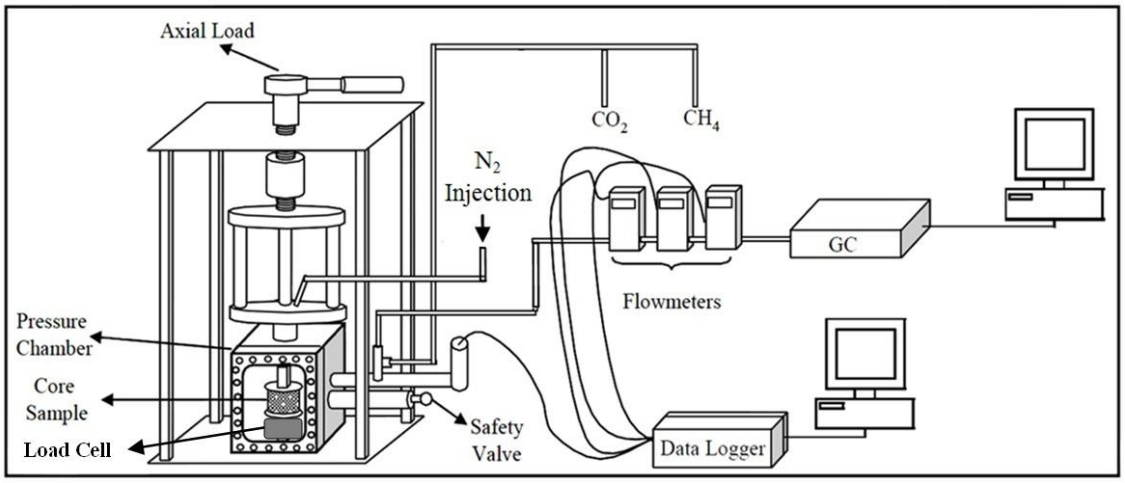

Figure 7.3: A combination set up of MFORR and GC (modified after Florentin *et al.*, 2010)

7.4.2 Coal sample preparation

The sample preparation for the flushing test is similar to preparing the sample for the permeability test with this apparatus. The sample for the flushing test was collected from the hard-to-drain area of panel MG22. A standard core samples with dimension of 54 mm in diameter and 50 mm in height were used. A 2 mm diameter hole was drilled in the middle of the cored coal. Prior to testing, two strain gauges were glued horizontally and vertically to the sample and both ends of the prepared specimen were sealed with a rubber layer. Figure 7.4 shows a snapshot of the sample.

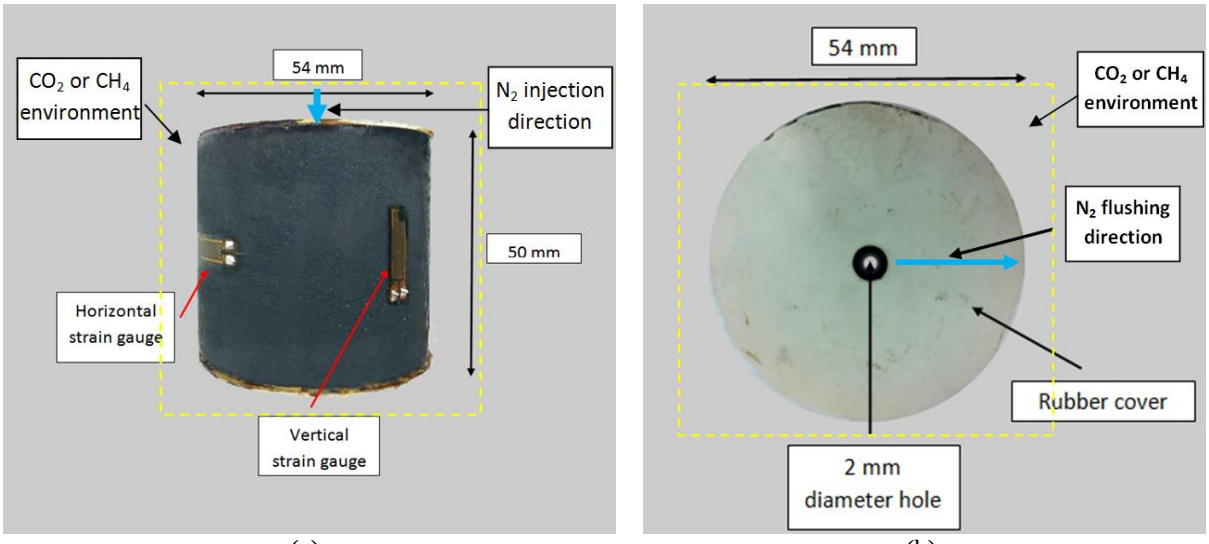

(a) (b)

Figure 7.4: Coal samples for N_2 flushing test

7.5 INJECTION OF N_2 TO FLUSH CO_2

7.5.1 Stage 1 - Coal sorption process

In stage 1, the gas chamber was sealed with the prepared coal sample inside, before the CO_2 sorption test. The system was evacuated to -100 kPa (relative pressure) to remove the air inside the chamber and degas the coal samples. The coal sample was then loaded axially to 3 MPa (axial load around 730 kg) initially and then charged with CO_2 to 3 MPa to keep the coal saturated with CO_2, two strain gauges were simultaneously logged during the whole process. The volumetric change in the coal sample due to pressurisation was monitored with the two strain gauges throughout the testing procedure. All the data from the test process were processed in a data logger and an online PC. The whole system was maintained in a non-leakage condition which was all operated properly by valves through the entire test. CO_2 gas was injected into the chamber to allow the CO_2 gas to diffuse into the coal and be adsorbed by the coal, until the coal reach sorption equilibrium at around 2 MPa gas pressure.

Figure 7.5 shows the coal strain gauges changes during coal sorption. The vertical and horizontal strain gauge readings continue to increase in the coal sorption process, with the vertical strain increasing from 1695 ppm to 4533 ppm and horizontal strain increasing from 2813 ppm to 5243 ppm respectively. This clearly indicates that coal continues to swell during the sorption process, with the gauge reading stabilising with the pressure inside the chamber, showing that coal will expand to a maximum degree when the coal gets saturated.

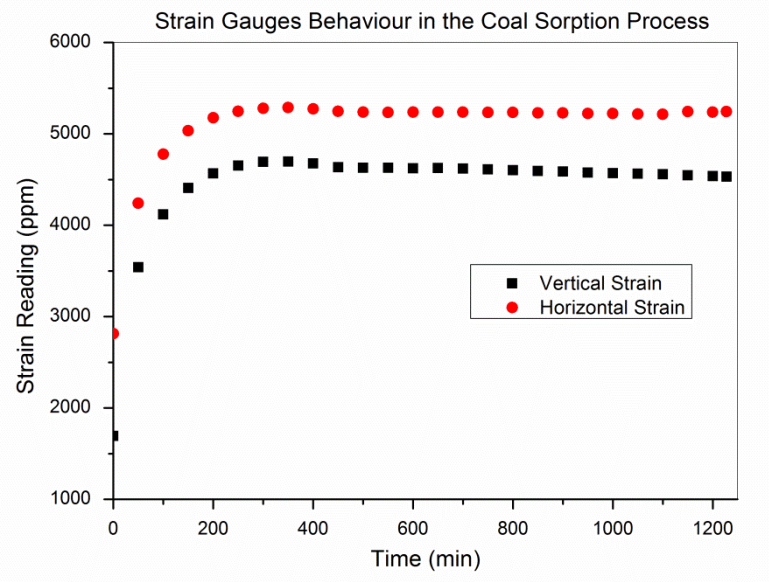

Figure 7.5: Coal strain gauges behaviour during coal sorption

7.5.2 Stage 2 - N_2 injection to flush CO_2 process

In concept, the principle of N_2-ECBM can be described as follows: N_2 is injected into a coal reservoir, it displaces the gaseous CSG from the cleat system, decreasing the CSG partial pressure and creating a compositional disequilibrium between the gaseous and adsorbed phases. These combined influences cause the CO_2 or CH_4 to desorb and diffuse into the cleat system, becoming the "stripped gas" from the matrix. The CSG then migrates to and is produced from production wells (Reeves and Oudinot, 2004).

Prior to the commencement of the N_2 injection test, the GC was calibrated to allow accurate measuring of the gas composition of CO_2, CH_4 and N_2 from the low to high range. N_2 gas flushing was carried out after the coal sample was saturated with CO_2 at the prescribed 2 MPa. The gas inside the chamber was tested by the GC to make sure that gas composition of CO_2 is pure (99.9 %), and the whole system is not contaminated by air.

At 2 MPa pressure, N_2 gas was then introduced to the gas chamber, charged through the central hole of the coal sample to allow N_2 gas to penetrate and permeate the coal sample along the radius and flow into the chamber. The directions of N_2 gas injection and N_2 gas flushing are described with testing coal sample in Figure 7.4. The released gas was systematically discharged from the side hole of the chamber at 6 min interval and then went through a measuring system and a line of gas flow meters (0-2 L/min and 0-15 L/min measurement range), the gas was collected in a 1 L storage capacity sample bag which was directly connected to the GC to test gas composition. The pressure inside the chamber, vertical and horizontal strain gauge readings are continuously logged during the whole process.

As shown in Figure 7.6, during the N_2 flushing process, the CO_2 percentage in the chamber gas gradually decreases and N_2 percentage increases, which indicates that CO_2 gas continues to be flushed out by N_2, the whole flushing test takes more than 13 h (800 min). At the lower concentration of CO_2, it seems that the flushing process is becoming harder as coal continues to desorb much CO_2 gas at low CO_2 partial pressure and apparently the injected N_2 gas helps this adsorbed gas to desorb into the chamber.

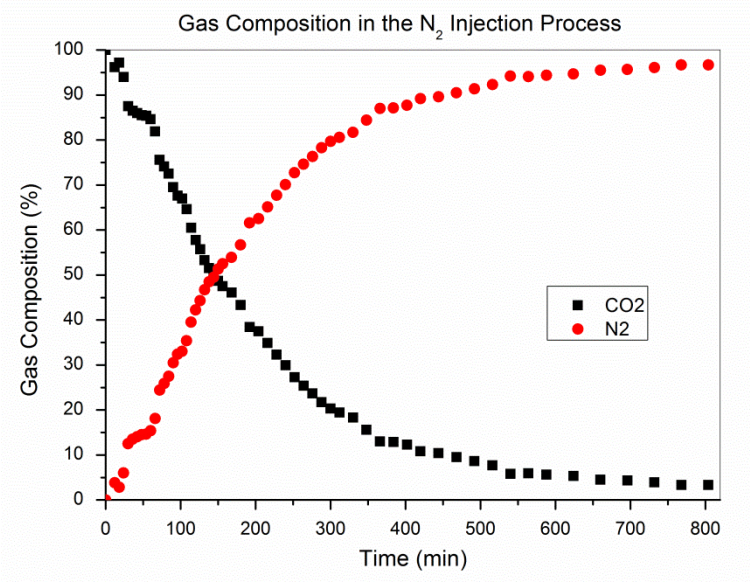

Figure 7.6: Gas composition during N_2 injection

As each step of the test, gas was discharged through the sample bag and 1 bag volume is equal to 1 L, so the total gas volume for each discharge from the chamber can be calculated combined with the gas composition data. Figure 7.7 shows the volume of the various gases being discharged out of the pressure chamber over the test period of 800 min.

The total gases consumed during the flushing test was estimated to be 100.9 L of N_2, liberating 33.1 L of CO_2 out of the system. Test results indicate that a greater volume of N_2 gas is needed to flush CO_2 gas out of coal, especially during the later stage of flushing, as the CO_2 level was declining.

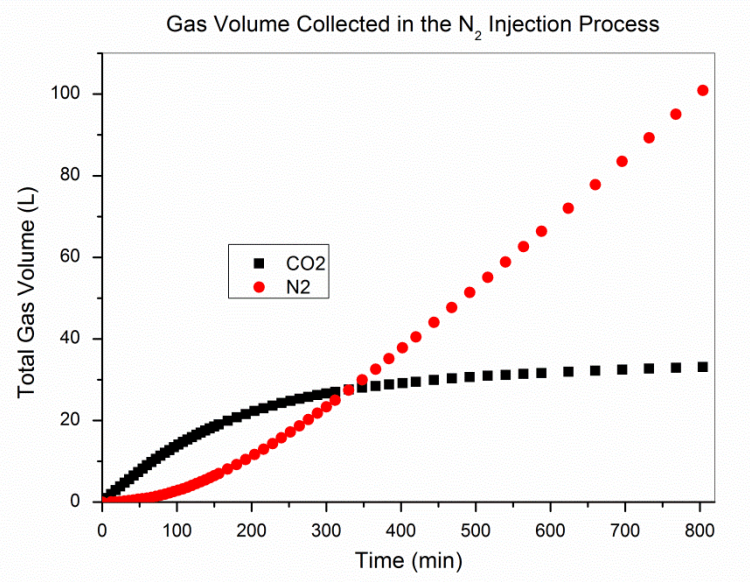

Figure 7.7: Gas volume during N_2 injection

Figure 7.8 shows the volumetric changes in coal during the N_2 flushing and CO_2 recovery test period, both vertical and horizontal strain gauge readings gradually decrease in the flushing process, with vertical strain reducing from 4668 ppm to 3160 ppm, while horizontal strain reducing from 5278 ppm to 4127 ppm, which indicates although the chamber pressure is maintained at around 2 MPa, coal shrinks in the process. The continued desorption of CO_2 during the flushing period has contributed significantly to the shrinkage behaviour.

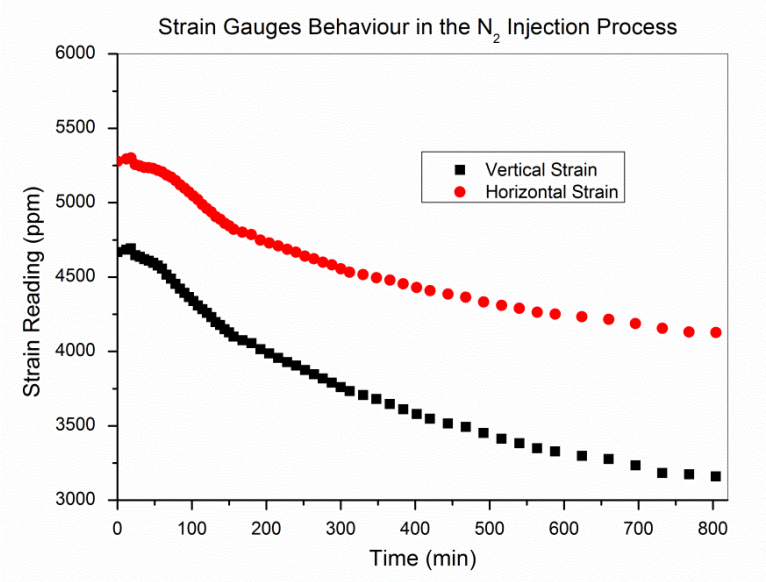

Figure 7.8: Coal strain gauges behaviour during N_2 injection

7.5.3 Stage 3 - Desorption test after N_2 injection

In stage 3, a desorption test was carried out following the N_2 injection test when the CO_2 percentage was around 3 %. The N_2 injection valve was closed. Gas pressure inside the chamber began to gradually drop as the remaining gas volume in the chamber was gradually removed. Figure 7.9 shows the pressure drop (relative pressure) in the desorption process.

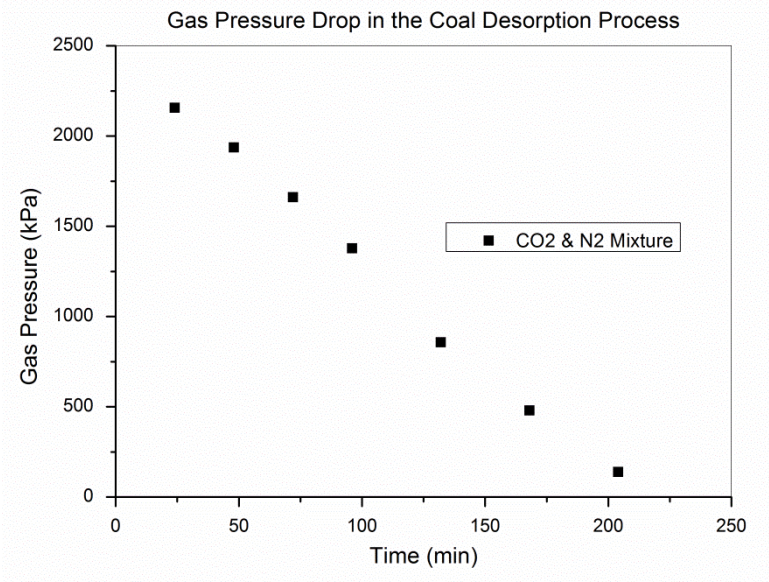

Figure 7.9: Gas pressure drop during desorption

Figure 7.10 shows the change of gas composition in the desorption process, the CO_2 percentage starts to increase from 3.4 % to 9.4 %, while the N_2 percentage deceases from 96.6 % to 90.6 % over a period of around 3 h (200 min), which shows that more CO_2 gas desorbs from the coal than N_2 when the gas pressure drops indicating greater CO_2 sorption capacity than N_2. Further measured data after overnight desorption in Figure 7.10 also confirm this conclusion, with CO_2 reaching 37.2 % and N_2 decreasing to 62.8 %. It should be noted that the pressure in the chamber was reduced to normal atmospheric level (101.320 kPa, absolute pressure).

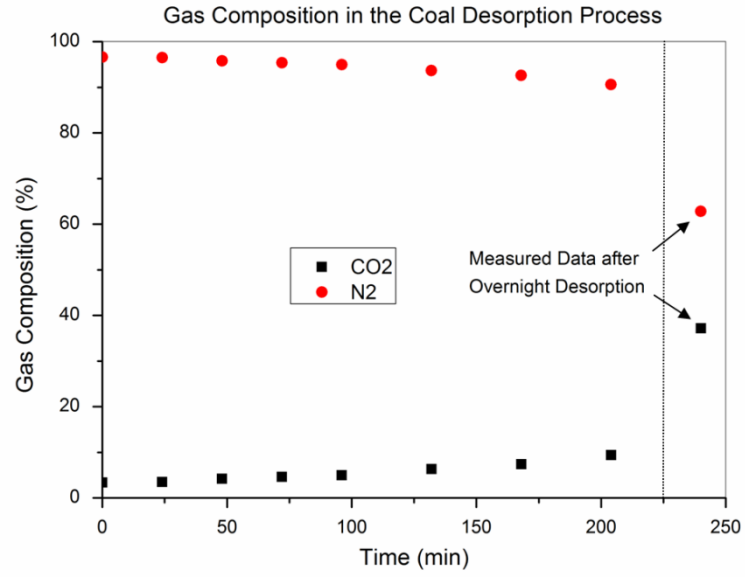

Figure 7.10: Gas composition during desorption

Figure 7.11 shows that the collected gas volume of CO_2 and N_2 in the desorption process, as there is a high concentration in the chamber after the flushing test, more N_2 is collected than CO_2. At the end of the test a total of 37.7 L of N_2 and 2.3 L of CO_2 are collected.

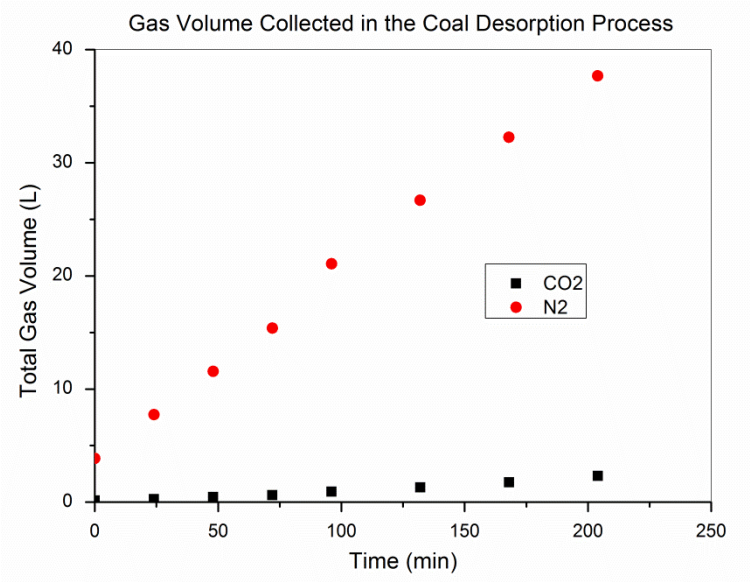

Figure 7.11: Gas volume during coal desorption

Figure 7.12 shows the coal volumetric changes in terms of strain gauge readings in the desorption process, the vertical and horizontal strain continues to decrease, with the vertical strain reducing from 3133 ppm to 2679 ppm and horizontal strain reducing from 4100 ppm to 3916 ppm, which shows that the coal sample shrinks in the desorption process, and the coal stops shrinking when the desorption process is finished.

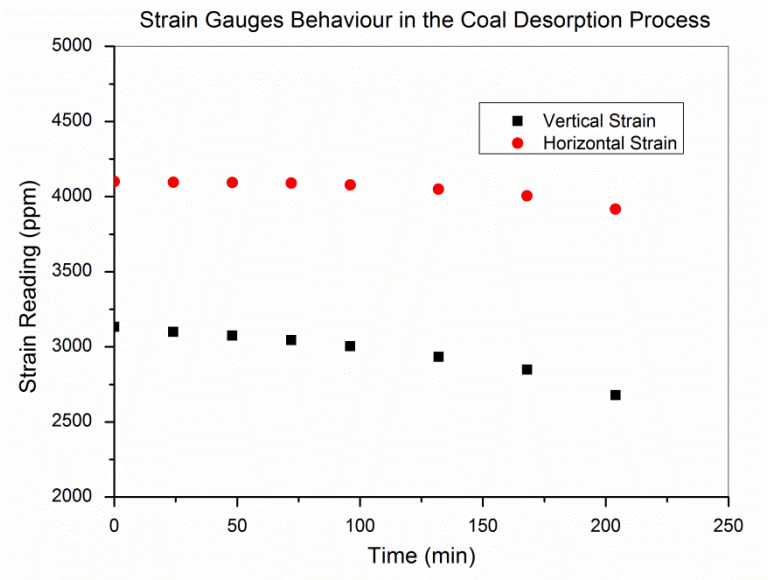

Figure 7.12: Coal strain gauges behaviour during desorption

7.6 INJECTION OF N_2 TO FLUSH CH_4

7.6.1 Stage 1 - Coal sorption process

In stage 1, the same procedure is used for the CO_2 flushing test. The gas chamber was sealed with the prepared coal sample inside, before the CH_4 sorption test, the system was evacuated and the coal sample was degassed. The coal sample was then loaded axially to 3 MPa initially and then charged with CH_4 to 3 MPa to keep the coal saturated with CH_4. CH_4 gas injection into the chamber continued to allow the CH_4 gas adsorbed by the coal, in the end the coal reached sorption equilibrium around 2 MPa gas pressure, the same as the CO_2 gas test.

Figure 7.13 shows the coal strain gauges behaviour in terms of coal sorption. The vertical and horizontal strain gauge readings continue to increase in the coal sorption process, with the vertical strain increasing from 934 ppm to 2134 ppm and horizontal strain increasing from 2589 ppm to 3637 ppm respectively. This clearly indicates that coal continues to swell during the sorption process which is similar with CO_2 gas test, with the gauge reading finally stabilising as coal expands to a maximum degree.

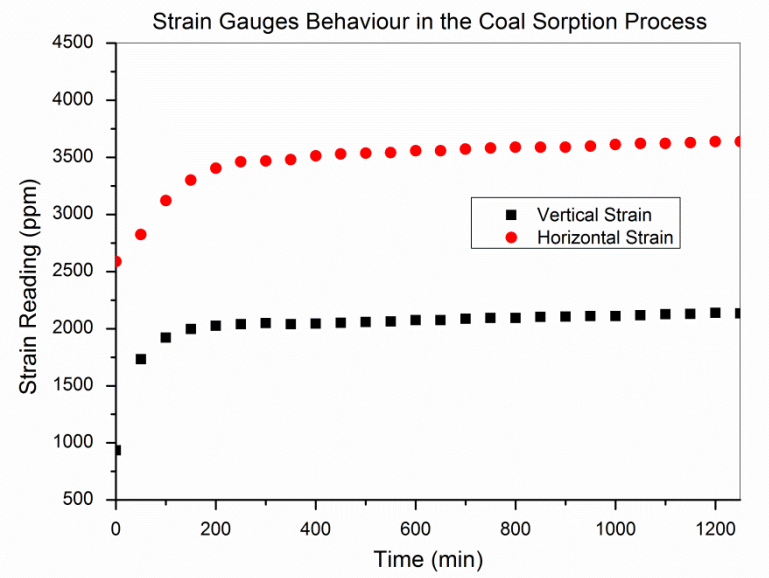

Figure 7.13: Coal strain gauges behaviour during coal sorption

7.6.2 Stage 2 - N_2 injection to flush CH_4 process

The same procedure is used for the CO_2 flushing test. Prior to the commencement of the N_2 injection test, the GC was calibrated to accurately measure the gas composition of CO_2, CH_4

and N_2. N_2 gas flushing test was carried out after the coal sample was saturated with CH_4 at the prescribed chamber pressure of 2 MPa. The gas inside the chamber was tested by the GC to make sure that the gas composition of CH_4 is nearly 100 % (99.9 %), and the whole system is not contaminated by air leakage.

At 2 MPa pressure, N_2 gas was then charged through the central hole of the coal sample to allow the N_2 gas to penetrate and permeate the coal sample along the radius and flow into the chamber. The released gas was systematically discharged from the side hole of the chamber at 6 minutes intervals and then went through a measuring system and gas flow meters. All the discharged gas was collected in 1 L storage capacity sample bags. The same as for the CO_2 flushing test, the pressure inside the chamber, and the vertical and horizontal strain gauge readings are continuously logged during the whole process.

As shown in Figure 7.14, during the N_2 flushing process, the CH_4 percentage in the chamber gradually decreases and the N_2 percentage increases, which indicates CH_4 gas also continues to be flushed out by N_2. This finding is in general agreement with the study of Florentin *et al.*, (2010), who did a similar test and found CSG can be flushed out with N_2 injection in the experimental test. The whole flushing test takes more than 8 h (500 min). At the lower CH_4 percentage stage, it confirms that it is hard to use N_2 to achieve effective flushing.

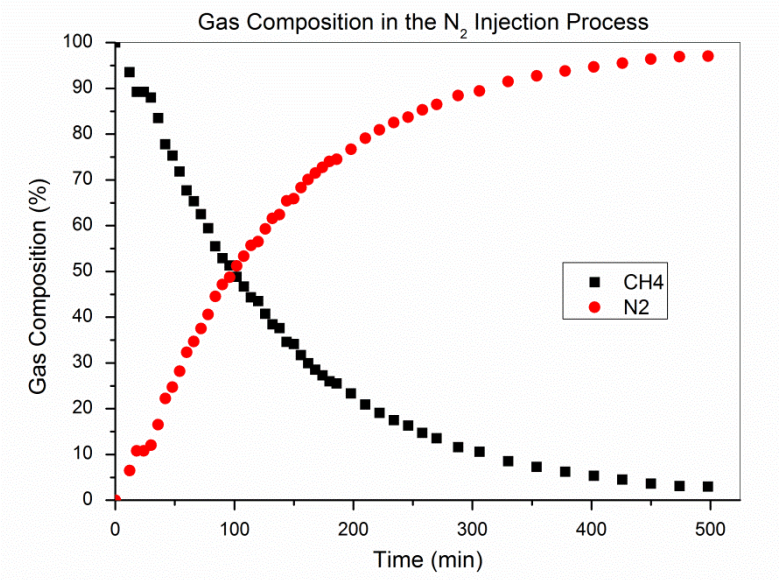

Figure 7.14: Gas composition during N_2 injection

As mentioned in the CO_2 flushing test, gas was discharged and collected. Figure 7.15 shows the volume of the various gases being discharged and collected out of the pressure chamber over the test period of 500 min. It was estimated that 61.0 L of N_2 were consumed in the

flushing test, liberating 22.0 L of CH_4 out of the system. It was also found that a greater volume of N_2 gas is needed to flush CH_4 gas during the later stage of flushing.

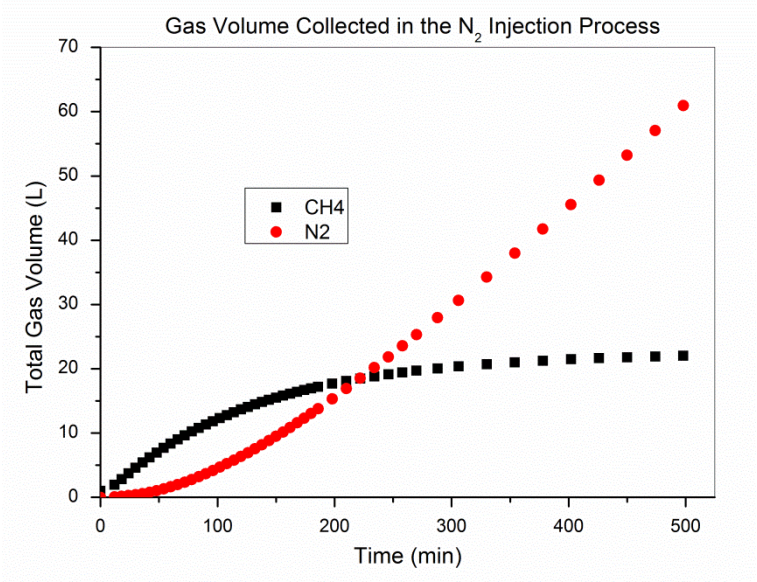

Figure 7.15: Gas volume during N_2 injection

Figure 7.16 shows the volumetric changes in coal during the N_2 flushing and CH_4 recovery test period. Both the vertical and horizontal strain gauge readings gradually decreases in the flushing process, with vertical strain reducing from 2187 ppm to 1607 ppm, while horizontal strain reduces from 3693 ppm to 3237 ppm, which indicates that coal shrinks in the whole process with the stable pressure of 2 MPa. The continued gas desorption contributes significantly to the shrinkage behaviour.

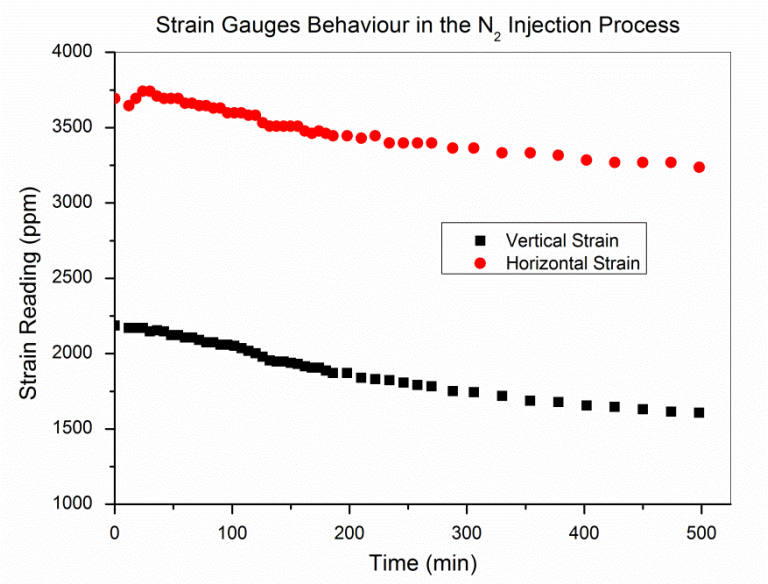

Figure 7.16: Coal strain gauges behaviour during N_2 injection

7.6.3 Stage 3 - Desorption test after N_2 injection

In stage 3, a desorption test was carried out after the N_2 injection test was finished and gas composition of CH_4 was around 3 %. The N_2 injection valve was closed and the gas pressure inside the chamber began to gradually drop as the remaining gas volume in the chamber was gradually removed. Figure 7.17 shows the pressure drop (relative pressure) in the desorption process.

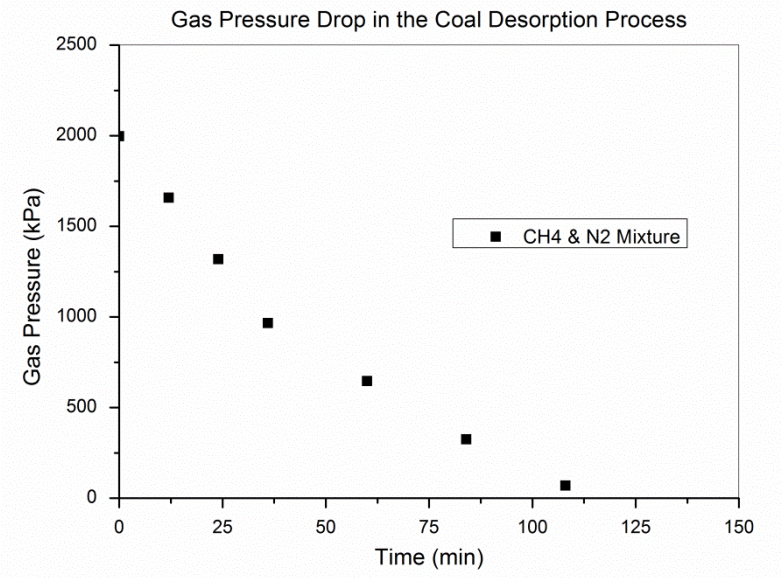

Figure 7.17: Gas pressure drop during desorption

Figure 7.18 shows the change of gas composition in the desorption process, CH_4 percentage starts to increase from 2.8 % to 6.0 %, while N_2 percentage deceases from 97.2 % to 94.0 % over a period of around 2 h (110 min), which shows that more CH_4 gas desorbs from the coal than N_2 when the gas pressure drops indicating greater CH_4 sorption capacity than N_2. Further measurement data after overnight desorption in Figure 10 also confirm this conclusion, with CH_4 percentage reaches 12.2 % and N_2 percentage decreases to 87.8 %.

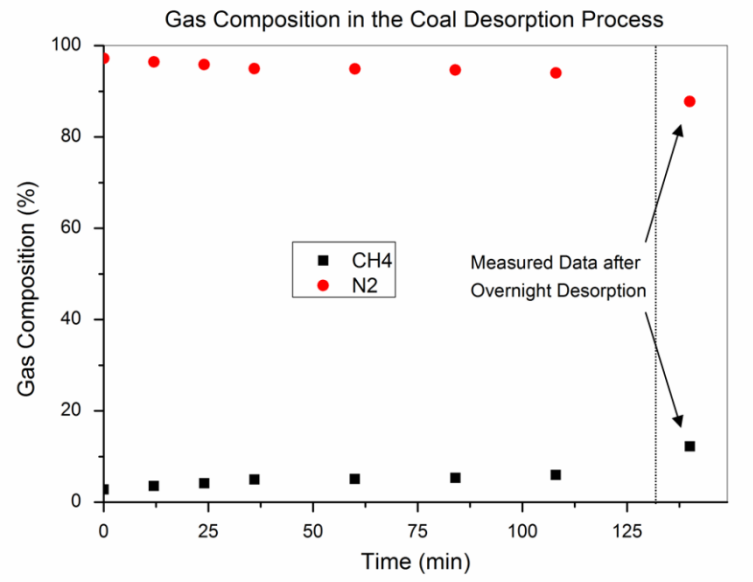

Figure 7.18: Gas composition during desorption

Figure 7.19 shows the collected gas volumes of CH_4 and N_2 in the desorption process, as there is a high concentration in the chamber after the flushing test, more N_2 is collected than CH_4, at the end of test a total 20.9 L of N_2 and 1.1 L of CH_4 is collected.

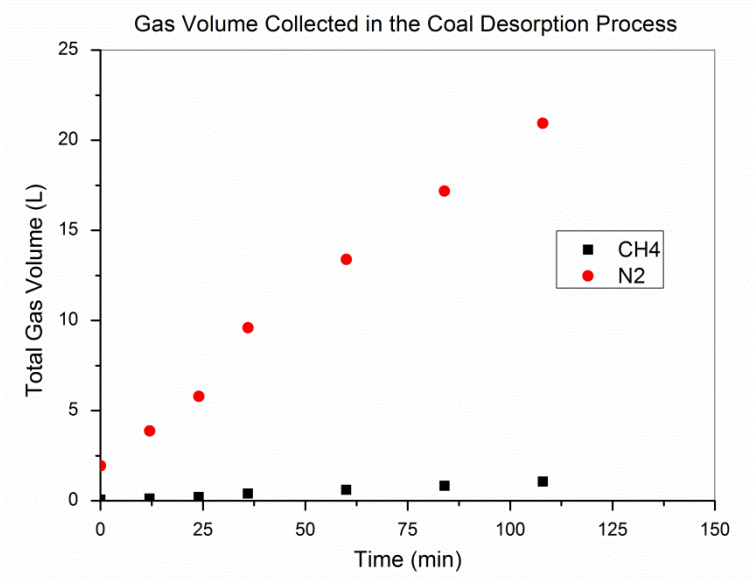

Figure 7.19: Gas volume during coal desorption

Figure 7.20 shows the coal volumetric changes in terms of strain gauge readings in the desorption process, the vertical and horizontal strain continues to decrease, with the vertical strain reducing continuously from 1594 ppm to 1326 ppm, but horizontal strain first increasing from 3238 ppm to 3346 ppm and then reducing from 3346 ppm to 3310 ppm, which shows that the coal sample shrinks in the desorption process in the vertical direction,

but first swells and then shrinks in the horizontal direction till the end of the desorption process.

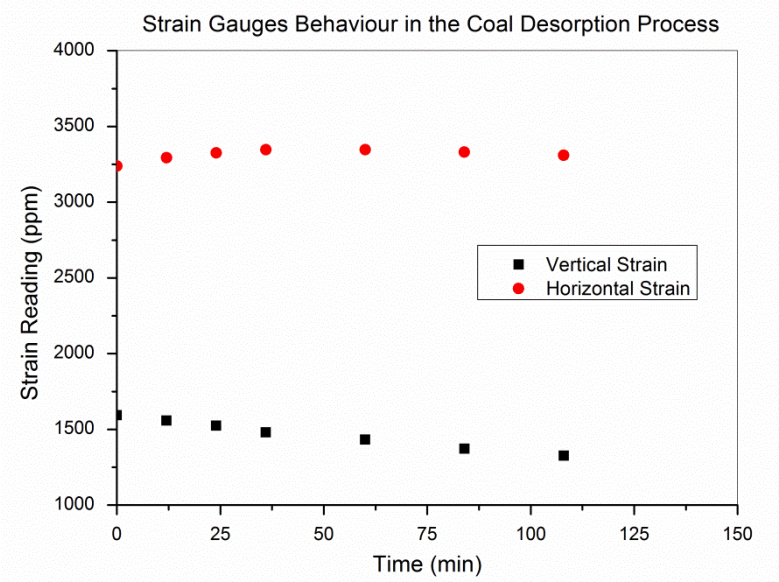

Figure 7.20: Coal strain gauges behaviour during desorption

7.7 COMPARISON OF N_2 TO FLUSH CO_2 AND CH_4

Table 7.2 and Table 7.3 shows the important stages of the CO_2 and CH_4 flushing test, the parameter of rig load indicates the vertical stress applied on the coal. Rig load is only set at the beginning of the whole test, the changes of the reading indicate coal swelling and shrinking behaviour. Both strain gauge reading and rig loading data show that gas sorption in coal is a swelling process, and the coal desorption and N_2 flushing process is generally a shrinking process.

Table 7.2: The important stages of flushing CO_2 test

Stage	Status	Rig Load (kg)	Vertical Strain (ppm)	Horizontal Strain (ppm)	Chamber Pressure (kPa)	Gas Composition of CO_2 (%)	Gas Composition of N_2 (%)
1	Origin status	732	939	2650	-100	0	0
2	Start of adsorbing	655	1695	2813	3020	99.9	0
3	End of adsorbing	752	4533	5243	1999	99.9	0
4	Start of flushing	726	4668	5278	2019	99	1
5	End of flushing	664	3160	4127	2050	3.4	96.6
6	End of desorption	737	2679	3916	45	9.4	90.6
7	End of desorption (overnight)	722	1186	2786	125	37.2	62.8

Table 7.3: The important stages of flushing CH_4 test

Stage	Status	Rig Load (kg)	Vertical Strain (ppm)	Horizontal Strain (ppm)	Chamber Pressure (kPa)	Gas Composition of CH_4 (%)	Gas Composition of N_2 (%)
1	Origin status	734	903	2634	-100	0	0
2	Start of adsorbing	703	934	2589	3030	99.9	0
3	End of adsorbing	745	2145	3644	1989	99.9	0
4	Start of flushing	721	2187	3693	2028	94.0	6.0
5	End of flushing	695	1607	3237	2046	2.8	97.2
6	End of desorption	740	1335	3317	64	6.0	94.0
7	End of desorption (overnight)	730	1008	2693	110	12.2	87.8

7.7.1 Stage 1 - Coal sorption comparison

Coal sorption of CO_2 or CH_4 is a coal swelling process. Figure 7.21 shows the comparison of strain change in the coal sorption process, for CO_2 sorption, vertical strain change and horizontal strain change is 2838 ppm and 2430 ppm, respectively. While for CH_4 sorption, vertical strain change and horizontal strain change is 1200 ppm and 1048 ppm, respectively. It is indicated that coal strain change is larger for CO_2 than CH_4 when coal starts to adsorb the gas to get equilibrium around 2 MPa, which confirms the reviews of coal behaviour with gas adsorption in Chapter Two.

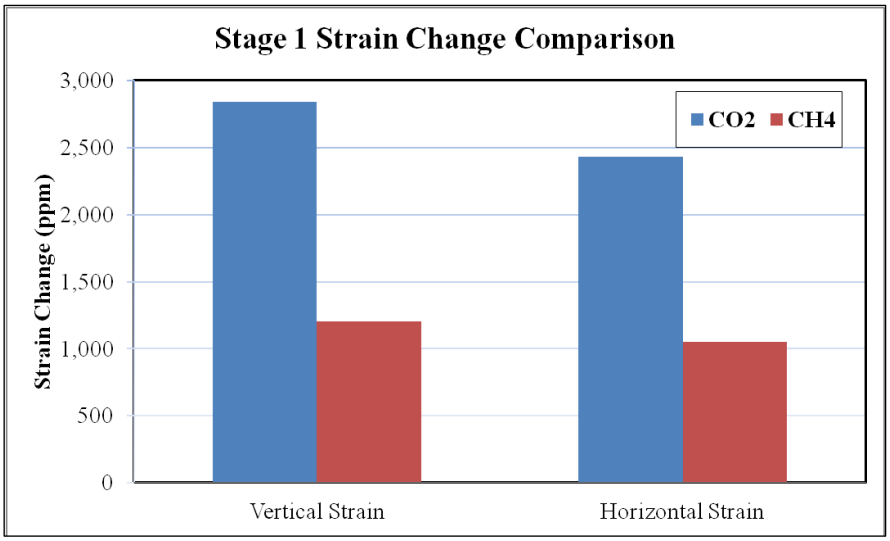

Figure 7.21: Comparison of strain change in Stage 1

7.7.2 Stage 2 - N_2 injection process comparison

As mentioned in previous section, the N_2 flushing process is a coal shrinkage process. Figure 7.22 shows a comparison of strain change in the N_2 flushing process. For the CO_2 flushing test, vertical strain change and horizontal strain change is 1508 ppm and 1151 ppm, respectively, while for CH_4 flushing test, vertical strain change and horizontal strain change is 580 ppm and 456 ppm, respectively. This indicates that coal keeps shrinking and permeability is enhanced in the N_2 flushing stage. It also indicates that coal strain change is larger for CO_2 than CH_4 during the whole flushing stage. For CO_2 and CH_4, larger vertical strain changes were observed in the flushing stage than desorption stage. In all the three stages, larger vertical strain change was observed than horizontal strain change.

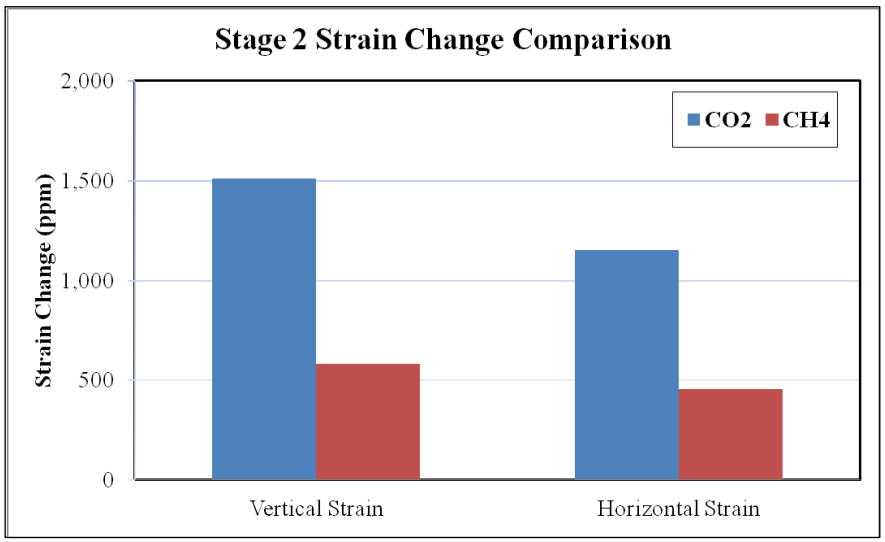

Figure 7.22: Comparison of strain change in Stage 2

Figure 7.23 shows a comparison of collected gas volume in the flushing stage for CO_2 and CH_4. It can be observed that more N_2 is consumed than the recovered CO_2 or CH_4. The ratio of collected volume of N_2:CO_2 is around 3.05 and the ratio of collected volume of N_2:CH_4 is around 2.77, which is relatively smaller than the CO_2 flushing test.

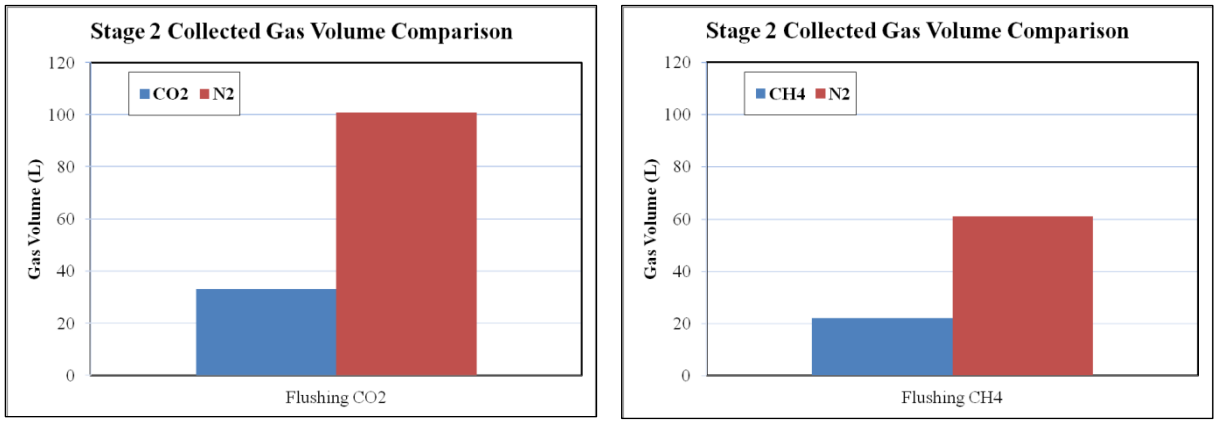

(a) (b)

Figure 7.23: Comparison of collected gas volume in Stage 2

According to the tested coal sorption isotherm of this typical hard-to-drain coal in Chapter Six, Langmuir parameters are as follows, V_L= 32.2 cc/g, P_L = 798.5 kPa for CO_2 and V_L = 18.9 cc/g, P_L = 1064.55 kPa for CH_4. Thus, by combining all the parameters and using the Langmuir equation, when coal is saturated at 2 MPa, the adsorbed gas content is 23.01 cc/g for CO_2 and 12.33 cc/g for CH_4. It should be noted that this calculation is based on the assumption that coal sample achieves complete saturation under the experimental conditions mentioned above. Because the coal sample mass in the flushing test is 160 g, the adsorbed volume of CO_2 is 3.68 L and 1.97 L for CH_4. All the adsorbed gas is flushed out during Stage 2 and Stage 3 and as the gas composition of CO_2 or CH_4 is very low at the end of the flushing stage, all the gas coming out in the stage 3 is assumed to be adsorbed gas, which is 2.3 L for CO_2 and 1.1 L for CH_4. Hence, the total adsorbed gas volume flushed in the Stage 2 is 1.38 L for CO_2 and 0.87 L for CH_4.

Based on the experimental data the following equation is adopted to calculate the gas content in coal during the flushing stage:

$$v_t = v_0 - \sum_{i=1}^{t} (c_{t-1} - c_t) \times \frac{\Delta v}{\Delta c} \qquad (7\text{-}1)$$

Where v_t is the gas content in coal during the flushing stage, v_0 is the gas content in coal at the time 0 (starting point of flushing stage), c_t and c_{t-1} are the gas composition in the chamber at the time t and t-1 during the flushing stage, respectively, Δv is the total gas content drop in coal in the flushing stage and Δc is the total gas composition drop in the chamber in the flushing stage, all the gas terms referred here is CO_2 or CH_4.

Figure 7.24 shows the gas content change in coal during the flushing stage, in total 1.38 L adsorbed CO_2 and 0.87 L of adsorbed CH_4 are flushed out of coal, helping reduce coal gas content of CO_2 from 23.01 cc/g to 14.385 cc/g and from 12.33 cc/g to 6.89 cc/g for CH_4. The reduction of 8.625 cc/g CO_2 gas content accounts for 37.5 % of the total adsorbed CO_2 gas content while the reduction of 5.44 cc/g accounts for 44.1 % of the total adsorbed CH_4 gas content, which indicates N_2 flushing plays a more effective role in reducing adsorbed CH_4 than CO_2. Also a longer flushing time is needed to flush CO_2 than CH_4 at the same equilibrium pressure (2 MPa) level.

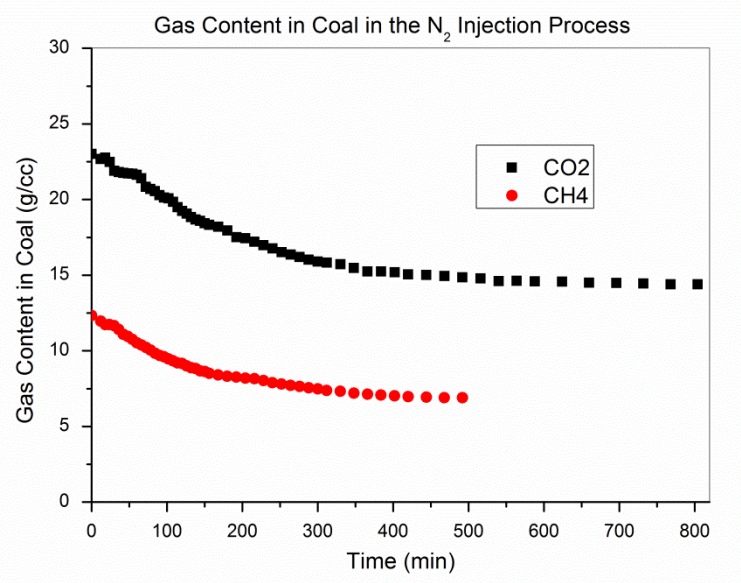

Figure 7.24: Comparison of gas content in coal in Stage 2

7.7.3 Stage 3 - Desorption process comparison

The gas desorption process is generally a shrinkage process. Figure 7.25 shows the comparison of strain change in the gas desorption process. For the CO_2 desorption test, vertical strain change and horizontal strain change is 454 ppm and 184 ppm, respectively, while for the CH_4 desorption test, vertical strain change and horizontal strain change is 268 ppm and 72 ppm, respectively. It is indicated that coal strain change is larger for CO_2 than CH_4 during the gas desorption stage, which confirms reported coal behaviours with gas adsorption in Chapter Two.

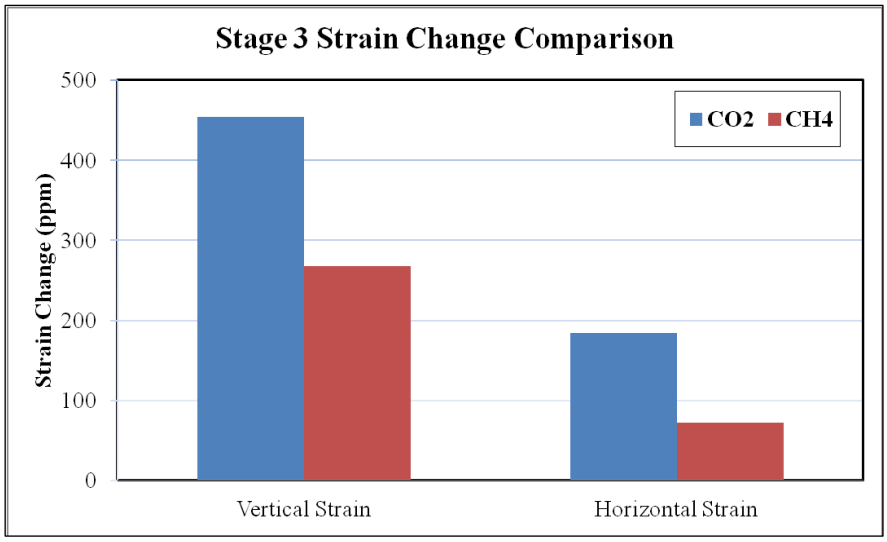

Figure 7.25: Comparison of strain change in Stage 3

Figure 7.26 shows the comparison of collected gas volume in the desorption stage for CO_2 and CH_4. It was found that more N_2 volume is collected than CO_2 or CH_4 was recovered. The ratio of collected volume of N_2:CO_2 is around 16.40 and the ratio of collected volume of N_2:CH_4 is around 19.0, which is relatively larger than the CO_2 flushing test.

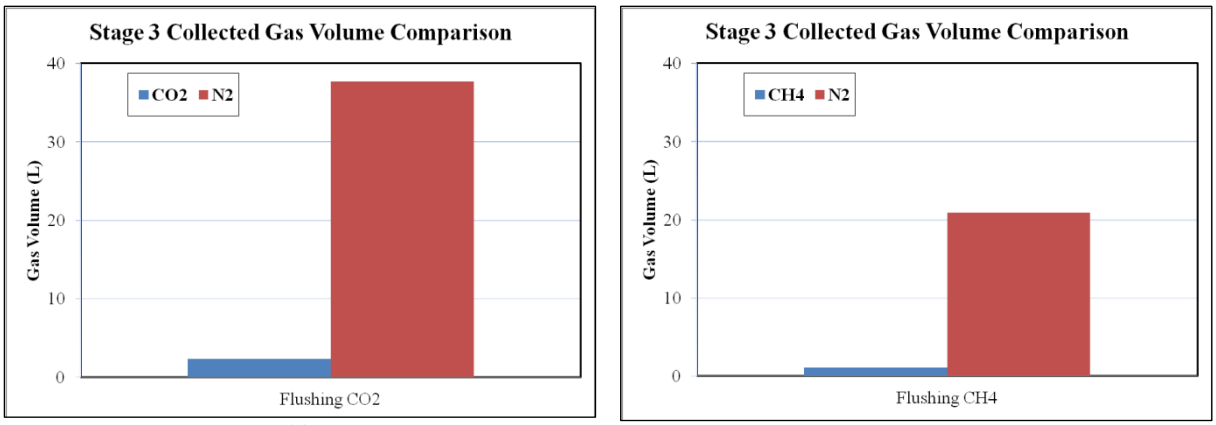

(a) (b)

Figure 7.26: Comparison of collected gas volume in Stage 3

All the adsorbed gas is flushed out during the Stage 2 and Stage 3 and as the gas composition of CO_2 or CH_4 is very low at the end of the flushing stage, all the gas coming out in the stage 3 is assumed to be adsorbed gas, which is 2.30 L for CO_2 and 1.10 L for CH_4.

Based on the experimental data the following equation is adopted to calculate the gas content during the desorption stage:

$$v_t = v_0 - \sum_{i=1}^{t}(c_t - c_{t-1}) \times \frac{\Delta v}{\Delta c} \qquad (7\text{-}2)$$

Where v_t is the gas content in coal during the desorption stage, v_0 is the gas content in coal at the time 0 (starting point of desorption stage), c_t and c_{t-1} are the gas composition in the chamber at the time t and t-1 during the desorption stage, respectively, Δv is the total gas content drop in coal in the desorption stage and Δc is the total gas composition increase in the chamber in the desorption stage, all the gas terms referred here is CO_2 or CH_4.

Packham *et al*. (2012) reported the continued injection of nitrogen would create conditions where the methane content of the coal could be reduced to negligible levels. Figure 7.27 shows the gas content change in coal during the desorption stage. A total of 2.30 L adsorbed CO_2 and 1.10 L of adsorbed CH_4 are desorbed from coal, to help reduce the remaining coal gas content, which is 14.385 cc/g for CO_2 and 6.89 cc/g for CH_4.The reduction accounts for 62.5 % of the total adsorbed CO_2 gas content and 55.8 % of the total adsorbed CH_4 gas content, respectively. It indicates gas desorption after N_2 flushing plays a more effective role in reducing adsorbed CO_2 than CH_4.

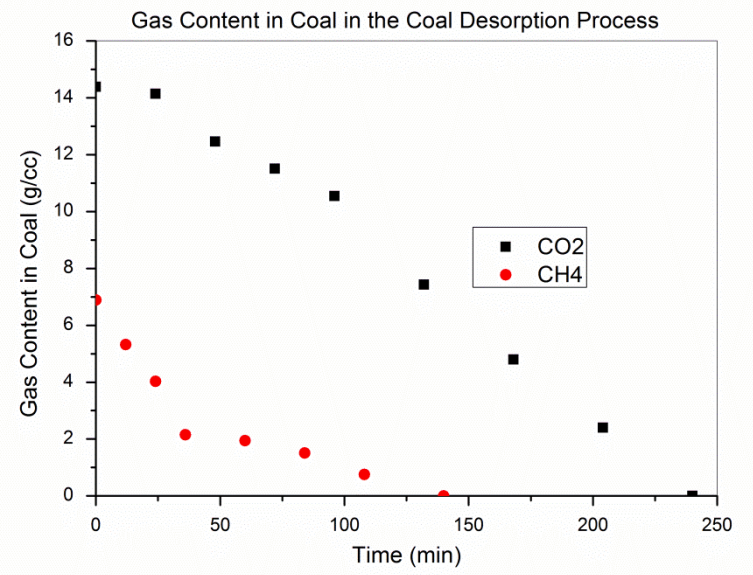

Figure 7.27: Comparison of gas content in coal in Stage 3

7.8 SUMMARY

The gas drainability of a coal seam is affected by many different factors. Especially, geological variation induced cleat system variation, poor coal porous structure, low coal

permeability, high coal sorption capacity and high CO_2 concentration are believed to contribute to the hard-to-drain problems.

Laboratory N_2 injection test shows that CSG (CO_2 and CH_4) can be flushed out by N_2 injection. During the N_2 flushing process, CO_2 and CH_4 percentage of the chamber gas gradually decreases and N_2 percentage increases, which indicates that CO_2 and CH_4 gas continues to be flushed out by N_2. With the N_2 flushing test approaching, the collected total gas volume of both CSG and N_2 increases. It is obvious that at low CO_2 or CH_4 concentration stage, it is hard to use N_2 to achieve effective flushing.

After the flushing test, a certain amount of CO_2 or CH_4 is still adsorbed inside the coal. In the desorption process, CO_2 or CH_4 percentage change starts to increase. More CO_2 and CH_4 gas desorbs from the coal than N_2. Strain gauge reading and rig loading data show that coal sorption process is a coal swelling process, coal desorption and N_2 flushing and gas desorption processes are generally a coal shrinking process.

A comparative study between flushing CO_2 and CH_4 shows that coals with CO_2 gas tests experience always a more strain change than CH_4 gas. The decreasing strain in the flushing and desorption stages indicates that coal continues shrinking and the coal permeability is recovered.

In the N_2 injection stage, the ratio of N_2:CO_2 collected volume is around 3.05 and the ratio is around 2.77 for N_2:CH_4. In the gas desorption stage, the ratio of N_2:CO_2 collected volume is around 16.40 and the ratio is around 19.0 for N_2:CH_4. During the flushing stage, N_2 injection help reduces the adsorbed gas content. The reduction of 8.625 cc/g CO_2 gas content accounts for 37.5 % of the total adsorbed CO_2 gas content while the reduction of 5.44 cc/g accounts for 44.1 % of the total adsorbed CH_4 gas content, which indicates N_2 flushing plays a more effective role in reducing adsorbed CH_4 than CO_2.

Comparatively, during the desorption stage, a total of 2.30 L adsorbed CO_2 and 1.10 L of adsorbed CH_4 are desorbed from coal. The reduction accounts for 62.5 % of the total adsorbed CO_2 gas content and 55.8 % of the total adsorbed CH_4 gas content, respectively. It indicates gas desorption after N_2 flushing plays a more effective role in reducing adsorbed CO_2 than CH_4.

The result clearly shows that N_2 gas flushing has a significant effect on the CO_2 and CH_4 desorption and removal from coal. The N_2 flushing application plays an apparent role in coal's behaviour in the whole process as well. Thus it is important to develop a nitrogen injection technique in the field trial, to enhance gas recovery in tight (hard-to-drain) and low permeable seams in future.

CHAPTER EIGHT – CONCLUSIONS AND RECOMMENDATIONS

8.1 CONCLUSIONS

Through the study of gas generation and flow mechanism in coal and coal sorption characteristics, the following conclusions have been made:

- Gas transport in coal in terms of desorption, diffusion and gas flow and different factors impacting on gas diffusion and gas flow in cleat are reviewed. Different types of technology to enhance both surface and underground gas drainage are introduced.
- Different coal sorption isotherm test methods were grouped into volumetric and gravimetric methods plus the confining stress sorption method and sorption direct determining method. The volumetric method was subdivided into volumetric method with sample cell (equilibrium cell) and injection pumps and volumetric method with both sample cell and reference cell (or reference volume). The gravimetric method was subdivided into gravimetric method with sample cell and suspension magnetic balance and gravimetric method with both sample cell and reference cell (or reference volume). The apparatus set up and the calculation method, uncertainties and comparisons regarding the sorption test are reviewed and introduced.
- Although the powdered coal samples provide a good indication of the gas sorption capacity, observations emphasize that it is necessary to use coal samples confined at representative *in situ* confining stress for reliable evaluation of the sorption capacities. Based on the isotherm testing apparatus and calculation method of the University of Wollongong, coal isotherms of Bulli Seam in the Southern Sydney Basin were tested. For both dry and moist coal tests, the adsorption capacity of coal linearly decreases with increasing temperature. The decreasing rate of adsorption capacity is greater for CO_2 than CH_4, and for each gas test, the decreasing rate is higher for dry coals. Greater reduction value for CO_2 than CH_4 is observed with increasing temperature on the adsorption capacity of coal.
- The moist coal sample isotherm for both CO_2 and CH_4 demonstrated a much lower sorption capacity. This clearly indicates that the moisture in the coal reduces the adsorption capacity. For the coal sample tested at several temperatures (35 ℃, 45 ℃ and

55 ℃), the average reduction ratio of coal adsorption capacity with moisture of CO_2 and CH_4 is 11.1 % and 14.0 %, respectively. The experimental result shows that moisture content in coal has more effect on CH_4 than on CO_2.

- The helium density of coal increases with increasing coal particle size and ash content. In the process of grinding, coal loses the higher density component and at the same time the pore accessibility increases, finally resulting in coal volume relatively increasing and with the helium density decreasing.
- Coal sorbed volume decreases with increasing coal particle size, both in dry and in dry ash free basis. The difference of CO_2 and CH_4 adsorption isotherms for different particle size coal samples calculated with dry ash free basis is smaller than dry basis. Langmuir volume decreases with the increasing coal particle size for CO_2 and CH_4 adsorption and desorption.
- Langmuir volume difference becomes larger between dry ash free and dry basis with increasing coal particle size, especially for CO_2 adsorption isotherms. Commercial laboratories prefer using coal powders in order to reduce the time required for saturation, will have the risk of overstating the sorption capacity of the coal.
- The tested coal isotherms of different coal particle sizes have apparent hysteresis for both CO_2 and CH_4. Larger particle size coals show a greater hysteresis. Langmuir volume decreases with increasing coal particle size. Langmuir volume differences become larger between adsorption and desorption with the increasing coal particle size, especially for CH_4 adsorption and desorption isotherms.
- The reduced surface tension value is reduced by increasing coal temperature and moisture and this value decreased with gas type and in the order of CO_2, CH_4 and N_2 respectively. The reduced surface tension value is relatively greater in the desorption process than in adsorption for both dry and moist coal samples. The experimental results showed that the theory of coal surface free energy tallied well with the experimental results and this can be used to explain both dry and moist coal sorption characteristics with CO_2, CH_4 and N_2 at higher temperatures.

Through the investigation of gas drainage performances at Metropolitan Colliery, the following conclusions have been made:

- Geological variations can lead to changes in seam gas compositions as well as impact on the performance of gas drainage. Geological survey of the Bulli seam in Metropolitan Colliery showed that there is a strike/slip fault and mylonite existing in the typical hard-

to-drain area (8-11 c/t, MG 22). This fault may be responsible for cleat system variations, CO_2 and CH_4 variations in this area and the high concentration of CO_2.

- Field observation of cleat system and gas drainage borehole arrangements were carried out and face and butt cleat systems can be clearly observed on the lump coal sample provided, which appears to support field observations that boreholes drilled perpendicular to the face cleat (from drilling stub towards Mains or outbye) tend to be more productive, whilst boreholes drilled inbye were less effective for degassing.
- SEM studies were carried out with coal from the both easy-to-drain area and the hard-to-drain area with SEM technology. It is observed that the microstructures of the hard-to-drain coal samples appear to be tighter and less porous when compared with the easy-to-drain samples, both from perpendicular and parallel to bedding directions.
- More coal porous structures are found with coals from the easy-to-drain area, especially along the parallel to bedding direction. The less porous structures may contribute to the problem of draining gas from coal sections of Bulli seam in the hard-to-drain area, where the coal structure is less fractured.
- Permeability of coal samples from MG22 of Metropolitan mine was tested with MFORR and Triaxial Compression Apparatus. Tests show at each of the vertical stress level that coal sample permeability decreases with increasing gas pressure and at higher gas pressure, coal permeability stays stable and undergoes minor changes under different vertical stress. The permeability converges to below 1 mD under increased stress conditions portraying the *in situ* conditions at Metropolitan mine, explaining the possible reason causing the problem of hard to drain.
- Strain gauge results from the MFORR test clearly demonstrate the coal samples experienced negative volumetric changes or shrinkage with increased confinement pressures axially and laterally. The degree of the volumetric changes is found to be dependent on the level of the applied axial and lateral pressures or stresses.
- Ash content tests showed low ash content around 7% with the hard-to-drain coal seam, and this can contribute to higher gas adsorption capacity, and hence lead to poor drainage. The Langmuir volume of CO_2 and CH_4 for the hard-to-drain area had no larger difference with both of the easy-to-drain areas. The Langmuir volume for CO_2 is much higher than for CH_4 which indicates the larger adsorption capacity for coal seams and higher undersaturation potential with higher gas composition value of CO_2 which is the case at Metropolitan Mine.

- An analysis of the whole gas database find that the Q_1, Q_2 and Q_3 components increased in response to increasing measured total gas content Q_M. Statistical analysis also shows an increase trend in the Q_1:Q_M and Q_2:Q_M ratio corresponding to increased Q_M, but a decreasing trend in the Q_3:Q_M ratio corresponding to increased Q_M.
- The greater statistical correlation indicates a power equation is considered to more accurately represent the relationship between each gas content component and Q_M especially for "Fail" samples. Analysis also shows that the Q_1 and Q_2 gas components increased more sharply than Q_3 with the increase of Q_M especially for "Fail" samples.
- According to the analysis of the whole database (519 samples) and typical hard-to-drain area (94 samples), "Fail" samples always appear with the higher CO_2 concentration. The zone of the whole database with CH_4/ (CH_4+CO_2) ratio less than 0.2 includes 171 "Fail" samples, accounting for 88.1 % of total "Fail" samples. The zone of typical hard-to-drain area with CH_4/ (CH_4+CO_2) ratio less than 0.2 includes 60 "Fail" samples, accounting for 93.8 % of total "Fail" samples. Including the "Pass" samples, 65.9 % of samples in the zone with CH_4/ (CH_4+CO_2) ratio less than 0.2 are failed.
- Comparative analysis among the three groups including whole database (CH_4<20 %), whole database (CH_4≥20 %) and the typical hard-to-drain area, shows that the value of gas component Q_1, Q_2, Q_3 and Q_M for "Fail" samples of typical hard-to-drain area remains the smallest compared with the other two groups; whilst, the value of gas component Q_1, Q_2, Q_3 and Q_M for "Pass" samples of the typical hard-to-drain area is the highest compared with the other two groups. The measured total gas content (Q_M) in the typical hard-to-drain area is relatively lower and the difference of Q_M between the "Fail" and "Pass" samples is marginal. The Q_3:Q_M ratio remains constant among the three groups, for "Fail" and "Pass" samples, i.e., around 70 % for "Fail" samples and 80 % for "Pass" samples.
- Apparently, the gas content and composition, in conjunction with other parameters, can be used as important indicators for identifying the hard-to-drain areas. A warning index for the hard-to-drain area can include relatively lower gas content (6-10 m^3/t), high gas composition of CO_2 (CO_2>80 %, CH_4<20 % or CH_4/(CH_4+CO_2)<0.2) and other geological variations. If the gas samples have all the above features then the mine should be cautious with their gas drainage in the area from where the samples are taken.
- Laboratory N_2 injection tests show that the CSG (CO_2 and CH_4) can be flushed out by N_2 injection. During the N_2 flushing process, CO_2 and CH_4 percentage of the gas in the

chamber gradually decreases and N_2 percentage increases, which indicates that CO_2 and CH_4 gas continues to be flushed out by N_2. This finding is generally agreed with the study of Florentin (2012), who did the similar test and find CSG can be flushed out with N_2 injection in the experimental test.

- With the N_2 flushing test approaching, the collected total gas volume of both CSG and N_2 increases. It is obvious that at low CO_2 or CH_4 concentration stage, it is hard to use N_2 to achieve effective flushing.
- After the flushing test, a certain amount of CO_2 or CH_4 is still adsorbed inside the coal. In the desorption process, CO_2 or CH_4 percentage change starts to increase. More CO_2 and CH_4 gas desorbs from the coal than N_2. Strain gauge reading and rig loading data show that coal sorption process is a coal swelling process, coal desorption and N_2 flushing and gas desorption processes are generally a coal shrinking process.
- A comparative study between flushing CO_2 and CH_4 shows that coals with CO_2 gas tests experience more strain change than CH_4 gas. The decreasing strain in the flushing and desorption stages indicates that coal continues shrinking and the coal permeability is recovered.
- In the N_2 injection stage, the ratio of N_2:CO_2 collected volume is around 3.05 and the ratio is around 2.77 for N_2:CH_4. In the gas desorption stage, the ratio of N_2:CO_2 collected volume is around 16.40 and the ratio is around 19.0 for N_2:CH_4. During the flushing stage, N_2 injection help reduces the adsorbed gas content. The reduction of 8.625 cc/g CO_2 gas content accounts for 37.5 % of the total adsorbed CO_2 gas content while the reduction of 5.44 cc/g accounts for 44.1 % of the total adsorbed CH_4 gas content, which indicates N_2 flushing plays a more effective role in reducing adsorbed CH_4 than CO_2. Comparatively, during the desorption stage, a total of 2.30 L adsorbed CO_2 and 1.10 L of adsorbed CH_4 are desorbed from coal. The reduction accounts for 62.5 % of the total adsorbed CO_2 gas content and 55.8 % of the total adsorbed CH_4 gas content, respectively. It indicates gas desorption after N_2 flushing plays a more effective role in reducing adsorbed CO_2 than CH_4.
- The result clearly shows that N_2 gas flushing has a significant effect on the CO_2 and CH_4 desorption and removal from coal. The N_2 flushing application plays an apparent role in coal's behaviour in the whole process as well. Thus it is important to develop a nitrogen injection technique for field trials, to enhance gas recovery in tight (hard-to-drain) and low permeable seams in the future.

8.2 RECOMMENDATIONS

The following areas are recommended for further research:

- Different apparatus and calculation methods for testing coal sorption isotherm are used in the world, but the variations of both inter and intra laboratories, indicates that a standard coal sample preparation, operation procedure and calculation method should be developed and adopted. Although powdered coal samples provide a good indication of the gas sorption capacity, it is necessary to use coal samples confined at representative *in situ* confining stress with *in situ* temperature and moisture content for reliable evaluation of the sorption capacities.
- Field permeability coal seam tests should be carried out within hard-to-drain areas. To compare with the laboratory testing results, field permeability tests may also be expanded to the whole range of the mining field to set up a database together with gas content and composition data to give early warning signs of hard-to-drain areas.
- Expand the analysis of the relationship between different gas components, gas content and composition to include additional coal collieries and different coal seams, in order to give a more general and detailed relationship about the different gas parameters for different coal seams.
- Further investigations of hard-to-drain seams can be carried out at other mine sites and adopt more analysis such as coal rank, coal type and petrographic parameters, thus setting up a more general quantitative benchmark to characterize gas drainage performances for these seams.
- Field tests of N_2 injection to flush CO_2 and CH_4 should be carried out to enhance underground coal seam gas drainage, especially for improving gas drainage performances from low gas saturation and low permeability hard-to-drain seams. Gas injection time, pressure, borehole arrangement and operation procedure parameters should be considered. Gas flow rate, gas pressure, coal behaviour and gas content as well as gas composition information of both injection borehole and the monitoring borehole should be collected.

REFERENCES

Alcañiz-Monge, J., Linares-Solano, A., Rand, B., 2002. Mechanism of adsorption of water in carbon micropores as revealed by a study of activated carbon fibres. *The Journal of Physical Chemistry B* 106(12), 3209-3216.

Australia Standard, 1989. Methods for the analysis and testing of coal and coke, AS 1038.3-1989.

Australian Standard, 1999. Guide to the determination of gas content of coal-Direct desorption method, AS 3980-1999.

Australia Standard, 2002. Coal and coke - analysis and testing, AS 1038.25 - 2002.

Aziz, N., Li, W. M., 1999. The effect of sorbed gas on the strength of coal – an experimental study. *Geotechnical and Geological Engineering* 17(3), 387-402.

Bae, J.-S., Bhatia, S. K., 2006. High-pressure adsorption of methane and carbon dioxide on coal. *Energy and Fuels* 20(6), 2599-2607.

Bartosiewicz, H., Hargraves, A. J., 1984. Catalogue of gas properties of Australian gassy black coals. *CSIRO Div. Geomech., AMIRA Project 82/P153, Final Report*, 12p.

Bartosiewicz, H., Hargraves, A. J., 1985. Gas properties of Australian coal. *Proc. Australia. Inst. Min. Metall* 290, 71-77.

Battino, S., Hargraves, A. J., 1982. Seam gas drainage experiments in some collieries of B.H.P. *Seam gas drainage with particular reference to the working seam*, (ed: Hargraves, A. J.), University of Wollongong, Wollongong, Australia, 157-171. http://www.uow.edu.au/eng/outburst/presentations_publications/ausimm_1982/S.Battino,%20Hargraves.PDF

Beamish, B., O'Donnell, G., 1992. Microbalance applications to sorption testing of coal. *Symposium on Coalbed Methane Research and Development in Australia*, Coalseam Gas Research Institute – James Cook University, Townsville, 19-21 November 4, 31-41. http://www.uow.edu.au/eng/outburst/presentations_publications/coal_methane_1992/Microbalance%20application-B.B.Bea.PDF

Bielicki, R. J., Perkins, J. H., Kissell, F. N., 1972. Methane diffusion parameters for sized coal particles: A measuring apparatus and some preliminary results. United StatesWed, Univ. of Tennessee Library, Knoxville, 12p.

Black, D., 2012. Factors affecting the drainage of gas from coal and methods to improve drainage effectiveness. *PhD thesis* (University of Wollongong). http://www.uow.edu.au/eng/outburst/html/Completed%20Thesis/D%20Black%20PhD%20Thesis.pdf

Black, D., Aziz, N., 2010. Impact of coal properties and operational factors on mine gas drainage. in *Proceeding of 10th Underground Coal Operators' Conference COAL 2010*, University of Wollongong and Australasian Institute of Mining and Metallurgy, (eds: Aziz, N. and Nemcik, J.), Wollongong, 11-12 February, 229-240. http://ro.uow.edu.au/coal/323/

Briggs, H., Sinha, R. P., 1933. Expansion and contraction of coal caused respectively by the sorption and discharge of gas. *Proceedings of the Royal Society of Edinburgh* 53, 48-53.

Busch, A., Alles, S., Gensterblum, Y., Prinz, D., Dewhurst, D. N., Raven, M. D., Stanjek, H., Krooss, B. M., 2008. Carbon dioxide storage potential of shales. *International Journal of Greenhouse Gas Control* 2(3), 297-308.

Busch, A., Gensterblum, Y., 2011. CBM and CO_2-ECBM related sorption processes in coal: A review. *International Journal of Coal Geology* 87(2), 49-71.

Busch, A., Gensterblum, Y., Krooss, B. M., 2003. Methane and CO_2 sorption and desorption measurements on dry Argonne premium coals: Pure components and mixtures. *International Journal of Coal Geology* 55(2-4), 205-224.

Busch, A., Gensterblum, Y., Krooss, B. M., 2007. High-pressure sorption of nitrogen, carbon dioxide, and their mixtures on Argonne premium coals. *Energy and Fuels* 21(3), 1640-1645.

Busch, A., Gensterblum, Y., Krooss, B. M., Littke, R., 2004. Methane and carbon dioxide adsorption-diffusion experiments on coal: Upscaling and modelling. *International Journal of Coal Geology* 60(2-4), 151-168.

Cai, F., Liu, Z., Zhang, C., Lin, B., 2007. Numerical simulation of improving permeability by deep-hole presplitting explosion in loose-soft and low permeability coal seam. *Journal of China Coal Society* 32 (5), 499-503.

Cervik, J., 1979. Methane control on longwalls - European and U.S. Practices. *Longwall-Shortwall Mining*, Art. Society of Mining Engineers of American Institute of Mining, Metallurgical, and Petroleum Engineers, New York, 75–80.

Chareonsuppanimit, P., Mohammad, S. A., Robinson, R. L., Gasem, K. A., 2012. High-pressure adsorption of gases on shales: Measurements and modelling. *International Journal of Coal Geology* 95(0), 34-46.

Charrière, D., Behra, P., 2010. Water sorption on coals. *Journal of Colloid and Interface Science* 344(2), 460-467.

Charrière, D., Pokryszka, Z., Behra, P., 2010. Effect of pressure and temperature on diffusion of CO_2 and CH_4 into coal from the Lorraine Basin (France). *International Journal of Coal Geology* 81(4), 373-380.

Chen, Z., Pan, Z., Liu, J., Connell, L. D., Elsworth, D., 2011. Effect of the effective stress coefficient and sorption-induced strain on the evolution of coal permeability: Experimental observations. *International Journal of Greenhouse Gas Control* 5(5), 1284-1293.

Clarkson, C. R., Bustin, R. M., 1999. The effect of pore structure and gas pressure upon the transport properties of coal: A laboratory and modelling study 2: Adsorption rate modelling. *Fuel* 78(11), 1345-1362.

Clarkson, C. R., Bustin, R. M., 2000. Binary gas adsorption/desorption isotherms: Effect of moisture and coal composition upon carbon dioxide selectivity over methane. *International Journal of Coal Geology* 42(4), 241-271.

Clayton, J. L., 1998. Geochemistry of coalbed gas - A review. *International Journal of Coal Geology* 35(1–4), 159-173.

Connell, L. D., Lu, M., Pan, Z., 2010. An analytical coal permeability model for tri-axial strain and stress conditions. *International Journal of Coal Geology* 84(2), 103-114.

Crank, J., 1975. The mathematics of diffusion. Second edition, Oxford University.

Crosdale, P., Saghafi, A., Williams, R., Yurakov, E., 2005. Interlaboratory comparative CH_4 isotherm measurement on Australian coals. *Bowen Basin Symposium 2005, The Future for Coal: Fuel for Thought*, Yeppoon, Qld., Geological Society of Australia Coal Geology Group and the Bowen Basin Geologists Group, 273–277.

Crosdale, P. J., Beamish, B. B., Valix, M., 1998. Coalbed methane sorption related to coal composition. *International Journal of Coal Geology* 35(1-4), 147-158.

Crosdale, P. J., Moore, T. A., Mares, T. E., 2008. Influence of moisture content and temperature on methane adsorption isotherm analysis for coals from a low-rank, biogenically-sourced gas reservoir. *International Journal of Coal Geology* 76(1-2), 166-174.

Cui, X., Busten, R., 2006. Controls of coal fabric on coalbed gas production and compositional shift in both field production and canister desorption tests. *SPE Journal* 111-119 (SPE-89035).

Cui, X., Bustin, R. M., Dipple, G., 2004. Differential transport of CO_2 and CH_4 in coalbed aquifers: Implications for coalbed gas distribution and composition. *The American Association of Petroleum Geologists.* 88, 1149-1161.

Cui, X., Bustin, R. M., Dipple, G., 2004. Selective transport of CO_2, CH_4, and N_2 in coals: Insights from modelling of experimental gas adsorption data. *Fuel* 83(3), 293-303.

Dabbous, M. K., Reznik, A. A., Taber, J. J., Fulton, P. F., 1974. The permeability of coal to gas and water. *SPE* 14 (6), 563-572.

Day, S., Fry, R., Sakurovs, R., 2008. Swelling of Australian coals in supercritical CO_2. *International Journal of Coal Geology* 74(1), 41-52.

Day, S., Sakurovs, R., Weir, S., 2008. Supercritical gas sorption on moist coals. *International Journal of Coal Geology* 74(3-4), 203-214.

Dutta, P., Bhowmik, S., Das, S., 2011. Methane and carbon dioxide sorption on a set of coals from India. *International Journal of Coal Geology* 85(3-4), 289-299.

Embleton, B. J. J., Schmidt, R. W., Hamilton, L. H., Riley, H. H., 1985. Dating volcanism in the Sydney Basin: Evidence from K–Ar ages and palaeomagnetism. North Ryde, N.S.W., CSIRO Division of Mineral Physics.

Esterhuizen, G. S., Karacan, C. Ö., 2005. Development of numerical models to investigate permeability changes and gas emission around longwall mining panels. *The AlaskaRocks 2005, 40th US Symposium on Rock Mechanics*, Anchorage, Alaska.

Facer, R. A., Carr, P. F., 1979. K–Ar dating of Permian and Tertiary igneous activity in the Southern Sydney Basin, New South Wales. *Journal of the Geological Society of Australia* 26, 73–79.

Faiz, M., Hutton, A. C., 1995. Geological controls on the distribution of CH_4 and CO_2 in coal seams of the southern coalfield, NSW, Australia. International Symposium-CUM-Workshop on Management and Control of High Gas Emissions and Outbursts in

Underground Coal Mines, Wollongong, NSW, Australia, 375-383. http://www.uow.edu.au/eng/outburst/pdfs/C3079%20Final%20Report.pdf

Faiz, M., Saghafi, A., Sherwood, N., Wang, I., 2007. The influence of petrological properties and burial history on coal seam methane reservoir characterisation, Sydney Basin, Australia. *International Journal of Coal Geology* 70(1–3), 193-208.

Faiz, M. M., 1993. Geological controls on the distribution of coal seam gases in the southern Sydney Basin. *PhD Thesis*. University of Wollongong. http://www.uow.edu.au/eng/outburst/html/Completed%20Thesis/Mohinudeen.html

Faiz, M. M., Saghafi, A., Barclay, S. A., Stalker, L., Sherwood, N. R., Whitford, D. J., 2007. Evaluating geological sequestration of CO_2 in bituminous coals: The Southern Sydney Basin, Australia as a natural analogue. *International Journal of Greenhouse Gas Control* 1(2), 223-235.

Faiz, M. M., Stalker, L., Sherwood, N., Saghafi, A., Wold, M., Barclay, S., Choudhury, J., Barker, W., Wang, I., 2003. Bioenhancement of coal bed methane resources in the Southern Sydney Basin. *J. Aust. Petrol. Prod. Explor. Assoc*. 43, 595–610.

Fan, Y., Wang, Z., 2012. Effect analysis of strengthening permeability in soft and low permeability outburst coal seam by hydraulic flushing. *Safety in Coal Mines* 06, 137-140.

Feng, Z., Wan, Z., Zhao, Y., Li, G., Zhang, Y., Wang, C., Zhu, N., 2010. Experimental study of permeability of anthracite and gas coal masses under high temperature and triaxial stress. *Chinese Journal of Rock Mechanics and Engineering* 29 (4), 689-696.

Florentin, R., 2012. Characterisation of the parameters influencing the storage and drainage of gas in coal. *PhD thesis* (University of Wollongong). http://www.uow.edu.au/eng/outburst/html/Completed%20Thesis/Raul%20Florentin.pdf

Florentin, R., Aziz, N., Black, D., Nghiem, L. and Baris, K., 2010. Recovery of stored gas in coal by nitrogen injection - A laboratory study, in *Proceeding of 10th Underground Coal Operators' Conference COAL 2010*, University of Wollongong and Australasian Institute of Mining and Metallurgy, (eds: Aziz, N. and Nemcik, J.), Wollongong, 11-12 February, 223-234. http://ro.uow.edu.au/cgi/viewcontent.cgi?article=1971&context=coal

Fredericks, L., 2008. Bulli seam permeability data files - 2003 to 2006. BHP Billiton Illawarra Coal Exploration - Confidential Test Reports.

Fujioka, M., Yamaguchi, S., Nako, M., 2010. CO_2-ECBM field tests in the Ishikari Coal Basin of Japan. *International Journal of Coal Geology* 82(3-4), 287-298.

Gamson, P. D., Beamish, B. B., 1992. Coal type, microstructure and gas flow behaviour of Bowen Basin coals. *Symposium on Coalbed Methane Research and Development in Australia*, Coalseam Gas Research Institute – James Cook University, Townsville, 43-64. http://www.uow.edu.au/eng/outburst/presentations_publications/coal_methane_1992/PDGamson%20and%20Beamish.PDF

Gamson, P. D., Beamish, B. B., Johnson, D. P., 1993. Coal microstructure and micropermeability and their effects on natural gas recovery. *Fuel* 72(1), 87-99.

Gensterblum, Y., van Hemert, P., Billemont, P., Battistutta, E., Busch, A., Krooss, B. M., De Weireld, G., Wolf, K. H. A. A., 2010. European inter-laboratory comparison of high pressure CO_2 sorption isotherms ii: Natural coals. *International Journal of Coal Geology* 84(2), 115-124.

Gensterblum, Y., van Hemert, P., Billemont, P., Busch, A., Charriére, D., Li, D., Krooss, B. M., de Weireld, G., Prinz, D., Wolf, K. H. A. A., 2009. European inter-laboratory comparison of high pressure CO_2 sorption isotherms. I: Activated carbon. *Carbon* 47(13), 2958-2969.

Gillies, A. D. S., Gray, I., Ham, B., 1995. Measurement of coal permeability using large samples. *International Symposium-CUM-Workshop on Management and Control of High Gas Emissions and Outbursts in Underground Coal Mines*, Wollongong, NSW, Australia, 317-322.
http://www.uow.edu.au/eng/outburst/pdfs/C3079%20Final%20Report.pdf

Gode, F., Pehlivan, E., 2005. Adsorption of Cr (III) ions by Turkish brown coals. *Fuel Processing Technology* 86(8), 875-884.

Goodman, A. L., Busch, A., Bustin, R. M., Chikatamarla, L., Day, S., Duffy, G. J., Fitzgerald, J. E., Gasem, K. A. M., Gensterblum, Y., Hartman, C., Jing, C., Krooss, B. M., Mohammed, S., Pratt, T., Robinson Jr, R. L., Romanov, V., Sakurovs, R., Schroeder, K., White, C. M., 2007. Inter-laboratory comparison II: CO_2 isotherms measured on moisture-equilibrated Argonne premium coals at 55 °C and up to 15 MPa. *International Journal of Coal Geology* 72(3-4), 153-164.

Goodman, A. L., Busch, A., Duffy, G. J., Fitzgerald, J. E., Gasem, K. A. M., Gensterblum, Y., Krooss, B. M., Levy, J., Ozdemir, E., Pan, Z., Robinson, R. L., Schroeder, K., Sudibandriyo, M., White, C. M., 2004. An inter-laboratory comparison of CO_2 isotherms measured on Argonne premium coal samples. *Energy and Fuels* 18(4), 1175-1182.

Gray, I., 1982. A study of seam gas drainage in Queensland. in *Proceedings of the Symposium on Seam Gas Drainage with Particular Reference to the Working Seam*, (ed: Hargraves, A. J.), Australasian Institute of Mining and Metallurgy - Illawarra Branch, University of Wollongong, Wollongong, Australia, 11-14 May, 218-231.
http://www.uow.edu.au/eng/outburst/presentations_publications/ausimm_1982/Ian%20Gray.PDF

Gregory, R. K., Ertekin, T., Schwerer, F. C., 1986. Numerical simulation of the transient behaviour of coal-seam degasification wells. *SPE Formation Evaluation*, p. 165.

Griffith, M., Hirst, W., 1944. Proceedings of a conference on the ultra fine structure of coals and coke. The British Coal Utilisation Research Association, London, p.80.

Gruszkiewicz, M. S., Naney, M. T., Blencoe, J. G., Cole, D. R., Pashin, J. C., Carroll, R. E., 2009. Adsorption kinetics of CO_2, CH_4, and their equimolar mixture on coal from the Black Warrior Basin, West-central Alabama. *International Journal of Coal Geology* 77(1-2), 23-33.

Gumma, S., Talu, O., 2003. Gibbs dividing surface and helium adsorption. *Adsorption* 9 (1), 17-28.

Guo, D., Pei, H., Song, J., Qin, F., Liu, X., 2008. Study on splitting mechanism of coal bed deep-hole cumulative blasting to improve permeability. *Journal of China Coal Society* 33 (12), 1381-1385.

Guo, Q., Han, W., Zhang, W., Wang, X., Hao, X., Ahato, D. A., 2011. Study on mechanism and application of hydraulic fracturing and permeability improvement gas drainage in underground mine. *Coal Science and Technology* 39 (12), 60-64.

Gurba, L. W., 2002a. Gas migration in coal on the microscopic scale. In: *Gas and coal outburst committee half day seminar, NSW Department of mineral resources*, Wollongong, NSW, Australia.

Gurba, L. W., 2002b. Microscopic studies of low permeability coal. In: *Outburst and gas drainage workshop*, Hanes, J., Australian coal association research program, 53-67.

Hadden, J. D., Sainato, A., 1969. Gas migration characteristics of coalbeds. *United States Bureau of Mines Methane Control Program*, Technical Progress Report – 12, p13.

Hargraves, A. J., 1983. Prevention of instantaneous outbursts of coal and gas. *Alleviation of Coal and Gas Outbursts in Coal Mines Seminar* (ed: Lama, R. D.), Co-ordinating Committee on Outburst Research.

Harpalani, S., Chen, G., 1997. Influence of gas production induced volumetric strain on permeability of coal. *Geotechnical and Geological Engineering* 15(4), 303-325.

Harpalani, S., Prusty, B. K., Dutta, P., 2006. Methane/CO_2 sorption modelling for coalbed methane production and CO_2 sequestration. *Energy and Fuels* 20(4), 1591-1599.

Harpalani, S., Schraufnagel, R. A., 1990. Shrinkage of coal matrix with release of gas and its impact on permeability of coal. *Fuel* 69(5), 551-556.

Hayes, P. J., 1982. Factors affecting gas release from the working seam. in *Proceedings of the Symposium on Seam Gas Drainage with Particular Reference to the Working Seam*, (ed: Hargraves, A.J.), Australasian Institute of Mining and Metallurgy – Illawarra Branch, University of Wollongong, Wollongong, Australia, 11-14 May, 62-69.

He, J., Shi, Y., Ahn, S., Kang, J. W., Lee, C.-H., 2010. Adsorption and desorption of CO_2 on Korean coal under subcritical to supercritical conditions. *The Journal of Physical Chemistry* B 114(14), 4854-4861.

Hol, S., Peach, C. J., Spiers, C. J., 2011. A new experimental method to determine the CO_2 sorption capacity of coal. *Energy Procedia* 4(0), 3125-3130.

Holditch, S. A., Ely, J. W., Carter, R. H., Hinkel, J., Jeffrey, R. G., 1988. Enhanced recovery of coalbed methane through hydraulic fracturing. in *Proceedings of the 63rd Annual Technical Conference and Exhibition of the Society of Petroleum Engineers*, Society of Petroleum Engineers, Houston, Texas, 2-5 October, 9p. (SPE-18250).

Holloway, S., 1997. An overview of the underground disposal of carbon dioxide. *Energy Conversion and Management* 38, Supplement, S193-S198.

Huang, B., Chen, Q., Liu, C., Wei, M., Fu, J., 2011. Hydraulic fracturing theory of coal-rock mass and its technical framework. *Journal of Mining and Safety Engineering* 28 (2), 167-173.

Hughes, B. D., Logan, T. L., 1990. How to design a coalbed methane well. *Petroleum Engineer International* 5, 16-20.

Hungerford, F., Ren, T., Aziz, N., 2012a. Directional control in longhole drilling. in *Proceeding of 12th Underground Coal Operators' Conference COAL 2012*, University of

Wollongong and Australasian Institute of Mining and Metallurgy, (eds: Aziz, N., Kininmonth, B., Nemcik, J. and Ren, T.), Wollongong, 16-17 February, 269-277. http://ro.uow.edu.au/cgi/viewcontent.cgi?article=2076&context=coal

Hungerford, F., Ren, T., Aziz, N., 2012b. Directional control in longhole drilling, ACARP Gas and Outburst Seminar, Wollongong, 27 June. http://www.uow.edu.au/eng/outburst/presentations_publications/outburst_2012_jul/Directional%20Control%20in%20Longhole%20Drilling%20-%20ACARP%20June%2012.pdf

Indraratna, B., Haque, A., 1999. Triaxial equipment for measuring the permeability and strength of intact and fractured rocks. *Geotechnique* 49, 515-521.

IUPAC, 2001. Manual of Symbols and Terminology for Physicochemical Quantities and Units.

Jackson, M., 2004. Permeability testing procedure, BHP Billiton Illawarra coal exploration/coal bed methane. Internal Operating Procedure, document reference - CBM-12-010.

Jasinge, D., Ranjith, P. G., Choi, S. K., 2011. Effects of effective stress changes on permeability of Latrobe Valley brown coal. *Fuel* 90(3), 1292-1300.

JEOL, 2012. JSM-6490 LV Key Product Features. Online document, available from: http://www.jeolusa.com/Default.aspx?tabid=194

Johnson, D., 2010. Perspectives on new CBM production, gas markets and carbon trading in Australia. Metgasco Limited, 15p.

Jones, A. H., Ahmed, U., Abou-Sayed, A. S., Mahyera, A., Sakashita, B., 1982. Fractured vertical wells versus horizontal boreholes for methane drainage in advance of mining U.S. Coals. in *Proceedings of the Symposium on Seam Gas Drainage with Particular Reference to the Working Seam*, (ed: Hargraves, A. J.), Australasian Institute of Mining and Metallurgy - Illawarra Branch, University of Wollongong, Wollongong, Australia, 11-14 May, 172-201. http://www.uow.edu.au/eng/outburst/presentations_publications/ausimm_1982/Fractured%20Vertical%20Wells%20Versus%20Horizontal%20Boreholes%20for%20Methane%20Drainage%20in%20Advance%20of%20Mining%20U.S.%20Coals.pdf

Joubert, J. I., Grein, C. T., Bienstock, D., 1973. Sorption of methane in moist coal. *Fuel* 52(3), 181-185.

Joubert, J. I., Grein, C. T., Bienstock, D., 1974. Effect of moisture on the methane capacity of American coals. *Fuel* 53(3), 186-191.

Kahil, A. A., Masszi, D., 1982. Technical considerations for the design of a demethanation program. *Seam gas drainage with particular reference to the working seam*, (ed: Hargraves, A. J.), University of Wollongong, Wollongong, Australia, 99-104.

Karacan, C. Ö., Esterhuizen, G. S., Schatzel, S. J., Diamond, W. P., 2007. Reservoir simulation-based modelling for characterizing longwall methane emissions and gob gas venthole production. *International Journal of Coal Geology* 71(2-3), 225-245.

Kendall, P. F., Briggs, H., 1933. The formation of rock joints and the cleat of coal. *Proc. R. Soc*. Edinburgh 53, 164–187.

Kinnon, E. C. P., Golding, S. D., Boreham, C. J., Baublys, K. A., Esterle, J. S., 2010. Stable isotope and water quality analysis of coal bed methane production waters and gases from the Bowen Basin, Australia. *International Journal of Coal Geology* 82(3-4), 219-231.

Kiyama, T., Nishimoto, S., Fujioka, M., Xue, Z., Ishijima, Y., Pan, Z., Connell, L. D., 2011. Coal swelling strain and permeability change with injecting liquid/supercritical CO_2 and N_2 at stress-constrained conditions. *International Journal of Coal Geology* 85(1), 56-64.

Kolesar, J. E., 1986. Nature of sorption and diffusion phenomena in the micropore structure of coal. *SPE* (1986), 40p.

Krooss, B. M., van Bergen, F., Gensterblum, Y., Siemons, N., Pagnier, H. J. M., David, P., 2002. High-pressure methane and carbon dioxide adsorption on dry and moisture-equilibrated Pennsylvanian coals. *International Journal of Coal Geology* 51(2), 69-92.

Kunz, O., Wagner, W., Jaeschke, M., 2007. The gerg-2004 wide-range reference equation of state for natural gases. *GERG Technical Monograph 15 Fortschritts - Berichte Verein Deutscher Ingenieue (VDI)* 6.

Lama, R. D., Bartosiewicz, H., 1982. Determination of gas content of coal seams. *Seam Gas Drainage with Particular Reference to the Working Seam.* University of Wollongong, NSW, Australia, 36-52.

Lama, R., Saghafi, A., 2002. Overview of gas outbursts and unusual emissions. in *Proceeding of 3rd Underground Coal Operators' Conference COAL 2002*, University of Wollongong and Australasian Institute of Mining and Metallurgy, (eds: Aziz, N.), Wollongong, 6-8 February, 74-88. http://www.uow.edu.au/eng/outburst/html/Completed%20Thesis/D%20Black%20PhD%20Thesis.pdf

Lama, R. D., 1995. Effect of stress, gas pressure and vacuum on permeability of Bulli coal samples. *International Symposium-CUM-Workshop on Management and Control of High Gas Emissions and Outbursts in Underground Coal Mines*, Wollongong, NSW, Australia, 293-301. http://www.uow.edu.au/eng/outburst/pdfs/C3079%20Final%20Report.pdf

Lama, R. D., Bodziony, J., 1996. Outburst of gas, coal and rock in underground coal mines. Wollongong, NSW, Australia. http://www.uow.edu.au/eng/outburst/pdfs/C4034%20Final%20Report.pdf

Lamarre, R. A., 2007. Downhole geomechanical analysis of critical desorption pressure and gas content for carbonaceous reservoirs. *SPE Annual Technical Workshop on Coalbed Methane*, Society of Petroleum Engineers, Durango, Colorado, 27-29 March, 31p. (SPE-111091).

Laubach, S. E., Marrett, R. A., Olson, J. E., Scott, A. R., 1998. Characteristics and origins of coal cleat: A review. *International Journal of Coal Geology* 35(1–4), 175-207.

Laxminarayana, C., Crosdale, P. J., 1999. Role of coal type and rank on methane sorption characteristics of Bowen Basin, Australia coals. *International Journal of Coal Geology* 40(4), 309-325.

Levy, J. H., Day, S. J., Killingley, J. S., 1997. Methane capacities of Bowen Basin coals related to coal properties. *Fuel* 76(9), 813-819.

Li, D., Liu, Q., Weniger, P., Gensterblum, Y., Busch, A., Krooss, B. M., 2010. High-pressure sorption isotherms and sorption kinetics of CH_4 and CO_2 on coals. *Fuel* 89(3), 569-580.

Li, Q., Liang, Y., Ren, K., Zeng, Y., Zhang, X., 2010. Experimental study of propagation of directional cracks with shaped charge under blasting load. *Chinese Journal of Rock Mechanics and Engineering* 29 (8), 1684-1689.

Li, X., Lu, Y., Zhao, Y., Kang, Y., Zhou, D., 2008. Study on improving the permeability of soft coal seam with high pressure pulsed water jet. *Journal of China Coal Society* 33 (12), 1386-1390.

Li, Z., Song, X., Wang, E., 2011. Feasibility of improving permeability by static blasting during uncovering coal seam in cross-cut. *Journal of Mining and Safety Engineering* 28 (1), 86-89.

Li, Z., Xian, X., 2009. Study on experiment of coal permeability with temperature and stress changing. *Journal of Liaoning Technical University* 28, 156-159.

Li, Z., Xian, X., Long, Q., 2009. Experiment study of coal permeability under different temperature and stress. *Journal of China University of Mining and Technology* 38 (4), 523-527.

Lin, B., Li, Z., Zhai, C., Bi, Q., Wen, Y., 2011. Pressure relief and permeability increasing technology based on high pressure pulsating hydraulic fracturing and its application. *Journal of Mining and Safety Engineering* 28 (3), 452-455.

Lingard, P. S., Phillips, H. R., Doig, I. D., 1982. The permeability of some Australian coals. *Seam gas drainage with particular reference to the working seam*, (ed: Hargraves, A. J.), University of Wollongong, Wollongong, Australia, 70-80.

Lingard, P. S., Phillips, H. R., Doig, I. D., 1984. Laboratory studies of the sorption characteristics and permeability of triaxially stressed coal samples. *Proceeding 3rd Int. congress on mine ventilation*, Harrogate, 143-150.

Liu, C. J., Wang, G. X., Sang, S. X., Rudolph, V., 2010. Changes in pore structure of anthracite coal associated with CO_2 sequestration process. *Fuel* 89(10), 2665-2672.

Liu, J., Chen, Z., Elsworth, D., Qu, H., Chen, D., 2011. Interactions of multiple processes during CBM extraction: A critical review. *International Journal of Coal Geology* 87(3–4), 175-189.

Liu, l., Cheng, Y., Wang, H., Wang, L., Ma, X., 2009. Principle and engineering application of pressure relief gas drainage in low permeability outburst coal seam. *Mining Science and Technology (China)* 19(3), 342-345.

Liu, M., Zhao, W., Liu, Y., Wei, J., 2010. Research and application of hydraulic flushing borehole to quickly eliminate outburst. *Coal Science and Technology* 38 (3), 58-61.

Liu, Y., Lu, Y., Li, X., Xia, B., 2010. Application of drilling in roof or floor with high pulse pressure water jet to improve gas drainage. *Journal of China Coal Society* 35 (7), 1115-1119.

Liu, Y., Ren, P., Xia, S., Sun, Y., 2009. Analysis of pressure-relief and permeability improvement effect of hydraulic flushing. *Journal of Henan Polytechnic University (Natural Science)* 28 (6), 695-699.

Liu, Z., Cai, F., Xiao, Y., 2008. Numerical simulation and analysis of effect of stress release and permeability improvement in coal seams by deep-hole presplit ting explosion. *Journal of Anhui University of Science and Technology (Natural Science)* 28 (4), 16-20.

Loftin, P., 2009. Tips and tricks for finding, developing and operating a coalbed methane field. *24th World Gas Conference*, Argentina, 5-9 October, 17p.

Lu, Y., Song, C., Liu, Y., Kang, Y., 2011. Mechanism analysis of permeability based on promoting coal matrix shrinkage by water jet. *Journal of Chongqing University* 34 (4), 20-23.

Lunarzewski, L. W., 2001. Gas drainage practices. *2001 Coal Operators' Geotechnology Colloquium*, University of Wollongong, NSW, Australia, 35-44.

Marecka, A., Mianowski, A., 1998. Kinetics of CO_2 and CH_4 sorption on high rank coal at ambient temperatures. *Fuel* 77(14), 1691-1696.

Massarotto, P., Golding, S. D., Bae, J. S., Iyer, R., Rudolph, V., 2010. Changes in reservoir properties from injection of supercritical CO_2 into coal seams - a laboratory study. *International Journal of Coal Geology* 82(3-4), 269-279.

Massarotto, P., Rudolph, V., Golding, S. (2000). New 3-D Permeability Equipment helps solve methane release problems. in *Proceedings of Second International Conference Methane Mitigation*. Novosibirsk, Russia, 18-23 June, 373-382.

Mavor, M. J., Close, J. C., Pratt, T. J., 1992. Review of recent US coalbed natural gas reservoir research. in *Proceedings of the Symposium on Coalbed Methane Research and Development in Australia*, Coalseam Gas Research Institute – James Cook University, Townsville, November 19-21 2, 109-152. http://www.uow.edu.au/eng/outburst/presentations_publications/coal_methane_1992/vol2/paper8.pdf

Mavor, M. J., Hartman, C., Pratt, T. J., 2004. Uncertainty in sorption isotherm measurements. *2004 CBM Symposium*, Tuscaloosa, Alabama, p. 14.

Mazumder, S., Wolf, K. H., 2008. Differential swelling and permeability change of coal in response to CO_2 injection for ECBM. *International Journal of Coal Geology* 74(2), 123-138.

McCulloch, C. M., Duel, M., Jeran, P. W., 1974. Cleat in bituminous coalbeds. *US Bureau of Mines, Report of investigations* 7910, 25p.

McCutcheon, A. L., Barton, W. A., 1998. Contribution of mineral matter to water associated with bituminous coals. *Energy and Fuels* 13(1), 160-165.

McCutcheon, A. L., Barton, W. A., Wilson, M. A., 2002. Characterization of water adsorbed on bituminous coals. *Energy and Fuels* 17(1), 107-112.

Meaney, K., Paterson, L., Pinczewski, W. V., Stevenson, M. D., 1995. Advances in coal seam reservoir simulation for mine gas drainage. *International Symposium on Management and Control of High Gas Emissions and Outburst in Underground Coal Mines*, (ed: Lama, R. D.), Wollongong, 20-24 March, 277-282.

Medek, J., Weishauptová, Z., Kovář, L., 2006. Combined isotherm of adsorption and absorption on coal and differentiation of both processes. *Microporous and Mesoporous Materials* 89(1-3), 276-283.

Meszaros, G., Boonen, P., Hale, M., 2007. New tools enable CBM horizontal drilling. *E&P Journal*, 50-53.

Moffat, D. H., Weale, K. E., 1955. Sorption by coal of methane at high pressures. *Fuel* 34, 593-601.

Mohammad, S., Fitzgerald, J., Robinson, R. L., Gasem, K. A. M., 2009. Experimental uncertainties in volumetric methods for measuring equilibrium adsorption. *Energy and Fuels* 23(5), 2810-2820.

Mohammad, S. A., Chen, J. S., Fitzgerald, J. E., Robinson, R. L., Gasem, K. A. M., 2008. Adsorption of pure carbon dioxide on wet Argonne coals at 328.2 K and pressures up to 13.8 MPa. *Energy and Fuels* 23(2), 1107-1117.

Murry, D. K., 1991. Coal bed methane; natural gas resources from coal seams, USA. 97-103.

Nakajima, I., Asakura, K., Yang, Q., Imai, T., 1995. Effect of earth temperature on gas permeability of stressed coal. *International Symposium-CUM-Workshop on Management and Control of High Gas Emissions and Outbursts in Underground Coal Mines*, Wollongong, NSW, Australia, 323-330. http://www.uow.edu.au/eng/outburst/pdfs/C3079%20Final%20Report.pdf

Nie, B., He, X., Wang, E., 2000. Surface free energy of coal and its calculation. *Journal of Taiyuan University of Technology* 31(4), 346-348.

Olague, N. E., Smith, D. M., 1989. Diffusion of gases in American coals. *Fuel* 68(11), 1381-1387.

Osisanya, S. A., Schaffitzel, R. F., 1996. A review of horizontal drilling and completion techniques for recovery of coalbed methane. *SPE International Conference on Horizontal Well Technology*, Society of Petroleum Engineers, Calgary, Canada, 18-20 November, 13p. (SPE-37131).

Ozdemir, E., Morsi, B. I., Schroeder, K., 2004. CO_2 adsorption capacity of Argonne premium coals. *Fuel* 83(7-8), 1085-1094.

Ozdemir, E., Schroeder, K., 2009. Effect of moisture on adsorption isotherms and adsorption capacities of CO_2 on coals. *Energy and Fuels* 23(5), 2821-2831.

Packham, R., Cinar, Y., Moreby, R., 2011. Simulation of an enhanced gas recovery field trial for coal mine gas management. *International Journal of Coal Geology* 85, 247–256.

Packham, R., Connell, L., Cinar, Y., Moreby, R., 2012. Observations from an enhanced gas recovery field trial for coal mine gas management. *International Journal of Coal Geology* 100(0), 82-92.

Palchik, V., 2003. Formation of fractured zones in overburden due to longwall mining. *Environmental Geology* 44(1), 28-38.

Palmer, I., 2010. Coalbed methane completions: A world view. *International Journal of Coal Geology* 82(3-4), 184-195.

Pan, Z., Connell, L. D., Camilleri, M., 2010. Laboratory characterisation of coal reservoir permeability for primary and enhanced coalbed methane recovery. *International Journal of Coal Geology* 82(3-4), 252-261.

Pan, Z., Connell, L. D., Camilleri, M., Connelly, L., 2010. Effects of matrix moisture on gas diffusion and flow in coal. *Fuel* 89(11), 3207-3217.

Perera, M. S. A., Ranjith, P. G., Choi, S. K., Airey, D., 2011. The effects of sub-critical and super-critical carbon dioxide adsorption-induced coal matrix swelling on the permeability of naturally fractured black coal. *Energy* 36(11), 6442-6450.

Perkins, J. H., Cervik, J., 1969. Sorption investigation of methane on coal. United States Department of the Interior, Bureau of Mines Methane Control Program, Technical Progress Report - 14, 9p.

Pone, J. D. N., Halleck, P. M., Mathews, J. P., 2009. Sorption capacity and sorption kinetic measurements of co2 and ch4 in confined and unconfined bituminous coal. *Energy and Fuels* 23(9), 4688-4695.

Pone, J. D. N., Halleck, P. M., Mathews, J. P., 2010. 3D characterization of coal strains induced by compression, carbon dioxide sorption, and desorption at in-situ stress conditions. *International Journal of Coal Geology* 82(3-4), 262-268.

Prusty, B. K., 2008. Sorption of methane and CO_2 for enhanced coalbed methane recovery and carbon dioxide sequestration. *Journal of Natural Gas Chemistry* 17(1), 29-38.

Qian, M., Liu, T., 1984. Mine pressure and control. China University of Mining and Technology Press, Beijing, 110-134.

Reeves, S., Oudinot, A., 2004. The Tiffany unit N_2 – ECBM pilot: A reservoir modelling study. *Topical Report U.S. Department of Energy***:** DE-FC26-20NT40924.

Reeves, S., Oudinot, A., 2005. The Tiffany unit N_2-ECBM pilot – a reservoir and economic analysis. *2005 International Coalbed Methane Symposium*. Tuscaloosa, Alabama, USA**:** Paper 0523.

Reeves, S., Taillefert, A., Pekot, L., Clarkson, C., 2002. The Allison unit CO_2 - ECBM pilot: A reservoir modelling study. *Topical Report U.S. Department of Energy*: DE-FC26-20NT40924.

Reimer, L., 1998. *Scanning Electron Microscopy*: Physics of Image Formation and Microanalysis, Second edition, Springer-Verlag Berlin Heidelberg New York.

Ruppel, T. C., Grein, C. T., Bienstock, D., 1974. Adsorption of methane on dry coal at elevated pressure. *Fuel* 53(3), 152-162.

Saghafi, A., 2010. Potential for ECBM and CO_2 storage in mixed gas Australian coals. *International Journal of Coal Geology* 82(3-4), 240-251.

Saghafi, A., Faiz, M., Roberts, D., 2007. CO_2 storage and gas diffusivity properties of coals from Sydney Basin, Australia. *International Journal of Coal Geology* 70(1-3), 240-254.

Saghafi, A., Roberts, D., 2008. Measurement of CO_2 and CH_4 reservoir properties of coals from West Cliff mine, *CSIRO Investigation report* ET/IR 1033R.

Sakurovs, R., Day, S., Weir, S., 2009. Causes and consequences of errors in determining sorption capacity of coals for carbon dioxide at high pressure. *International Journal of Coal Geology* 77(1–2), 16-22.

Sakurovs, R., Day, S., Weir, S., Duffy, G., 2008. Temperature dependence of sorption of gases by coals and charcoals. *International Journal of Coal Geology* 73(3–4), 250-258.

Sang, S., Xu, H., Fang, L., Li, G., Huang, H., 2010. Stress relief coalbed methane drainage by surface vertical wells in China. *International Journal of Coal Geology* 82(3-4), 196-203.

Santillan, M., 2004. Underground desgasification and coal mine methane projects at Minerales Monclova, Minerales Monclova, Report, 2004.

Scott, A. R., 2002. Hydrogeologic factors affecting gas content distribution in coal beds. *International Journal of Coal Geology* 50(1-4), 363-387.

Seidle, J. P., O'Connor, L. S., 2007. The impact of undersaturation on coal gas economics. *SPE Rocky Mountain Oil and Gas Technology Symposium*, Society of Petroleum Engineers, Denver, Colorado 16-18 April, 12p. (SPE-107731).

Sereshki, F., 2005. Improving coal mine safety by identifying factors that influence the sudden release of gases in outburst prone zones. *PhD thesis* (University of Wollongong). http://www.uow.edu.au/eng/outburst/html/Completed%20Thesis/thesis%201.pdf

Seri-Levy, A., Avnir, D., 1993. Effects of heterogeneous surface geometry on adsorption. *Langmuir* 9(11), 3067-3076.

Setzmann, U., Wagner, W., 1991. A new equation of state and tables of thermodynamic properties for methane covering the range from the melting line to 625 K at pressures up to 1000 MPa. *Journal of Physical and Chemical Reference Data* 20, 1061–1155.

Shen, C., Lin, B., Wu, H., 2011. High-pressure water jet slotting and influence on permeability of coal seams. *Journal of China Coal Society* 36 (12), 2058-2063.

Shi, J. Q., Durucan, S., 2005. A model for changes in coalbed permeability during primary and enhanced methane recovery. SPEREE, 291-300.

Siemons, N., Busch, A., 2007. Measurement and interpretation of supercritical CO_2 sorption on various coals. *International Journal of Coal Geology* 69(4), 229-242.

Singh, A., Singh, B. D., 1999. Methane gas: An unconventional energy resource. Indian Academy of Science.

Singh, M. M., Kendorski, F. S., 1981. Strata disturbance prediction for mining beneath surface water and waste impoundments. *Proceedings of 1st Conference on Ground Control in Mining*, 76–89.

Smith, J. W., Pallasser, R. J., 1996. Microbial origin of Australian coalbed methane. *Am. Assoc. Petrol. Geologists Bull* 80, 807–891.

Solano-Acosta, W., Mastalerz, M., Schimmelmann, A., 2007. Cleats and their relation to geologic lineaments and coalbed methane potential in Pennsylvanian coals in Indiana. *International Journal of Coal Geology* 72(3–4), 187-208.

Somerton, W. H., Söylemezoğlu, I. M., Dudley, R. C., 1975. Effect of stress on permeability of coal. *International Journal of Rock Mechanics and Mining Sciences and amp; Geomechanics Abstracts* 12(5–6), 129-145.

Song, W., Wang, Z., Tang, J., 2011. Principle of gas extraction by increasing permeability of coal seam with hydraulic cutting and its application. *China Safety Science Journal* 21 (4), 78-82.

Spafford, S., 2007. Recent production from laterals in coal seams. *SPE ATW on Coalbed Methane*. Durango, Colorado. March 27–29.

State Administration of Work Safety (SAWS), 2006. The predicted method of mine gas emission rate (AQ1018-2006).

Statistical Review of World Energy (SRWE), 2012. Published by British Petroleum. http://en.wikipedia.org/wiki/List_of_countries_by_coal_production

Span, R., Wagner, W., 1996. A new equation of state for carbon dioxide covering the fluid region from the triple-point temperature to 1100 K at pressures up to 800 MPa. *Journal of Physical and Chemical Reference Data* 25 (6), 1509–1596.

Speight, J. G., 1983. The chemistry and technology of coal. Marcel Dekker, Inc., New York and Basel, 528p.

Stevenson, M., Pinczewski, W., Somers, M., 1991. Adsorption/desorption of multi-component gas mixtures at in seam conditions. *SPE Asia-Pacific Conference*, Perth, Australia.

Stewart, W. J., Barro, L., 1982. Coal seam degasification by use of hydraulic fracturing in vertical wells case histories. *Seam gas drainage with particular reference to the working seam*, (ed: Hargraves, A. J.), University of Wollongong, Wollongong, Australia, 89-98.

Su, X., Feng, Y., Chen, J., Pan, J., 2001. The characteristics and origins of cleat in coal from western north China. *International Journal of Coal Geology* 47(1), 51-62.

Sudibandriyo, M., Pan, Z., Fitzgerald, J. E., Robinson, R. L., Gasem, K. A. M., 2003. Adsorption of methane, nitrogen, carbon dioxide, and their binary mixtures on dry activated carbon at 318.2 K and pressures up to 13.6 MPa. *Langmuir* 19(13), 5323-533.

Sun, B., Wang, Z., Wu, H., 2010. Hydraulic pressurized cracking and permeability improvement technology applied to gas drainage. *Coal Science and Technology* 38 (11), 78-81.

Sun, X., Lin, B., Dong, T., Hui, G., Zhang, Z., Zhu, C., Wang, H., 2010. Deep crossing-hole controlled hydraulic blasting and its application in outburst prevention. *Journal of Mining and Safety Engineering* 27 (1), 82-86.

Tang, G. Q., Jessen, K., Kovscek, A. R., 2005. Laboratory and simulation investigation of enhanced coalbed methane recovery by gas injection. *Annual Technical Conference and Exhibition*, Dallas 8–12, 14p (SPE 9594).

Thakur, P. C., 1981. Methane control for longwall gobs. *Proceedings of longwall– shortwall mining, state of the art*. Society of Mining Engineers of American Institute of Mining, Metallurgical, and Petroleum Engineers, New York, 81-86.

Thimons, E. D., Kissell, F. N., 1973. Diffusion of methane through coal. *Fuel* 52(4), 274-280.

Thomson, S., 1998. The role of directional drilling for safety in coal mining. in *Proceedings of the 11th Turkish Coal Congress*, Bartin-Amasra, Turkey, 10-12 June, 10p.

Thomson, S., Adam, S., 2007. Intelligent drilling systems. *Australian Coal Association Research Program*, Project Report C14034.

Thomson, S and MacDonald, D, 2003. The application of medium radius directional drilling for coal bed methane extraction, 11p. http://www.lucas.com.au/eWebUploadedFiles/MRD%20for%20coal%20seam%20gas.pdf

United States Environmental Protection Agency (USEPA), 2009. Coal mine methane recovery: a primer, *Coalbed Methane Outreach Program*, Report No. EPA-430-R-09-013. http://www.epa.gov/cmop/docs/cmm_primer.pdf

University of Wyoming (UWYO), 2002. The anatomy of a coal forming swamp, *The Science and Mathematics Teaching Centre*, University of Wyoming. http://www.wsgs.uwyo.edu/coalweb/swamp/anatomy.aspx

Van der Meer, L. G. H., 2004. An excellent simulation tool SIMED II, TNO-NITG, Information.

Van Hemert, P., Wolf, K.-H. A. A., Bruining, J., 2007. The intrinsic reliability of manometric sorption apparatus using supercritical carbon dioxide. *SPE Annual Technical Conference and Exhibition*, Anaheim, CA, p. 11.

Van Krevelen, D. W., 1993. Coal: Typology-physics-chemistry-constitution. *Elsevier*, 1002p.

Viete, D. R., Ranjith, P. G., 2006. The effect of CO_2 on the geomechanical and permeability behaviour of brown coal: Implications for coal seam CO_2 sequestration. *International Journal of Coal Geology* 66(3), 204-216.

Wallace, J. A., 1990. Coalbed methane production- an operator's perspective. *Coalbed methane in Alberta what's it all about?* (eds: Nikols, D., Treasure, S., Stuhec, S., Goulet, D.), Edmonton, Alberta Canada, 17p.

Wang, F. Y., Zhu, Z. H., Massarotto, P., Rudolph, V., 2007. Mass transfer in coal seams for CO_2 sequestration. *AIChE Journal* 53(4), 1028-1049.

Wang, K., Xue, S., 2008. Gas drainage practices and challenges in coal mines of China. in *Proceeding of 8th Underground Coal Operators' Conference COAL 2008*, University of Wollongong and Australasian Institute of Mining and Metallurgy, (eds: Aziz, N. and Nemcik, J.), Wollongong, 14-15 February, 178-185. http://ro.uow.edu.au/cgi/viewcontent.cgi?article=1018&context=coal

Wang, X., Shi, B., Mu, C., 2012. Study on formation mechanism of gas emission partition in hydraulic flushing coal seam. *Journal of China Coal Society* 37 (3), 467-471.

Wang, Z., Ting, R., Zhang, L., 2011. Review of gas emission prediction and control methods for multi-seam mining in Chinese coal mines. in *Proceeding of 11th Underground Coal Operators' Conference COAL 2011*, University of Wollongong and Australasian Institute of Mining and Metallurgy, (eds: Aziz, N., Kininmonth, B., Nemcik, J. and Ren, T.), Wollongong, 10-11 February, 315-325. http://ro.uow.edu.au/cgi/viewcontent.cgi?article=2034&context=coal

Weireld, D., Frere, M., Jadot, R., 1999. Automated determination of high-temperature and high-pressure gas adsorption isotherms using a magnetic suspension balance. *Measurement Science and Technology* 10, 117-126.

Weniger, P., Kalkreuth, W., Busch, A., Krooss, B. M., 2010. High-pressure methane and carbon dioxide sorption on coal and shale samples from the Paraná Basin, Brazil. *International Journal of Coal Geology* 84(3–4), 190-205.

White, C. M., Smith, D. H., Jones, K. L., Goodman, A. L., Jikich, S. A., LaCount, R. B., DuBose, S. B., Ozdemir, E., Morsi, B. I., Schroeder, K. T., 2005. Sequestration of carbon dioxide in coal with enhanced coalbed methane recovery - A review. *Energy and Fuels* 19(3), 659-724.

Whittaker, B. N., Singh, R. N., Neate, C. J., 1979. Effect of longwall mining on ground permeability and subsurface drainage. *Proceedings of the First International Mine Drainage Symposium*, 161–183.

Whittles, D. N., Lowndes, I. S., Kingman, S. W., Yates, C., Jobling, S., 2006. Influence of geotechnical factors on gas flow experienced in a UK longwall coal mine panel. *International Journal of Rock Mechanics and Mining Sciences* 43(3), 369-387.

Williams, R. J., 1999. Assessment and control of gas hazards in Queensland collieries. Longwall Mining Summit, Capricorn Resort, Yeppoon.

Wolf, K. H. A. A., Bertheux, W., Bruining, J., Ephraim, R., 2001. CO_2 injection in and CH_4 production from coal seams: Laboratory experiments and image analysis for simulations. *First National Conference on Carbon Sequestration*, Washington, DC, USA.

Wollenweber, J., Alles, S., Busch, A., Krooss, B. M., Stanjek, H., Littke, R., 2010. Experimental investigation of the CO_2 sealing efficiency of caprocks. *International Journal of Greenhouse Gas Control* 4(2), 231-241.

Wong, S., Macdonald, D., Andrei, S., Gunter, W. D., Deng, X., Law, D., Ye, J., Feng, S., Fan, Z., Ho, P., 2010. Conceptual economics of full scale enhanced coalbed methane production and CO_2 storage in anthracitic coals at south Qinshui Basin, Shanxi, China. *International Journal of Coal Geology* 82(3-4), 280-286.

Wu, J., 1994. Coal absorption method of calculation-coal surface energy and its significance. *Coal Geology and Exploration* 22(2), 18-23.

Xie, J., Guo, Y., Wu, S., 2004. Study on adsorption of methane on coal at normal temperature. *Journal of Taiyuan University of Technology* 35(5), 562-564.

Xu, J., Zhang, D., Peng, S., Nie, W., Wang, L., Chen, Y., 2011. Experimental research on impact of temperature on seepage characteristics of coal containing methane under triaxial stress. *Chinese Journal of Rock Mechanics and Engineering* 30 (9), 1848-1854.

Xue, S., Thomas, J. L., 1995. Laboratory investigation on the permeability of coal to mixture of methane and carbon dioxide. *International Symposium-CUM-Workshop on Management and Control of High Gas Emissions and Outbursts in Underground Coal Mines*, Wollongong, NSW, Australia, 311-315. http://www.uow.edu.au/eng/outburst/pdfs/C3079%20Final%20Report.pdf

Yang, H., Zhang, T., Wang, Z., Zhao, C., 2010. Experimental study on technology of accelerating methane release by nitrogen injection in coalbed. *Journal of China Coal Society* 35 (5), 792-796.

Yang, R. T., Saunders, J. T., 1985. Adsorption of gases on coals and heattreated coals at elevated temperature and pressure: 1. Adsorption from hydrogen and methane as single gases. *Fuel* 64(5), 616-620.

Yang, X., Zhang, Y., 2008. Experimental study of the temperature influence on the gas-solid coupling coal gas permeability law. *Journal of Geomechanics* 14 (4), 374-379.

Yi, J., Akkutlu, I. Y., Karacan, C. Ö., Clarkson, C. R., 2009. Gas sorption and transport in coals: A poroelastic medium approach. *International Journal of Coal Geology* 77(1–2), 137-144.

Yin, G., Jiang, C., Xu, J., Peng, S., Li, W., 2011. Experimental study of thermo-fluid-solid coupling seepage of coal containing gas. *Journal of China Coal Society* 36 (9), 1495-1500.

You, H., Li, B., Zhang, F., 2008. Comprehensive gas control technique for fully mechanised top coal caving face in Yangquan mining area. China Coal Industry Publishing House. Beijing.

You, H., 2008. The safe and efficient exploitation of high gassy and spontaneous prone seam by enhancing both ventilation and gas drainage simultaneously. *International symposium on theory and practice of safe, efficient, and green mining*. Xuzhou, China

Yu, B., 2005. Preventing gas disaster in coal mines and utilization technology handbook. China University of Mining and Technology Press, Beijing, 275–784

Yu, Q., 1992. Mine gas control. China University of Mining and Technology Press. Xuzhou.

Yu, Q., Cheng, Y., Jiang, C., 2004. Principles and applications of exploitation of coal and pressure relief gas in thick and high gas seams. *Journal of China University of Mining and Technology* 2, 127–131.

Yu, Y., Yang, X., Liang, W., Wang, J., 2007. Testing research of improving mine gas drainage under suction by controlling blasting to cause crack. *Journal of China Coal Society* 32 (4), 377-381.

Yuan, L., 2008. The technique of coal mining and gas extraction by roadway retaining and borehole drilling. *Journal of China Coal Society* 33(8), 898-902.

Zahid, S., Bhatti, A. A., Khan, H. A., Ahmad, T., 2007. Development of unconventional gas resources: Stimulation perspective. *SPE Production and Operations Symposium*, Society of Petroleum Engineers, Oklahoma City, Oklahoma, 31 March – 3 April, 11p. (SPE-107053).

Zhai, C., Li, X., Li, Q., 2011. Research and application of coal seam pulse hydraulic fracturing technology. *Journal of China Coal Society* 36 (12), 1996-2001.

Zhang, J., Lin, B., Zhai, C., 2012. Research on outburst prevention technology of high pressure hydraulic-cutting seam through layer and its application. *Journal of Mining and Safety Engineering* 29 (3), 411-415.

Zhang, L., Aziz, N., Ren, T., Nemcik, J., Wang, Z., 2012. Permeability testing of Bulli seam coal under triaxial condition. *18th Coal Congress of Turkey*, Zonguldak, Turkey, 71-83.

Zhang, L., Aziz, N., Ren, T., Wang, Z., 2011. Influence of temperature on the gas content of coal and sorption modelling. in *Proceeding of 11th Underground Coal Operators' Conference COAL 2011*, University of Wollongong and Australasian Institute of Mining and Metallurgy, (eds: Aziz, N., Kininmonth, B., Nemcik, J. and Ren, T.), Wollongong, 10-11 February, 269-276.
http://ro.uow.edu.au/cgi/viewcontent.cgi?article=2028&context=coal

Zhang, L., Aziz, N., Ren, T. X., Wang, Z., 2011. Influence of temperature on coal sorption characteristics and the theory of coal surface free energy. *Procedia Engineering* 26, 1430-1439.

Zhang, L., Ren, T., Aziz, N., Nemcik, J., Wang, Z., 2012. Investigation into variations in the drainability of coal in different sections of the Bulli seam, NSW, Australia. *18th Coal Congress of Turkey*, Zonguldak, Turkey, 173-184.

Zhang, L., Ren, T., Aziz, N., Wang, Z., 2011. Influence of temperature and moisture on the gas content of coal. *The 3rd Asia Pacific Coalbed Methane Symposium*, Brisbane, Queensland, Australia, Paper 11.

Zhao, C., 1996. Gas drainage technique and utilization in Yangquan mining area. Technology of Yangquan Mining Area 4, Shanxi, China.

Zhu, J., Zhao, C., Qi, J., 1997. A study on gas governing by high gas drainage gate on strike at up-near seam of the full-mechanised mining caving face. *Shanxi Coal* 17(4), 26-30.

Zutshi, Z., Harpalani, S., 2005. Gas flow characterization of Illinois coal: Assessment for recovery of coalbed methane and carbon sequestration potential. in *Proceedings of the*

2005 International Coalbed Methane Symposium, University of Alabama, Tuscaloosa, 18-19 May, Paper no.0514, 10p.

APPENDICES

APPENDIX A: LANGMUIR EQUATION

The Langmuir equation is used to model gas sorption and calculate the coal sorption capacity. The equation of adsorption of gases on plane surfaces is based on three main assumptions: (a) the surface of the adsorbent is uniform, all the adsorption sites are equal; (b) adsorbed molecules do not interact with each other; (c) when the maximum adsorption state is achieved, only a monolayer is formed. The Langmuir equation is expressed as:

$$\frac{V}{V_L} = \frac{P}{P + P_L}$$

Where V_L is Langmuir volume (maximum sorption amount) and P_L is the Langmuir pressure (pressure at half of the Langmuir volume is achieved).

The formulas involved in the Langmuir equation are followed, adsorption rate:

$$\frac{d\Theta}{dt} = k_a P(1 - \Theta)$$

Where, $d\Theta$ is the differential coverage of the surface; dt is the differential time; k_a is the adsorption constant; P is gas pressure; Θ is the surface coverage, desorption rate:

$$\frac{d\Theta}{dt} = k_d \Theta$$

When the equilibrium of adsorption and desorption is achieved, adsorption rate is equal to desorption rate:

$$k_a P(1 - \Theta) = k_d \Theta$$

When $k = k_a/k_d$, surface coverage at pressure P will be:

$$\Theta = \frac{kP}{1 + kP}$$

APPENDIX B: SOAVE-REDLICH-KWONG EQUATION OF STATE

Soave-Redlich-Kwong (SRK) equation is a real gas law and widely used to accurately express the relationship of gas pressure, temperature and gas volume.

The difference between SRK equation and ideal gas law is that, SRK equation takes the different gas molecular geometry and polarity into consideration. Soave-Redlich-Kwong EOS is expressed as:

$$P = \frac{RT}{V_m - b} - \frac{a\alpha}{V_m(V_m + b)}$$

Where P is gas pressure; R is universal gas content per mole; T is the absolute temperature; V_m is the specific molar volume; b is volume correction; a is molecular interaction parameter and α is a parameter calculated by ω and T.

The formulas involved in the Langmuir equation are followed:

$$a = 0.42748 \frac{R^2 {T_c}^2}{P_c}$$

Where T_c is the critical temperature and P_c is the critical pressure.

$$b = 0.08664 \frac{RT_c}{P_c}$$

The parameter α can be calculated by the following equation:

$$\alpha = (1 + m(1 - {T_r}^{0.5}))^2$$

$$T_r = \frac{T}{T_c}$$

The parameter m can be calculated by the following equation:

$$m = 0.48508 + 1.55171\omega - 0.15613\omega^2$$

Where ω is the acentric factor for the species.

APPENDIX C: COAL SOPRTION ISOTHERM CALCULATION WITH SRK EQUATION METHOD

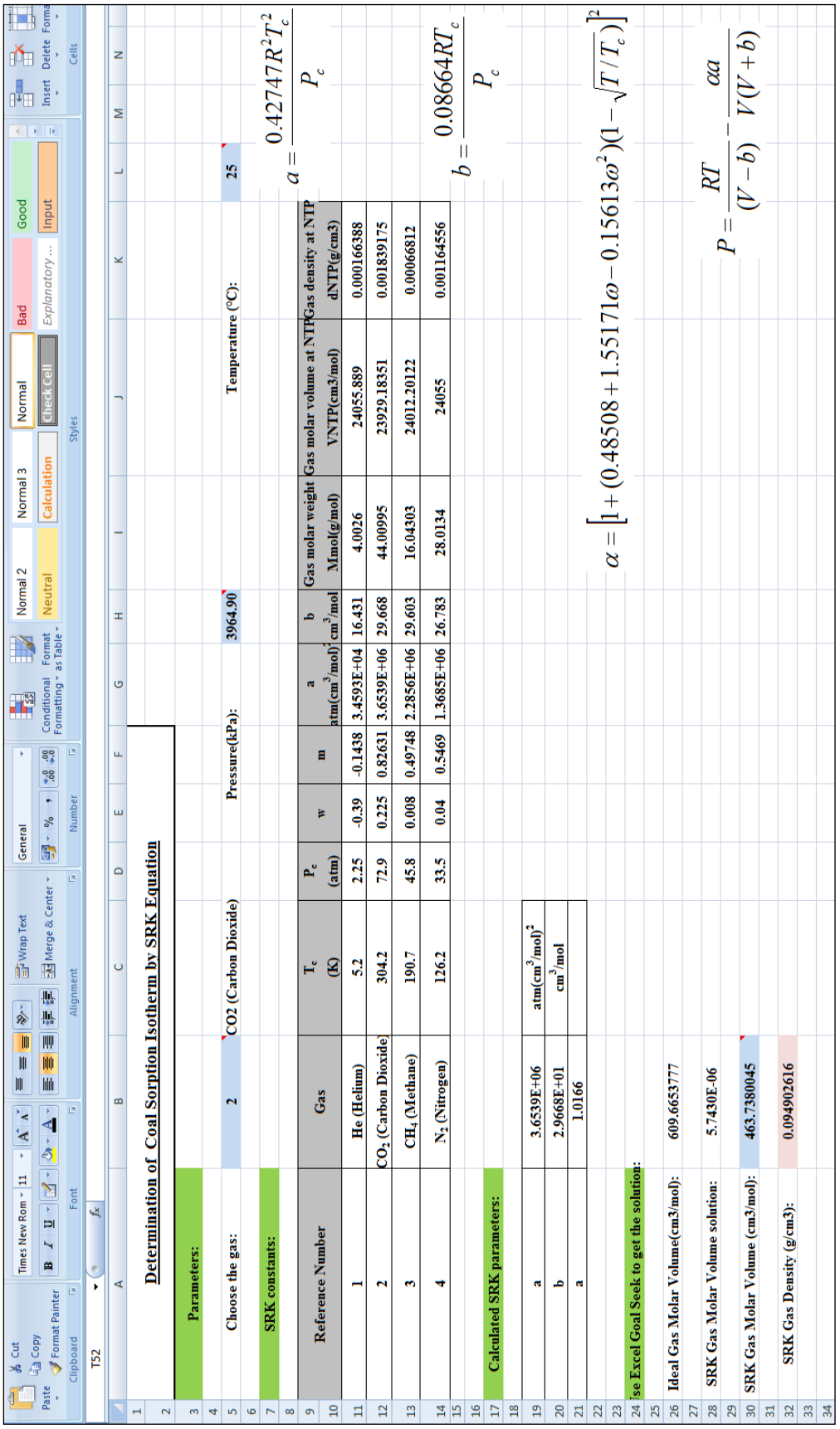

Determination of Coal Sorption Isotherm by SRK Equation

Parameters:

Choose the gas:	2	CO2 (Carbon Dioxide)	Pressure(kPa):		3964.90			Temperature (°C):	25	
SRK constants:										
Reference Number	Gas	T_c (K)	P_c (atm)	w	m	a atm(cm³/mol)²	b cm³/mol	Gas molar weight Mmol(g/mol)	Gas molar volume at NTP VNTP(cm3/mol)	Gas density at NTP dNTP(g/cm3)
1	He (Helium)	5.2	2.25	-0.39	-0.1438	3.4593E+04	16.431	4.0026	24055.889	0.000166388
2	CO_2 (Carbon Dioxide)	304.2	72.9	0.225	0.82631	3.6539E+06	29.668	44.00995	23929.18351	0.001839175
3	CH_4 (Methane)	190.7	45.8	0.008	0.49748	2.2856E+06	29.603	16.04303	24012.20122	0.00066812
4	N_2 (Nitrogen)	126.2	33.5	0.04	0.5469	1.3685E+06	26.783	28.0134	24055	0.001164556

$$a = \frac{0.42747 R^2 T_c^2}{P_c}$$

$$b = \frac{0.08664 R T_c}{P_c}$$

Calculated SRK parameters:

a	3.6539E+06	atm(cm³/mol)²
b	2.9668E+01	cm³/mol
a	1.0166	

$$\alpha = \left[1 + (0.48508 + 1.55171\omega - 0.15613\omega^2)(1 - \sqrt{T/T_c})\right]^2$$

Use Excel Goal Seek to get the solution:

Ideal Gas Molar Volume(cm3/mol):	609.6653777
SRK Gas Molar Volume solution:	5.7430E-06
SRK Gas Molar Volume (cm3/mol):	463.7380045
SRK Gas Density (g/cm3):	0.094902616

$$P = \frac{RT}{(V-b)} - \frac{\alpha a}{V(V+b)}$$

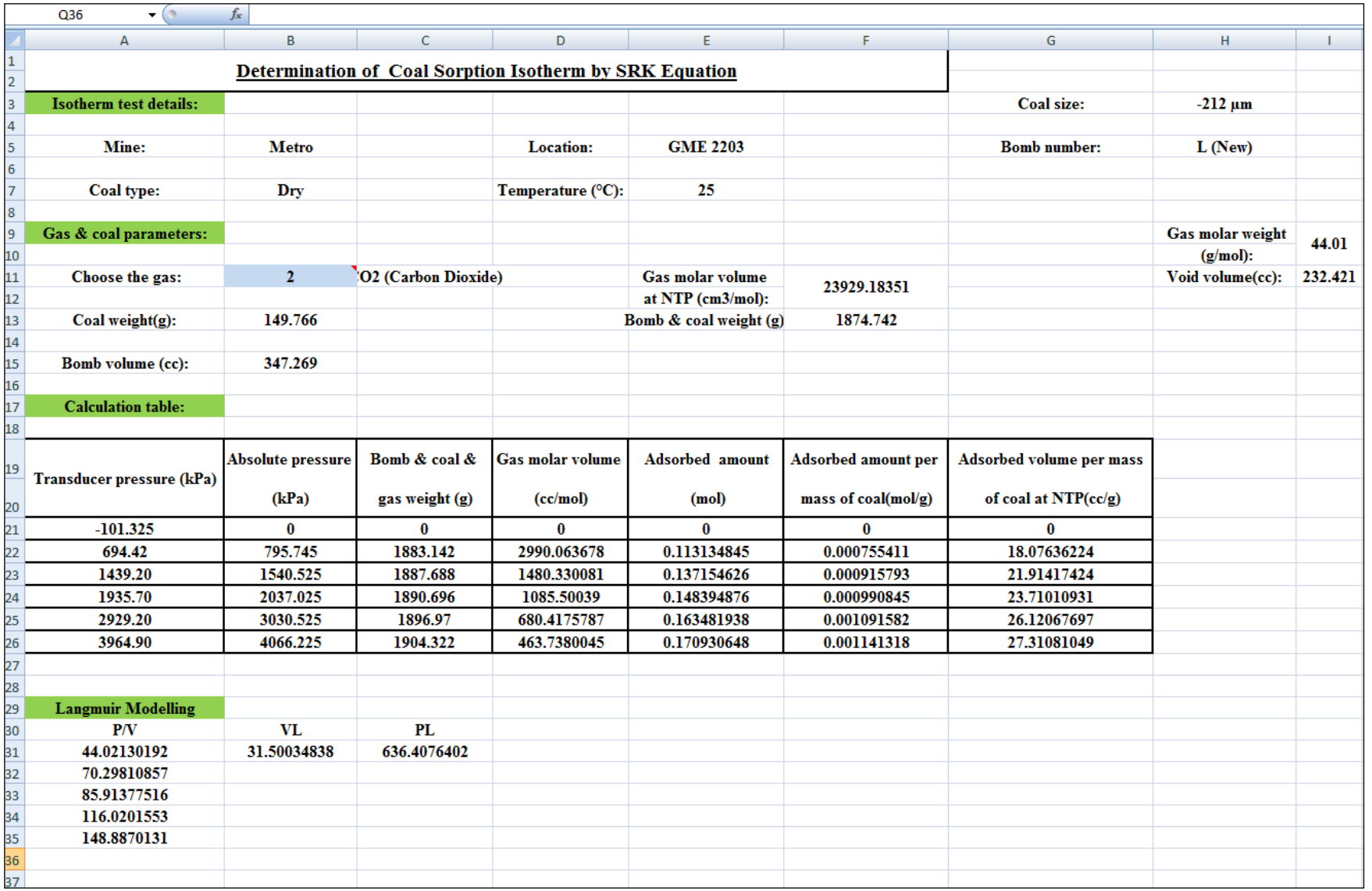

Q36

	A	B	C	D	E	F	G	H	I
1									
2			**Determination of Coal Sorption Isotherm by SRK Equation**						
3	**Isotherm test details:**						**Coal size:**	**-212 µm**	
4									
5	**Mine:**	**Metro**		**Location:**	**GME 2203**		**Bomb number:**	**L (New)**	
6									
7	**Coal type:**	**Dry**		**Temperature (°C):**	**25**				
8									
9	**Gas & coal parameters:**							**Gas molar weight (g/mol):**	**44.01**
10									
11	**Choose the gas:**	**2**	**CO2 (Carbon Dioxide)**		**Gas molar volume at NTP (cm3/mol):**	**23929.18351**		**Void volume(cc):**	**232.421**
12									
13	**Coal weight(g):**	**149.766**			**Bomb & coal weight (g)**	**1874.742**			
14									
15	**Bomb volume (cc):**	**347.269**							
16									
17	**Calculation table:**								
18									
19	**Transducer pressure (kPa)**	**Absolute pressure (kPa)**	**Bomb & coal & gas weight (g)**	**Gas molar volume (cc/mol)**	**Adsorbed amount (mol)**	**Adsorbed amount per mass of coal(mol/g)**	**Adsorbed volume per mass of coal at NTP(cc/g)**		
20									
21	-101.325	0	0	0	0	0	0		
22	694.42	795.745	1883.142	2990.063678	0.113134845	0.000755411	18.07636224		
23	1439.20	1540.525	1887.688	1480.330081	0.137154626	0.000915793	21.91417424		
24	1935.70	2037.025	1890.696	1085.50039	0.148394876	0.000990845	23.71010931		
25	2929.20	3030.525	1896.97	680.4175787	0.163481938	0.001091582	26.12067697		
26	3964.90	4066.225	1904.322	463.7380045	0.170930648	0.001141318	27.31081049		
27									
28									
29	**Langmuir Modelling**								
30	**P/V**	**VL**	**PL**						
31	44.02130192	31.50034838	636.4076402						
32	70.29810857								
33	85.91377516								
34	116.0201553								
35	148.8870131								
36									
37									

APPENDIX D: COAL SOPRTION ISOTHERM CALCULATION WITH CALIBRATION CUREVE METHOD

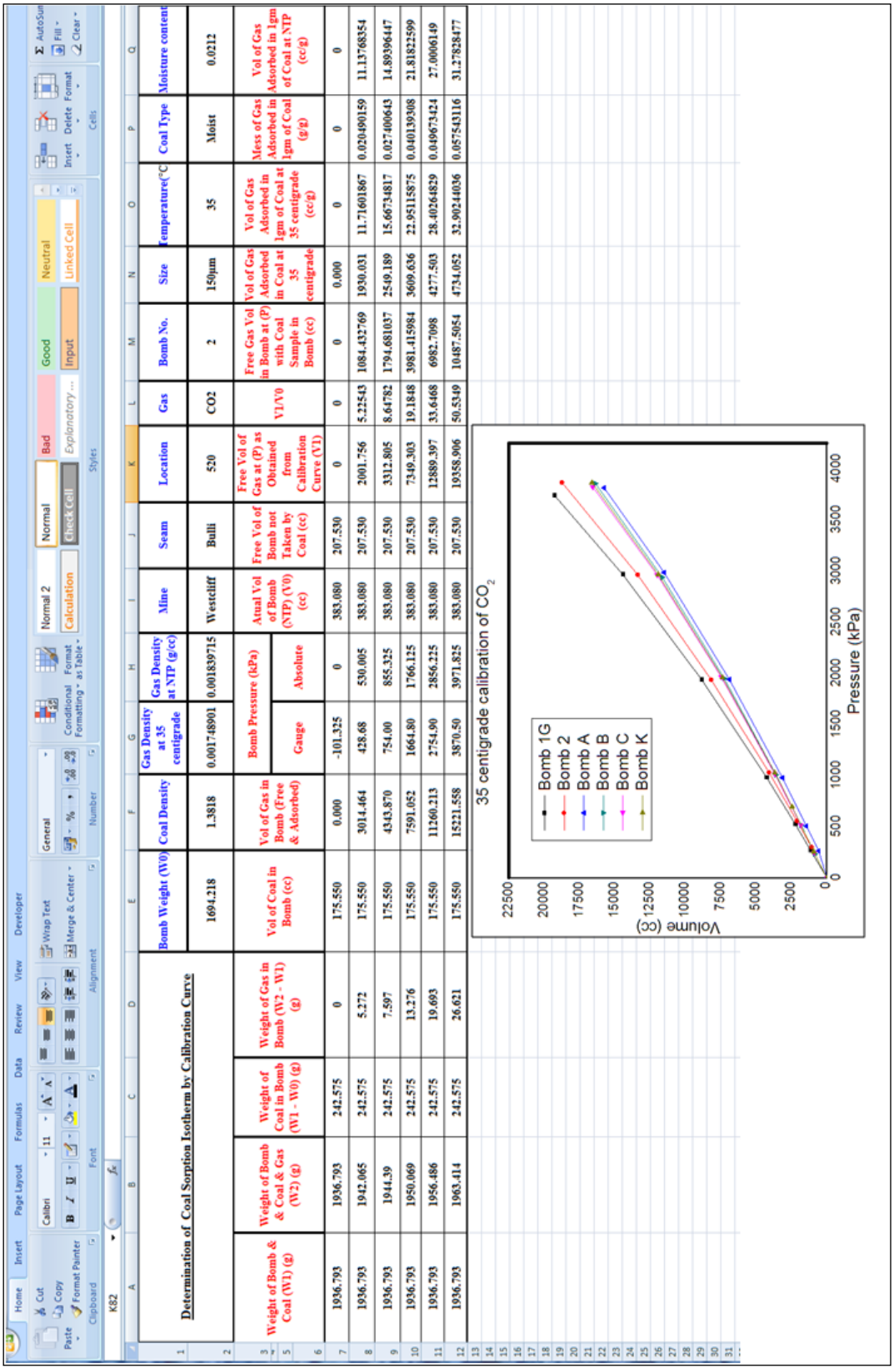

Determination of Coal Sorption Isotherm by Calibration Curve																		
Weight of Bomb & Coal (W1) (g)	Weight of Bomb & Coal & Gas (W2) (g)	Weight of Coal in Bomb (W1 - W0) (g)	Weight of Gas in Bomb (W2 - W1) (g)	Bomb Weight (W0)	Vol of Coal in Bomb (cc)	Coal Density	Vol of Gas in Bomb (Free & Adsorbed)	Gas Density at 35 centigrade	Bomb Pressure (kPa)		Gas Density at NTP (g/cc)	Mine	Seam	Location	Gas	Bomb No.	Size	Temperature(°C	Coal Type	Moisture content
									Gauge	Absolute										
				1694.218		1.3818	0.000	0.001748901	-101.325	0	0.001839715	Westcliff	Bulli	520	CO2	2	150µm	35	Moist	0.0212
1936.793	1936.793	242.575	0	175.550	0.000	-101.325	0	383.080	207.530	0	2001.756	5.22543	1084.432769	1930.031	11.71601867	0.020490159	11.13768354			
1936.793	1942.065	242.575	5.272	175.550	3014.464	428.68	530.005	383.080	207.530	2001.756	5.22543	1084.432769	1930.031	11.71601867	0.020490159	11.13768354				
1936.793	1944.39	242.575	7.597	175.550	4343.870	754.00	855.325	383.080	207.530	3312.805	8.64782	1794.681037	2549.189	15.66734817	0.027400643	14.89396447				
1936.793	1950.069	242.575	13.276	175.550	7591.052	1664.80	1766.125	383.080	207.530	7349.303	19.1848	3981.415984	3609.636	22.95115875	0.040139308	21.81822599				
1936.793	1956.486	242.575	19.693	175.550	11260.213	2754.90	2856.225	383.080	207.530	12889.397	33.6468	6982.7098	4277.503	28.40264829	0.049673424	27.0006149				
1936.793	1963.414	242.575	26.621	175.550	15221.558	3870.50	3971.825	383.080	207.530	19358.906	50.5349	10487.5054	4734.052	32.90244036	0.057543116	31.27828477				

APPENDIX E: COAL PERMEABILITY TEST RESULT WITH MFORR

MFORR TEST RESULT			
Vertical stress 1 MPa		**Vertical stress 2 MPa**	
Gas Pressure MPa	**Permeability mD**	**Gas Pressure MPa**	**Permeability mD**
0.19622	13.34799	0.16861	9.12493
0.46537	3.54365	0.46346	2.3169
0.59801	2.4917	0.5823	1.73614
0.77507	1.81091	0.76693	1.21933
0.95369	1.38156	0.94554	0.98834
1.1536	1.07841	1.169	0.78929
1.3806	0.90918	1.356	0.69054
1.59	0.75258	1.567	0.59845
1.7864	0.65474	1.7971	0.55332
2.0044	0.56414	1.9861	0.50019
2.509	0.42632	2.49	0.3926
2.9915	0.34541	2.98	0.32165
Vertical stress 3 MPa		**Vertical stress 4 MPa**	
Gas Pressure MPa	**Permeability mD**	**Gas Pressure MPa**	**Permeability mD**
0.24343	5.76343	0.22005	4.37581
0.34231	2.77316	0.38988	2.0354
0.57501	1.44274	0.62794	1.20354
0.74385	1.09981	0.79104	0.97737
1.0118	0.81583	0.9882	0.79216
1.1744	0.71832	1.1932	0.67442
1.3623	0.62992	1.3828	0.59934
1.5897	0.54922	1.6161	0.53301
1.8308	0.50846	1.8167	0.4582
1.9791	0.47405	2.0482	0.42918
2.499	0.38357	2.4561	0.37418
2.9937	0.31555	2.9208	0.31452

APPENDIX F: COAL PERMEABILITY TEST RESULT WITH TRIAXIAL COMPRESSION APPARATUS

TRIAXIAL COMPRESSION APPARATUS TEST RESULT			
Vertical Stress 3 MPa			
Horizontal Stress 2 MPa		**Horizontal Stress 2.5 MPa**	
Gas Pressure MPa	**Permeability mD**	**Gas Pressure MPa**	**Permeability mD**
0.20425	1.75053	0.20041	1.44892
0.41085	1.47934	0.39227	1.23248
0.59558	1.377	0.60213	1.10272
0.80222	1.21664	0.81725	0.98511
1.0049	1.19493	1.0235	0.92375
1.1982	1.12416	1.1958	0.89843
1.4023	1.12184	1.3999	0.88002
1.6035	1.11378	1.6038	0.8405
		1.819	0.83379
		2.0092	0.8407
		2.1909	0.8668
Vertical Stress 4 MPa			
Horizontal Stress 3 MPa		**Horizontal Stress 3.5 MPa**	
Gas Pressure MPa	**Permeability mD**	**Gas Pressure MPa**	**Permeability mD**
0.1983	1.33991	0.21037	1.03707
0.41167	0.95459	0.41895	0.81027
0.61992	0.83793	0.61575	0.73732
0.82206	0.78811	0.79958	0.69306
0.98652	0.75969	0.99939	0.63675
1.2039	0.73324	1.2114	0.61265
1.3966	0.70959	1.4187	0.58194
1.5847	0.69058	1.6188	0.56605
1.8028	0.67058	1.8052	0.5546
2.0401	0.64672	2.0248	0.55371
2.5053	0.64239	2.4913	0.53195
		3.0096	0.52613

TRIAXIAL COMPRESSION APPARATUS TEST RESULT			
Vertical Stress 6 MPa			
Horizontal Stress 4 MPa		**Horizontal Stress 5 MPa**	
Gas Pressure MPa	**Permeability mD**	**Gas Pressure MPa**	**Permeability mD**
0.2366	0.84501	0.23393	0.66028
0.41088	0.66973	0.39544	0.51702
0.61036	0.57006	0.60961	0.42277
0.81994	0.54514	0.79608	0.39846
1.0253	0.52065	1.0108	0.38395
1.2192	0.50127	1.2147	0.36685
1.4156	0.48153	1.4008	0.3612
1.6044	0.47081	1.6408	0.34771
1.8309	0.45544	1.827	0.34449
2.023	0.4424	2.0166	0.33647
2.5249	0.42957	2.5277	0.31686
3.0301	0.41472	3.0459	0.30658
3.3373	0.41362	3.3338	0.3012
Vertical Stress 8 MPa			
Horizontal Stress 4 MPa		**Horizontal Stress 5 MPa**	
Gas Pressure MPa	**Permeability mD**	**Gas Pressure MPa**	**Permeability mD**
0.22014	0.62057	0.23766	0.56791
0.39332	0.39198	0.41605	0.3567
0.62298	0.30045	0.6008	0.28942
0.82333	0.27939	0.80055	0.2688
1.0463	0.26681	1.0003	0.25368
1.196	0.26043	1.2082	0.23995
1.4111	0.24968	1.4067	0.22923
1.6233	0.24397	1.6192	0.22049
1.8273	0.24097	1.7691	0.22185
2.0341	0.24123	2.0138	0.21527
2.5199	0.23824	2.5243	0.20758
3.0193	0.24142	2.9935	0.20163
3.3072	0.24778	3.2933	0.20157

APPENDIX G: COMPARISON OF ADSORPTION ISOTHERMS (HARD-TO-DRAIN AND EASY-TO-DRAIN AREAS)

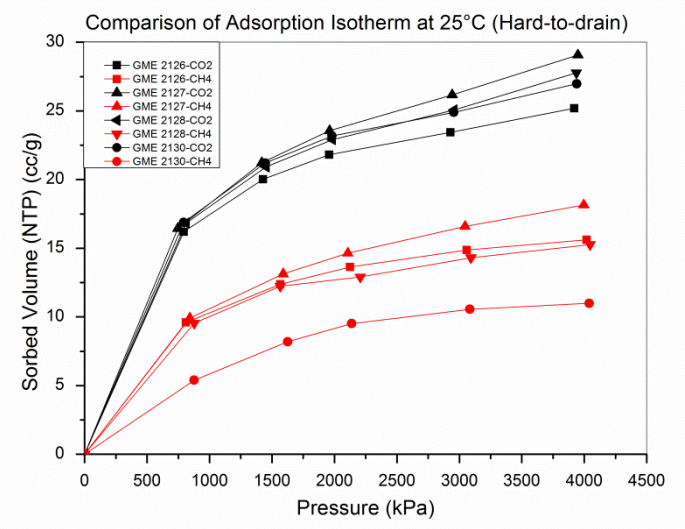

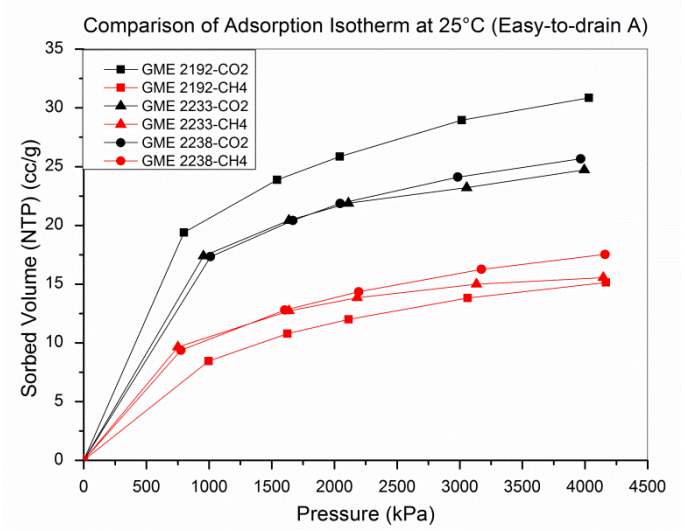

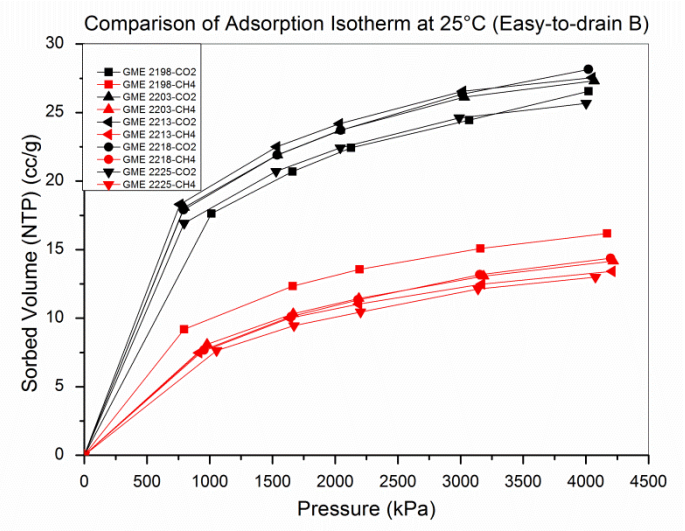

APPENDIX H: SUMMARY OF GAS CONTENT AND GAS COMPOSITION DATA (WHOLE DATABASE-PASS SAMPLES)

Core Sample	CO2 Composition (%)	CH4 Composition (%)	Gas Composition CH4/(CO2+CH4) (%)	Measured Gas Content QM (m3/t)	Mining Limit Level (m3/t)	Q1 (m3/t)	Q2 (m3/t)	Q3 (m3/t)	Q1/QM (%)	Q2/QM (%)	Q3/QM (%)	Pass/Fail
GME1719	61.94	31.68	33.8%	6.58	7.18	0.20	1.33	5.05	3.0%	20.2%	76.7%	Pass
GME1721	4.84	89.80	94.9%	2.47	9.32	0.41	0.15	1.91	16.6%	6.1%	77.3%	Pass
GME1722	24.35	73.19	75.0%	7.30	8.62	0.11	0.58	6.61	1.5%	7.9%	90.5%	Pass
GME1723	43.31	53.70	55.4%	6.79	7.94	0.08	0.36	6.35	1.2%	5.3%	93.5%	Pass
GME1724	1.84	92.64	98.1%	5.86	9.43	0.12	0.45	5.29	2.0%	7.7%	90.3%	Pass
GME1725	88.32	7.98	8.3%	5.52	6.29	0.11	1.11	4.30	2.0%	20.1%	77.9%	Pass
GME1726	44.49	55.05	55.3%	7.51	7.93	0.20	0.65	6.66	2.7%	8.7%	88.7%	Pass
GME1727	75.88	17.44	18.7%	6.05	6.65	0.17	1.18	4.70	2.8%	19.5%	77.7%	Pass
GME1728	7.35	91.24	92.5%	7.36	9.24	0.54	2.51	4.31	7.3%	34.1%	58.6%	Pass
GME1734	92.10	7.33	7.4%	4.48	6.26	0.04	0.50	3.94	0.9%	11.2%	87.9%	Pass
GME1735	11.86	86.11	87.9%	8.65	9.06	0.44	1.66	6.55	5.1%	19.2%	75.7%	Pass
GME1736	49.65	49.53	49.9%	7.59	7.75	0.49	1.89	5.21	6.5%	24.9%	68.6%	Pass
GME1739	86.99	8.72	9.1%	6.08	6.32	0.42	1.39	4.27	6.9%	22.9%	70.2%	Pass
GME1740	77.54	15.31	16.5%	6.23	6.58	0.44	1.32	4.47	7.1%	21.2%	71.7%	Pass
GME1741	72.29	17.63	19.6%	6.39	6.69	0.06	0.84	5.49	0.9%	13.1%	85.9%	Pass
GME1742	76.74	2.44	3.1%	3.48	6.11	0.01	0.59	2.88	0.3%	17.0%	82.8%	Pass
GME1743	57.89	23.44	28.8%	5.80	7.01	0.27	0.78	4.75	4.7%	13.4%	81.9%	Pass
GME1745	52.56	40.40	43.5%	2.95	7.52	0.02	0.51	2.42	0.7%	17.3%	82.0%	Pass
GME1746	91.16	2.06	2.2%	4.04	6.08	0.09	0.50	3.45	2.2%	12.4%	85.4%	Pass
GME1747	86.48	6.52	7.0%	5.48	6.25	0.03	0.70	4.75	0.5%	12.8%	86.7%	Pass
GME1749	75.69	12.60	14.3%	4.27	6.50	0.23	0.56	3.48	5.4%	13.1%	81.5%	Pass
GME1750	50.39	0.46	0.9%	2.71	6.03	0.02	0.46	2.23	0.7%	17.0%	82.3%	Pass
GME1751	62.42	31.10	33.3%	6.16	7.16	0.30	0.68	5.18	4.9%	11.0%	84.1%	Pass
GME1752	70.34	24.84	26.1%	6.81	6.91	0.49	0.91	5.41	7.2%	13.4%	79.4%	Pass
GME1753	84.82	15.13	15.1%	5.93	6.53	0.24	0.62	5.07	4.0%	10.5%	85.5%	Pass
GME1755	72.63	21.92	23.2%	6.79	6.81	0.31	1.12	5.36	4.6%	16.5%	78.9%	Pass
GME1756	72.84	17.82	19.7%	6.11	6.69	0.07	0.84	5.20	1.1%	13.7%	85.1%	Pass
GME1758	68.04	1.16	1.7%	2.79	6.06	0.01	0.44	2.34	0.4%	15.8%	83.9%	Pass
GME1759	50.45	28.20	35.9%	3.75	7.25	0.02	0.47	3.26	0.5%	12.5%	86.9%	Pass
GME1760	43.71	8.30	16.0%	2.99	6.56	0.06	0.46	2.47	2.0%	15.4%	82.6%	Pass
GME1761	58.89	24.65	29.5%	3.44	7.03	0.49	0.60	2.35	14.2%	17.4%	68.3%	Pass
GME1762	74.39	6.68	8.2%	5.24	6.29	0.05	0.51	4.68	1.0%	9.7%	89.3%	Pass
GME1763	86.67	0.89	1.0%	2.61	6.04	0.08	0.37	2.16	3.1%	14.2%	82.8%	Pass
GME1765	83.13	0.22	0.3%	2.41	6.01	0.03	0.32	2.06	1.2%	13.3%	85.5%	Pass
GME1767	77.05	10.54	12.0%	5.69	6.42	0.36	0.84	4.49	6.3%	14.8%	78.9%	Pass
GME1769	75.80	0.59	0.8%	2.67	6.03	0.05	0.30	2.32	1.9%	11.2%	86.9%	Pass
GME1773	55.55	31.19	36.0%	4.29	7.26	0.10	0.58	3.61	2.3%	13.5%	84.1%	Pass
GME1775	52.29	11.29	17.8%	3.46	6.61	0.07	0.61	2.78	2.0%	17.6%	80.3%	Pass
GME1776	60.03	12.83	17.6%	3.46	6.59	0.11	0.54	2.81	3.2%	15.6%	81.2%	Pass
GME1777	62.02	2.85	4.4%	2.65	6.15	0.01	0.35	2.29	0.4%	13.2%	86.4%	Pass
GME1779	84.82	0.44	0.5%	3.10	6.02	0.02	0.30	2.78	0.6%	9.7%	89.7%	Pass
GME1783	92.00	0.11	0.1%	4.22	6.00	0.15	0.46	3.61	3.6%	10.9%	85.5%	Pass
GME1785	56.06	9.87	15.0%	4.66	6.52	0.29	0.68	3.69	6.2%	14.6%	79.2%	Pass
GME1786	73.66	18.95	20.5%	5.85	6.72	0.15	0.61	5.09	2.6%	10.4%	87.0%	Pass
GME1792	75.40	11.10	12.8%	3.38	6.45	0.15	0.42	2.81	4.4%	12.4%	83.1%	Pass
GME1794	65.46	26.29	28.7%	5.61	7.00	0.50	0.92	4.19	8.9%	16.4%	74.7%	Pass
GME1795	66.83	13.74	17.1%	2.19	6.60	0.06	0.42	1.71	2.7%	19.2%	78.1%	Pass
GME1796	31.92	61.44	65.8%	2.18	8.30	0.03	0.35	1.80	1.4%	16.1%	82.6%	Pass
GME1797	47.03	47.80	50.4%	2.76	7.76	0.05	0.42	2.29	1.8%	15.2%	83.0%	Pass
GME1798	85.13	6.28	6.9%	4.29	6.24	0.09	0.44	3.76	2.1%	10.3%	87.6%	Pass
GME1799	49.26	36.08	42.3%	2.15	7.48	0.04	0.27	1.84	1.9%	12.6%	85.6%	Pass
GME1800	40.75	51.29	55.7%	3.25	7.95	0.07	0.32	2.86	2.2%	9.8%	88.0%	Pass
GME1802	64.10	28.47	30.8%	5.31	7.08	0.25	0.57	4.49	4.7%	10.7%	84.6%	Pass
GME1803	65.70	23.91	26.7%	5.58	6.93	0.29	0.48	4.81	5.2%	8.6%	86.2%	Pass
GME1804	57.35	41.38	41.9%	6.32	7.47	0.65	1.32	4.35	10.3%	20.9%	68.8%	Pass
GME1805	80.99	0.90	1.1%	3.23	6.04	0.12	0.45	2.66	3.7%	13.9%	82.4%	Pass
GME1806	67.81	24.20	26.3%	5.11	6.92	0.33	0.61	4.17	6.5%	11.9%	81.6%	Pass
GME1807	95.34	0.23	0.2%	5.95	6.01	0.25	0.58	5.12	4.2%	9.7%	86.1%	Pass
GME1809	74.80	21.77	22.5%	4.96	6.79	0.36	1.17	3.43	7.3%	23.6%	69.2%	Pass
GME1810	78.23	14.06	15.2%	4.65	6.53	0.19	0.48	3.98	4.1%	10.3%	85.6%	Pass
GME1813	85.37	7.73	8.3%	4.85	6.29	0.23	0.44	4.18	4.7%	9.1%	86.2%	Pass
GME1814	81.43	12.68	13.5%	3.74	6.47	0.06	0.47	3.21	1.6%	12.6%	85.8%	Pass
GME1815	78.52	12.90	14.1%	4.40	6.49	0.17	0.38	3.85	3.9%	8.6%	87.5%	Pass
GME1816	78.52	13.11	14.3%	5.51	6.50	0.44	0.88	4.19	8.0%	16.0%	76.0%	Pass
GME1817	48.65	30.65	38.7%	2.60	7.36	0.05	0.44	2.11	1.9%	16.9%	81.2%	Pass
GME1819	77.72	14.15	15.4%	3.79	6.54	0.19	0.49	3.11	5.0%	12.9%	82.1%	Pass
GME1820	87.57	0.64	0.7%	4.76	6.03	1.18	0.57	3.01	24.8%	12.0%	63.2%	Pass
GME1821	88.42	6.59	6.9%	3.61	6.24	0.00	0.48	3.13	0.0%	13.3%	86.7%	Pass
GME1822	88.32	1.44	1.6%	5.16	6.06	0.17	0.70	4.29	3.3%	13.6%	83.1%	Pass
GME1823	36.78	36.71	50.0%	4.32	7.75	0.11	0.44	3.77	2.5%	10.2%	87.3%	Pass
GME1824	40.70	31.54	43.7%	4.52	7.53	0.29	0.51	3.72	6.4%	11.3%	82.3%	Pass
GME1825	71.13	16.95	19.2%	4.33	6.67	0.43	0.52	3.38	9.9%	12.0%	78.1%	Pass
GME1826	79.12	15.18	16.1%	5.62	6.56	0.64	0.92	4.06	11.4%	16.4%	72.2%	Pass
GME1827	66.59	19.81	22.9%	4.27	6.80	0.04	0.48	3.75	0.9%	11.2%	87.8%	Pass
GME1828	73.81	0.52	0.7%	2.59	6.02	0.04	0.30	2.25	1.5%	11.6%	86.9%	Pass
GME1829	65.59	0.32	0.5%	2.62	6.02	0.05	0.38	2.19	1.9%	14.5%	83.6%	Pass
GME1830	82.18	2.53	3.0%	3.90	6.10	0.14	0.42	3.34	3.6%	10.8%	85.6%	Pass
GME1831	78.28	2.19	2.7%	2.96	6.09	0.10	0.49	2.37	3.4%	16.6%	80.1%	Pass
GME1832	18.32	67.45	78.6%	2.76	8.75	0.03	0.29	2.44	1.1%	10.5%	88.4%	Pass
GME1833	14.35	32.84	69.6%	3.55	8.36	0.07	0.28	3.20	2.0%	7.9%	90.1%	Pass
GME1835	48.95	32.13	39.6%	1.74	7.38	0.05	0.24	1.45	2.9%	13.8%	83.3%	Pass
GME1836	57.93	24.72	29.9%	2.52	7.05	0.03	0.29	2.20	1.2%	11.5%	87.3%	Pass
GME1837	92.61	2.14	2.3%	5.31	6.08	0.13	0.44	4.74	2.4%	8.3%	89.3%	Pass
GME1838	82.48	14.60	15.0%	5.67	6.53	0.48	0.70	4.49	8.5%	12.3%	79.2%	Pass
GME1843	53.40	41.09	43.5%	6.77	7.52	0.36	0.87	5.54	5.3%	12.9%	81.8%	Pass
GME1844	89.87	3.01	3.2%	4.58	6.11	0.43	0.74	3.41	9.4%	16.2%	74.5%	Pass
GME1845	86.34	3.69	4.1%	3.32	6.14	0.00	0.38	2.94	0.0%	11.4%	88.6%	Pass
GME1846	74.93	15.97	17.6%	4.69	6.61	0.18	0.60	3.91	3.8%	12.8%	83.4%	Pass
GME1847	76.89	11.84	13.3%	4.85	6.47	0.84	1.03	2.98	17.3%	21.2%	61.4%	Pass
GME1848	80.69	11.65	12.6%	3.94	6.44	0.25	0.58	3.11	6.3%	14.7%	78.9%	Pass
GME1849	80.04	14.17	15.0%	3.85	6.53	0.04	0.57	3.24	1.0%	14.8%	84.2%	Pass
GME1850	81.02	12.67	13.5%	4.55	6.47	0.17	0.64	3.74	3.7%	14.1%	82.2%	Pass
GME1851	78.28	14.44	15.6%	3.90	6.54	0.25	0.71	2.94	6.4%	18.2%	75.4%	Pass
GME1852	73.21	15.37	17.4%	3.60	6.61	0.02	0.50	3.08	0.6%	13.9%	85.6%	Pass
GME1853	95.40	0.75	0.8%	3.58	6.03	0.13	0.71	2.74	3.6%	19.8%	76.5%	Pass
GME1854	87.54	2.12	2.4%	3.65	6.08	0.01	0.37	3.27	0.3%	10.1%	89.6%	Pass
GME1855	82.23	1.25	1.5%	3.40	6.05	0.08	0.39	2.93	2.4%	11.5%	86.2%	Pass
GME1856	90.61	4.10	4.3%	5.85	6.15	0.58	0.87	4.40	9.9%	14.9%	75.2%	Pass
GME1857	84.40	6.08	6.7%	3.56	6.23	0.08	0.47	3.01	2.2%	13.2%	84.6%	Pass
GME1858	76.50	13.76	15.2%	4.00	6.53	0.04	0.45	3.51	1.0%	11.3%	87.8%	Pass

Core Sample	CO2 Composition (%)	CH4 Composition (%)	Gas Composition CH4/(CO2+CH4) (%)	Measured Gas Content QM (m3/t)	Mining Limit Level (m3/t)	Q1 (m3/t)	Q2 (m3/t)	Q3 (m3/t)	Q1/QM (%)	Q2/QM (%)	Q3/QM (%)	Pass/Fail
GME1859	85.74	4.01	4.5%	3.09	6.16	0.02	0.33	2.74	0.6%	10.7%	88.7%	Pass
GME1860	80.44	1.28	1.6%	2.82	6.05	0.02	0.43	2.37	0.7%	15.2%	84.0%	Pass
GME1861	62.93	33.93	35.0%	4.72	7.23	0.25	0.57	3.90	5.3%	12.1%	82.6%	Pass
GME1862	82.73	5.06	5.8%	2.71	6.20	0.06	0.37	2.28	2.2%	13.7%	84.1%	Pass
GME1863	95.61	2.85	2.9%	5.90	6.10	0.48	0.99	4.43	8.1%	16.8%	75.1%	Pass
GME1864	93.30	1.41	1.5%	2.66	6.05	0.05	0.37	2.24	1.9%	13.9%	84.2%	Pass
GME1865	74.31	15.03	16.8%	4.01	6.59	0.25	0.61	3.15	6.2%	15.2%	78.6%	Pass
GME1866	84.93	1.94	2.2%	2.50	6.08	0.01	0.25	2.24	0.4%	10.0%	89.6%	Pass
GME1867	80.03	3.95	4.7%	2.50	6.16	0.06	0.37	2.07	2.4%	14.8%	82.8%	Pass
GME1868	86.99	5.36	5.8%	4.90	6.20	0.12	0.54	4.24	2.4%	11.0%	86.5%	Pass
GME1869	75.49	15.30	16.9%	4.06	6.59	0.01	0.38	3.67	0.2%	9.4%	90.4%	Pass
GME1870	72.43	18.54	20.4%	3.71	6.71	0.10	0.43	3.18	2.7%	11.6%	85.7%	Pass
GME1871	86.29	3.44	3.8%	3.31	6.13	0.05	0.39	2.87	1.5%	11.8%	86.7%	Pass
GME1872	86.12	3.29	3.7%	3.61	6.13	0.00	0.46	3.15	0.0%	12.7%	87.3%	Pass
GME1873	89.10	3.64	3.9%	4.94	6.14	0.20	0.86	3.88	4.0%	17.4%	78.5%	Pass
GME1874	76.73	0.66	0.9%	2.25	6.03	0.03	0.37	1.85	1.3%	16.4%	82.2%	Pass
GME1875	83.23	0.18	0.2%	3.35	6.01	0.02	0.37	2.96	0.6%	11.0%	88.4%	Pass
GME1881	90.07	2.79	3.0%	5.26	6.11	0.38	0.71	4.17	7.2%	13.5%	79.3%	Pass
GME1883	93.09	0.67	0.7%	3.38	6.02	0.05	0.51	2.82	1.5%	15.1%	83.4%	Pass
GME1885	93.70	1.87	2.0%	5.11	6.07	0.32	0.65	4.14	6.3%	12.7%	81.0%	Pass
GME1887	92.79	0.18	0.2%	2.77	6.01	0.00	0.32	2.45	0.0%	11.6%	88.4%	Pass
GME1889	84.48	0.10	0.1%	2.65	6.00	0.04	0.44	2.17	1.5%	16.6%	81.9%	Pass
GME1890	91.16	0.20	0.2%	3.06	6.01	0.05	0.46	2.55	1.6%	15.0%	83.3%	Pass
GME1891	89.42	0.24	0.3%	3.01	6.01	0.03	0.40	2.58	1.0%	13.3%	85.7%	Pass
GME1892	89.43	0.34	0.4%	3.08	6.01	0.00	0.41	2.67	0.0%	13.3%	86.7%	Pass
GME1895	89.15	0.34	0.4%	3.53	6.01	0.12	0.55	2.86	3.4%	15.6%	81.0%	Pass
GME1897	92.20	5.68	5.8%	3.58	6.20	0.08	0.41	3.09	2.2%	11.5%	86.3%	Pass
GME1898	86.45	8.46	8.9%	3.20	6.31	0.09	0.28	2.83	2.8%	8.8%	88.4%	Pass
GME1900	85.91	3.66	4.1%	2.82	6.14	0.06	0.40	2.36	2.1%	14.2%	83.7%	Pass
GME1901	76.36	13.60	15.1%	3.00	6.52	0.01	0.37	2.62	0.3%	12.3%	87.3%	Pass
GME1902	75.18	19.24	20.4%	4.52	6.71	0.00	0.35	4.17	0.0%	7.7%	92.3%	Pass
GME1904	78.32	9.22	10.5%	3.42	6.37	0.39	0.45	2.58	11.4%	13.2%	75.4%	Pass
GME1905	89.56	2.12	2.3%	3.33	6.08	0.29	0.62	2.42	8.7%	18.6%	72.7%	Pass
GME1906	74.12	16.60	18.3%	3.17	6.64	0.11	0.32	2.74	3.5%	10.1%	86.4%	Pass
GME1907	94.87	1.06	1.1%	3.33	6.04	0.05	0.37	2.91	1.5%	11.1%	87.4%	Pass
GME1908	82.54	2.22	2.6%	3.80	6.09	0.19	0.48	3.13	5.0%	12.6%	82.4%	Pass
GME1909	91.39	2.05	2.2%	4.55	6.08	0.11	0.69	3.75	2.4%	15.2%	82.4%	Pass
GME1911	87.25	0.78	0.9%	3.27	6.03	0.04	0.41	2.82	1.2%	12.5%	86.2%	Pass
GME1912	84.04	1.98	2.3%	2.58	6.08	0.00	0.39	2.19	0.0%	15.1%	84.9%	Pass
GME1913	77.13	0.45	0.6%	2.80	6.02	0.02	0.36	2.42	0.7%	12.9%	86.4%	Pass
GME1915	91.26	2.43	2.6%	3.53	6.09	0.05	0.51	2.97	1.4%	14.4%	84.1%	Pass
GME1916	87.34	3.90	4.3%	3.27	6.15	0.01	0.47	2.79	0.3%	14.4%	85.3%	Pass
GME1917	88.84	2.24	2.5%	2.93	6.09	0.02	0.41	2.50	0.7%	14.0%	85.3%	Pass
GME1918	74.37	12.62	14.5%	4.97	6.51	0.06	0.48	4.43	1.2%	9.7%	89.1%	Pass
GME1919	90.49	4.45	4.7%	3.83	6.16	0.14	0.55	3.14	3.7%	14.4%	82.0%	Pass
GME1921	86.47	1.00	1.1%	3.39	6.04	0.03	0.29	3.07	0.9%	8.6%	90.6%	Pass
GME1923	95.00	2.55	2.6%	5.63	6.09	0.05	0.42	5.16	0.9%	7.5%	91.7%	Pass
GME1924	95.20	1.37	1.4%	3.87	6.05	0.00	0.35	3.52	0.0%	9.0%	91.0%	Pass
GME1925	83.65	13.40	13.8%	6.06	6.48	0.35	0.79	4.92	5.8%	13.0%	81.2%	Pass
GME1928	62.59	28.54	31.3%	4.09	7.10	0.03	0.71	3.35	0.7%	17.4%	81.9%	Pass
GME1929	78.24	17.89	18.6%	5.55	6.65	0.52	0.81	4.22	9.4%	14.6%	76.0%	Pass
GME1930	77.30	18.51	19.3%	4.28	6.68	0.38	0.82	3.08	8.9%	19.2%	72.0%	Pass
GME1931	71.28	18.61	20.7%	4.08	6.72	0.14	0.62	3.32	3.4%	15.2%	81.4%	Pass
GME1932	83.35	14.28	14.6%	6.32	6.51	1.15	0.85	4.32	18.2%	13.4%	68.4%	Pass
GME1933	91.49	0.28	0.3%	3.66	6.01	0.04	0.46	3.16	1.1%	12.6%	86.3%	Pass
GME1934	89.62	0.71	0.8%	3.71	6.02	0.08	0.46	3.17	2.2%	12.4%	85.4%	Pass
GME1935	92.85	0.64	0.7%	3.68	6.02	0.04	0.48	3.16	1.1%	13.0%	85.9%	Pass
GME1936	87.77	0.36	0.4%	3.21	6.01	0.01	0.33	2.87	0.3%	10.3%	89.4%	Pass
GME1937	71.71	22.53	23.9%	5.53	6.84	0.16	0.45	4.92	2.9%	8.1%	89.0%	Pass
GME1938	78.20	18.66	19.3%	6.30	6.67	0.13	0.97	5.20	2.1%	15.4%	82.5%	Pass
GME1939	90.15	0.15	0.2%	3.06	6.01	0.01	0.51	2.54	0.3%	16.7%	83.0%	Pass
GME1940	92.83	0.87	0.9%	3.89	6.03	0.07	0.45	3.37	1.8%	11.6%	86.6%	Pass
GME1941	80.53	15.72	16.3%	5.89	6.57	0.19	0.78	4.92	3.2%	13.2%	83.5%	Pass
GME1942	83.40	0.20	0.2%	3.31	6.01	0.01	0.33	2.97	0.3%	10.0%	89.7%	Pass
GME1943	69.73	26.28	27.4%	6.31	6.96	0.18	1.20	4.93	2.9%	19.0%	78.1%	Pass
GME1944	88.22	11.77	11.8%	5.84	6.41	0.59	1.17	4.08	10.1%	20.0%	69.9%	Pass
GME1945	82.95	12.40	13.0%	5.43	6.45	0.30	0.75	4.38	5.5%	13.8%	80.7%	Pass
GME1946	86.57	11.87	12.1%	5.98	6.42	0.44	0.92	4.62	7.4%	15.4%	77.3%	Pass
GME1947	79.64	13.41	14.4%	4.69	6.50	0.05	0.43	4.21	1.1%	9.2%	89.8%	Pass
GME1948	82.66	14.49	14.9%	5.66	6.52	0.43	0.68	4.55	7.6%	12.0%	80.4%	Pass
GME1949	93.30	6.65	6.7%	6.18	6.23	0.53	1.66	3.99	8.6%	26.9%	64.6%	Pass
GME1955	80.90	15.65	16.2%	5.93	6.57	0.15	0.76	5.02	2.5%	12.8%	84.7%	Pass
GME1956	81.32	15.42	15.9%	5.08	6.56	0.81	0.66	3.61	15.9%	13.0%	71.1%	Pass
GME1957	80.74	15.91	16.5%	6.54	6.58	0.48	0.87	5.19	7.3%	13.3%	79.4%	Pass
GME1963	82.05	13.89	14.5%	5.44	6.51	0.21	0.71	4.52	3.9%	13.1%	83.1%	Pass
GME1969	83.35	10.89	11.6%	6.23	6.40	0.13	1.29	4.81	2.1%	20.7%	77.2%	Pass
GME1970	87.86	10.43	10.6%	4.04	6.47	0.15	0.87	3.02	3.7%	21.5%	74.8%	Pass
GME1973	84.11	11.36	11.9%	4.56	6.42	0.03	0.58	3.95	0.7%	12.7%	86.6%	Pass
GME1975	92.59	4.92	5.0%	4.97	6.18	0.28	0.82	3.87	5.6%	16.5%	77.9%	Pass
GME1977	81.03	12.02	12.9%	5.45	6.45	0.14	0.84	4.47	2.6%	15.4%	82.0%	Pass
GME1978	88.37	11.08	11.1%	5.97	6.39	0.19	1.01	4.77	3.2%	16.9%	79.9%	Pass
GME1984	83.79	10.95	11.6%	6.37	6.40	0.47	0.97	4.93	7.4%	15.2%	77.4%	Pass
GME1989	85.34	11.11	11.5%	6.33	6.40	0.12	0.75	5.46	1.9%	11.8%	86.3%	Pass
GME1991	82.90	11.84	12.5%	5.43	6.44	0.32	1.09	4.02	5.9%	20.1%	74.0%	Pass
GME1993	85.80	11.37	11.7%	6.35	6.41	0.24	2.08	4.03	3.8%	32.8%	63.5%	Pass
GME1995	39.32	59.38	60.2%	5.97	8.10	0.43	0.77	4.77	7.2%	12.9%	79.9%	Pass
GME2002	79.56	15.72	16.5%	4.22	6.58	0.04	0.66	3.52	0.9%	15.6%	83.4%	Pass
GME2003	89.27	5.59	5.9%	5.12	6.21	0.12	0.67	4.33	2.3%	13.1%	84.6%	Pass
GME2005	88.21	9.88	10.1%	6.17	6.35	0.31	1.29	4.57	5.0%	20.9%	74.1%	Pass
GME2008	88.28	9.64	9.8%	4.29	6.34	0.12	0.86	3.31	2.8%	20.0%	77.2%	Pass
GME2009	86.08	12.85	13.0%	5.46	6.45	0.17	1.14	4.15	3.1%	20.9%	76.0%	Pass
GME2010	86.06	11.94	12.2%	5.53	6.43	0.19	0.66	4.68	3.4%	11.9%	84.6%	Pass
GME2012	72.18	16.77	18.9%	5.01	6.66	0.04	0.57	4.40	0.8%	11.4%	87.8%	Pass
GME2013	78.74	16.67	17.5%	6.53	6.61	0.14	0.74	5.65	2.1%	11.3%	86.5%	Pass
GME2014	72.64	17.70	19.6%	6.19	6.69	0.14	0.81	5.24	2.3%	13.1%	84.7%	Pass
GME2016	92.14	7.74	7.7%	5.97	6.27	0.13	0.75	5.09	2.2%	12.6%	85.3%	Pass
GME2021	83.70	15.06	15.2%	4.51	6.53	0.07	0.53	3.96	1.5%	11.6%	86.8%	Pass
GME2023	83.98	12.47	12.9%	5.20	6.45	0.16	0.96	4.21	3.0%	18.0%	79.0%	Pass
GME2025	90.90	5.97	6.2%	5.19	6.22	0.15	0.84	4.32	2.8%	15.8%	81.4%	Pass
GME2026	89.93	6.31	6.6%	5.21	6.23	0.13	0.56	4.63	2.4%	10.5%	87.0%	Pass
GME2027	84.93	11.97	12.4%	5.30	6.43	0.28	0.84	4.41	5.1%	15.2%	79.7%	Pass
GME2028	84.42	10.43	11.0%	5.13	6.49	0.09	0.67	4.44	1.7%	12.9%	85.4%	Pass
GME2029	85.59	8.26	8.8%	5.71	6.31	0.27	1.08	4.58	4.6%	18.2%	77.2%	Pass
GME2035	79.25	12.95	14.0%	5.14	6.49	0.22	0.76	4.34	4.1%	14.3%	81.6%	Pass
GME2037	88.03	11.09	11.2%	6.08	6.39	0.20	0.56	5.49	3.2%	9.0%	87.8%	Pass
GME2042	89.57	6.14	6.4%	5.66	6.22	0.05	1.39	4.26	0.9%	24.4%	74.7%	Pass
GME2057	51.57	11.65	18.4%	2.93	6.62	0.41	0.38	2.14	14.0%	13.0%	73.0%	Pass
GME2058	80.41	14.20	15.0%	5.32	6.53	0.31	0.67	4.34	5.8%	12.6%	81.6%	Pass
GME2061	42.97	43.56	50.3%	2.38	7.76	0.03	0.24	2.11	1.3%	10.1%	88.7%	Pass
GME2062	53.06	32.67	38.1%	1.88	7.33	0.01	0.34	1.53	0.5%	18.1%	81.4%	Pass
GME2063	41.71	39.74	48.8%	2.32	7.71	0.01	0.34	1.97	0.4%	14.7%	84.9%	Pass
GME2064	39.56	48.19	54.9%	3.24	7.92	0.10	0.48	2.66	3.1%	14.8%	82.1%	Pass
GME2065	37.56	44.57	54.3%	2.52	7.90	0.01	0.37	2.14	0.4%	14.7%	84.9%	Pass
GME2066	46.46	39.62	46.0%	2.65	7.61	0.03	0.52	2.10	1.1%	19.6%	79.2%	Pass

Core Sample	CO2 Composition (%)	CH4 Composition (%)	Gas Composition CH4/(CO2+CH4) (%)	Measured Gas Content QM (m3/t)	Mining Limit Level (m3/t)	Q1 (m3/t)	Q2 (m3/t)	Q3 (m3/t)	Q1/QM (%)	Q2/QM (%)	Q3/QM (%)	Pass/Fail
GME2066	46.46	39.62	46.0%	2.65	7.61	0.03	0.52	2.10	1.1%	19.6%	79.2%	Pass
GME2067	34.80	52.80	60.3%	3.18	8.11	0.01	0.43	2.74	0.3%	13.5%	86.2%	Pass
GME2068	91.64	1.00	1.1%	4.46	6.04	0.06	0.52	3.88	1.3%	11.7%	87.0%	Pass
GME2078	85.75	2.63	3.0%	3.50	6.10	0.05	0.55	2.90	1.4%	15.7%	82.9%	Pass
GME2079	92.48	0.66	0.7%	4.01	6.02	0.17	0.49	3.35	4.2%	12.2%	83.5%	Pass
GME2092	34.36	48.90	58.7%	1.93	8.05	0.04	0.17	1.72	2.1%	8.8%	89.1%	Pass
GME2093	33.48	51.00	60.4%	2.28	8.11	0.00	0.27	2.01	0.0%	11.8%	88.2%	Pass
GME2094	32.35	50.55	61.0%	2.22	8.13	0.07	0.29	1.86	3.2%	13.1%	83.8%	Pass
GME2095	28.30	63.17	69.1%	4.45	8.42	0.06	0.67	3.72	1.3%	15.1%	83.6%	Pass
GME2096	24.28	62.14	71.9%	3.35	8.52	0.06	0.31	2.98	1.8%	9.3%	89.0%	Pass
GME2097	29.75	58.32	66.2%	2.55	8.32	0.00	0.30	2.25	0.0%	11.8%	88.2%	Pass
GME2098	37.55	56.78	60.2%	3.14	8.11	0.04	0.42	2.68	1.3%	13.4%	85.4%	Pass
GME2099	27.81	66.37	70.5%	4.03	8.46	0.31	0.54	3.18	7.7%	13.4%	78.9%	Pass
GME2100	82.09	10.72	11.6%	5.55	6.40	0.33	0.74	4.48	5.9%	13.3%	80.7%	Pass
GME2101	38.48	46.14	54.5%	1.99	7.91	0.08	0.32	1.59	4.0%	16.1%	79.9%	Pass
GME2102	37.46	50.35	57.3%	1.96	8.00	0.03	0.26	1.67	1.5%	13.3%	85.2%	Pass
GME2103	79.73	11.50	12.6%	5.34	6.44	0.19	0.80	4.35	3.6%	15.0%	81.5%	Pass
GME2104	80.81	11.38	12.3%	5.48	6.43	0.22	0.80	4.46	4.0%	14.6%	81.4%	Pass
GME2105	85.75	11.31	11.7%	5.51	6.41	0.39	0.75	4.37	7.1%	13.6%	79.3%	Pass
GME2106	86.71	12.70	12.8%	5.76	6.45	0.52	1.30	3.94	9.0%	22.6%	68.4%	Pass
GME2107	83.15	12.71	13.3%	5.68	6.46	0.51	1.28	3.89	9.0%	22.5%	68.5%	Pass
GME2108	84.79	11.30	11.8%	5.71	6.41	0.47	1.53	3.71	8.2%	26.8%	65.0%	Pass
GME2109	83.35	11.46	12.1%	5.31	6.42	0.23	0.75	4.33	4.3%	14.1%	81.5%	Pass
GME2111	78.67	12.01	13.2%	4.97	6.46	0.20	0.62	4.15	4.0%	12.5%	83.5%	Pass
GME2113	86.16	7.98	8.5%	5.36	6.30	0.07	0.57	4.72	1.3%	10.6%	88.1%	Pass
GME2114	84.86	12.13	12.5%	5.35	6.44	0.61	0.81	3.93	11.4%	15.1%	73.5%	Pass
GME2115	81.44	12.05	12.9%	5.20	6.45	0.15	0.62	4.43	2.9%	11.9%	85.2%	Pass
GME2120	85.31	12.39	12.7%	5.78	6.44	0.33	0.99	4.74	5.4%	16.3%	78.2%	Pass
GME2121	85.74	10.94	11.3%	4.77	6.40	0.49	0.74	3.94	9.5%	14.3%	76.2%	Pass
GME2126	84.96	8.07	8.7%	5.01	6.30	0.06	0.74	4.26	1.2%	14.6%	84.2%	Pass
GME2127	85.04	9.70	10.2%	5.59	6.36	0.14	0.78	4.79	2.5%	13.7%	83.9%	Pass
GME2129	85.97	10.05	10.5%	4.25	6.37	0.03	0.86	3.36	0.7%	20.2%	79.1%	Pass
GME2131	87.67	8.80	9.1%	4.80	6.32	0.43	0.77	3.60	9.0%	16.0%	75.0%	Pass
GME2132	95.83	4.17	4.2%	5.79	6.15	0.13	1.15	4.51	2.2%	19.9%	77.9%	Pass
GME2134	90.07	8.17	8.3%	4.50	6.29	0.18	0.84	3.48	4.0%	18.7%	77.3%	Pass
GME2139	50.37	32.72	39.4%	2.00	7.38	0.08	0.23	1.69	4.0%	11.5%	84.5%	Pass
GME2141	5.98	87.49	93.6%	5.14	9.27	0.04	0.53	4.57	0.8%	10.3%	88.9%	Pass
GME2142	32.76	60.56	64.9%	3.51	8.27	0.02	0.32	3.17	0.6%	9.1%	90.3%	Pass
GME2145	82.95	0.40	0.5%	2.84	6.02	0.01	0.40	2.43	0.4%	14.1%	85.6%	Pass
GME2148	22.21	69.51	75.8%	3.72	8.65	0.09	0.41	3.22	2.4%	11.0%	86.6%	Pass
GME2149	2.70	92.66	97.2%	4.18	9.40	0.09	0.36	3.73	2.2%	8.6%	89.2%	Pass
GME2157	7.57	84.11	91.7%	3.88	9.21	0.04	0.50	3.34	1.0%	12.9%	86.1%	Pass
GME2158	6.10	84.19	93.2%	4.29	9.26	0.11	0.36	3.82	2.6%	8.4%	89.0%	Pass
GME2160	5.98	86.23	93.5%	6.34	9.27	0.05	0.53	5.76	0.8%	8.4%	90.9%	Pass
GME2163	15.29	80.87	84.1%	4.86	8.94	0.20	0.77	3.89	4.1%	15.8%	80.0%	Pass
GME2163	15.29	80.87	84.1%	4.86	8.94	0.20	0.77	3.89	4.1%	15.8%	80.0%	Pass
GME2165	47.78	45.44	48.7%	2.58	7.70	0.04	0.30	2.24	1.6%	11.6%	86.8%	Pass
GME2167	86.85	8.14	8.6%	2.80	6.30	0.07	0.41	2.32	2.5%	14.6%	82.9%	Pass
GME2168	87.68	9.83	10.1%	5.71	6.35	0.33	1.27	4.11	5.8%	22.2%	72.0%	Pass
GME2169	90.26	5.99	6.2%	4.40	6.22	0.21	0.66	3.53	4.8%	15.0%	80.2%	Pass
GME2170	88.37	7.56	7.9%	6.12	6.28	0.18	0.71	5.23	2.9%	11.6%	85.5%	Pass
GME2172	83.26	11.40	12.0%	5.70	6.42	0.26	0.48	4.96	4.6%	8.4%	87.0%	Pass
GME2173	91.63	6.59	6.7%	5.16	6.23	0.28	0.99	3.89	5.4%	19.2%	75.4%	Pass
GME2174	89.97	7.53	7.7%	5.95	6.27	0.28	1.09	4.58	4.7%	18.3%	77.0%	Pass
GME2177	86.53	11.18	11.4%	6.30	6.40	0.29	1.06	4.95	4.6%	16.8%	78.6%	Pass
GME2179	88.38	7.07	7.4%	4.31	6.26	0.28	0.63	3.40	6.5%	14.6%	78.9%	Pass
GME2180	17.86	78.55	81.5%	7.98	8.85	0.43	1.78	5.77	5.4%	22.3%	72.3%	Pass
GME2181	89.64	7.05	7.3%	5.53	6.26	0.07	0.56	4.90	1.3%	10.1%	88.6%	Pass
GME2184	85.35	10.74	11.2%	5.93	6.39	0.58	0.66	4.69	9.8%	11.1%	79.1%	Pass
GME2185	89.30	7.55	7.8%	6.08	6.27	0.05	0.51	5.52	0.8%	8.4%	90.8%	Pass
GME2186	83.50	12.51	13.0%	5.91	6.46	0.39	1.09	4.43	6.6%	18.4%	75.0%	Pass
GME2187	82.99	12.20	12.8%	6.37	6.45	0.66	1.49	4.22	10.4%	23.4%	66.2%	Pass
GME2188	88.72	0.36	0.4%	3.36	6.01	0.09	0.63	2.64	2.7%	18.8%	78.6%	Pass
GME2189	85.91	8.47	9.0%	6.05	6.31	0.14	0.65	5.26	2.3%	10.7%	86.9%	Pass
GME2190	86.91	0.84	1.0%	2.67	6.03	0.00	0.34	2.33	0.0%	12.7%	87.3%	Pass
GME2191	90.87	1.26	1.4%	3.02	6.05	0.25	0.36	2.41	8.3%	11.9%	79.8%	Pass
GME2192	74.11	18.58	20.0%	5.90	6.70	0.29	0.87	4.74	4.9%	14.7%	80.3%	Pass
GME2193	89.85	0.36	0.4%	2.74	6.01	0.07	0.34	2.33	2.6%	12.4%	85.0%	Pass
GME2194	90.27	0.31	0.3%	2.82	6.01	0.07	0.34	2.41	2.5%	12.1%	85.5%	Pass
GME2195	79.65	13.58	14.6%	5.65	6.51	0.27	0.57	4.81	4.8%	10.1%	85.1%	Pass
GME2196	88.71	1.98	2.2%	2.86	6.08	0.08	0.33	2.45	2.8%	11.5%	85.7%	Pass
GME2197	79.89	0.11	0.1%	2.90	6.00	0.11	0.35	2.44	3.8%	12.1%	84.1%	Pass
GME2198	89.09	0.30	0.3%	3.03	6.01	0.11	0.45	2.47	3.6%	14.9%	81.5%	Pass
GME2199	89.90	0.86	0.9%	2.83	6.03	0.16	0.38	2.31	5.7%	13.4%	81.6%	Pass
GME2200	93.26	1.59	1.7%	3.02	6.06	0.16	0.43	2.43	5.3%	14.2%	80.5%	Pass
GME2201	8.99	67.28	88.2%	2.84	9.08	0.08	0.33	2.43	2.8%	11.6%	85.6%	Pass
GME2202	92.92	2.55	2.7%	2.88	6.09	0.03	0.38	2.47	1.0%	13.2%	85.8%	Pass
GME2203	85.65	1.93	2.2%	2.72	6.08	0.07	0.34	2.31	2.6%	12.5%	84.9%	Pass
GME2204	89.50	2.54	2.8%	2.78	6.10	0.23	0.40	2.15	8.3%	14.4%	77.3%	Pass
GME2206	79.52	0.46	0.6%	2.79	6.02	0.07	0.39	2.33	2.5%	14.0%	83.5%	Pass
GME2207	84.54	0.24	0.3%	2.82	6.01	0.01	0.38	2.43	0.4%	13.5%	86.2%	Pass
GME2209	88.53	0.91	1.0%	2.83	6.04	0.09	0.46	2.28	3.2%	16.3%	80.6%	Pass
GME2210	31.82	60.05	65.4%	6.13	8.29	0.24	0.71	5.18	3.9%	11.6%	84.5%	Pass
GME2212	87.34	1.87	2.1%	3.40	6.07	0.06	0.35	2.99	1.8%	10.3%	87.9%	Pass
GME2213	89.45	2.93	3.2%	5.51	6.11	0.69	0.82	4.00	12.5%	14.9%	72.6%	Pass
GME2216	99.17	0.28	0.3%	4.14	6.01	0.24	0.73	3.17	5.8%	17.6%	76.6%	Pass
GME2224	80.96	0.43	0.5%	2.46	6.02	0.27	0.41	1.78	11.0%	16.7%	72.4%	Pass
GME2225	90.16	1.09	1.2%	3.70	6.04	0.18	0.43	3.09	4.9%	11.6%	83.5%	Pass
GME2228	90.49	0.18	0.2%	4.17	6.01	0.23	0.60	3.34	5.5%	14.4%	80.1%	Pass
GME2229	89.71	0.23	0.3%	5.54	6.01	0.43	0.75	4.36	7.8%	13.5%	78.7%	Pass
GME2230	93.83	0.10	0.1%	4.69	6.00	0.39	0.64	3.66	8.3%	13.6%	78.0%	Pass
GME2234	80.96	0.43	0.5%	2.46	6.02	0.27	0.41	1.78	11.0%	16.7%	72.4%	Pass
GME2235	78.66	15.73	16.7%	5.86	6.58	0.68	0.99	4.19	11.6%	16.9%	71.5%	Pass
GME2236	79.65	9.90	11.1%	5.31	6.39	0.33	0.87	4.11	6.2%	16.4%	77.4%	Pass
GME2237	37.49	44.22	54.1%	2.18	7.89	0.24	0.29	1.65	11.0%	13.3%	75.7%	Pass
GME2238	29.62	54.14	64.6%	4.30	8.26	0.19	0.51	3.60	4.4%	11.9%	83.7%	Pass
GME2241	85.19	0.31	0.4%	2.90	6.01	0.09	0.56	2.25	3.1%	19.3%	77.6%	Pass
GME2242	86.44	2.91	3.3%	2.81	6.11	0.02	0.40	2.39	0.7%	14.2%	85.1%	Pass
GME2243	83.86	1.36	1.6%	3.54	6.06	0.17	0.50	2.87	4.8%	14.1%	81.1%	Pass
GME2244	81.75	0.56	0.7%	3.38	6.02	0.01	0.40	2.97	0.3%	11.8%	87.9%	Pass
GME2249	86.09	0.58	0.7%	3.47	6.02	0.04	0.48	2.95	1.2%	13.8%	85.0%	Pass
GME2253	77.63	9.82	11.2%	4.80	6.39	0.04	0.71	4.05	0.8%	14.8%	84.4%	Pass
GME2256	79.71	10.40	11.5%	5.49	6.40	0.45	0.57	4.47	8.2%	10.4%	81.4%	Pass
GME2257	82.45	10.57	11.4%	6.06	6.40	0.78	0.98	4.30	12.9%	16.2%	71.0%	Pass
GME2258	87.81	12.18	12.2%	5.81	6.42	0.56	0.88	4.37	9.6%	15.1%	75.2%	Pass
GME2259	88.95	11.01	11.0%	5.05	6.38	0.54	1.08	3.43	10.7%	21.4%	67.9%	Pass
GME2273	77.01	14.33	15.7%	6.35	6.55	0.35	0.93	5.07	5.5%	14.6%	79.8%	Pass
GME2274	78.80	16.64	17.4%	6.48	6.61	0.88	1.81	3.79	13.6%	27.9%	58.5%	Pass
GME2275	77.61	11.54	12.9%	5.54	6.45	0.46	0.47	4.61	8.3%	8.5%	83.2%	Pass
GME2276	82.98	11.52	12.2%	6.10	6.43	0.78	0.98	4.34	12.8%	16.1%	71.1%	Pass
GME2277	75.97	12.91	14.5%	4.96	6.51	0.47	0.64	3.85	9.5%	12.9%	77.6%	Pass
GME2278	74.87	12.76	14.6%	4.36	6.51	0.03	0.57	3.76	0.7%	13.1%	86.2%	Pass

APPENDIX I: SUMMARY OF GAS CONTENT AND GAS COMPOSITION DATA (WHOLE DATABASE-FAIL SAMPLES)

Core Sample	CO2 Composition (%)	CH4 Composition (%)	Gas Composition CH4/(CO2+CH4) (%)	Measured Gas Content QM (m3/t)	Mining Limit Level (m3/t)	Q1 (m3/t)	Q2 (m3/t)	Q3 (m3/t)	Q1/QM (%)	Q2/QM (%)	Q3/QM (%)	Pass/Fail
GME1720	60.45	29.15	32.53%	7.57	7.14	1.05	1.01	5.51	13.87%	13.34%	72.79%	Fail
GME1729	2.71	95.43	97.24%	10.96	9.40	1.81	3.55	5.60	16.51%	32.39%	51.09%	Fail
GME1730	47.32	42.29	47.19%	8.71	7.65	0.20	1.29	7.22	2.30%	14.81%	82.89%	Fail
GME1731	76.94	19.91	20.56%	6.79	6.72	0.78	1.73	4.28	11.49%	25.48%	63.03%	Fail
GME1732	11.62	81.71	87.55%	12.90	9.06	0.75	4.02	8.13	5.81%	31.16%	63.02%	Fail
GME1733	12.22	86.94	87.68%	10.93	9.07	0.69	2.04	8.20	6.31%	18.66%	75.02%	Fail
GME1737	35.89	63.93	64.05%	8.47	8.24	0.82	2.32	5.33	9.68%	27.39%	62.93%	Fail
GME1738	36.18	58.75	61.89%	11.83	8.17	0.81	2.85	8.17	6.85%	24.09%	69.06%	Fail
GME1744	83.62	13.19	13.62%	6.57	6.48	0.39	1.18	5.00	5.94%	17.96%	76.10%	Fail
GME1748	90.82	2.20	2.37%	8.01	6.08	0.62	0.81	6.58	7.74%	10.11%	82.15%	Fail
GME1754	85.92	12.99	13.13%	7.48	6.46	0.79	1.83	4.86	10.56%	24.47%	64.97%	Fail
GME1757	88.66	8.24	8.50%	7.52	6.30	0.20	1.69	5.63	2.66%	22.47%	74.87%	Fail
GME1764	93.40	1.21	1.28%	9.65	6.04	0.80	0.93	7.92	8.29%	9.64%	82.07%	Fail
GME1766	87.25	7.25	7.67%	7.45	6.27	0.28	1.38	5.79	3.76%	18.52%	77.72%	Fail
GME1768	75.85	13.10	14.73%	7.02	6.51	0.42	1.06	5.54	5.98%	15.10%	78.92%	Fail
GME1770	83.71	15.69	15.78%	14.86	6.55	3.52	5.96	5.38	23.69%	40.11%	36.20%	Fail
GME1771	84.43	10.85	11.39%	14.01	6.40	0.87	4.84	8.30	6.21%	34.55%	59.24%	Fail
GME1772	89.59	10.36	10.37%	8.51	6.36	0.53	1.51	6.47	6.23%	17.74%	76.03%	Fail
GME1774	99.84	0.13	0.13%	7.62	6.00	0.55	2.01	5.06	7.22%	26.38%	66.40%	Fail
GME1778	92.80	5.85	5.93%	17.07	6.21	2.72	6.58	7.77	15.93%	38.55%	45.52%	Fail
GME1780	64.99	31.55	32.68%	7.35	7.14	0.30	0.92	6.13	4.08%	12.52%	83.40%	Fail
GME1781	92.28	4.80	4.94%	8.39	6.17	0.66	1.57	6.16	7.87%	18.71%	73.42%	Fail
GME1782	89.42	6.01	6.30%	7.19	6.22	0.85	0.96	5.38	11.82%	13.35%	74.83%	Fail
GME1784	97.49	0.98	1.00%	11.85	6.04	2.29	3.03	6.53	19.32%	25.57%	55.11%	Fail
GME1788	90.27	1.06	1.16%	6.42	6.04	0.40	0.86	5.16	6.23%	13.40%	80.37%	Fail
GME1789	87.07	6.78	7.22%	6.71	6.25	0.12	0.55	6.04	1.79%	8.20%	90.01%	Fail
GME1790	60.41	37.23	38.13%	9.64	7.33	0.69	1.53	7.42	7.16%	15.87%	76.97%	Fail
GME1791	92.33	3.92	4.07%	6.88	6.14	0.40	1.46	5.02	5.81%	21.22%	72.97%	Fail
GME1793	77.94	17.71	18.52%	15.37	6.65	3.17	6.04	6.16	20.62%	39.30%	40.08%	Fail
GME1801	95.92	4.03	4.03%	8.57	6.14	1.69	1.57	5.31	19.72%	18.32%	61.96%	Fail
GME1808	92.31	5.33	5.46%	14.66	6.19	2.22	3.51	8.93	15.14%	23.94%	60.91%	Fail
GME1811	80.25	18.83	19.00%	12.88	6.67	2.08	2.96	7.84	16.15%	22.98%	60.87%	Fail
GME1812	93.15	0.93	0.99%	6.81	6.03	0.47	1.10	5.24	6.90%	16.15%	76.95%	Fail
GME1834	70.25	18.64	20.97%	13.80	6.73	3.33	6.35	4.12	24.13%	46.01%	29.86%	Fail
GME1876	98.17	0.52	0.53%	10.59	6.02	1.25	3.06	6.28	11.80%	28.90%	59.30%	Fail
GME1877	99.27	0.72	0.72%	17.75	6.03	4.26	7.97	5.52	24.00%	44.90%	31.10%	Fail
GME1878	96.90	1.04	1.06%	7.87	6.04	0.35	1.24	6.28	4.45%	15.76%	79.80%	Fail
GME1879	92.19	2.06	2.19%	7.46	6.08	0.24	0.93	6.29	3.22%	12.47%	84.32%	Fail
GME1880	98.79	1.04	1.04%	14.33	6.04	1.48	4.07	8.78	10.33%	28.40%	61.27%	Fail
GME1884	81.19	14.19	14.88%	8.94	6.52	1.23	1.90	5.81	13.76%	21.25%	64.99%	Fail
GME1888	87.19	7.19	7.62%	7.16	6.27	0.38	0.92	5.86	5.31%	12.85%	81.84%	Fail
GME1882	96.54	1.35	1.38%	17.03	6.05	3.41	5.89	7.73	20.02%	34.59%	45.39%	Fail
GME1886	88.01	7.93	8.27%	6.36	6.29	0.34	0.63	5.39	5.35%	9.91%	84.75%	Fail
GME1893	94.67	0.49	0.51%	6.14	6.02	0.13	0.59	5.42	2.12%	9.61%	88.27%	Fail
GME1894	79.52	17.92	18.39%	6.87	6.64	0.50	0.92	5.45	7.28%	13.39%	79.33%	Fail
GME1896	76.52	20.68	21.28%	7.94	6.74	0.69	0.99	6.26	8.69%	12.47%	78.84%	Fail
GME1899	98.85	1.11	1.11%	7.78	6.05	0.68	1.27	5.83	8.74%	16.32%	74.94%	Fail
GME1903	96.15	1.64	1.68%	7.00	6.06	0.60	1.40	5.00	8.57%	20.00%	71.43%	Fail
GME1910	83.01	8.86	9.64%	6.94	6.34	0.54	1.07	5.33	7.78%	15.42%	76.80%	Fail
GME1914	89.72	4.48	4.76%	6.43	6.17	0.05	0.80	5.58	0.78%	12.44%	86.78%	Fail
GME1920	85.38	11.43	11.81%	7.02	6.41	0.65	0.85	5.52	9.26%	12.11%	78.63%	Fail
GME1922	92.05	2.95	3.11%	6.85	6.11	0.11	0.77	5.97	1.61%	11.24%	87.15%	Fail
GME1926	98.32	1.27	1.28%	11.75	6.04	0.95	2.33	8.47	8.09%	19.83%	72.09%	Fail
GME1927	97.48	0.62	0.63%	6.76	6.02	0.39	1.10	5.27	5.77%	16.27%	77.96%	Fail
GME1950	81.94	14.65	15.17%	8.35	6.53	0.80	1.29	6.26	9.58%	15.45%	74.97%	Fail
GME1951	90.88	8.07	8.16%	6.66	6.29	0.40	1.08	5.18	6.01%	16.22%	77.78%	Fail
GME1952	85.01	14.97	14.97%	7.31	6.52	0.66	1.84	4.81	9.03%	25.17%	65.80%	Fail
GME1953	79.27	20.71	20.71%	8.57	6.72	1.46	2.05	5.06	17.04%	23.92%	59.04%	Fail
GME1954	84.99	14.17	14.29%	8.44	6.50	0.98	1.27	6.19	11.61%	15.05%	73.34%	Fail
GME1958	80.74	15.91	16.46%	6.66	6.50	0.18	1.07	5.41	2.70%	16.07%	81.23%	Fail
GME1959	93.91	6.08	6.08%	6.90	6.21	0.63	1.38	4.89	9.13%	20.00%	70.87%	Fail
GME1960	83.25	16.73	16.73%	10.19	6.59	2.50	3.20	4.49	24.53%	31.40%	44.06%	Fail
GME1961	84.95	12.13	12.49%	6.55	6.44	0.38	0.66	5.55	5.80%	10.08%	84.73%	Fail
GME1962	86.66	11.62	11.82%	6.85	6.41	0.87	1.94	4.04	12.70%	28.32%	58.98%	Fail
GME1964	86.25	11.76	12.00%	6.48	6.42	0.48	1.73	4.27	7.41%	26.70%	65.90%	Fail
GME1965	84.06	12.95	13.35%	8.13	6.47	0.03	1.33	6.77	0.37%	16.36%	83.27%	Fail
GME1966	78.68	17.12	17.87%	8.59	6.63	0.20	1.87	6.52	2.33%	21.77%	75.90%	Fail
GME1967	79.54	18.95	19.24%	8.09	6.67	0.93	2.21	4.95	11.50%	27.32%	61.19%	Fail
GME1968	80.71	16.65	17.10%	7.86	6.67	0.88	2.46	4.52	11.20%	31.30%	57.51%	Fail
GME1971	81.31	12.00	12.86%	7.39	6.45	0.35	1.41	5.63	4.74%	19.08%	76.18%	Fail
GME1972	80.40	14.76	15.51%	8.21	6.54	0.42	1.76	6.03	5.12%	21.44%	73.45%	Fail
GME1974	79.18	16.49	17.24%	6.60	6.60	0.26	1.04	5.30	3.94%	15.76%	80.30%	Fail
GME1976	91.06	6.63	6.79%	6.60	6.24	0.53	1.88	4.19	8.03%	28.48%	63.48%	Fail
GME1979	83.40	15.28	15.48%	7.60	6.54	0.50	1.29	5.81	6.58%	16.97%	76.45%	Fail
GME1980	83.20	15.58	15.77%	7.84	6.55	0.23	1.36	6.25	2.93%	17.35%	79.72%	Fail
GME1981	78.58	20.18	20.43%	7.75	6.71	0.25	1.28	6.22	3.23%	16.52%	80.26%	Fail
GME1982	81.10	18.02	18.18%	7.85	6.64	0.36	1.59	5.90	4.59%	20.25%	75.16%	Fail
GME1983	82.88	15.14	15.45%	8.08	6.54	0.38	1.96	5.74	4.70%	24.26%	71.04%	Fail
GME1985	76.58	18.20	19.20%	7.87	6.67	0.36	1.19	6.32	4.57%	15.12%	80.30%	Fail
GME1986	91.66	6.48	6.60%	7.45	6.23	0.32	0.94	6.19	4.30%	12.62%	83.09%	Fail
GME1987	85.24	13.56	13.72%	6.73	6.48	0.47	1.42	4.84	6.98%	21.10%	71.92%	Fail
GME1988	82.26	14.69	15.15%	7.73	6.53	0.23	0.99	6.51	2.98%	12.81%	84.22%	Fail
GME1990	87.13	12.42	12.48%	6.81	6.44	0.54	1.32	4.95	7.93%	19.38%	72.69%	Fail
GME1992	72.94	16.83	18.75%	6.99	6.66	0.04	0.67	6.28	0.57%	9.59%	89.84%	Fail
GME1994	82.18	11.56	12.33%	7.05	6.43	0.33	1.14	5.58	4.68%	16.17%	79.15%	Fail
GME1996	84.31	14.65	14.80%	8.69	6.63	0.92	2.27	5.50	10.59%	26.12%	63.29%	Fail
GME1997	83.73	14.02	14.34%	8.63	6.50	0.39	2.05	6.19	4.52%	23.75%	71.73%	Fail
GME1998	79.70	17.19	17.74%	7.10	6.62	0.14	0.86	6.10	1.97%	12.11%	85.92%	Fail
GME1999	83.89	12.10	12.61%	7.23	6.44	0.48	1.93	4.82	6.64%	26.69%	66.67%	Fail
GME2000	79.07	17.10	17.78%	6.99	6.62	0.30	0.93	5.76	4.29%	13.30%	82.40%	Fail
GME2001	82.81	14.64	15.02%	7.02	6.53	0.35	1.58	5.09	4.99%	22.51%	72.51%	Fail
GME2004	89.15	6.43	6.73%	7.20	6.24	0.16	1.19	5.85	2.22%	16.53%	81.25%	Fail
GME2006	79.05	16.87	17.59%	8.49	6.62	0.52	2.18	5.79	6.12%	25.68%	68.20%	Fail
GME2007	82.89	14.02	14.47%	8.71	6.51	0.58	2.59	5.54	6.66%	29.74%	63.61%	Fail
GME2011	84.17	12.17	12.63%	6.56	6.44	0.75	1.85	3.96	11.43%	28.20%	60.37%	Fail

Core Sample	CO2 Composition (%)	CH4 Composition (%)	Gas Composition CH4/(CO2+CH4) (%)	Measured Gas Content QM (m3/t)	Mining Limit Level (m3/t)	Q1 (m3/t)	Q2 (m3/t)	Q3 (m3/t)	Q1/QM (%)	Q2/QM (%)	Q3/QM (%)	Pass/Fail
GME2015	86.43	12.67	12.79%	8.57	6.45	0.20	1.64	6.73	2.33%	19.14%	78.53%	Fail
GME2017	93.23	6.76	6.76%	6.53	6.24	0.15	1.04	5.34	2.30%	15.93%	81.78%	Fail
GME2018	86.34	11.10	11.39%	7.39	6.40	0.03	1.10	6.26	0.41%	14.88%	84.71%	Fail
GME2019	84.00	14.35	14.59%	7.28	6.51	0.23	1.54	5.51	3.16%	21.15%	75.69%	Fail
GME2020	86.96	10.65	10.91%	7.12	6.38	0.22	1.03	5.87	3.09%	14.47%	82.44%	Fail
GME2024	88.37	6.87	7.21%	6.27	6.25	0.25	0.74	5.28	3.99%	11.80%	84.21%	Fail
GME2030	82.18	10.09	10.94%	8.43	6.38	0.88	2.63	4.92	10.44%	31.20%	58.36%	Fail
GME2031	78.75	16.91	17.68%	8.14	6.62	0.70	1.23	6.21	8.60%	15.11%	76.29%	Fail
GME2032	82.41	16.84	16.97%	8.43	6.59	0.69	1.51	6.23	8.19%	17.91%	73.90%	Fail
GME2033	90.70	7.29	7.44%	7.89	6.26	0.28	1.21	6.40	3.55%	15.34%	81.12%	Fail
GME2034	87.41	9.55	9.85%	7.74	6.34	0.56	1.05	6.13	7.24%	13.57%	79.20%	Fail
GME2036	85.47	11.04	11.44%	8.52	6.40	0.47	1.72	6.33	5.52%	20.19%	74.30%	Fail
GME2038	86.17	10.57	10.93%	7.85	6.38	0.56	1.61	5.68	7.13%	20.51%	72.36%	Fail
GME2039	76.62	6.08	7.35%	7.55	6.26	0.91	1.70	4.94	12.05%	22.52%	65.43%	Fail
GME2040	83.60	15.05	15.26%	8.06	6.53	0.80	2.10	5.16	9.93%	26.05%	64.02%	Fail
GME2041	89.67	8.28	8.45%	6.61	6.30	0.74	1.63	4.24	11.20%	24.66%	64.15%	Fail
GME2043	87.50	8.16	8.53%	8.99	6.30	0.92	1.96	6.11	10.23%	21.80%	67.96%	Fail
GME2044	84.14	13.23	13.59%	8.47	6.48	0.72	3.16	4.59	8.50%	37.31%	54.19%	Fail
GME2045	86.23	10.53	10.88%	7.95	6.38	0.31	2.49	5.15	3.90%	31.32%	64.78%	Fail
GME2046	89.31	7.22	7.48%	8.44	6.26	0.46	1.55	6.43	5.45%	18.36%	76.18%	Fail
GME2047	85.47	10.96	11.37%	8.93	6.40	0.49	1.86	6.58	5.49%	20.83%	73.68%	Fail
GME2048	84.39	11.53	12.02%	8.88	6.42	0.87	2.17	5.84	9.80%	24.44%	65.77%	Fail
GME2049	77.80	16.90	17.85%	9.42	6.62	0.49	2.74	6.19	5.20%	29.09%	65.71%	Fail
GME2050	79.98	16.52	17.12%	8.05	6.60	0.38	2.49	5.18	4.72%	30.93%	64.35%	Fail
GME2051	89.94	6.52	6.76%	8.33	6.24	0.41	1.81	6.11	4.92%	21.73%	73.35%	Fail
GME2052	84.88	10.04	10.58%	8.02	6.37	0.38	1.31	6.33	4.74%	16.33%	78.93%	Fail
GME2053	79.54	18.46	18.84%	7.93	6.66	0.64	2.36	4.93	8.07%	29.76%	62.17%	Fail
GME2054	86.67	8.54	8.97%	7.08	6.31	0.30	1.18	5.60	4.24%	16.67%	79.10%	Fail
GME2055	90.26	6.44	6.66%	6.81	6.23	0.03	0.68	6.10	0.44%	9.99%	89.57%	Fail
GME2056	88.33	9.06	9.30%	7.94	6.33	0.63	0.92	6.39	7.93%	11.59%	80.48%	Fail
GME2059	84.02	14.79	14.97%	9.93	6.52	0.59	2.00	7.34	5.94%	20.14%	73.92%	Fail
GME2060	82.68	14.74	15.13%	9.03	6.53	0.51	1.25	7.27	5.65%	13.84%	80.51%	Fail
GME2069	90.25	7.91	8.06%	7.96	6.28	0.76	3.10	4.10	9.55%	38.94%	51.51%	Fail
GME2070	88.29	10.58	10.70%	8.42	6.37	1.30	3.31	3.81	15.44%	39.31%	45.25%	Fail
GME2071	87.35	6.52	6.95%	6.84	6.24	0.06	1.14	5.64	0.88%	16.67%	82.46%	Fail
GME2072	88.16	11.11	11.19%	6.88	6.39	0.39	1.67	4.82	5.67%	24.27%	70.06%	Fail
GME2073	76.84	14.69	16.05%	7.06	6.56	0.10	1.02	5.94	1.42%	14.45%	84.14%	Fail
GME2074	88.20	8.79	9.06%	8.06	6.32	0.83	2.06	5.17	10.30%	25.56%	64.14%	Fail
GME2075	83.22	13.23	13.72%	8.64	6.48	0.56	1.22	6.86	6.48%	14.12%	79.40%	Fail
GME2076	88.55	9.43	9.62%	8.87	6.34	1.14	3.42	4.31	12.85%	38.56%	48.59%	Fail
GME2077	90.50	8.47	8.56%	8.58	6.30	0.98	2.28	5.32	11.42%	26.57%	62.00%	Fail
GME2080	86.08	11.17	11.49%	8.28	6.40	0.64	1.40	6.24	7.73%	16.91%	75.36%	Fail
GME2081	88.50	10.53	10.63%	6.37	6.37	0.60	1.50	4.27	9.42%	23.55%	67.03%	Fail
GME2082	88.67	10.30	10.41%	8.51	6.36	1.29	2.89	4.33	15.16%	33.96%	50.88%	Fail
GME2083	88.26	9.14	9.38%	8.17	6.33	0.67	1.81	5.69	8.20%	22.15%	69.65%	Fail
GME2084	80.90	15.81	16.35%	6.74	6.57	0.23	1.06	5.45	3.41%	15.73%	80.86%	Fail
GME2085	86.09	12.14	12.36%	7.90	6.43	0.51	1.55	5.84	6.46%	19.62%	73.92%	Fail
GME2086	89.73	9.78	9.83%	8.33	6.34	0.91	2.12	5.30	10.92%	25.45%	63.63%	Fail
GME2087	86.47	10.98	11.27%	8.63	6.39	0.30	1.65	6.68	3.48%	19.12%	77.40%	Fail
GME2088	86.92	7.45	7.89%	7.43	6.28	0.14	1.58	5.71	1.88%	21.27%	76.85%	Fail
GME2089	89.37	7.61	7.85%	7.23	6.27	0.52	0.82	5.89	7.19%	11.34%	81.47%	Fail
GME2090	92.27	5.65	5.77%	12.36	6.20	1.07	3.35	7.94	8.66%	27.10%	64.24%	Fail
GME2091	90.23	9.05	9.12%	14.52	6.32	1.17	4.01	9.34	8.06%	27.62%	64.33%	Fail
GME2110	93.99	3.12	3.21%	16.90	6.11	4.81	6.87	5.22	28.46%	40.65%	30.89%	Fail
GME2112	97.96	2.01	2.01%	25.44	6.07	6.86	6.51	12.07	26.97%	25.59%	47.44%	Fail
GME2116	85.99	9.96	10.38%	7.06	6.36	0.27	0.89	5.90	3.82%	12.61%	83.57%	Fail
GME2122	99.33	0.66	0.66%	17.91	6.02	3.08	8.37	6.46	17.20%	46.73%	36.07%	Fail
GME2123	99.31	0.68	0.68%	17.52	6.02	5.16	5.85	6.51	29.45%	33.39%	37.16%	Fail
GME2124	96.98	0.69	0.71%	16.66	6.02	5.04	4.81	6.81	30.25%	28.87%	40.88%	Fail
GME2125	97.54	0.74	0.75%	19.74	6.03	5.08	7.17	7.49	25.73%	36.32%	37.94%	Fail
GME2133	97.52	1.08	1.10%	17.19	6.04	5.72	5.64	5.83	33.28%	32.81%	33.92%	Fail
GME2135	91.71	8.24	8.24%	7.59	6.29	1.12	2.20	4.27	14.76%	28.99%	56.26%	Fail
GME2137	99.34	0.59	0.59%	17.25	6.02	3.19	6.00	8.06	18.49%	34.78%	46.72%	Fail
GME2143	43.14	50.68	54.02%	8.51	7.89	0.42	1.20	6.89	4.94%	14.10%	80.96%	Fail
GME2144	31.62	65.08	67.30%	10.91	8.36	1.36	3.53	6.02	12.47%	32.36%	55.18%	Fail
GME2146	98.11	0.51	0.52%	16.76	6.02	6.43	4.40	5.93	38.37%	26.25%	35.38%	Fail
GME2147	99.19	0.55	0.55%	13.05	6.02	4.34	4.16	4.55	33.26%	31.88%	34.87%	Fail
GME2152	20.78	72.97	77.83%	10.16	8.72	0.58	1.70	7.88	5.71%	16.73%	77.56%	Fail
GME2156	24.57	71.98	74.55%	9.22	8.61	0.22	1.29	7.71	2.39%	13.99%	83.62%	Fail
GME2166	45.71	49.60	52.04%	7.96	7.82	0.40	1.13	6.43	5.03%	14.20%	80.78%	Fail
GME2171	90.02	8.11	8.26%	6.82	6.29	0.58	1.18	5.06	8.50%	17.30%	74.19%	Fail
GME2175	81.86	11.11	11.95%	6.71	6.42	0.62	0.93	5.16	9.24%	13.86%	76.90%	Fail
GME2176	89.16	7.45	7.71%	6.55	6.27	0.38	1.11	5.06	5.80%	16.95%	77.25%	Fail
GME2178	87.52	8.12	8.49%	6.87	6.30	0.17	0.83	5.87	2.47%	12.08%	85.44%	Fail
GME2182	94.00	4.35	4.42%	6.87	6.15	0.29	0.89	5.69	4.22%	12.95%	82.82%	Fail
GME2183	89.26	7.90	8.13%	6.72	6.28	0.36	0.80	5.56	5.36%	11.90%	82.74%	Fail
GME2214	92.11	3.69	3.85%	17.10	6.13	5.26	4.74	7.10	30.76%	27.72%	41.52%	Fail
GME2215	90.52	2.69	2.89%	7.90	6.10	0.73	1.40	5.77	9.24%	17.72%	73.04%	Fail
GME2217	93.30	3.55	3.67%	8.27	6.13	0.63	1.57	6.07	7.62%	18.98%	73.40%	Fail
GME2218	98.10	1.87	1.87%	14.03	6.07	3.51	4.60	5.92	25.02%	32.79%	42.20%	Fail
GME2219	94.58	0.80	0.84%	12.28	6.03	2.15	3.83	6.30	17.51%	31.19%	51.30%	Fail
GME2220	94.89	1.29	1.34%	15.97	6.05	2.18	4.48	9.31	13.65%	28.05%	58.30%	Fail
GME2221	93.74	1.96	2.05%	13.61	6.07	2.20	3.25	8.16	16.16%	23.88%	59.96%	Fail
GME2222	92.92	1.84	1.94%	16.92	6.07	3.19	6.67	7.06	18.85%	39.42%	41.73%	Fail
GME2223	63.21	31.00	32.91%	13.08	7.15	2.00	3.32	7.76	15.29%	25.38%	59.33%	Fail
GME2226	9.25	83.83	90.06%	11.33	9.15	1.25	2.65	7.43	11.03%	23.39%	65.58%	Fail
GME2227	25.11	65.80	72.38%	10.80	8.53	0.92	2.78	7.10	8.52%	25.74%	65.74%	Fail
GME2231	96.93	0.33	0.34%	13.32	6.01	2.96	3.89	6.47	22.22%	29.20%	48.57%	Fail
GME2232	89.83	4.47	4.74%	10.44	6.17	0.95	2.91	6.58	9.10%	27.87%	63.03%	Fail
GME2233	63.21	31.00	32.91%	13.08	7.15	2.00	3.32	7.76	15.29%	25.38%	59.33%	Fail
GME2239	83.95	10.09	10.73%	8.48	6.38	0.78	2.25	5.45	9.20%	26.53%	64.27%	Fail
GME2240	85.06	10.48	10.97%	10.31	6.38	1.81	2.60	5.90	17.56%	25.22%	57.23%	Fail
GME2252	84.05	9.46	10.12%	8.46	6.35	0.59	1.35	6.52	6.97%	15.96%	77.07%	Fail
GME2267	83.98	10.12	10.75%	9.56	6.38	1.48	3.06	5.02	15.48%	32.01%	52.51%	Fail
GME2268	86.26	7.69	8.19%	12.06	6.29	1.55	2.77	7.74	12.85%	22.97%	64.18%	Fail
GME2269	83.14	7.49	8.26%	7.17	6.29	0.40	1.69	5.08	5.58%	23.57%	70.85%	Fail
GME2270	75.21	14.71	16.36%	7.24	6.57	0.46	1.62	5.16	6.35%	22.38%	71.27%	Fail
GME2271	79.78	9.11	10.25%	8.41	6.36	0.99	1.59	5.83	11.77%	18.91%	69.32%	Fail
GME2272	76.33	18.82	19.78%	9.77	6.69	1.55	2.68	5.54	15.86%	27.43%	56.70%	Fail

APPENDIX J: SUMMARY OF GAS CONTENT AND GAS COMPOSITION DATA (HARD-TO-DRAIN DATABASE)

Core Sample	CO2 Composition (%)	CH4 Composition (%)	Gas Composition CH4/(CO2+CH4) (%)	Measured Gas Content QM (m3/t)	Mining Limit Level (m3/t)	Q1 (m3/t)	Q2 (m3/t)	Q3 (m3/t)	Q1/QM (%)	Q2/QM (%)	Q3/QM (%)	Pass/Fail
GME2009	86.08	12.85	12.99%	5.46	6.45	0.17	1.14	4.15	3.11%	20.88%	76.01%	Pass
GME2016	92.14	7.74	7.75%	5.97	6.27	0.13	0.75	5.09	2.18%	12.56%	85.26%	Pass
GME1957	80.74	15.91	16.46%	6.54	6.58	0.48	0.87	5.19	7.34%	13.30%	79.36%	Pass
GME1891	89.42	0.24	0.27%	3.01	6.01	0.03	0.40	2.58	1.00%	13.29%	85.71%	Pass
GME2003	89.27	5.59	5.89%	5.12	6.21	0.12	0.67	4.33	2.34%	13.09%	84.57%	Pass
GME2115	81.44	12.05	12.89%	5.20	6.45	0.15	0.62	4.43	2.88%	11.92%	85.19%	Pass
GME2127	85.04	9.70	10.24%	5.71	6.36	0.14	0.78	4.79	2.45%	13.66%	83.89%	Pass
GME2126	84.96	8.07	8.67%	5.06	6.30	0.06	0.74	4.26	1.19%	14.62%	84.19%	Pass
GME2167	86.85	8.14	8.57%	2.80	6.30	0.07	0.41	2.32	2.50%	14.64%	82.86%	Pass
GME2177	86.53	11.18	11.44%	6.30	6.40	0.29	1.06	4.95	4.60%	16.83%	78.57%	Pass
GME2168	87.68	9.83	10.08%	5.71	6.35	0.33	1.27	4.11	5.78%	22.24%	71.98%	Pass
GME2173	91.63	6.59	6.71%	5.16	6.23	0.28	0.99	3.89	5.43%	19.19%	75.39%	Pass
GME2174	89.97	7.53	7.72%	5.95	6.27	0.28	1.09	4.58	4.71%	18.32%	76.97%	Pass
GME2185	89.30	7.55	7.80%	6.08	6.27	0.05	0.51	5.52	0.82%	8.39%	90.79%	Pass
GME2132	95.83	4.17	4.17%	5.79	6.15	0.13	1.15	4.51	2.25%	19.86%	77.89%	Pass
GME2134	90.07	8.17	8.32%	4.50	6.29	0.18	0.84	3.48	4.00%	18.67%	77.33%	Pass
GME2131	87.67	8.80	9.12%	4.80	6.32	0.43	0.77	3.60	8.96%	16.04%	75.00%	Pass
GME2079	92.48	0.66	0.71%	4.01	6.02	0.17	0.49	3.35	4.24%	12.22%	83.54%	Pass
GME2129	85.97	10.05	10.47%	4.25	6.37	0.03	0.86	3.36	0.71%	20.24%	79.06%	Pass
GME2114	84.86	12.13	12.51%	5.35	6.44	0.61	0.81	3.93	11.40%	15.14%	73.46%	Pass
GME2113	86.16	7.98	8.48%	5.36	6.30	0.07	0.57	4.72	1.31%	10.63%	88.06%	Pass
GME2042	89.57	6.14	6.42%	5.70	6.22	0.05	1.39	4.26	0.88%	24.39%	74.74%	Pass
GME2026	89.93	6.31	6.56%	5.32	6.23	0.13	0.56	4.63	2.44%	10.53%	87.03%	Pass
GME2025	90.90	5.97	6.16%	5.31	6.22	0.15	0.84	4.32	2.82%	15.82%	81.36%	Pass
GME1975	92.59	4.92	5.05%	4.97	6.18	0.28	0.82	3.87	5.63%	16.50%	77.87%	Pass
GME1949	93.30	6.65	6.65%	6.18	6.23	0.53	1.66	3.99	8.58%	26.86%	64.56%	Pass
GME1885	93.70	1.87	1.96%	5.11	6.07	0.32	0.65	4.14	6.26%	12.72%	81.02%	Pass
GME1963	82.05	13.89	14.48%	5.44	6.51	0.21	0.71	4.52	3.86%	13.05%	83.09%	Pass
GME1948	82.66	14.49	14.92%	5.66	6.52	0.43	0.68	4.55	7.60%	12.01%	80.39%	Pass
GME2014	72.64	17.70	19.59%	6.19	6.69	0.14	0.81	5.24	2.26%	13.09%	84.65%	Pass
GME1973	84.11	11.36	11.90%	4.56	6.42	0.03	0.58	3.95	0.66%	12.72%	86.62%	Pass
GME1950	81.94	14.65	15.17%	8.35	6.53	0.80	1.29	6.26	9.58%	15.45%	74.97%	Fail
GME1960	83.25	16.73	16.73%	10.19	6.59	2.50	3.20	4.49	24.53%	31.40%	44.06%	Fail
GME1980	83.20	15.58	15.77%	7.84	6.55	0.23	1.36	6.25	2.93%	17.35%	79.72%	Fail
GME2006	79.05	16.87	17.59%	8.49	6.62	0.52	2.18	5.79	6.12%	25.68%	68.20%	Fail
GME2019	84.00	14.35	14.59%	7.28	6.51	0.23	1.54	5.51	3.16%	21.15%	75.69%	Fail
GME1952	85.01	14.97	14.97%	7.31	6.52	0.66	1.84	4.81	9.03%	25.17%	65.80%	Fail
GME1998	79.70	17.19	17.74%	7.10	6.62	0.14	0.86	6.10	1.97%	12.11%	85.92%	Fail
GME1981	78.58	20.18	20.43%	7.75	6.71	0.25	1.28	6.22	3.23%	16.52%	80.26%	Fail
GME1967	79.54	18.95	19.24%	8.09	6.67	0.93	2.21	4.95	11.50%	27.32%	61.19%	Fail
GME1896	76.52	20.68	21.28%	7.94	6.74	0.69	0.99	6.26	8.69%	12.47%	78.84%	Fail
GME1953	79.27	20.71	20.71%	8.57	6.72	1.46	2.05	5.06	17.04%	23.92%	59.04%	Fail
GME1982	81.10	18.02	18.18%	7.85	6.64	0.36	1.59	5.90	4.59%	20.25%	75.16%	Fail
GME2000	79.07	17.10	17.78%	6.99	6.62	0.30	0.93	5.76	4.29%	13.30%	82.40%	Fail
GME1968	80.71	16.65	17.10%	7.86	6.67	0.88	2.46	4.52	11.20%	31.30%	57.51%	Fail
GME2084	80.90	15.81	16.35%	6.74	6.57	0.23	1.06	5.45	3.41%	15.73%	80.86%	Fail
GME2050	79.98	16.52	17.12%	8.05	6.60	0.38	2.49	5.18	4.72%	30.93%	64.35%	Fail
GME2073	76.84	14.69	16.05%	7.06	6.56	0.10	1.02	5.94	1.42%	14.45%	84.14%	Fail
GME2049	77.80	16.90	17.85%	9.42	6.62	0.49	2.74	6.19	5.20%	29.09%	65.71%	Fail
GME2032	82.41	16.84	16.97%	8.43	6.59	0.69	1.51	6.23	8.19%	17.91%	73.90%	Fail
GME2085	86.09	12.14	12.36%	7.90	6.43	0.51	1.55	5.84	6.46%	19.62%	73.92%	Fail
GME2074	88.20	8.79	9.06%	8.06	6.32	0.83	2.06	5.17	10.30%	25.56%	64.14%	Fail
GME2116	85.99	9.96	10.38%	7.06	6.36	0.27	0.89	5.90	3.82%	12.61%	83.57%	Fail
GME2087	86.47	10.98	11.27%	8.63	6.39	0.30	1.65	6.68	3.48%	19.12%	77.40%	Fail
GME2047	85.47	10.96	11.37%	8.93	6.40	0.49	1.86	6.58	5.49%	20.83%	73.68%	Fail
GME2075	83.22	13.23	13.72%	8.64	6.48	0.56	1.22	6.86	6.48%	14.12%	79.40%	Fail
GME2048	84.39	11.53	12.02%	8.88	6.42	0.87	2.17	5.84	9.80%	24.44%	65.77%	Fail
GME2030	82.18	10.09	10.94%	8.43	6.38	0.88	2.63	4.92	10.44%	31.20%	58.36%	Fail
GME2086	89.73	9.78	9.83%	8.33	6.34	0.91	2.12	5.30	10.92%	25.45%	63.63%	Fail
GME2088	86.92	7.45	7.89%	7.43	6.28	0.14	1.58	5.71	1.88%	21.27%	76.85%	Fail
GME2076	88.55	9.43	9.62%	8.87	6.34	1.14	3.42	4.31	12.85%	38.56%	48.59%	Fail
GME2176	89.16	7.45	7.71%	6.55	6.27	0.38	1.11	5.06	5.80%	16.95%	77.25%	Fail
GME2082	88.67	10.30	10.41%	8.51	6.36	1.29	2.89	4.33	15.16%	33.96%	50.88%	Fail
GME2053	79.54	18.46	18.84%	7.93	6.66	0.64	2.36	4.93	8.07%	29.76%	62.17%	Fail
GME2031	78.75	16.91	17.68%	8.14	6.62	0.70	1.23	6.21	8.60%	15.11%	76.29%	Fail
GME2040	83.60	15.05	15.26%	8.06	6.53	0.80	2.10	5.16	9.93%	26.05%	64.02%	Fail
GME2044	84.14	13.23	13.59%	8.47	6.48	0.72	3.16	4.59	8.50%	37.31%	54.19%	Fail
GME2070	88.29	10.58	10.70%	8.42	6.37	1.30	3.31	3.81	15.44%	39.31%	45.25%	Fail
GME2043	87.50	8.16	8.53%	8.99	6.30	0.92	1.96	6.11	10.23%	21.80%	67.96%	Fail
GME2046	89.31	7.22	7.48%	8.44	6.26	0.46	1.55	6.43	5.45%	18.36%	76.18%	Fail
GME2054	86.67	8.54	8.97%	7.08	6.31	0.30	1.18	5.60	4.24%	16.67%	79.10%	Fail
GME2069	90.25	7.91	8.06%	7.96	6.28	0.76	3.10	4.10	9.55%	38.94%	51.51%	Fail
GME2056	88.33	9.06	9.30%	7.94	6.33	0.63	0.92	6.39	7.93%	11.59%	80.48%	Fail
GME2045	86.23	10.53	10.88%	7.95	6.38	0.31	2.49	5.15	3.90%	31.32%	64.78%	Fail
GME2072	88.16	11.11	11.19%	6.88	6.39	0.39	1.67	4.82	5.67%	24.27%	70.06%	Fail
GME2052	84.88	10.04	10.58%	8.02	6.37	0.38	1.31	6.33	4.74%	16.33%	78.93%	Fail
GME2055	90.26	6.44	6.66%	6.81	6.23	0.03	0.68	6.10	0.44%	9.99%	89.57%	Fail
GME2051	89.94	6.52	6.76%	8.33	6.24	0.41	1.81	6.11	4.92%	21.73%	73.35%	Fail
GME2071	87.35	6.52	6.95%	6.84	6.24	0.06	1.14	5.64	0.88%	16.67%	82.46%	Fail
GME1951	90.88	8.07	8.16%	6.66	6.29	0.40	1.08	5.18	6.01%	16.22%	77.78%	Fail
GME1888	87.19	7.19	7.62%	7.16	6.27	0.38	0.92	5.86	5.31%	12.85%	81.84%	Fail
GME1986	91.66	6.48	6.60%	7.45	6.23	0.32	0.94	6.19	4.30%	12.62%	83.09%	Fail
GME2024	88.37	6.87	7.21%	6.27	6.25	0.25	0.74	5.28	3.99%	11.80%	84.21%	Fail
GME2004	89.15	6.43	6.73%	7.20	6.24	0.16	1.19	5.85	2.22%	16.53%	81.25%	Fail
GME1976	91.06	6.63	6.79%	6.60	6.24	0.53	1.88	4.19	8.03%	28.48%	63.48%	Fail
GME1959	93.91	6.08	6.08%	6.90	6.21	0.63	1.38	4.89	9.13%	20.00%	70.87%	Fail
GME1985	76.58	18.20	19.20%	7.87	6.67	0.36	1.19	6.32	4.57%	15.12%	80.30%	Fail
GME2001	82.81	14.64	15.02%	7.02	6.53	0.35	1.58	5.09	4.99%	22.51%	72.51%	Fail
GME1974	79.18	16.49	17.24%	6.60	6.60	0.26	1.04	5.30	3.94%	15.76%	80.30%	Fail
GME1884	81.19	14.19	14.88%	8.94	6.52	1.23	1.90	5.81	13.76%	21.25%	64.99%	Fail
GME1962	86.66	11.62	11.82%	6.85	6.41	0.87	1.94	4.04	12.70%	28.32%	58.98%	Fail
GME1958	80.74	15.91	16.46%	6.66	6.50	0.18	1.07	5.41	2.70%	16.07%	81.23%	Fail
GME1964	86.25	11.76	12.00%	6.48	6.42	0.48	1.73	4.27	7.41%	26.70%	65.90%	Fail
GME1961	84.95	12.13	12.49%	6.55	6.44	0.38	0.66	5.55	5.80%	10.08%	84.73%	Fail